



NUREG/CR-7284
ORNL/TM-2017/278

SCALE 6.2 Lattice Physics Performance Assessment

AVAILABILITY OF REFERENCE MATERIALS IN NRC PUBLICATIONS

NRC Reference Material

As of November 1999, you may electronically access NUREG-series publications and other NRC records at the NRC's Library at www.nrc.gov/reading-rm.html. Publicly released records include, to name a few, NUREG-series publications; *Federal Register* notices; applicant, licensee, and vendor documents and correspondence; NRC correspondence and internal memoranda; bulletins and information notices; inspection and investigative reports; licensee event reports; and Commission papers and their attachments.

NRC publications in the NUREG series, NRC regulations, and Title 10, "Energy," in the *Code of Federal Regulations* may also be purchased from one of these two sources:

1. The Superintendent of Documents

U.S. Government Publishing Office
Washington, DC 20402-0001
Internet: <https://bookstore.gpo.gov/>
Telephone: (202) 512-1800
Fax: (202) 512-2104

2. The National Technical Information Service

5301 Shawnee Road
Alexandria, VA 22312-0002
Internet: <https://www.ntis.gov/>
1-800-553-6847 or, locally, (703) 605-6000

A single copy of each NRC draft report for comment is available free, to the extent of supply, upon written request as follows:

Address: **U.S. Nuclear Regulatory Commission**
Office of Administration
Digital Communications and Administrative
Services Branch
Washington, DC 20555-0001
E-mail: Reproduction.Resource@nrc.gov
Facsimile: (301) 415-2289

Some publications in the NUREG series that are posted at the NRC's Web site address www.nrc.gov/reading-rm/doc-collections/nuregs are updated periodically and may differ from the last printed version. Although references to material found on a Web site bear the date the material was accessed, the material available on the date cited may subsequently be removed from the site.

Non-NRC Reference Material

Documents available from public and special technical libraries include all open literature items, such as books, journal articles, transactions, *Federal Register* notices, Federal and State legislation, and congressional reports. Such documents as theses, dissertations, foreign reports and translations, and non-NRC conference proceedings may be purchased from their sponsoring organization.

Copies of industry codes and standards used in a substantive manner in the NRC regulatory process are maintained at—

The NRC Technical Library

Two White Flint North
11545 Rockville Pike
Rockville, MD 20852-2738

These standards are available in the library for reference use by the public. Codes and standards are usually copyrighted and may be purchased from the originating organization or, if they are American National Standards, from—

American National Standards Institute

11 West 42nd Street
New York, NY 10036-8002
Internet: www.ansi.org
(212) 642-4900

Legally binding regulatory requirements are stated only in laws; NRC regulations; licenses, including technical specifications; or orders, not in NUREG-series publications. The views expressed in contractor prepared publications in this series are not necessarily those of the NRC.

The NUREG series comprises (1) technical and administrative reports and books prepared by the staff (NUREG-XXXX) or agency contractors (NUREG/CR-XXXX), (2) proceedings of conferences (NUREG/CP-XXXX), (3) reports resulting from international agreements (NUREG/IA-XXXX), (4) brochures (NUREG/BR-XXXX), and (5) compilations of legal decisions and orders of the Commission and the Atomic and Safety Licensing Boards and of Directors' decisions under Section 2.206 of the NRC's regulations (NUREG-0750), (6) Knowledge Management prepared by NRC staff or agency contractors (NUREG/KM-XXXX).

DISCLAIMER: This report was prepared as an account of work sponsored by an agency of the U.S. Government. Neither the U.S. Government nor any agency thereof, nor any employee, makes any warranty, expressed or implied, or assumes any legal liability or responsibility for any third party's use, or the results of such use, of any information, apparatus, product, or process disclosed in this publication, or represents that its use by such third party would not infringe privately owned rights.

SCALE 6.2 Lattice Physics Performance Assessment

Manuscript Completed: November 2022
Date Published: March 2023

Prepared by:
Ugur Mertuyrek
Matthew A. Jessee
Benjamin R. Betzler
Stephen M. Bowman

Oak Ridge National Laboratory
Managed by UT-Battelle, LLC
Oak Ridge, TN 37831-617

Lucas Kyriazidis, NRC Project Manager

ABSTRACT

The US Nuclear Regulatory Commission relies on the lattice physics analysis capabilities of the SCALE code system to perform confirmatory licensing analyses. Either SCALE lattice physics code—TRITON/NEWT or Polaris—can be used to generate cross section data used by the PARCS nodal core simulator for full-core neutronics calculations. This report presents an assessment of the accuracy of SCALE lattice physics codes for preparation of lattice physics data that are used to support simulator codes such as the NRC's PARCS, for UO₂-mixed oxide (MOX)/Zr fueled light water reactor (LWR) analyses.

Due to the nature of lattice physics calculations, critical reactor experiment benchmarks cannot be modeled in explicit detail in a lattice physics code. However, this limitation does not mean that these measurement data are not usable for lattice physics studies. Therefore, either geometry approximations or axial buckling must be implemented to determine the critical water height. These modeling limitations have led to development of a three-phase assessment strategy.

In the first phase, selected critical experiment benchmarks are modeled using the SCALE 3D continuous-energy (CE) Monte Carlo (MC) code KENO, which is the most rigorous neutron transport method available in SCALE, with no approximations in the spatial, angle, or energy treatments. Biases and statistical uncertainties in quantities of interest such as k_{eff} and pin power distributions are determined by comparing CE KENO results to experimental data. This first phase in the accuracy assessment is to demonstrate and establish the use of CE KENO as a reference solution for the second phase.

In the second phase, 14 numerical test suites are used to compare SCALE lattice physics calculations with CE KENO as a reference solution.

In the third phase, SCALE lattice physics depletion calculations are performed, and the spent fuel isotopic results are compared with available radiochemical assay measurements. Isotopic measurement comparisons provide quantitative assessment of isotopic density distribution predictions with the depletion models in SCALE lattice physics codes.

This report documents results for all test suites. The assessment was performed using standard production techniques unless otherwise noted. Both TRITON/NEWT and Polaris exhibited acceptable accuracy for most test cases. For the few test cases in which acceptable accuracy criteria were not met, further code and data development are planned.

The computer codes used in this assessment are as follows:

- SCALE 6.2 rev19189 (pre-release of 6.2.1) was used for CE KENO, TRITON/NEWT and Polaris (PWR only) calculations.
- SCALE 6.2.2 was used for Polaris calculations to address several updates in support of support boiling water reactor (BWR) lattice geometries. For this work, there is no difference between SCALE 6.2.1 and SCALE 6.2.2 beyond the inclusion of the Polaris BWR analysis capability.
- The ENDF/B-VII.1 continuous energy and 252 group libraries deployed in SCALE 6.2 were generated with AMPX 6.2 that is distributed with SCALE.

TABLE OF CONTENTS

ABSTRACT		iii
LIST OF FIGURES		vii
LIST OF TABLES		xi
ACKNOWLEDGMENTS		xv
ABBREVIATIONS AND ACRONYMS		xvii
1	INTRODUCTION AND BACKGROUND	1-1
2	TWO-STEP REACTOR CORE SIMULATION	2-1
3	SCALE CODE DESCRIPTIONS AND MAJOR ASSUMPTIONS	3-1
	3.1 KENO	3-1
	3.2 TRITON/NEWT	3-1
	3.3 Polaris	3-3
	3.4 ORIGEN	3-5
4	CODE ASSESSMENT TESTING	4-1
	4.1 Parametric Studies	4-1
	4.2 2D Numerical Benchmark Test Suites	4-8
5	SUMMARY OF RESULTS	5-1
	5.1 Test Suite 1 – BOL LWR Assemblies Baseline	5-1
	5.2 Test Suite 2 – Control Elements	5-2
	5.3 Test Suite 3 – MOX Fuel	5-3
	5.4 Test Suite 4 – Reactivity Worth of Depleted Fuel	5-4
	5.5 Test Suite 5 – Depletion Calculations	5-5
	5.6 Test Suite 6 – Boron Injection	5-6
	5.7 Test Suite 7 – Enrichment	5-7
	5.8 Test Suite 8 – Fuel Temperature	5-8
	5.9 Test Suite 9 – Burnable Poison Loading	5-9
	5.10 Test Suite 10 – Burnable Poison Spatial Variations	5-10
	5.11 Test Suite 11 – PARCS Parameters for Fuel-Only Model	5-11
	5.12 Test Suite 12 – PARCS Parameters for Fuel/Reflector Model	5-12
	5.13 Test Suite 13 – International Numerical Benchmarks	5-13
	5.14 Test Suite 14 – Variations in Vanished Zone Patterns	5-14
	5.15 RCA Measurements	5-15
6	CONCLUSIONS	6-1
	6.1 Overall Conclusions	6-1
	6.2 Lessons Learned	6-3
	6.3 Future Work	6-4

7	REFERENCES	7-1
APPENDIX A	CE KENO LATTICE CALCULATIONS ACCURACY ASSESSMENT	A-1
APPENDIX B	2D NUMERICAL BENCHMARK ASSESSMENT	B-1
APPENDIX C	RCA MEASUREMENTS FOR DEPLETION ASSESSMENT.....	C-1
APPENDIX D	INPUT AND OUTPUT FILES	D-1
APPENDIX E	PROPRIETARY INPUT AND OUTPUT FILES	E-1
APPENDIX F	SCALE 6.2.4 UPDATE.....	F-1

LIST OF FIGURES

Figure 2-1	Fuel and Reflector Lattice Geometry Configurations	2-1
Figure 2-2	Cross Section Evaluation for Two-Step Calculations.....	2-2
Figure 3-1	TRITON/NEWT Lattice Physics Calculation Flow.....	3-2
Figure 3-2	Polaris Lattice Physics Calculation Flow	3-4
Figure A-1	C/E Values for LEU-COMP-THERM Systems Using SCALE 6.2 [24].....	A-2
Figure A-2	C/E Values for MIX COMP-THERM Systems Using SCALE 6.2 [24]	A-3
Figure A-3	B&W Core 1 Pin Power Differences for CE KENO	A-5
Figure A-4	B&W Core 5 Pin Power Differences for CE KENO	A-5
Figure A-5	B&W Core 12 Pin Power Differences for CE KENO	A-6
Figure A-6	B&W Core 14 Pin Power Differences for CE KENO	A-6
Figure A-7	B&W Core 18 Pin Power Differences for CE KENO	A-7
Figure A-8	B&W Core 20 Pin Power Differences for CE KENO	A-7
Figure B-1	Test Suite 1: BWR k_{inf} Comparisons for Uncontrolled Cases	B-3
Figure B-2	Test Suite 1: BWR k_{inf} Comparisons for Controlled Cases	B-4
Figure B-3	Test Suite 1: Void Fraction Trend for GE14-DOM Lattice.....	B-4
Figure B-4	Test Suite 1: 10 × 10 DOM Zone Pin Power Differences at 0% Void Fraction for NEWT and Polaris.....	B-7
Figure B-5	Test Suite 1: 10 × 10 DOM Zone Pin Power Differences at 40% Void Fraction for NEWT and Polaris.....	B-8
Figure B-6	Test Suite 1: 10 × 10 DOM Zone Pin Power Differences at 40% Void Fraction for NEWT and Polaris Controlled Cases.....	B-9
Figure B-7	Test Suite 1: 10 × 10 DOM Zone Pin Power Differences at 70% Void Fraction for NEWT and Polaris.....	B-10
Figure B-8	Test Suite 1: 10 × 10 DOM Zone Pin Power Differences at 90% Void Fraction for NEWT and Polaris.....	B-11
Figure B-9	Test Suite 1: 9 × 9 DOM Zone Pin Power Differences at 40% Void Fraction for NEWT and Polaris.....	B-12
Figure B-10	Test Suite 1: 8 × 8 DOM Zone Pin Power Differences at 40% Void Fraction for NEWT and Polaris.....	B-13
Figure B-11	Test Suite 1: 8 × 8 DOM Zone Pin Power Differences at 40% Void Fraction for NEWT and Polaris Controlled Cases.....	B-14
Figure B-12	Test Suite 1: ATRIUM10 DOM Zone Pin Power Differences at 40% Void Fraction for NEWT	B-15
Figure B-13	Test Suite 1: PWR k_{inf} Comparisons for Uncontrolled Cases.....	B-18
Figure B-14	Test Suite 1: PWR k_{inf} Comparisons for Controlled Cases	B-18
Figure B-15	Test Suite 1: Effect of Boron Concentration on k_{inf} Differences for Uncontrolled Cases.....	B-19

Figure B-16	Test Suite 1: Effect of Boron Concentration on k_{inf} Differences for Controlled Cases	B-20
Figure B-17	Test Suite 1: 17 × 17 Lattice Pin Power Differences at Nominal Conditions for NEWT (top) and Polaris (bottom).....	B-22
Figure B-18	Test Suite 1: 17 × 17 Lattice Pin Power Differences at Nominal Controlled Conditions for NEWT (top) and Polaris (bottom)	B-23
Figure B-19	Test Suite 1: 14 × 14 Lattice Pin Power Differences at Cold Controlled Conditions for NEWT (top) and Polaris (bottom)	B-24
Figure B-20	Test Suite 1: 14 × 14 Lattice Pin Power Differences at Nominal Conditions for NEWT (top) and Polaris (bottom).....	B-25
Figure B-21	Test Suite 1: 16 × 16 CE Lattice Pin Power Differences at Nominal Conditions for NEWT (top) and Polaris (bottom)	B-26
Figure B-22	Test Suite 1: 18 × 18 Lattice Pin Power Differences at Nominal Conditions for NEWT (top) and Polaris (bottom).....	B-27
Figure B-23	Test Suite 2: MG KENO and NEWT k_{inf} Void Fraction Trends for Different Control Blade Types	B-29
Figure B-24	Test Suite 2: k_{inf} MG KENO and Polaris Void Fraction Trends for Different Control Blade Types	B-30
Figure B-25	Test Suite 2: k_{inf} Boron Trends for Different Control Rod Types	B-31
Figure B-26	BWR MOX Lattice Design [13].....	B-32
Figure B-27	Test Suite 3: MOX BWR k_{inf} Differences for Uncontrolled Cases.....	B-33
Figure B-28	Test Suite 3: MOX BWR k_{inf} Differences for Controlled Cases	B-34
Figure B-29	Test Suite 3 MOX BWR Pin Power Differences at 40% Void	B-35
Figure B-30	Test Suite 3 MOX BWR Pin Power Differences at 90% Void	B-36
Figure B-31	Test Suite 3: PWR MOX Lattice Designs	B-37
Figure B-32	Test suite 3 17 × 17 MOX PWR Lattice k_{inf} Differences for Uncontrolled Cases	B-38
Figure B-33	Test suite 3 17 × 17 MOX PWR Lattice k_{inf} Differences for Controlled Cases	B-39
Figure B-34	Test Suite 3: 15 × 15 MOX PWR Lattice k_{inf} Differences for Uncontrolled Cases	B-40
Figure B-35	Test suite 3 15 × 15 MOX PWR Lattice k_{inf} Differences for Controlled Cases	B-41
Figure B-36	Test Suite 3: 17 × 17 lattice Pin Power Differences at Nominal Conditions for NEWT (Top) and Polaris (Bottom)	B-42
Figure B-37	Test suite 3 17×17 Lattice Pin Power Differences at Nominal Controlled Conditions for NEWT (Top) and Polaris (Bottom).....	B-43
Figure B-38	Test Suite 4: 10 × 10 BWR Lattice k_{inf} Differences	B-45
Figure B-39	Test Suite 4: 17 × 17 PWR Lattice k_{inf} Differences	B-46

Figure B-40	Test Suite 5: 8 × 8 BWR Lattice NEWT k_{inf} Differences.....	B-48
Figure B-41	Test suite 5 8 × 8 BWR Lattice Polaris k_{inf} Differences.....	B-49
Figure B-42	Test Suite 5: 17 × 17 PWR Lattice k_{inf} Differences	B-51
Figure B-43	Test Suite 6: BWR Lattice k_{inf} Differences for Boron Variations.....	B-53
Figure B-44	Test Suite 6 10 × 10 DOM Zone Pin Power Differences at HZP Conditions at 2,000 ppm Boron Concentration	B-54
Figure B-45	Test Suite 6: PWR Lattice k_{inf} Differences for Boron Variations.....	B-56
Figure B-46	Test Suite 6 17 × 17 Lattice Pin Power Differences at HFP Conditions at 0 ppm Boron Concentration	B-57
Figure B-47	Test Suite 7: BWR Lattice Design	B-60
Figure B-48	Test Suite 7: k_{inf} Differences for Uncontrolled BWR Cases.....	B-61
Figure B-49	Test Suite 7: k_{inf} Differences for Controlled BWR Cases	B-61
Figure B-50	Test Suite 7: 10 × 10 DOM Zone Pin Power Differences at HFP Conditions, 40% Void Fraction, and 10% ²³⁵ U Enrichment.....	B-62
Figure B-51	Test Suite 7: k_{inf} Differences for Uncontrolled and Controlled PWR Cases.....	B-64
Figure B-52	Test Suite 7: 17 × 17 Lattice Pin Power Differences at HFP Conditions at 10% ²³⁵ U Enrichment	B-65
Figure B-53	Test Suite 8: k_{inf} Differences for Uncontrolled BWR Cases.....	B-67
Figure B-54	Test Suite 8: k_{inf} Differences for Uncontrolled PWR Cases.....	B-68
Figure B-55	Test suite 9: k_{inf} Differences for Uncontrolled BWR Cases	B-70
Figure B-56	Test suite 9: 10 × 10 DOM Zone Pin Power Differences at HFP Conditions, 40% Void Fraction, and 10% Gadolinia Loading.....	B-71
Figure B-57	Test Suite 9: k_{inf} Differences for Uncontrolled PWR Cases.....	B-73
Figure B-58	Test Suite 9: 17 × 17 Lattice Pin Power Differences at HFP, 1,300 ppm Boron, and 4 g/cm ³ B ₄ C Conditions.....	B-74
Figure B-59	Test Suite 10: Gadolinia Rod Patterns	B-75
Figure B-60	Test Suite 10: k_{inf} Differences for BWR Uncontrolled Cases.....	B-77
Figure B-61	Test Suite 10: k_{inf} Differences for BWR Controlled Cases	B-78
Figure B-62	Test Suite 10: 10 × 10 DOM Zone Pin Power Differences at HFP Conditions, 40% Void Fraction, Edge Gadolinia Loading	B-79
Figure B-63	Test Suite 10: 10 × 10 DOM Zone Pin Power Differences at HFP Conditions, 40% Void Fraction, Internal Gadolinia Loading.....	B-80
Figure B-64	Test Suite 10: PWR BP Loading Patterns	B-81
Figure B-65	Test Suite 10: PWR Integral BP Loading Patterns	B-82
Figure B-66	Test Suite 10: PWR k_{inf} Differences	B-83
Figure B-67	Test Suite 10: 17 × 17 Lattice Pin Power Differences at HFP, 1,300 ppm boron, and 4 B ₄ C Rods	B-84

Figure B-68	Test Suite 12: BWR Bottom Reflector Geometry.....	B-99
Figure B-69	Test Suite 12: BWR Top Reflector Geometry.....	B-99
Figure B-70	Test Suite 12: BWR Radial Reflector Geometry.....	B-100
Figure B-71	Test Suite 13: BWR k_{inf} Differences with Depletion for 0% Void Fraction	B-108
Figure B-72	Test Suite 13: BWR k_{inf} Differences with Depletion for 40% Void Fraction ...	B-109
Figure B-73	Test Suite 13: BWR k_{inf} Differences with Depletion for 70% Void Fraction ...	B-109
Figure B-74	Test Suite 14: Vanished Zone Patterns.....	B-114
Figure B-75	Test Suite 14: k_{inf} Differences.....	B-115
Figure C-1	Comparison of addnux=3 and addnux=4 Isotope Sets on Calvert Cliffs-1 MKP 109-3 Sample.....	C-2
Figure C-2	Comparison of Isotopic Distributions for Calvert Cliffs-1 MKP 109-3 Sample	C-2
Figure C-3	Comparison of isotopic Distributions for Calvert Cliffs-1 MKP 109-2 Sample	C-3
Figure C-4	Comparison of Isotopic Distributions for Fukushima SF98-5 Sample	C-3
Figure C-5	Comparison of Isotopic Distributions for Fukushima SF98-6 Sample	C-4
Figure C-6	Comparison of Isotopic Distributions for Gundremmingen GRM-1 Sample	C-4
Figure D-1	Main Directory Structure of Input and Output Repository.	D-1
Figure D-2	Directory Structure (Partially Expanded) of APPENDIX A Inputs and Outputs.....	D-2
Figure D-3	Directory Structure of APPENDIX B Inputs and Outputs	D-3
Figure D-4	Directory structure of APPENDIX A Test Suite 3 inputs and outputs.....	D-4
Figure D-5	Expanded Directory Structure of APPENDIX A Test Suite 3 PWR Inputs	D-4
Figure D-6	Expanded Directory Structure of APPENDIX A Test Suite 3 BWR Inputs	D-5
Figure D-7	Partially Expanded Directory Structure of APPENDIX C Inputs and Outputs.....	D-6
Figure D-8	Polaris Input File for Fukushima Daini SF98-5 Fuel Sample	D-9
Figure D-9	TRITON/CE-KENO Input File for Fukushima Daini SF98-5 Fuel Sample.....	D-11
Figure E-1	Main Directory Structure of Proprietary Input Repository.....	E-1
Figure F-2	Test Suite 10: Updated PWR k_{inf} Differences	F-2

LIST OF TABLES

Table 4-1	Effect of CE KENO Parameters on Pin Power Distribution Statistics.....	4-2
Table 4-2	Change in Unrodded k_{eff} with NEWT Input Parameters.....	4-3
Table 4-3	Change in Unrodded k_{eff} with Polaris Input Parameters.....	4-4
Table 4-4	SCALE Solution Parameters Used in Testing	4-5
Table 4-5	Test Suite Coverage for 2D Numerical Benchmarks	4-11
Table 4-6	Test Suite Coverage for RCA Benchmarks ^a	4-13
Table 5-1	Summary of Test Suite 1 Results.....	5-1
Table 5-2	Summary of Test Suite 2 Results.....	5-2
Table 5-3	Summary of Test Suite 3 Results.....	5-3
Table 5-4	Summary of Test Suite 4 Results.....	5-4
Table 5-5	Summary of Test Suite 5 Results.....	5-5
Table 5-6	Summary of Test Suite 6 Results.....	5-6
Table 5-7	Summary of Test Suite 7 Results.....	5-7
Table 5-8	Summary of Test Suite 8 Results.....	5-8
Table 5-9	Summary of Test Suite 9 Results.....	5-9
Table 5-10	Summary of Test Suite 10 Results.....	5-10
Table 5-11	Summary of Test Suite 11 Results.....	5-11
Table 5-12	Summary of Test Suite 12 Results.....	5-12
Table 5-13	Summary of Test Suite 13 Results.....	5-13
Table 5-14	Summary of Test Suite 14 Results.....	5-14
Table 5-15	Summary of RCA Results	5-15
Table 6-1	Summary of SCALE Lattice Physics Test Suite Results.....	6-2
Table 6-2	Summary of SCALE RCA Comparisons for Depletion Validation	6-3
Table A-1	Critical Experiment Summary for UOX fuel	A-1
Table A-2	Critical Experiment Summary for MOX fuel	A-1
Table A-3	Critical Experiment Comparison for UOX fuel	A-3
Table A-4	Critical Experiment Comparison for MOX fuel	A-4
Table A-5	Critical Experiment Summary for B&W 1810.....	A-4
Table A-6	Critical Experiment Comparison for B&W 1810.....	A-7
Table A-7	Serpent and CE KENO k_{inf} Comparisons	A-8
Table B-1	Test Suite BWR Assembly Geometries.....	B-1
Table B-2	BWR Standard Case Matrix for Uncontrolled And Controlled Cases	B-2
Table B-3	BWR Standard Case Matrix MG KENO Δk_{inf} (pcm) Statistics.....	B-5

Table B-4	BWR Standard Case Matrix NEWT Δk_{inf} (pcm) Statistics	B-5
Table B-5	BWR Standard Case Matrix Polaris Δk_{inf} (pcm) Statistics	B-6
Table B-6	Test Suite 1: PWR Assembly Geometries	B-16
Table B-7	PWR Standard Case Matrix for Uncontrolled And Controlled Cases	B-16
Table B-8	PWR Standard Case Matrix MG KENO Δk_{inf} (pcm) Statistics	B-20
Table B-9	PWR Standard Case Matrix NEWT Δk_{inf} (pcm) Statistics	B-21
Table B-10	PWR Standard Case Matrix Polaris Δk_{inf} (pcm) Statistics	B-21
Table B-11	Test Suite 2: BWR Case Matrix.....	B-28
Table B-12	Test Suite 2: PWR Case Matrix.....	B-30
Table B-13	Test Suite 3: BWR Case Matrix.....	B-32
Table B-14	BWR 9 × 9-1 Lattice MOX Δk_{inf} (pcm) Statistics	B-34
Table B-15	PWR MOX Δk_{inf} (pcm) Statistics.....	B-41
Table B-16	Test Suite 4: BWR Case Matrix.....	B-44
Table B-17	Test Suite 4: PWR Case Matrix.....	B-45
Table B-18	Test Suite 5: BWR Case Matrix.....	B-47
Table B-19	Test Suite 5: BWR Relative Differences in Major Actinide Concentrations at 8 GWd/MTU.....	B-49
Table B-20	Test Suite 5: BWR Relative Differences in Major Actinide Concentrations at 14 GWd/MTU	B-50
Table B-21	Test Suite 5: PWR Relative Differences in Major Actinide Concentrations at 30 GWd/MTU and 80 GWd/MTU	B-51
Table B-22	Test Suite 6: BWR Case Matrix.....	B-52
Table B-23	Test Suite 6: PWR Case Matrix.....	B-55
Table B-24	Test Suite 7: BWR case matrix	B-59
Table B-25	Test Suite 7: PWR Case Matrix.....	B-63
Table B-26	Test Suite 8: BWR Case Matrix.....	B-66
Table B-27	Test Suite 8: PWR Case Matrix.....	B-67
Table B-28	Test Suite 9: BWR Case Matrix.....	B-69
Table B-29	Test Suite 9: PWR Case Matrix.....	B-72
Table B-31	Test Suite 10: PWR Case Matrix.....	B-82
Table B-32	Test Suite 10: PWR Variations in Number of bp Rods	B-83
Table B-33	Test Suite 11: Cross Section Comparison for GE14 10 × 10 DOM Lattice at 0% Void Fraction.....	B-88
Table B-34	Test Suite 11: Cross Section Comparison for GE14 10 × 10 DOM Lattice at 40% Void Fraction.....	B-89

Table B-35	Test Suite 11: Cross Section Comparison for GE14 10 × 10 DOM Lattice at 70% Void Fraction.....	B-90
Table B-36	Test Suite 11: Cross Section Comparison for GE14 10 × 10 DOM Lattice at 90% Void Fraction.....	B-91
Table B-37	Test Suite 11: Fission Product Yield and Kinetics Parameter Comparison for GE14 10 × 10 DOM Lattice at 0% Void Fraction	B-92
Table B-38	Test Suite 11: Fission Product Yield and Kinetics Parameter Comparison for GE14 10 × 10 DOM Lattice at 40% Void Fraction	B-93
Table B-39	Test Suite 11: Fission Product Yield and Kinetics Parameter Comparison for GE14 10 × 10 DOM Lattice at 70% Void Fraction	B-94
Table B-40	Test Suite 11: Fission Product Yield and Kinetics Parameter Comparison for GE14 10 × 10 DOM Lattice at 90% Void Fraction	B-95
Table B-41	²³⁵ U and ²³⁸ U Kinetics Parameters	B-96
Table B-42	Comparison of Serpent and Polaris for GE14 10 × 10 DOM Lattice at 40% Void Fraction.....	B-96
Table B-43	Test Suite 11: Cross Section Comparison for 17 × 17 WE Lattice.....	B-97
Table B-44	Test Suite 11: Fission Product Yield and Kinetics Parameter Comparison for 17 × 17 WE Lattice	B-98
Table B-45	Test Suite 12: BWR Case Matrix.....	B-99
Table B-46	Test Suite 12: Reflector Cross Section Comparison for GE14 10 × 10 DOM Lattice at 0% Void Fraction	B-101
Table B-47	Test Suite 12: Reflector Cross Section Comparison for GE14 10 × 10 DOM Lattice at 40% Void Fraction	B-102
Table B-48	Test Suite 12: Reflector Cross Section Comparison for GE14 10 × 10 DOM Lattice at 70% Void Fraction	B-103
Table B-49	Test Suite 12: Reflector Cross Section Comparison for GE14 10 × 10 DOM Lattice at 90% Void Fraction	B-104
Table B-50	Test Suite 12: PWR Case Matrix.....	B-105
Table B-51	Test Suite 12: Reflector Cross Section Comparison for 17 × 17 WE Lattice	B-106
Table B-52	Test Suite 13: BWR Numerical Benchmark.....	B-107
Table B-53	Test Suite 13: Relative Differences in Isotopic Concentrations for 0% Void Fraction.....	B-110
Table B-54	Test Suite 13: Relative Differences in Isotopic Concentrations for 40% Void Fraction.....	B-111
Table B-55	Test Suite 13: Relative Differences in Isotopic Concentrations for 70% Void Fraction.....	B-112
Table B-56	Test Suite 13: PWR Numerical Benchmark.....	B-113

Table B-57 EPRI IFBA Depletion Reactivity Benchmark Results..... B-113

Table B-58 Test Suite 14: BWR Case Matrix..... B-114

Table C-1 Selected RCA Samples.....C-1

Table D-1 List of terms used in “Reactor-Lattice-State.Branch.Control.inp” Naming
Convention for 2D Numerical Benchmark Assessment Test Suite Input
Files.....D-7

ACKNOWLEDGMENTS

This document was written under contract with the US Nuclear Regulatory Commission (NRC) Office of Nuclear Regulatory Research. The authors acknowledge NRC project manager Lucas Kyriazidis, NRC staff members Mourad Aissa (fmr.), Don Algama (fmr.), Drew Barto, Peter Yarsky, Andrew Bielen, Scott Krepel, Amrit Patel (fmr.), Nathanael Hudson, Joseph Staudenmeier, and Andrew Ward of the University of Michigan, for their valuable feedback to this work. The authors also thank ORNL staff members: Brian Ade, B. J. Marshall and Germina Ilas for their review of this report; Briana Hiscox and Joseph Burns for simulations supporting Appendix F of the report; and Rose Raney, Kathy Jones, and John Batson for final document preparation.

ABBREVIATIONS AND ACRONYMS

1D	One-Dimensional
2D	Two-Dimensional
3D	Three-Dimensional
Acceptance Accuracy	Minimum Acceptable Accuracy in the Test Results Before Further Methodology and Modeling Improvements are Considered Necessary
Average	$= \frac{\sum_i^N x}{N}$
ADF	Assembly Discontinuity Factor
AIC	Ag-In-Cd
ATWS	Anticipated Transient Without Scram
BC	Boundary Condition
BOC	Beginning of Cycle
BOL	Beginning of Life
BP	Burnable Poison
BPRA	Burnable Poison Rod Assembly
BWR	Boiling Water Reactor
C/E	Ratio of Calculated Value to Expected Value
CE	Combustion Engineering
CE	Continuous Energy
CPU	Central Processing Unit
Controlled Lattice:	Control Rods or Control Blades Are Inserted/Included in the Lattice Geometry
CR	Control Rod
DOM	Dominant Lattice Type
EGBUC	Expert Group on Burn-Up Credit
EGUNF	Expert Group on Used Nuclear Fuel Criticality
ENDF	Evaluated Nuclear Data File
EOC	End of Cycle
EOL	End of Life
EPRI	Electric Power Research Institute
ESC	Extended Step Characteristics
ESSM	Embedded Self-Shielding Method
GE	General Electric
GNF	Global Nuclear Fuel
GT	Guide Tube

HFP	Hot Full Power
HZP	Hot Zero Power
ICSBEP	International Criticality Safety Benchmark Evaluation Project
IFBA	Integral Fuel Absorber
JENDL	Japanese Evaluated Nuclear Data Library
k_{eff}	k eigenvalue (k-effective)
k_{inf}	zero leakage assumption k eigenvalue (k-infinity)
Δk	$(k) - (k_{reference})$
LEU	Low Enriched Uranium
LWR	Light Water Reactor
max	$\max (x_i)$
min	$\min (x_i)$
MC	Monte Carlo
MG	Multigroup
MOC	Method of Characteristics
MOL	Middle of Life
MOX	Mixed Oxide
NAT	Natural Enrichment Blankets
NRC	US Nuclear Regulatory Commission
OEM	Original Equipment Manufacturer
ORIGEN	Oak Ridge Isotope Generation
ORNL	Oak Ridge National Laboratory
PC	Soluble Boron Concentration
pcm	$10^{-5} \Delta k$ (percent mille)
PLE	Plenum Lattice
PWR	Pressurized Water Reactor
PYREX	Borosilicate Glass Burnable Poison
QA	Quality Assurance
QOI	Quantities of Interest
RCA	Radiochemical Assay
RMS	Root Mean Square
	$RMS = \sqrt{\frac{\sum_i^N (x_i)^2}{N}}$
RSICC	Radiation Safety Information Computational Center
σ	Standard Deviation (Sigma)

$$\sigma = \sqrt{\frac{\sum_i^N (x_i - \bar{x})^2}{N-1}}$$

S/U	Sensitivity and Uncertainty
Target Accuracy	Intended Long-Term Accuracy in The Test Results; Test Results that Do Not Satisfy This Accuracy Will Be Considered for Future Methodology Improvements
TC	Coolant Temperature
TDEPL	TRITON/NEWT Depletion
TF	Fuel Temperature
Uncontrolled Lattice	Control Rods or Control Blades are Withdrawn/Removed from the Lattice Geometry
UM	University of Michigan
UOX	Uranium Oxide
VAN	Vanished Lattice
WABA	Wet Annular Burnable Absorber

1 INTRODUCTION AND BACKGROUND

The US Nuclear Regulatory Commission (NRC) relies on the lattice physics analysis capabilities of the SCALE code system [1] to perform confirmatory licensing analyses. Either SCALE lattice physics code—TRITON/NEWT or Polaris—can be used to generate cross section data used by the PARCS nodal core simulator for full-core neutronics calculations. Depending on the type of analysis needed, PARCS [2] may be used as a stand-alone reactor simulator, or it may be coupled to the TRACE [3] reactor system safety analyses code. The results of PARCS stand-alone steady-state simulations or transient simulations are impacted by the quality of the few-group cross section data prepared by SCALE lattice physics calculations.

This report presents an assessment of the accuracy of SCALE lattice physics codes for preparation of PARCS cross section data for light water reactor (LWR) analysis. The underlying basis for this work is to compare SCALE's lattice physics methods in TRITON/NEWT and Polaris to the methods used in SCALE's KENO continuous energy (CE) Monte Carlo (MC) code capability to understand the impact of using multigroup cross sections and geometry approximations.

Due to the nature of lattice physics calculations, critical reactor experiment benchmarks cannot be modeled in explicit detail in a lattice physics code. Therefore, either geometry approximations or axial buckling must be implemented to determine the critical water height. These modeling limitations have led to development of a three-phase assessment strategy.

In the first phase, selected critical experiment benchmarks are modeled using the SCALE 3D CE MC code KENO. CE KENO is the most rigorous neutron transport method available in SCALE 6.2, with no calculational approximations in the spatial, angle, or energy treatments. Biases and statistical uncertainties in calculated quantities of interest (QOIs) such as k_{eff} and pin power distributions are determined by comparing CE KENO results to experimental data. This first phase in the accuracy assessment is to demonstrate and establish the use of CE KENO as a reference solution for the second phase.

For the second phase, 14 numerical test suites are used to compare SCALE lattice physics calculations with CE KENO as a reference solution:

1. LWR assemblies' beginning of life (BOL) baseline
2. Control elements
3. Mixed oxide (MOX) fuel
4. Reactivity worth of depleted fuel
5. Depletion calculations
6. Boron injection
7. Enrichment
8. Fuel temperature
9. Burnable poison (BP) loading
10. BP spatial variations
11. PARCS QOIs parameters
12. Fuel reflector models
13. International benchmarks
14. Boiling water reactor (BWR) vanished zone patterns

In the third phase, SCALE lattice physics depletion calculations are performed, and the spent fuel isotopic results are compared with available radiochemical assay (RCA) measurements. Comparison of the RCA measurement data with the corresponding calculated data provides a measure of the accuracy in predicting isotopic concentrations with the depletion models in SCALE physics codes.

This report is organized as follows. Section 2 describes the two-step reactor core calculation procedure. Section 3 summarizes the methods and calculational details for the SCALE lattice physics codes and CE KENO. Section 4 presents the 14 test suites developed for this assessment. Section 5 presents concise lattice physics test results for each test suite, and conclusions are provided in Section 6. Finally, the appendices provide (A) CE KENO 3D critical experiment results, (B) detailed code-to-code comparisons for the 14 test suites, and (C) RCA experiment isotopic benchmark comparisons.

2 TWO-STEP REACTOR CORE SIMULATION

Two-step reactor core simulation refers to the procedure of lattice physics calculations (step 1) used to generate cross section data for reactor core calculations (step 2). As shown in Figure 2-1, the two types of lattice physics calculations are *fuel calculations* and *reflector calculations*, both of which model a 2D slice of a reactor's fuel assembly with the boundary conditions (BCs) shown. Fuel-based lattice physics calculations model a 2D radial (x-y) slice of a fuel assembly. For this reason, multiassembly models are not considered in this report, and the transport geometry is assumed to be infinite in the axial direction with reflective radial boundary conditions. Cross section data for the fuel assembly are computed based on the 2D neutron transport and depletion calculations. Reflector-based lattice physics calculations model a 2D lattice adjacent to a reflector region, which is modeled as a set of slab material zones.

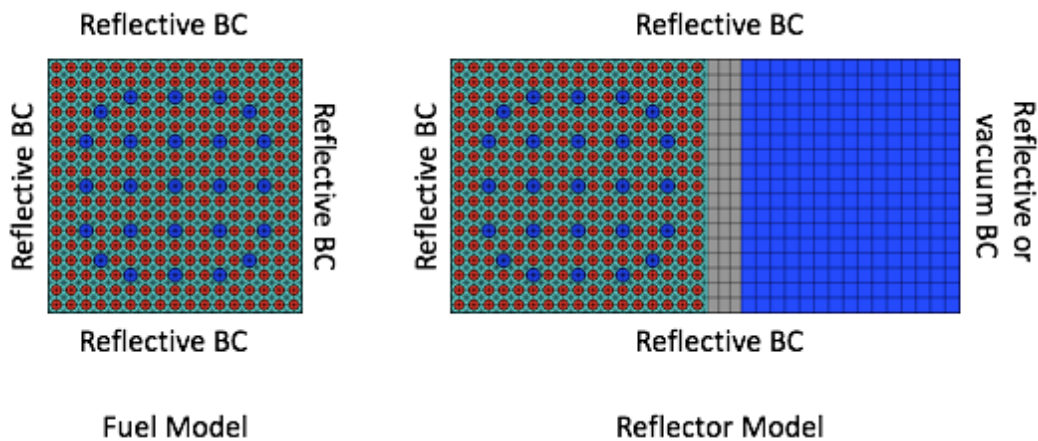


Figure 2-1 Fuel and Reflector Lattice Geometry Configurations

As mentioned above, the PARCS reactor simulations depend on the quality of the cross section data computed by lattice physics calculations. Cross sections are generally described as the probability of interaction of a target of interest such as a nuclide and a projectile of interest such as a neutron. The processes for evaluating cross sections at different computational levels in the two-step approach are shown in Figure 2-2.

In the first column of Figure 2-2, cross sections are measured, evaluated, and tabulated into nuclear data files. Evaluated nuclear data files (ENDFs) are processed into library formats used by downstream neutron transport calculations. ENDF/B-VII.1 nuclear data files are the basis for all SCALE calculations in this report. For SCALE, the AMPX code system is used to prepare SCALE cross section libraries from the ENDF/B data. The SCALE lattice physics codes TRITON/NEWT and Polaris use the SCALE cross section libraries to generate lattice physics cross section data in T16 file format. GenPMAXS, an interface code developed by the PARCS code developers at the University of Michigan (UM), is used to convert the lattice physics cross section data into the appropriate PMAXS format for PARCS.

To establish the quality of PARCS core simulations, the following aspects should be considered regarding the process outlined in Figure 2-2:

- The uncertainty or biases associated with cross section data measurements,
- The approximations and assumptions made by each computational process,
- The two-step approximation for reactor simulation, and
- The code verification and quality assurance (QA) of the following computational processes:
 - Evaluation,
 - AMPX processing,
 - SCALE lattice physics,
 - GenPMAXS conversion, and
 - PARCS core simulations.

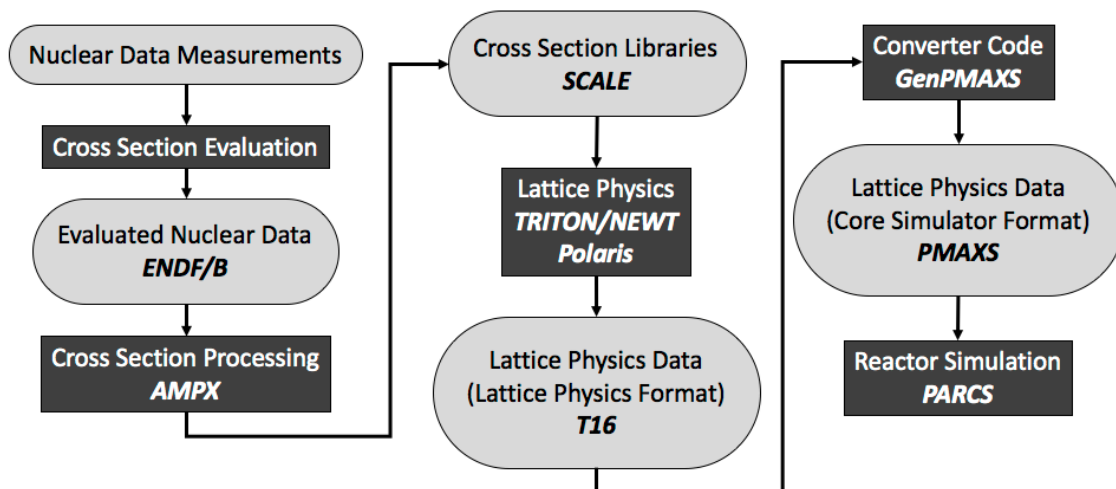


Figure 2-2 Cross Section Evaluation for Two-Step Calculations

This report focuses on assessment of the performance of the SCALE lattice physics codes, TRITON/NEWT and Polaris, as part of this process. This report does not address propagation of uncertainties and biases throughout the computational process. It also does not address two-step approximation for reactor core simulation, code verification, and QA of each code. Descriptions of the codes used in this work and the approximations and assumptions made by them are discussed in Section 3.

The SCALE computer code system is distributed through ORNL's Radiation Safety Information Computational Center (RSICC), and the QA program is available on the SCALE public website. SCALE is compliant with ISO-9001-2008, US Department of Energy Order 414.1D, NRC NUREG/BR-0167, and the ORNL Standards-Based Management System. SCALE 6.2 was released in April 2016 and is the official version of SCALE used for this report. Two micro updates were deployed for SCALE 6.2 in 2016-2017: SCALE 6.2.1 in July 2016, and SCALE 6.2.2 in May 2017. SCALE 6.2 rev19189 (pre-release of 6.2.1) was used for CE KENO,

TRITON/NEWT and Polaris (PWR only) calculations. SCALE 6.2.2 was used for Polaris BWR calculations to address several updates in support of BWR lattice geometries. AMPX ENDF/B-VII.1 CE and 252 group libraries were used for CE and multigroup (MG) calculations, respectively. As of 2014, the AMPX code system was developed in compliance with the SCALE QA plan and was released with SCALE 6.2 in April 2016. This 6.2 version of AMPX was used to generate the ENDF/B-VII.1 libraries deployed in SCALE 6.2.

3 SCALE CODE DESCRIPTIONS AND MAJOR ASSUMPTIONS

The SCALE codes used in this assessment are described briefly below, along with the major assumptions and approximations.

3.1 KENO

The KENO MC code performs 3D eigenvalue neutronics calculations. KENO-VI uses the SCALE Generalized Geometry Package, which provides a quadratic-based geometry system with flexibility in problem modeling. KENO performs eigenvalue calculations for neutron transport primarily to calculate multiplication factors (k_{eff}) and flux distributions of fissile systems in both CE and multigroup (MG) modes. CE KENO is the most rigorous method available in SCALE 6.2 for neutron transport, with no approximations made in the spatial, angle, and energy treatments. CE KENO (SCALE 6.2.1) was used for all reference calculations in this code assessment.

Major assumptions or approximations of CE KENO are as follows:

- A sufficient number of particles is used to ensure small MC uncertainty in QOIs.
- The source is appropriately converged.
- The correlation between generations of random particles is leading to non-conservative estimates of the MC uncertainty.

3.2 TRITON/NEWT

The TRITON computer code is a multipurpose SCALE control module for transport, depletion, and sensitivity and uncertainty (S/U) analysis. TRITON can be used to provide automated, problem-dependent cross section processing followed by MG transport calculations for 1D, 2D, and 3D configurations. This functionality can also be used in tandem with the Oak Ridge Isotope Generation (ORIGEN) depletion module to predict isotopic concentrations, source terms, and decay heat and to generate few-group homogenized cross sections for nodal core calculations. TRITON provides the capability to perform deterministic transport analysis for 1D geometries using XSDRNPM and for 2D geometries using NEWT. TRITON also includes 3D MC depletion capabilities using KENO V.a and KENO-VI. For MC depletion calculations, TRITON supports both MG and CE options.

Detailed descriptions of the methods and calculational approach for TRITON and NEWT are provided by DeHart and Bowman [4]. The TRITON/NEWT depletion sequence (TDEPL) shown in Figure 3-1 is designed to perform 2D lattice physics calculations. This sequence was tested extensively in this assessment. In addition, the TRITON/KENO-VI depletion sequence (T-DEPL6) was used to perform reference depletion calculations with MG and CE KENO. All TRITON calculations documented in this report were performed with SCALE 6.2.1.

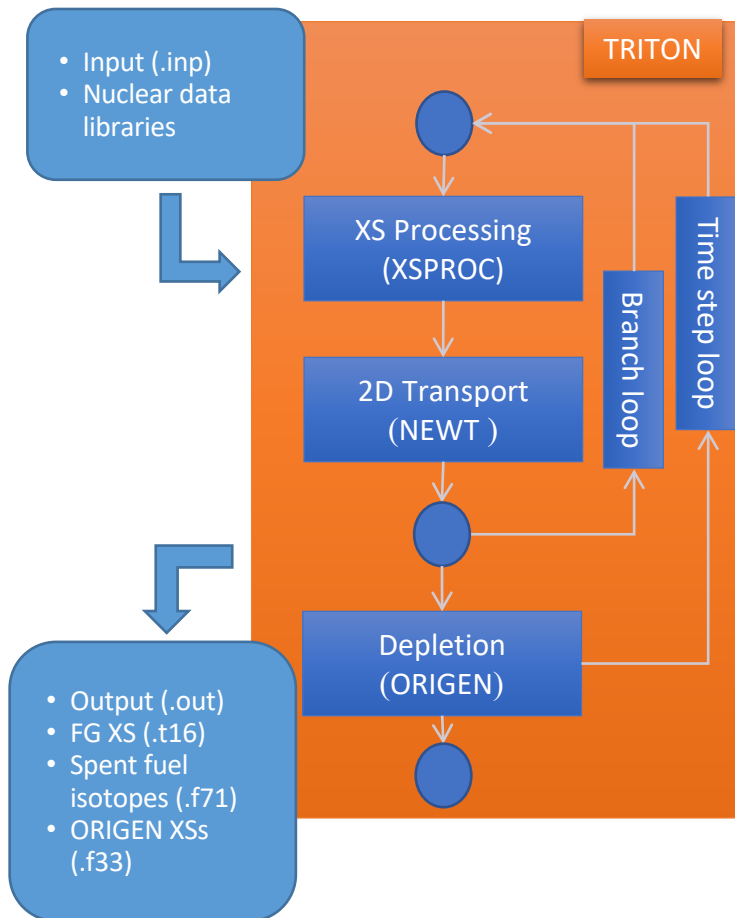


Figure 3-1 TRITON/NEWT Lattice Physics Calculation Flow

The TRITON/NEWT lattice physics capability is based on MG neutron transport coupled with the ORIGEN depletion/decay module for time-dependent transmutation of depletion materials. Resonance self-shielding calculations are performed for each defined unit cell. TRITON currently supports three self-shielding methods [1]:

- The equivalence-theory Bondarenko method,
- The pointwise slowing down calculation (resolved-resonance range only), and
- The double-heterogeneous method for TRISO-particle compositions (not applicable to LWR fuel).

The transport calculation is performed with NEWT, which uses discrete ordinate angle treatment and the extended step characteristic (ESC) method for spatial treatment. The ESC implementation in NEWT requires that the region boundaries within the transport geometry must be straight line segments, so a curved surface must be approximated by a polygon.

The major assumptions or approximations of TRITON/NEWT include [1]

- MG approximation: MG energy structure, thermal upscattering cutoff energy (5 eV), and flux weighting spectrum all impact the accuracy in the QOI calculation
- The equivalence-theory Bondarenko unit cell approximation:
 - Neglects resonance interference phenomena between resonance-absorbing nuclides in a given material.
 - Does not consider intra-pin self-shielding effects for strong-absorbing materials.
 - Assumes that spatial self-shielding effects by neighboring pin cells, guide tubes, water rods, or assembly structures may be approximated by a Dancoff factor.
- The pointwise slowing down unit cell calculation:
 - Provides rigorous spatial and energy resolution for the transport calculation within the unit cell.
 - Is limited to s-wave scattering treatment in the current implementation.
 - Includes a unit cell approximation that implies that the self-shielding effects from neighboring cells, guide tubes, water rods, or assembly structures are captured via the appropriate definition of a buffer region surrounding the unit cell.
- The discrete ordinate angle approximation:
 - Includes an angular flux which is determined over a discrete set of angles.
 - Requires that the user select an appropriate quadrature set to resolve the angular flux distribution because NEWT currently employs level-symmetric quadrature sets or product-quadrature sets with Gauss-Legendre quadratures for the polar angle.
- The ESC spatial discretization: assumes a constant flux over each spatial region in the geometry, so the spatial mesh must be appropriately selected so that the flux variation is very small over each volumetric region.

3.3 Polaris

Polaris is a module in SCALE 6.2 that provides 2D lattice physics analysis capability designed for LWR fuel designs. A detailed description of the methods and calculational approach of Polaris is provided by Jessee et al. [5]. As in TRITON/NEWT, the Polaris lattice physics capability is based on MG neutron transport coupled with the ORIGEN depletion/decay module for time-dependent transmutation of depletion materials. The major differences between Polaris and TRITON/NEWT lie in the resonance self-shielding and transport methods. Polaris employs the embedded self-shielding method (ESSM) for resonance self-shielding [6]. ESSM is similar to the subgroup method in that it is a global self-shielding method: the slowing-down and self-shielding effects of neighboring fuel pins, guide tubes, water rods, and assembly structures are accounted for in the calculation. For the transport calculation, Polaris employs the method of characteristics (MOC), which is sometimes referred to as *long characteristics*. MOC solves the characteristic transport equation over a set of equally spaced particle tracks across the lattice geometry. Polaris provides an easy-to-use input format allowing users to set up lattice models with a minimal amount of input.

Polaris was tested extensively in this assessment. The Polaris calculation flow is shown in Figure 3-2. All Polaris pressurized water reactor (PWR) calculations documented in this report were performed with SCALE 6.2.1, and all Polaris BWR calculations were performed with SCALE 6.2.2 since it is the first version that contained complete BWR modeling capabilities.

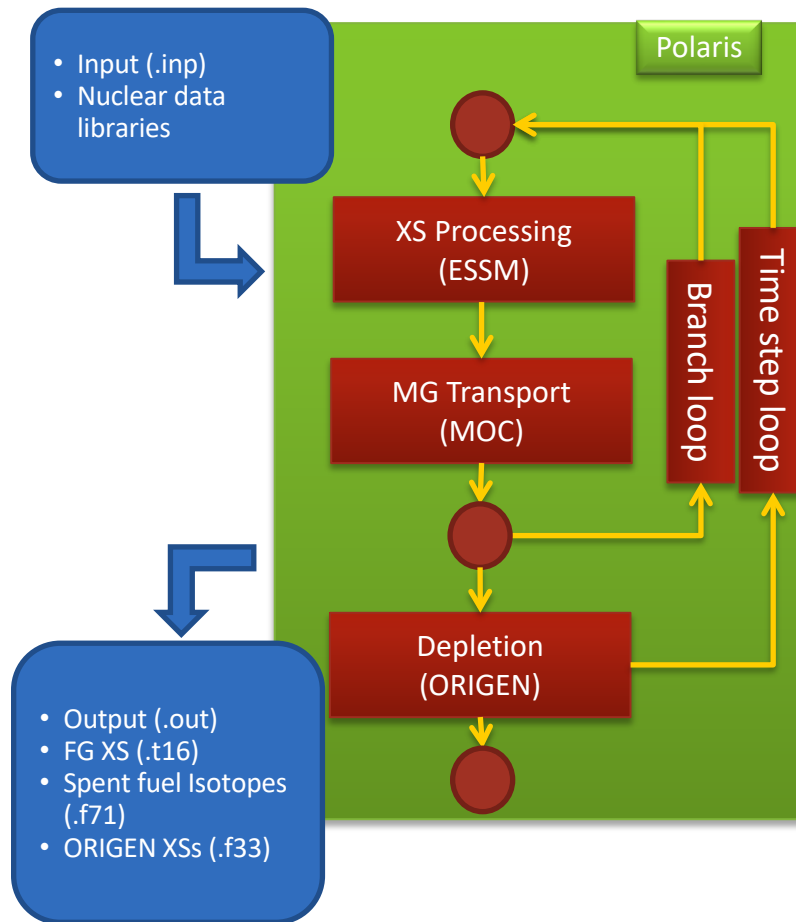


Figure 3-2 Polaris Lattice Physics Calculation Flow

The major assumptions or approximations of Polaris include [1]:

- The MG approximation: the MG energy structure, the thermal upscattering cutoff energy (5 eV), and the flux weighting spectrum all impact the accuracy in QOI calculation.
- The ESSM approximation:
 - Neglects resonance interference phenomena between resonance-absorbing nuclides in a given material.
 - Can conceptually model intra-pin self-shielding effects and temperature distributions, but the approximations currently employed require further investigation.
- The discrete ordinate angle approximation:
 - Has an angular flux that is determined over a discrete set of angles.
 - Employs a set of optimized quadrature sets for 2D MOC calculations in Polaris.
- The MOC spatial discretization:
 - Assumes a constant flux over each spatial region in the geometry, so this assumption requires that the spatial mesh must be appropriately selected so the scatter/fission source is very small over each volumetric region.
 - Requires that spacing between the characteristic particle tracks be appropriately selected so that the volumetric flux in each spatial region is accurate.

3.4 **ORIGEN**

The Oak Ridge Isotope Generation (ORIGEN) code calculates time-dependent concentrations, activities, and radiation source terms for a large number of isotopes simultaneously generated or depleted by neutron transmutation, fission, and radioactive decay. ORIGEN is used internally within SCALE's TRITON and Polaris sequences to perform depletion and decay.

The major assumptions or approximations in the ORIGEN depletion coupling in TRITON and Polaris are presented below:

- The size and number of depletion steps is appropriate for the midpoint depletion scheme employed in TRITON and the predictor-corrector scheme in Polaris. The depletion step size is tested in the depletion calculations of test suite 5.
- In CE KENO depletion, the propagation of MC uncertainties through the depletion calculation is small and can be neglected.

4 CODE ASSESSMENT TESTING

The goal in this work is to determine the degree to which TRITON/NEWT or Polaris is an accurate representation of a 2D assembly model with reflective boundary conditions. In this context, the code assessment includes assessing the quality of the nuclear data for 2D assembly calculations and substantiating the calculational methods employed in SCALE outlined in the previous section.

Because available critical reactor experiment benchmarks cannot be modeled with TRITON/NEWT or Polaris directly, a three-phase approach will be used to assess the prediction of QOIs.

In the first phase, selected critical experiments will be modeled using the CE KENO 3D MC code. Biases and statistical uncertainties in k_{eff} , and pin power distributions will be determined for the CE KENO calculations by comparing CE KENO results to experimental data. The critical benchmark experiments to be used are primarily from the *International Handbook of Evaluated Criticality Safety Benchmark Experiments* (International Criticality Safety Benchmark Evaluation Project [ICSBE]) [7] and the *International Handbook of Evaluated Reactor Physics Benchmark Experiments* (IRPhE) [8]. The selection of representative benchmark experiments, as documented in Appendix A, should translate the modeling accuracy of the benchmark experiments to the modeling accuracy of 2D assembly calculations. This phase is hereafter referred to as *CE KENO lattice calculations accuracy assessment* in this report and is primarily focused on assessing the quality of nuclear data and the accuracy of MC physics methods for assembly calculations.

In the second phase, CE KENO, TRITON/NEWT, and Polaris assembly models will be generated for a large set of test problems. The CE KENO result for each assembly model will be used as the reference solution to establish bias and uncertainties in the TRITON and Polaris calculations. A large set of assembly test problems for 14 test suites has been defined based on the intended range of applications. This phase is hereafter referred to as *2D numerical benchmark assessment* in this report, and it primarily substantiates the use of the self-shielding and transport methods employed in TRITON/NEWT and Polaris, the MG energy treatment, and the selection of group structure.

In the third phase, the isotopic predictions from Polaris and TRITON/NEWT depletion calculations will be compared to available RCA measurements. The measured isotopic density distributions of the fuel samples will be compared with isotopic density distributions calculated from Polaris and TRITON/NEWT depletion calculations. In addition, TRITON/NEWT and Polaris calculations will be benchmarked using applicable mixed oxide (MOX) and uranium oxide (UOX) fuel international numerical benchmarks for neutronic parameters and depletion calculations. The numerical benchmark results will provide an opportunity to compare TRITON/NEWT and Polaris results to well-recognized lattice physics code results.

4.1 Parametric Studies

Results of parametric studies are used to establish an optimum set of input parameters for CE KENO (number of particles/generation, number of active/inactive generations), NEWT (quadrature set, grid spacing), and Polaris (quadrature set, ray spacing, number of rings and sectors) models.

CE KENO pin power calculations parametric study:

A short study shows that based on a PWR CE 14 × 14 geometry, MC parameters set to 400,000 particles/generation, 2,500 active generations with 250 inactive generations produce a converged pin power distribution. Table 4-1 shows comparison of pin power distribution statistics with respect to the reference distribution for variations in the CE KENO MC parameters. Final CE KENO input parameters selected for the code assessment are provided in Table 4-4.

Table 4-1 Effect of CE KENO Parameters on Pin Power Distribution Statistics

CE KENO parameters			Pin power statistics (%)		
Active generations	Inactive generations	Particles/generation	Max	Mean	Root mean square (RMS)
2,500	250	400,000	0	0	0
2,500	250	10,000	0.41	0.084	0.113
2,500	250	50,000	0.16	0.035	0.047
2,500	250	100,000	0.09	0.024	0.034
2,500	250	200,000	0.08	0.031	0.037
2,500	250	300,000	0.09	0.038	0.038
750	250	400,000	0.08	0.015	0.026
500	500	400,000	0.09	0.027	0.036
1,750	250	400,000	0.04	0.007	0.015
1,500	500	400,000	0.10	0.023	0.033

NEWT calculations parametric study:

NEWT spatial mesh refinements are performed in two steps. In the first step, the number of polygon faces approximating the guide tube (GT) circles is increased. In the second step, the same refinement is implemented for the fuel rod geometries. Following the same steps, spatial grids used in unit cell definitions are refined. Table 4-2 shows some of the tested mesh refinement, angle quadrature, and scattering order studies for the NEWT geometry. Final NEWT input parameters selected for the code assessment are provided in Table 4-4.

Polaris calculations parametric study:

Spatial meshes were refined by increasing the number of material rings and the number of sectors in fuel, burnable absorbers, and GT regions. Uniform and material-dependent refinements and rotational (non-aligning) sector configurations were also tested. The resolution of the MOC solution was increased by decreasing ray spacing and increasing the number of azimuthal and polar angles. Different combinations of ray spacing, different numbers of angles, and different scattering orders were tested. In this study, the smallest ray spacing was 0.003 cm, the largest number of azimuthal angles was 32, and the largest number of polar angles was 4. Table 4-3 shows some of the tested configurations. Final Polaris input parameters selected for the code assessment are provided in Table 4-4.

Table 4-2 Change in Unrodded k_{eff} with NEWT Input Parameters

Parameters	k_{eff}	k(pcm)
CE KENO reference	1.25751	0
$P_n^a = 1$ $S_n^b = 6$ Sides = 12 Grid ^c = 4 × 4 (base)	1.25696	55
Grid(GT ^d) = 8 × 8	1.25692	59
Sides ^e (GT) = 40	1.25697	54
Grid = 8 × 8	1.25612	139
Grid = 16 × 16	1.25590	161
$S_n = 16$	1.25742	9
$S_n = 10$	1.25726	25
$P_n(\text{Fuel}^f) = 2$	1.25697	54
$P_n(\text{Moderator}^f) = 3$	1.25689	62
Grid = 8 × 8 $S_n = 16$	1.25672	79
Grid = 16 × 16 $S_n = 16$	1.25650	101
Grid = 16 × 16 $S_n = 16$ Sides = 20	1.25669	82
Grid = 16 × 16 $S_n = 16$ Sides = 40	1.25668	83

^a = P_n : scattering order

^b = S_n : angle quadrature

^c = Grid: unit grid used in geometry

^d = GT: applies only to guide tube

^e = Sides: number of polygon sides for approximating circular geometries

^f = Fuel: applies only to fuel

Table 4-3 Change in Unrodded k_{eff} with Polaris Input Parameters

Parameters	k_{eff}	k (pcm)
CE KENO reference	1.25751	0
MOC ^a ($\omega^b = 0.08$ $\theta^c = 16$ $\phi^d=2$) ESSM ^e ($\omega = 0.02$ $\theta = 3$ $\phi = 2$) Pn = 0	1.25664	87
MOC($\phi = 3$)	1.25682	69
MOC($\theta = 32$)	1.25725	26
MOC($\omega = 0.01$)	1.25682	69
MOC($\omega = 0.01$ $\theta = 32$ $\phi = 3$)	1.25741	10
MOC($\omega = 0.01$ $\theta = 32$ $\phi = 3$) ESSM($\omega = 0.01$)	1.25741	10
MOC($\omega = 0.01$ $\theta = 32$ $\phi = 3$) ESSM($\omega = 0.01$) GT ^f (3-1-1,8-16-24)	1.25711	40
MOC($\omega = 0.01$ $\theta = 32$ $\phi = 3$) ESSM($\omega = 0.01$) Pn = 2	1.25646	105
MOC($\omega = 0.01$ $\theta = 32$ $\phi = 3$) ESSM($\omega = 0.01$) Pn = 3	1.25636	115
MOC($\omega = 0.04$ $\theta = 32$ $\phi = 3$) ESSM($\omega = 0.01$) Pn=2	1.25646	105
MOC($\omega = 0.04$ $\theta = 20$ $\phi = 3$) ESSM($\omega = 0.01$) Pn = 2	1.25636	115
MOC($\omega = 0.04$ $\theta = 20$ $\phi = 3$) ESSM($\omega = 0.02$) Pn = 2	1.25636	115
MOC($\omega = 0.04$ $\theta = 20$ $\phi = 3$) ESSM($\omega = 0.01$) Pn = 2	1.25639	112
MOC($\omega = 0.01$ $\theta = 32$ $\phi = 3$) GT(1-1-1,16-16-16) Fuel ^g (1-1-1-1,16-16-16-16) Pn = 3	1.25625	126
MOC($\omega = 0.01$ $\theta = 32$ $\phi = 3$) GT(3-1-2,16-16-16) Fuel(3-1-1-2,16-16-16-16) Pn = 3	1.25644	107

^a = MOC: MOC solver parameters

^b = ω : ray spacing

^c = θ : number of azimuthal angles

^d = ϕ : number of polar angles

^e = ESSM: ESSM cross section processing solver parameters

^f = GT: Number of rings and sectors in each material region of GT cell

^g = Fuel: Number of rings and sectors in each material region of fuel cell

Solution Parameters:

Considering the individual contribution of each solution parameter to QOI (eigenvalue and pin powers) and CPU time, a set of optimum solution parameters is selected. Any attempt to increase solution resolution beyond its default value results in considerable increase to the run time. Therefore, input parameter changes that impact the calculated k_{eff} less than 20 pcm are ignored. Table 4-4 shows the solution parameters used in testing for CE KENO, NEWT, and Polaris. Step sizes for depletion calculations are selected based on the accuracy of the TRITON midpoint depletion algorithm, although Polaris allows larger depletion steps due to a higher order predictor-corrector scheme.

Table 4-4 SCALE Solution Parameters Used in Testing

Code	Problem Type	Solution Parameters
CE KENO	k_{inf}	Particles/generation: 10,000 Active generations: (until converged in 10 pcm) Inactive generations: 500
CE KENO	pin power	Particles/generation: 100,000 Active generations: 1,000 Inactive generations: 500
NEWT	IFBA lattice	Grid = 8×8 Sides ^a = 50, Sn = 16 for IFBA loaded lattices
NEWT	All others	Grid = 8×8 Sides ^a = 20 Sn = 16 for all others
Polaris	IFBA lattice	MOC ^b ($\omega^c = 0.003$ $\theta^d = 20$ $\phi^e = 3$) ESSM ^f ($\omega = 0.02$) for IFBA loaded lattices
Polaris	All others	MOC($\omega = 0.04$ $\theta = 20$ $\phi = 3$) ESSM ^f ($\omega = 0.02$) for all others (Default)
ALL	Depletion	0.25 GWd/MTU steps until burnable absorber is depleted

^a = Sides: number of polygon sides for approximating circular geometries

^b = MOC: MOC solver parameters

^c = ω : ray spacing

^d = θ : number of azimuthal angles

^e = ϕ : number of polar angles

^f = ESSM: ESSM cross section processing solver parameters

Coverage

To assess the quality of SCALE lattice physics calculations, a wide range of operating conditions and assembly designs were selected to cover past and current commercial PWRs and BWRs. The coverage is defined based on the intended application of SCALE lattice physics codes for LWR core analysis with PARCS. The application range and features are specified in terms of assembly design parameters and are provided below.

Geometry:

The code assessment is performed for available commercial PWR and BWR assembly geometries. The BWR assemblies include General Electric (GE), Global Nuclear Fuel (GNF), Areva (ATRIUM), and Westinghouse (SVEA) fuel designs. The PWR assemblies include Westinghouse Electric Company (WE) and Combustion Engineering (CE) fuel designs.

BWR

1. 8×8
 - a. Two small water rods (GE5)
 - b. One large water rod (GE8, GE9, GE10)

2. 9 × 9
 - a. Two water rods (GE13)
 - b. One large water rod (GNF-step3)
 - c. Centered water box (ATRIUM9)

3. 10 × 10
 - a. Two water rods (GE12, GE14, GNF1)
 - b. Off-centered water box (ATRIUM10)
 - c. Water diamond and wings (SVEA96-Optima2)

PWR

1. 14 × 14 WE (small guide tubes)
2. 15 × 15 WE
3. 16 × 16 CE (large guide tubes)
4. 17 × 17
 - a. Standard WE
 - b. Optimized fuel assembly (OFA) WE
5. 18 × 18 WE

The majority of the assembly geometries listed above is covered in 2D numerical benchmark validations. The remaining older designs are included in the RCA measurement validations.

For the design features and operating conditions covered in the test suites below, GE14 10 × 10, WE standard 17 × 17, and WE 15 × 15 (MOX fuel only) are selected as the nominal assembly geometries because they are the most common and recent assembly designs.

Enrichment:

Assembly designs with ²³⁵U enrichments ranging from 0.71–10 wt% are included. For PWR UOX assemblies, the nominal ²³⁵U enrichment selected is 3.1 wt%. For the BWR UOX assembly, the nominal design used is GE14 10 × 10 with an enrichment pattern [9] of 2.3–4.95 wt%. Zone patterns for other BWR assemblies [10,11] are adapted from the GE14 10 × 10 design.

MOX assemblies include recycled fuel and weapons-grade plutonium vectors with 59.7–93.6 wt % ²³⁹Pu. MOX enrichment zones for BWR and PWR assemblies are obtained from available designs [12,13].

Boron Concentration:

Soluble boron concentrations of up to 2,500 ppm for PWR are modeled. A boron concentration of 1,300 ppm natural boron is used as the nominal value for PWR assemblies because it represents a typical beginning of cycle (BOC) hot full power (HFP) concentration.

Accident conditions (anticipated transient without scram [ATWS]) for BWR are also covered by using boron concentrations up to 2,000 ppm at cold and hot zero power (HZP) conditions. This approach is conservative for testing the most reactive conditions with high density coolant and low temperature fuel.

Burnable Poisons:

Both integral and discrete burnable poison (BP) types are included. For BWRs, only integral gadolinia-loaded fuel with gadolinia loadings ranging from 0–10% Gd_2O_3 are considered, because it is the BP type commonly used. For PWRs, all BP types listed below are considered.

- 1. Gadolinia (Gd_2O_3):**
 - 0–10 wt % natural gadolinia
 - 4- and 12-rod patterns
- 2. Wet annular burnable absorber (WABA):**
 - 14.0 wt% B_4C content in an Al_2O_3 - B_4C mixture
- 3. Burnable poison rod assembly (BPRA):**
 - 1 g/cm³, 2 g/cm³ and 4 g/cm³ B_4C densities
 - 4-, 12-, and 24-rod patterns
- 4. Borosilicate glass (PYREX):**
 - 12.5 wt% B_2O_3 content
 - 4-, 12-, and 24-rod patterns
- 5. Integral fuel absorber (IFBA):**
 - 1.5 and 4 mg ¹⁰B/inch boron loadings with 3.1 wt % ²³⁵U
 - 80-, 104-, and 120-rod patterns with 3.1 wt% ²³⁵U enrichment

Fuel Temperature:

Fuel temperatures ranging from 293–3,000 K are included. A nominal fuel temperature of 900 K is selected at hot fuel conditions for PWR assembly models, and 950 K is selected for BWR assembly models.

Burnup:

The average assembly burnup range extends to 80 GWd/MTU of depleted fuel, which is beyond the highest reported commercial LWR fuel assembly in the United States.

Moderator Density:

Moderator densities range from 0–90% void fraction for BWR assemblies at HFP conditions. Moderator densities for 293 K cold and 560 K HZP conditions are also modeled. Moderator densities corresponding to moderator temperatures ranging from 293–600 K are included for PWR assemblies.

Control Rod/Control Blade Types:

The tested fuel assembly control element models include the following control rod types for PWR assemblies:

1. Ag-In-Cd (AIC)
2. B_4C
3. Inconel absorber

The following control blade types are used for BWR assemblies:

1. Standard original equipment manufacturer (OEM, B₄C)
2. Marathon
3. Standard OEM (hafnium)

Other Features:

The following modeling options are also tested using the nominal assembly designs:

1. Fuel/reflector cross section calculations
2. Time-dependent changes to operating conditions for RCA benchmarks

4.2 2D Numerical Benchmark Test Suites

As described above in Section 4.1, a range of assembly designs with different fuel loadings and operating conditions are tested for the accuracy assessment of the TRITON/NEWT and Polaris lattice physics calculations. Except for the depletion test suites, all tests are performed with fresh fuel or with depleted fuel isotopics calculated by TRITON/NEWT depletion calculations. Unless stated otherwise, k_{inf} and pin power distributions—relative fission rate distributions—are compared to the reference CE KENO values. All CE KENO k_{inf} calculations are converged to a maximum of 10 pcm uncertainty. Pin power uncertainties vary based on the lattice design and test suite. Statistics for pin power uncertainties are provided, along with pin power comparisons.

In addition to Polaris and TRITON/NEWT (hereafter referred as NEWT), MG KENO results are also included in code-to-code comparisons to provide insight about the accuracy of the TRITON MG cross section processing and the transport solution. Since MG KENO shares the same cross sections with NEWT and the same transport solver with CE KENO, it allows the contribution of the cross section library and the transport solver to be separated based on the differences seen in the results. As in the CE KENO calculations, MG KENO k_{inf} calculations are converged to 10 pcm maximum uncertainty.

The success of each test is determined by acceptance accuracy and target accuracy for each QOI. **Acceptance accuracy** is the maximum acceptable difference between the reference and the calculated QOIs. A test would be declared failed if the difference exceeds this determined value. Each failed case will be investigated in detail, and if necessary, modeling and methodology improvements will be considered. **Target accuracy** is the desired accuracy between the reference and the calculated values to ensure that SCALE codes meet or exceed the accuracy of state-of-the-art lattice physics codes. If a test result passes the acceptance accuracy test but does not meet the target accuracy, it will be included in future code development plans.

Acceptance accuracy and target accuracy criteria are selected based on a review of licensing topical reports, published papers of industry standard codes, and personal communications with experts [14,15,16,17,18]. The primary QOIs under investigation are k_{inf} and pin power. The k_{inf} comparisons provide insight on the prediction of the global reactivity of the lattice configuration. Pin power comparisons provide insight on the prediction of the local power and flux distributions within the lattice.

The target and acceptance accuracy for k_{inf} and pin power distribution are determined as follows:

k_{inf} and pin power target accuracy:

- BWR:
 - 200 pcm difference in k_{inf}
 - 1% RMS difference in pin power distribution
 - 1.5% maximum difference in pin power distribution
- PWR:
 - 200 pcm difference in k_{inf}
 - 0.5% RMS difference in pin power distribution
 - 1.5% maximum difference in pin power distribution

k_{inf} and pin power acceptance accuracy:

- BWR and PWR:
 - 400 pcm difference in k_{inf}
 - 1.5% RMS difference in pin power distribution
 - 2.5% maximum difference in pin power distribution

It is also important to assess the few-group cross sections used in the full-core PARCS analysis. The few-group cross sections are post-processed from the multigroup cross sections and flux distributions within the lattice. Therefore, errors in k_{inf} and pin powers may suggest that there are errors in the few-group cross sections. However, post-processing edits such as transport cross sections, kinetics parameters, and fission product yields are influenced by nuclear data that are independent of the neutronics calculation.

Because CE KENO was designed as a criticality safety analysis code, it is not capable of generating lattice physics parameters required by core simulator codes. There are current SCALE development efforts to replace KENO with the Shift MC code [19] to provide the depletion capabilities and the data output necessary for lattice physics calculations. The Serpent MC code [20] is used to compare and assess NEWT and Polaris calculations of few-group cross section QOIs, given its capabilities of generating few-group cross sections as function of depletion. Note that Serpent uses ENDF/B-VII nuclear data generated by NJOY, which will contribute to small differences in results.

If sensitivities of core QOIs (e.g., k_{eff} , peak pin power) to few-group cross sections are known, acceptance criteria for few-group cross sections can be determined based on the acceptable biases in core QOIs. However, calculation of these sensitivities is not straightforward. Moreover, these sensitivities will differ based on spatial location of the lattice in the core (3D), burnup, state of the core, control rod patterns, and core loadings. Sensitivity analysis (adjoint, stochastic, and parametric) will require additional efforts and will be part of the next phase in the accuracy assessment task.

However, based on previously set acceptance criteria for k_{inf} two accuracy criteria are applied for these calculations, as described in the following paragraphs.

For the first criterion, the nu-fission, absorption, and scattering cross sections can be used to compute the 4-factor formula for k_{inf} and the fast-to-thermal flux ratio. The 4-factor formula is appropriate for use in this study, as the lattice physics problems are infinite medium problems. The 4-factor formula provides an additional set of quantitative metrics for global reactivity balance with respect to the fast and thermal neutron groups. For the purposes of this report, the

target and acceptance accuracy for k_{inf} is applied to each term of the 4-factor formula to identify cancellation of errors among fast and thermal cross sections.

In the second criterion, target and acceptance accuracies must be provided for direct comparison of NEWT and Polaris few-group cross sections with Serpent. For the purposes of this report, the target accuracy is 1.5% relative difference, and the acceptance accuracy is 3% relative difference.

Few-group cross section target accuracy:

- 4-factor k_{inf} formula: 200 pcm difference
- Cross sections, assembly discontinuity factors (ADFs), flux ratios, transport cross sections, kappa values, kinetics parameters, and fission product yields: 1.5% relative difference unless noted otherwise

Few-group cross section acceptance accuracy:

- 4-factor k_{inf} formula: 400 pcm difference
- Cross sections, ADFs, flux ratio, transport cross sections, kappa values, kinetics parameters, and fission product yields: 3.0% relative difference unless noted otherwise

For depletion calculations, concentrations of important isotopes must be compared at different burnups. For the numerical depletion benchmarks presented in this report, the target accuracy and acceptance accuracy for isotopic concentrations are as follows:

Isotopic concentration target accuracy: 1.5% relative difference in uranium and plutonium isotopes mass

Isotopic concentration acceptance accuracy: 2.5% relative difference in uranium and plutonium isotopes mass

Table 4-5 summarizes test coverage for 2D numerical benchmarks, and Table 4-6 summarizes RCA measurement data.

Table 4-5 Test Suite Coverage for 2D Numerical Benchmarks

Test suite	Objective	Test case range
Test Suite 1: baseline	Tests modeling capability of various lattice types and possible biases due to lattice type and operating condition by comparing k_{inf} and pin power distribution of common PWR and BWR lattice types (all axial zones for BWR).	BWR: controlled and uncontrolled cold, HZP, 0, 40, 70, and 90% void HFP, Doppler branches at HFP 0, 40, 70, and 90% void PWR: controlled and uncontrolled, cold (0, 1,000,1,300, 2,000, and 2,500 ppm boron), HFP (560 and 600K coolant temperatures), HZP (0,1,000,1,300, 2,000, and 2,500 ppm boron), and Doppler branch
Test Suite 2: control elements	Tests accuracy and possible biases in k_{inf} and pin power distribution of BWR and PWR lattices with respect to different types of control blades and control rods.	BWR: controlled HFP 0, 40, 70, and 90% with B ₄ C, Marathon, and Hafnium control blades PWR: Controlled HFP with AIC, B ₄ C and Inconel control rods
Test Suite 3: MOX fuel	Tests accuracy and possible biases in k_{inf} and pin power distribution of BWR and PWR lattices containing MOX fuel (4 and 10 wt% Pu total with 50 and 95 wt% ²³⁹ Pu).	BWR: controlled and uncontrolled cold, HZP, 0, 40, 70, and 90% void HFP, Doppler branches at HFP 0, 40, 70, and 90% void PWR: controlled and uncontrolled, cold (0,1,000,1,300, 2,000, and 2,500 ppm boron), HFP (560 and 600 K coolant temperatures), HZP (0,1,000,1,300, 2,000, and 2,500 ppm boron), and Doppler branch
Test Suite 4: reactivity worth of depleted fuel	Tests accuracy and possible biases in reactivity worth of BWR and PWR lattices containing 40 GWd/MTU and 80 GWd/MTU depleted UOX fuel.	BWR: HFP 0, 40, 70, and 90% void HFP PWR: HFP
Test Suite 5: depletion calculations	Tests accuracy and possible biases in k_{inf} and U/Pu isotopic distributions with depletion of UOX for BWR (14 GWd/MTU) and for PWR (80 GWd/MTU) lattices.	BWR: 0, 40, 70% void, HFP PWR: HFP

Table 4-5 Test Suite Coverage for 2D Numerical Benchmarks (Continued)

Test suite	Objective	Test case range
Test Suite 6: boron injection	Tests accuracy and possible biases in k_{inf} and pin power distributions due to variations in the moderator boron concentration.	BWR: 1,000 and 2,000 ppm, cold and HZP
Test Suite 7: enrichment	Tests accuracy and possible biases in k_{inf} and pin power distributions due to increasing ^{235}U enrichment (2, 6, and 10 wt%) in BWR and PWR lattices.	BWR: 0, 40, 70, and 90% void, HFP PWR: HFP
Test Suite 8: fuel temperature	Tests accuracy and possible biases in k_{inf} and pin power distributions due to increasing fuel temperatures in BWR and PWR lattices.	BWR: 0, 40, 70, and 90% void, HFP at 500, 950, 1,500, and 3,000 K fuel temperatures PWR: HFP at 560, 900, 2,500, and 3,000 K fuel temperatures
Test Suite 9: burnable poison loading	Tests accuracy and possible biases in k_{inf} and pin power distributions due to increasing burnable poison loadings for BWR (2–10wt% Gd) and PWR (Gd, BPRA, IFBA) lattices.	BWR: controlled and uncontrolled, 0, 40, 70, and 90% void HFP PWR: HFP
Test Suite 10: burnable poison spatial variations	Tests accuracy and possible biases in k_{inf} and pin power distributions due to location of burnable poisons in BWR and PWR lattices.	BWR: 0, 40, 70, and 90% void, HFP PWR: HFP
Test Suite 11: PARCS parameters for fuel-only model	Tests accuracy and possible biases in PARCS QOI parameters with respect to nominal BWR and PWR lattice types at different lattice conditions.	BWR: 0, 40, 70, and 90% void, HFP PWR: HFP
Test Suite 12: PARCS parameters for fuel/reflector model	Tests accuracy of few group reflector cross sections generated by using BWR and PWR lattices.	BWR: 0, 40, 70, 90% void, HFP PWR: HFP

Table 4-5 Test Suite Coverage for 2D Numerical Benchmarks (Continued)

Test suite	Objective	Test case range
Test Suite 13: numerical benchmarks	Provides comparisons of k_{inf} and isotopic concentrations with well recognized lattice physics codes for BWR and PWR international benchmarks.	
Test Suite 14: variations in vanished zone patterns	Tests performance of the lattice physics calculations with respect to different vanished rod patterns in BWR lattices.	BWR: 0, 40, 70, and 90% void, HFP

Table 4-6 Test Suite Coverage for RCA Benchmarks^a

Reactor	Fuel	Assembly design	Enrichment ²³⁵ U wt %	Pu ^{fiss} wt %	# of samples	Burnup (GWd/MTU)
Calvert Cliffs-1	PWR UOX	14 × 14	3.038	n/a	2	37.12 44.34
Fukushima Daini-2	BWR UOX	8 × 8	3.41–3.91	n/a	2	43.99 39.99
Gundremmingen	BWR MOX	9 × 9	0.253	1.15– 5.53	1	51.7

^a = RCA benchmark data are provided in previous reports [21,22,23].

5 SUMMARY OF RESULTS

This section summarizes the calculational results for each test suite and provides high-level observations of code performance trends. Detailed results and associated discussions are found in the appendices.

5.1 Test Suite 1 – BOL LWR Assemblies Baseline

Table 5-1 Summary of Test Suite 1 Results

QOI		MC uncertainty	Target criteria	Acceptance criteria
k_{inf}		<10 pcm	200 pcm	400 pcm
Pin power (BWR)		~0.1%	1.0% RMS, 1.5% MAX	1.5% RMS, 2.5% MAX
Pin power (PWR)		~0.1%	0.5% RMS, 1.5% MAX	1.5% RMS, 2.5% MAX
Code	Category	Number of cases	Passed target criteria	Passed acceptance criteria
NEWT	BWR (u) ^a	172	128	170
	BWR (c) ^b	167	102	167
	PWR (u)	88	87	88
	PWR (c)	86	48	86
	Total	513	365	511
	Polaris	BWR (u)	172	143
BWR (c)		167	141	167
PWR (u)		88	88	84
PWR (c)		86	68	86
Total		513	440	502
Reference calculation – CE KENO: 500 inactive generations, 1,000 active generations, 100,000 particles/generation				

^a(u) = uncontrolled

^b(c) = controlled

Observations are as follows:

- Nearly all cases pass the acceptance criteria.

- All BWR lattice tests pass except Polaris 90% void, natural zone test ($\Delta k=470$ pcm). NEWT and Polaris cold-controlled cases and 90% void cases have the largest k_{inf} differences in BWR lattices and do not meet the target criteria.
- Several PWR-controlled cases fail to meet target criteria. All instances were at cold 0 ppm boron conditions.
- Both codes exhibit trends in k_{inf} difference vs void fraction for BWR lattices and k_{inf} difference vs coolant boron concentration in PWR lattices.

5.2 Test Suite 2 – Control Elements

Table 5-2 Summary of Test Suite 2 Results

QOI		MC uncertainty	Target criteria	Acceptance criteria
k_{inf}		<10 pcm	200 pcm	400 pcm
Pin power (BWR)		~0.1%	1.0% RMS, 1.5% MAX	1.5% RMS, 2.5% MAX
Pin power (PWR)		~0.1%	0.5% RMS, 1.5% MAX	1.5% RMS, 2.5% MAX
Code	Category	Number of cases	Passed target criteria	Passed acceptance criteria
NEWT	BWR	12	12	12
	PWR	6	6	6
	Total	18	18	18
Polaris	BWR	12	12	12
	PWR	6	6	6
	Total	18	18	18
Reference calculation – CE KENO:				
500 inactive generations, 1,000 active generations, 100,000 particles/generation				

Observations are as follows:

- All cases pass the acceptance criteria.
- Polaris and NEWT results indicate a small bias (<100 pcm) in k_{inf} differences between hafnium and B₄C control blades.
- Marathon control blades also show a similar bias in Polaris results.
- Compared with other PWR control rod types, AIC results show a small bias (<100 pcm) for all codes.

5.3 Test Suite 3 – MOX Fuel

Table 5-3 Summary of Test Suite 3 Results

QOI		MC uncertainty	Target criteria	Acceptance criteria
k_{inf}		<10 pcm	200 pcm	400 pcm
Pin power (BWR)		~0.1%	1.0% RMS, 1.5% MAX	1.5% RMS, 2.5% MAX
Pin power (PWR)		~0.1%	0.5% RMS, 1.5% MAX	1.5% RMS, 2.5% MAX
Code	Category	Number of cases	Passed target criteria	Passed acceptance criteria
NEWT	BWR (u) ^a	17	11	14
	BWR (c) ^b	15	12	15
	PWR (u)	29	29	29
	PWR (c)	29	29	29
	Total	90	81	89
Polaris	BWR (u)	17	14	17
	BWR (c)	15	15	15
	PWR (u)	29	29	29
	PWR (c)	29	29	29
	Total	90	87	90
Reference calculation: CE KENO: 500 inactive generations, 1,000 active generations, 100,000 particles/generation				

^a(u) = uncontrolled

^b(c) = controlled

Observations are as follows:

- As in UOX fuel, there is a strong trend in k_{inf} differences vs void fraction.
- Unlike UOX, MOX results for MG KENO and NEWT show a trend in the opposite direction.
- MG KENO and NEWT results fail to meet the target criteria after the void fraction exceeds 40%. NEWT results fail to meet the acceptance criteria at 90% void fraction. Further investigation is required.
- Polaris results pass acceptance and target criteria for hot cases, while k_{inf} differences are higher than the target criteria for cold cases (~370 pcm).

- All codes pass target criteria for controlled BWR lattices except for NEWT case at 90% void fraction.
- All codes pass target criteria for PWR lattices for all state points.

5.4 Test Suite 4 – Reactivity Worth of Depleted Fuel

Table 5-4 Summary of Test Suite 4 Results

QOI		MC uncertainty	Target criteria	Acceptance criteria
k_{inf}		<10 pcm	200 pcm	400 pcm
Pin power (BWR)		~0.1%	1.0% RMS, 1.5% MAX	1.5% RMS, 2.5% MAX
Pin power (PWR)		~0.1%	0.5% RMS, 1.5% MAX	1.5% RMS, 2.5% MAX
Code	Category	Number of cases	Passed target criteria	Passed acceptance criteria
NEWT	BWR	12	9	12
	PWR	3	3	3
	Total	15	12	15
Polaris	BWR	12	9	12
	PWR	3	3	3
	Total	15	12	15
Reference calculation – CE KENO: 500 inactive generations, 1,000 active generations, 100,000 particles/generation				

Observations are as follows:

- Both codes pass target criteria for all PWR tests.
- Trends in k_{inf} associated with void fraction were observed for all BWR depleted fuel configurations for both codes; the trends strongly depend on the burnup.
- While BWR 0% void fraction has the largest difference at BOC, 90% void fraction has the largest difference in k_{inf} at EOC for NEWT.
- Both codes fail to meet the target criteria for BWR depleted fuel at 90% void fraction.

5.5 Test Suite 5 – Depletion Calculations

Table 5-5 Summary of Test Suite 5 Results

QOI		MC Uncertainty	Target criteria	Acceptance criteria
k_{inf}		<10 pcm	200 pcm	400 pcm
U and Pu number density		n/a	1.5%	2.5%
Code	Category	Number of cases	Passed target criteria	Passed acceptance criteria
NEWT	BWR	57	48	57
	PWR	19	11	17
	Total	76	59	74
Polaris	BWR	57	44	57
	PWR	19	8	17
	Total	76	52	74
Reference calculation – CE KENO: 500 inactive generations, 1,000 active generations, 100,000 particles/generation				

Observations are as follows:

- For PWR depletion, Polaris and NEWT pass acceptance criteria for k_{inf} .
- Polaris results pass target criteria for k_{inf} , while NEWT results fail target criteria beyond 43 GWd/MTU.
- MG KENO analysis shows that cross section processing introduces 250 pcm bias in depletion results.
- In general, ^{238}Pu concentrations show larger relative differences than other isotopes. ^{235}U concentrations fail acceptance criteria for NEWT by -4.6% and for Polaris by -3.7% at 80 GWd/MTU burnups.
- For BWR depletion, Polaris and NEWT pass acceptance criteria for k_{inf} at all void fractions.
- Polaris results pass target criteria for k_{inf} , while NEWT results fail target criteria at 0% and 70% void fractions.
- All isotope differences pass acceptance criteria for both codes

- ²³⁸Pu concentrations show larger relative differences than other isotopes and fail target criteria for both codes.

5.6 Test Suite 6 – Boron Injection

Table 5-6 Summary of Test Suite 6 Results

QOI		MC uncertainty	Target criteria	Acceptance criteria
k_{inf}		<10 pcm	200 pcm	400 pcm
Pin power (BWR)		~0.1%	1.0% RMS, 1.5% MAX	1.5% RMS, 2.5% MAX
Pin power (PWR)		~0.1%	0.5% RMS, 1.5% MAX	1.5% RMS, 2.5% MAX
Code	Category	Number of cases	Passed target criteria	Passed acceptance criteria
NEWT	BWR	6	6	6
	PWR	15	15	15
	Total	21	21	21
Polaris	BWR	6	5	6
	PWR	15	15	15
	Total	21	20	21
Reference calculation – CE KENO: 500 inactive generations, 1,000 active generations, 100,000 particles/generation				

Observations are as follows:

- Both codes pass the acceptance criteria for all BWR borated lattice tests.
- Both codes exhibit a trend with boron concentration in k_{inf} differences at cold conditions. This trend disappears with increasing fuel temperature at HZP condition.
- Polaris fails the target criteria for BWRs at high boron cold condition (~260 pcm).
- Both codes pass the target criteria for all PWR borated lattice tests.

5.7 Test Suite 7 – Enrichment

Table 5-7 Summary of Test Suite 7 Results

QOI		MC uncertainty	Target criteria	Acceptance criteria
k_{inf}		<10 pcm	200 pcm	400 pcm
Pin power (BWR)		~0.1%	1.0% RMS, 1.5% MAX	1.5% RMS, 2.5% MAX
Pin power (PWR)		~0.1%	0.5% RMS, 1.5% MAX	1.5% RMS, 2.5% MAX
Code	Category	Number of cases	Passed target criteria	Passed acceptance criteria
NEWT	BWR (u) ^a	20	17	20
	BWR (c) ^b	20	19	20
	PWR (u)	5	5	5
	PWR (c)	5	5	5
	Total	50	46	50
Polaris	BWR (u) ^a	20	13	20
	BWR (c) ^b	20	19	20
	PWR (u)	5	5	5
	PWR (c)	5	5	5
	Total	50	42	50
Reference calculation – CE KENO: 500 inactive generations, 1,000 active generations, 100,000 particles/generation				

^a(u) = uncontrolled

^b(c) = controlled

Observations are as follows:

- All BWR lattice tests pass acceptance criteria.
- For Polaris, void fraction trends are observed across all enrichments. As fuel enrichment increases, the biases in k_{inf} also increase. A similar trend in enrichment is observed for NEWT results, while it is less noticeable for NEWT uncontrolled cases.
- There is a significant bias between NEWT and Polaris results for uncontrolled configurations. The bias decreases for controlled cases.
- Polaris results fail to pass the target criteria at high void fraction (90%).

- NEWT results fail to pass the target criteria at no void fraction (0%).
- All PWR lattice tests pass the target criteria.

5.8 Test Suite 8 – Fuel Temperature

Table 5-8 Summary of Test Suite 8 Results

QOI		MC uncertainty	Target criteria	Acceptance criteria
k_{inf}		<10 pcm	200 pcm	400 pcm
Pin power (BWR)		~0.1%	1.0% RMS, 1.5% MAX	1.5% RMS, 2.5% MAX
Pin power (PWR)		~0.1%	0.5% RMS, 1.5% MAX	1.5% RMS, 2.5% MAX
Code	Category	Number of cases	Passed target criteria	Passed acceptance criteria
NEWT	BWR	16	16	16
	PWR	4	4	4
	Total	20	20	20
Polaris	BWR	16	16	16
	PWR	4	4	4
	Total	20	20	20
Reference calculation – CE KENO: 500 inactive generations, 1,000 active generations, 100,000 particles/generation				

Observations are as follows:

- For consistent comparison, CE KENO calculations do not enable resonance upscattering calculations.
- All BWR and PWR lattice tests pass the target criteria.
- No significant biases or trends are observed with respect to increasing fuel temperature.

5.9 Test Suite 9 – Burnable Poison Loading

Table 5-9 Summary of Test Suite 9 Results

QOI		MC uncertainty	Target criteria	Acceptance criteria
k_{inf}		<10 pcm	200 pcm	400 pcm
Pin power (BWR)		~0.1%	1.0% RMS, 1.5% MAX	1.5% RMS, 2.5% MAX
Pin power (PWR)		~0.1%	0.5% RMS, 1.5% MAX	1.5% RMS, 2.5% MAX
Code	Category	Number of cases	Passed target criteria	Passed acceptance criteria
NEWT	BWR	12	9	11
	PWR	7	4	7
	Total	19	13	18
Polaris	BWR	12	10	12
	PWR	7	7	7
	Total	19	17	19
Reference calculation – CE KENO:				
500 inactive generations, 1,000 active generations, 100,000 particles/generation				

Observations are as follows:

- Increasing gadolinium loading in BWR lattices increases bias in void fraction trends for both codes.
- High void fraction (90%) NEWT results for 0% gadolinium loading fail to meet the acceptance criteria.
- All nonzero gadolinium loadings at 0% void fractions fail to meet the target criteria for NEWT results.
- Except for the 90% void fraction 10% gadolinium loading case, all Polaris results pass the target accuracy for BWR lattices.
- Polaris results pass the target accuracy for all PWR lattice tests.
- NEWT results fail to pass the target criteria for IFBA and gadolinium (~207 pcm) BP types. IFBA results can be improved by increasing geometry details of the absorber region.

5.10 Test Suite 10 – Burnable Poison Spatial Variations

Table 5-10 Summary of Test Suite 10 Results

QOI		MC uncertainty	Target criteria	Acceptance criteria
k_{inf}		<10 pcm	200 pcm	400 pcm
Pin power (BWR)		~0.1%	1.0% RMS, 1.5% MAX	1.5% RMS, 2.5% MAX
Pin power (PWR)		~0.1%	0.5% RMS, 1.5% MAX	1.5% RMS, 2.5% MAX
Code	Category	Number of cases	Passed target criteria	Passed acceptance criteria
NEWT	BWR (u) ^a	8	7	8
	BWR (c) ^b	8	8	8
	PWR (u)	14	11	14
	Total	30	26	30
Polaris	BWR (u) ^a	8	8	8
	BWR (c) ^b	8	7	8
	PWR (u) ^a	14	14	14
	Total	30	29	30
Reference calculation – CE KENO: 500 inactive generations, 1,000 active generations, 100,000 particles/generation				

^a(u) = uncontrolled

^b(c) = controlled

Observations are as follows:

- The magnitude of the k_{inf} differences depends on the BP type and spatial variation. For BWRs, the k_{inf} difference as a function of void fraction has the same shape across the different BP variations.
- NEWT 0% void fraction fails to pass the target criteria for the uncontrolled internal gadolinia pattern.
- Polaris 0% void fraction fails to pass the target criteria for the controlled internal gadolinia pattern.
- Polaris passes the target criteria for all PWR lattice BP loading patterns.
- NEWT fails the target criteria for IFBA loading patterns.

5.11 Test Suite 11 – PARCS Parameters for Fuel-Only Model

Table 5-11 Summary of Test Suite 11 Results

QOI		MC uncertainty	Target criteria	Acceptance criteria
$k_{inf}, \eta_f, \rho, \varepsilon$		<10 pcm	200 pcm	400 pcm
nu-fission, absorption, downscatter, kappa, fast-to-thermal flux, transport, ADF		< 0.1%	1.5% relative difference	3% relative difference
Upscatter		< 0.2%	5% relative difference	10% relative difference
Code	Category	Number of cases	Passed target criteria	Passed acceptance criteria
NEWT	BWR	68	52	61
	PWR	15	14	14
	Total	83	66	75
Polaris	BWR	68	60	67
	PWR	15	13	15
	Total	83	73	82
Reference calculation – Serpent: 200 inactive generations, 1,000 active generations, 100,000 particles/generation				

Observations are as follows:

- Polaris has good agreement for most cases except for the 90% void fraction case. Cross section processing in the unresolved resonance energy range and above requires further investigation.
- NEWT has good agreement for most cases. Thermal upscattering convergence requires investigation, along with spatial mesh refinement.
- Kappa values require additional investigation.
- See Appendix B, section B.11 for discussion on comparison of transport cross sections, fission product yields, and kinetics parameters.

5.12 Test Suite 12 – PARCS Parameters for Fuel/Reflector Model

Table 5-12 Summary of Test Suite 12 Results

QOI		MC uncertainty	Target criteria	Acceptance criteria
Absorption, downscatter, transport, ADF		<0.1%	1.5% relative difference	3% relative difference
Upscatter		< 0.5%	5% relative difference	10% relative difference
Code	Category	Number of cases	Passed target criteria	Passed acceptance criteria
NEWT	BWR	96	49	74
	PWR	24	13	20
	Total	120	62	94
Polaris	BWR	48	42	48
	PWR	12	7	10
	Total	60	49	58
Reference calculation – Serpent: 200 inactive generations, 1,000 active generations, 100,000 particles/generation				

Observations are as follows:

- Polaris has good agreement for most cases except for the upscatter cross section for the radial reflector.
- NEWT has good agreement for most cases except for the upscatter cross section and the reflector ADF. Thermal upscattering convergence requires investigation, along with the reflector ADF methodology.
- See Appendix B.12 for discussion on thermal upscatter and reflector ADF comparisons.

5.13 Test Suite 13 – International Numerical Benchmarks

Table 5-13 Summary of Test Suite 13 Results

QOI		Target criteria	Acceptance criteria	
k_{inf}		200 pcm	400 pcm	
U/Pu mass		2% relative	5% relative	
Code	Category	Number of cases	Passed target criteria	Passed acceptance criteria
CE KENO	BWR	57	N/A	N/A
	PWR	6	6	6
	Total	63	6	6
NEWT	BWR	57	N/A	N/A
	PWR	6	6	6
	Total	63	3	4
Polaris	BWR	57	N/A	N/A
	PWR	6	4	4
	Total	63	4	4
Reference calculation – benchmark results				

Observations are as follows:

- CE KENO and NEWT show good agreement with reference CASMO results from the EPRI PWR benchmark. Polaris results do not meet acceptance criteria after 50 GWd/MTU.
- There are large differences in (~800 pcm) in Serpent and SWAT code k_{inf} results for the Expert Group on Used Nuclear Fuel Criticality (EGUNF) Phase II BWR benchmark. Therefore, no reference solution was selected for the BWR benchmark.
- In contrast to large differences in k_{inf} results, U isotopes are in good agreement for all codes. The largest differences are observed in ^{238}Pu (14%) and ^{239}Pu (4%) isotopes.

5.14 Test Suite 14 – Variations in Vanished Zone Patterns

Table 5-14 Summary of Test Suite 14 Results

QOI		MC uncertainty	Target criteria	Acceptance criteria
k_{inf}		<10 pcm	200 pcm	400 pcm
Pin power (BWR)		~0.1%	1.0% RMS, 1.5% MAX	1.5% RMS, 2.5% MAX
Code	Category	Number of cases	Passed target criteria	Passed acceptance criteria
NEWT	BWR	12	10	12
Polaris	BWR	12	12	12
Reference calculation – CE KENO: 500 inactive generations, 1,000 active generations, 100,000 particles/generation				

Observations are as follows:

- Polaris passes the target criteria for all patterns.
- NEWT fails the target criteria for 0% void fractions.

5.15 RCA Measurements

Table 5-15 Summary of RCA Results

QOI				Target criteria	Acceptance criteria
U/Pu mass				2% relative	5% relative
Code	RCA sample	Sample Burnup ^a (GWd/MTU)	Number of isotopes	Passed target criteria	Passed acceptance criteria
CE KENO	Calvert Cliffs-1 MKP 109-3	44.34	9	3	6
	Calvert Cliffs-1 MKP 109-2	37.12	9	6	9
	Fukushima SF98-5	43.99	9	8	9
	Fukushima SF98-6	39.92	9	7	4
	Gundremmingen GRM-1	51.7	9	7	9
	Total			45	31
NEWT	Calvert Cliffs-1 MKP 109-3	44.34	9	5	6
	Calvert Cliffs-1 MKP 109-2	37.12	9	7	9
	Fukushima SF98-5	43.99	9	5	7
	Fukushima SF98-6	39.92	9	2	4
	Gundremmingen GRM-1	51.7	9	6	9
	Total			45	25
Polaris	Calvert Cliffs-1 MKP 109-3	44.34	9	6	8
	Calvert Cliffs-1 MKP 109-2	37.12	9	8	9
	Fukushima SF98-5	43.99	9	5	8
	Fukushima SF98-6	39.92	9	3	4
	Gundremmingen GRM-1	51.7	9	5	8
	Total			45	27

^a = Reported burnup values (Reference measured isotopic data)

Observations are as follows:

- The nine isotopes considered for comparisons in the table above are U and Pu isotopes: ²³⁴U, ²³⁵U, ²³⁶U, ²³⁸U, ²³⁸Pu, ²³⁹Pu, ²⁴⁰Pu, ²⁴¹Pu, and ²⁴²Pu.
- Good agreement between calculated and measured isotope concentrations is observed for major actinides (²³⁵U and ²³⁹Pu) for all three codes.

- Relative differences between calculated (C) and measured (E) isotope concentrations do not show any clear trends with respect to fuel (UOX, MOX) or reactor type (BWR, PWR).
- The difference in C/E ratios can be significant between CE KENO and Polaris for ^{235}U (6%) and ^{239}Pu (3%) for some samples. However, it is difficult to reach any conclusion based on the limited number of measurements for burnup, enrichment, void fraction and reactor type used in this test suite.

6 CONCLUSIONS

6.1 Overall Conclusions

This report provides a thorough, detailed assessment of the SCALE lattice physics codes for generation of few-group cross section data for the PARCS core simulator. The detailed results are summarized in Section 5 and are provided in the appendices. This assessment included 14 test suites in which the NEWT and Polaris results were compared to CE KENO MC reference calculations. Table 6-1 below summarizes the results for the 14 test suites. Nearly all cases passed the acceptance accuracy criteria, and the majority of cases passed the more stringent target accuracy criteria.

In addition, isotopic depletion results from NEWT, CE KENO, and Polaris were compared to RCA-measured isotopic concentrations. Table 6-2 summarizes the RCA results. The Polaris and NEWT results used different methodologies but were consistent with each other. These results agreed well with the measured data for most isotopes and were generally consistent with past SCALE depletion validation studies except for ^{238}Pu results, which need further investigation.

This report demonstrates that with few exceptions, NEWT and Polaris provide acceptable predictions of (1) k_{inf} , pin power distributions and (2) few-group cross section data for PARCS LWR core simulation. The exceptions, which are described in further detail in Appendix B, are subject to further investigation. Areas that will be investigated further are summarized below:

- Polaris void trend: The numeric test suites reveal a trend in the k_{inf} bias with respect to BWR void fraction. As void fraction increases from 0 to 90%, the bias between Polaris k_{inf} and CE KENO k_{inf} increases. At this writing, enhancements to the self-shielding methodology in Polaris have been identified that improve the bias trend to the point that the bias is a nearly constant function of void fraction. These enhancements will be introduced in the SCALE 6.3 release.
- Polaris boron trend: The numeric test suites reveal a trend in the k_{inf} bias with respect to PWR boron concentration. As boron concentration increases, the bias between Polaris k_{inf} and CE KENO k_{inf} increases. As in the BWR void trend, enhancements to the self-shielding methodology in Polaris improve the bias trend. These enhancements will be introduced in the SCALE 6.3 release.
- Source of biases in MOX fuel results: The numeric test suites reveal that biases and trends with MOX fuel are larger in magnitude when compared to the equivalent UO_2 models for both NEWT and Polaris. As shown in Section 4.1, the parameters used in each code were determined based on UO_2 CE 14×14 calculation. MOX fuel assemblies exhibit different flux spectrum when compared to UO_2 fuel. Initial future investigations will examine the sensitivity of the MOX QOIs to quadrature and spatial mesh selection specific to each code.
- High burnup depletion of IFBA loaded assemblies: The EPRI Benchmark shows larger than expected reactivity worth for depleted fuel at burnups above 50 GWd/MTU using Polaris. This trend is not observed in numerical depletions calculation tests (Test Suite 5). Even at extremely high burnups of up to 80 GWd/MTU, Polaris results show acceptable bias compared to results using CE KENO. Furthermore, good agreements in isotope distributions observed in comparisons to PWR RCA measurements do not

indicate any inherent problems in depletion calculations. A detailed analysis of burnup-dependent isotopic distributions and Polaris solution parameters is expected to identify sources of deviations.

Table 6-1 Summary of SCALE Lattice Physics Test Suite Results

Test suite	NEWT	Polaris	Comments
	acceptance accuracy (pass / total)		
1 – BOL LWR assemblies baseline	511 / 513	502 / 513	Both codes exhibit trends in k_{inf} difference vs void fraction for BWR lattices and k_{inf} difference vs coolant boron concentration for PWR lattices.
2 – control elements	18 / 18	18 / 18	All cases meet target and acceptance criteria.
3 – MOX fuel	87 / 90	90 / 90	NEWT cases fail acceptance criteria at 90% void fraction for BWR uncontrolled lattices.
4 – reactivity worth of depleted fuel	15 / 15	15 / 15	All cases meet acceptance criteria. Both codes fail to meet the target criteria for BWR fuel at 90% void fraction. Both codes pass target criteria for all PWR tests.
5 – depletion calculations	74 / 76	74 / 76	Polaris results meet target and accuracy criteria for k_{inf} . NEWT results fail target criteria at high burnups for PWR and at low and high void fractions for BWR. Both codes fail to pass target criteria for isotopic comparisons at high burnups for PWR.
6 – boron Injection	21 / 21	21 / 21	All cases meet acceptance criteria. NEWT cases meet target criteria. Polaris cases meet the target criteria except for the high boron cold condition.
7 – enrichment	50 / 50	50 / 50	All cases meet acceptance criteria. All PWR cases meet target criteria. Some BWR cases fail target criteria.
8 – fuel temperature	20 / 20	20 / 20	All cases meet target and acceptance criteria.
9 – BP loading	18 / 19	19 / 19	All Polaris cases meet target and acceptance criteria except for 2 PWR cases that fail target criteria. All NEWT cases meet acceptance criteria except for 1 BWR case at 90% void fraction. Several other NEWT cases fail target criteria.
10 – BP spatial variations	30 / 30	30 / 30	All Polaris cases meet target and acceptance criteria except for 1 BWR controlled case that fails target criteria. All NEWT cases meet target and acceptance criteria except for 4 cases that fail target criteria.

Table 6-1 Summary of SCALE Lattice Physics Test Suite Results (Continued)

Test suite	NEWT	Polaris	Comments
	acceptance (pass / total)	accuracy (pass / total)	
11 – PARCS parameters for fuel-only model	66 / 83	75 / 83	Polaris 90% void cases need further investigation. NEWT upscatter cross section needs investigation.
12 – PARCS parameters for fuel/reflector model	120 / 194	58 / 60	Polaris shows good agreement. NEWT upscatter cross section needs investigation.
13 – International numerical benchmarks	6 / 6	4 / 6	Polaris results at high burnups need investigation for the PWR tests.
14 – Vanished zone patterns	12 / 12	12 / 12	All Polaris cases meet the target and acceptance criteria. All NEWT cases meet the target and acceptance criteria with the exception of 2 cases that fail the target criteria at 0% void fraction.

Table 6-2 Summary of SCALE RCA Comparisons for Depletion Validation

Nuclide	Range of results for (C/E-1) (%)		
	CE KENO	NEWT	Polaris
²³⁴ U	[-4, 8]	[-4, 6]	[-3, 10]
²³⁵ U	[-4, 7]	[-6, 3]	[-6, 2]
²³⁶ U	[-2, 2]	[-1, 3]	[-2, 3]
²³⁸ Pu	[1, 16]	[0, 15]	[0, 12]
²³⁹ Pu	[-5, 7]	[-9, 4]	[-8, 2]
²⁴⁰ Pu	[-2, 4]	[-3, 2]	[-4, 1]
²⁴¹ Pu	[-3, 1]	[-7, -1]	[-6, -2]
²⁴² Pu	[-4, -2]	[-4, 2]	[-3, 2]

Isotope concentrations are normalized to ²³⁸U at discharge burnup.

6.2 Lessons Learned

The SCALE lattice physics code assessment reveals that many default or traditionally adopted solution parameters are too coarse, most notably for CE KENO pin power calculations and

NEWT calculations. The focus of this work is to assess the bias between well-converged NEWT and Polaris calculations with well-converged CE KENO calculations to identify deficiencies, trends, or biases in methods or multigroup structure. Selection of solution parameters—particle count, space/angle discretization, burnup step size, etc.—must be balanced between run time and fidelity of solution. Coarse parameter selection implies faster calculations at the cost of degraded solution fidelity. Mesh-converged parameter selection implies a higher fidelity solution at the cost of slower run times. The solution fidelity is not to be confused with solution accuracy; that is, the coarse parameter selection may lead to smaller bias due to cancellation of error.

The following list summarizes the recommended solution parameters for well-converged SCALE lattice physics calculations based on the parametric study presented in Section 4.1. The solution parameters are not default values in SCALE 6.2 unless otherwise noted and require 2x to 3x more CPU time.

1. CE KENO k_{eff} calculations with 10,000 particles per generations with 500 in active generations
2. CE KENO pin-power calculations with 100,000 particles per generation, 1,000 active and 500 inactive generations.
3. CE KENO depletion calculations with the same parameters as CE KENO pin-power calculations
4. NEWT k_{eff} and pin-power calculations with 8×8 grids per unit cell with 20 sides for polygons representing circles and $S_N=16$ quadrature set.
5. NEWT k_{eff} and pin-power calculations for IFBA loaded PWR lattices with 50 sides for polygons representing circles and the same solution parameters as other lattice types
6. Polaris k_{eff} and pin-power calculations with 0.04 cm MOC ray spacing, 0.02 cm ESSM ray spacing, 20 azimuthal angles, and 3 polar angles (These solution parameters are the defaults in Polaris in SCALE 6.2.2.)
7. Polaris k_{eff} and pin-power calculations for IFBA loaded PWR lattices with 0.003 cm MOC ray spacing and the same solution parameters as other lattice types. Noting that this ray spacing results in unpractical runtimes compared to typical lattice calculations and a ray spacing of 0.01 cm have acceptable accuracy.
8. CE KENO and TRITON/NEWT depletion step size not larger than 0.25 GWd/MTU until IFBA or Gd-based burnable absorbers deplete
9. Polaris depletions step size not larger than 0.5 GWd/MTU until IFBA or Gd-based burnable absorbers deplete

6.3 Future Work

Assessment of Polaris accuracy will continue be the point of emphasis for LWR lattice physics analysis. This is the first assessment in a series of activities applied for NRC LWR confirmatory analysis with Polaris and PARCS. These future activities include:

1. Polaris lattice physics assessments for high burnup, extended enrichment, and accident tolerant fuels.
2. SCALE coarse group libraries will be assessed to develop recommendations on usage and influence future development on broad group libraries to succeed the current 56-group structure.
3. Polaris and PARCS validation using core operating data for available PWRs and BWRs such as Watts Bar, Hatch, Cofrentes, and TMI. This will include cycle boron letdown (PWR only), control rod worths, reactivity coefficients, and detector measurements.
4. PARCS assessment of methodology accuracy such as effect of interpolation strategy, nodal methodology, and thermal hydraulics on core quantities of interest.
5. SCALE fine group libraries will be assessed as part of Polaris run-time optimization efforts that include on-the-fly energy condensation methods.

7 REFERENCES

- B. T. Rearden and M. A. Jessee, Eds., *SCALE Code System*, ORNL/TM-2005/39, Version 6.2.2, Oak Ridge National Laboratory, Oak Ridge, Tennessee (2017). Available from Radiation Safety Information Computational Center as CCC-834.
- T. Downar, et al., "PARCS, NRC - v3.3.2 Release," University of Michigan, Ann Arbor, MI, 2020.
- US NRC, *TRACE V5. 0 assessment manual, Main Report*, Washington, DC, USA (2005).
- M. D. DeHart and S. M. Bowman. "Reactor Physics Methods and Analysis Capabilities in SCALE," *Nucl. Technol.* 174(2), 196–213, May 2011.
- M. A. Jessee, W. A. Wieselquist, et al. "Polaris: A New Two-Dimensional Lattice Physics Analysis Capability for the SCALE Code System." *Proceedings, PHYSOR 2014*, Kyoto, Japan (2014).
- M. L. Williams and K. S. Kim. "The Embedded Self-Shielding Method." *Proceedings, PHYSOR 2012*, Knoxville, Tennessee, USA (2012).
- OECD NEA, *International Handbook of Evaluated Criticality Safety Benchmark Experiments*, NEA/NSC/DOC(95)03, OECD and at www.oecd-nea.org/science/wpncs/icsbep/.
- OECD NEA, *International Handbook of Evaluated Reactor Physics Benchmark Experiments*, NEA/NSC/DOC(2006)1, OECD and at www.oecd-nea.org/science/wprs/irphe (2006).
- M. L. Fensin. *Optimum Boiling Water Reactor Fuel Design Strategies to Enhance Reactor Shutdown by the Standby Liquid Control System*, Master's Thesis, University of Florida (2004).
- A New Comparative Analysis of LWR Fuel Designs*, NUREG-1754 (2001).
- N. E. Todreas. *Thermal Hydraulics Design Limits*, Class Note II, 9/7/06, MIT (2006).
- V. M. Mourogov et al. "MOX Fuel Cycle Technologies for Medium and Long Term Deployment." *Proceedings, IAEA*, Vienna, 1999, IAEA-CSP-3/P ISSN 1563–0153 (1999).
- U. Merturek and I. C. Gauld. "Development of ORIGEN Libraries for Mixed Oxide (MOX) Fuel Assembly Designs," *Nucl. Eng. and Design*, 297, 220–230 (2016).
- V. Xulubana et al., "Accuracy evaluation of pin exposure calculations in current LWR core design codes," *Annals of Nuclear Energy*, Volume 35, Issue 3 (March 2008).
- Merturek et al. "Validation of the lattice physics code Lancer02 with ENDF/B-VII library - 076." *Proceedings, PHYSOR 2010*, Pittsburgh, Pennsylvania (2010).
- E. Martinolli et al., "APOLLO2-A – Areva's New Generation Lattice Physics Code: Methodology and Validation," *Proceedings, PHYSOR 2010*, Pittsburgh, Pennsylvania (2010).
- F. Jatuf et al., "Experimental Validation of Pin Power Distributions for a BWR Assembly with Hafnium Control Blades," *Proceedings, PHYSOR 2004*, Chicago, Illinois (2004).

- M. Ouisloumen et al., "The new lattice code Paragon and its qualification for PWR core applications." *Proceedings, International Conference on Supercomputing in Nuclear Applications*, SNA'2003, France (2003).
- T. Pandya et al., "Implementation, capabilities, and benchmarking of Shift, a massively parallel Monte Carlo radiation transport code," *Journal of Computational Physics*, 308: pp. 239–272 (2016).
- J. Leppanen et al., "The Serpent Monte Carlo code: Status, development and applications in 2013," *Annals of Nuclear Energy*, 82: pp. 142–150 (2015).
- P. R. Thorne, G. J. O'Connor, and R. L. Bowden. *Problem Specification for the OECD/NEANSO Burnup Credit Benchmark Phase IV-B: Mixed Oxide (MOX) Fuels*, BNFL, Risley, Warrington, Cheshire, UK (2002).
- G. Ilas, I. C. Gauld, and G. Radulescu. "Validation of new depletion capabilities and ENDF/B-VII data libraries in SCALE," *Annals of Nuclear Energy*, 46, 43–55 (2012).
- U. Merturek, M. W. Francis, and I. C. Gauld, *SCALE 5 Analysis of BWR Spent Nuclear Fuel Isotopic Compositions for Safety Studies*, ORNL/TM-2010/286, Oak Ridge National Laboratory, Oak Ridge, TN (2010).
- B. J. Marshall et al., "Validation of SCALE 6.2 Criticality Calculations Using KENO V.a and KENO-VI," *ICNC 2015*, Charlotte, North Carolina, 13–17 Sep (2015).
- L. W. Newman, *Urania-Gadolinia: Nuclear Model Development and Critical Experiment Benchmark*, BAW-1810, Babcock and Wilcox (1984).
- T. Bahadir and S-Ö Lindahl, "SIMULATE-4 Pin Power Calculations," *Proceedings, PHYSOR 2006*, Vancouver, Canada (2006).
- D. Wang et al., *Cross Section Generation Guidelines for TRACE/PARCS*, NUREG/CR-7164 (2013).
- K. Suyama et al. *Burnup Credit Criticality Benchmark Phase IIIC*. OECD/NEA (2012).
- K. Lassmann et al. "The Radial Distribution of Plutonium in High Burn-up UO₂ fuels," *Journal of Nuclear Materials*, 208: pp. 223–231 (1994).
- J. Komatsu, T. Tachibana, and K. Konashi, "The Melting Temperature of Irradiated Oxide Fuel." *Journal of Nuclear Materials*, 154: pp. 38–44 (1994).
- B. R. Herman et al., "Improved diffusion coefficients generated from Monte Carlo codes," *Proceedings, M&C 2013*, Sun Valley, Idaho (2013).
- K. Xu et al., "Two-Step Analysis of Watts Bar Nuclear 1 Cycle 1 with SCALE/PARCS," *Proceedings, ANS National Meeting*, San Francisco, CA (2016).
- Depletion Reactivity Benchmark for the International Handbook of Evaluated Reactor Physics Benchmark Experiments*, EPRI Report No: 3002000306 (2013).

APPENDIX A

CE KENO LATTICE CALCULATIONS ACCURACY ASSESSMENT

A.1 Criticality Benchmarks

Purpose: A set of critical experiments applicable to LWRs, flux spectra, and fuel materials are used to assess 3D CE KENO k_{eff} calculations for LWR fuel. The k_{eff} biases from these experiments provide a basis for the accuracy of the CE KENO results.

Description: The range of temperatures, fuel enrichments, and pin cell geometries are summarized in Table A-1 and Table A-2.

Table A-1 Critical Experiment Summary for UOX fuel

Description	Number of cases	Enrichment ²³⁵ U	Pitch	Temperature (°C)
LEU-COMP-THERM-001	8	2.35	2.032	Ambient
LEU-COMP-THERM-002	5	4.31	2.54	Ambient
LEU-COMP-THERM-008	17	2.46	1.63576	Ambient
LEU-COMP-THERM-010	30	4.31	2.54–1.892	Ambient
LEU-COMP-THERM-017	29	2.35	2.032–1.684	Ambient
LEU-COMP-THERM-042	7	2.35	1.684	Ambient
LEU-COMP-THERM-046	18	4.35	1.5	14–85
LEU-COMP-THERM-050	18	4.74	1.3	Ambient
LEU-COMP-THERM-078	15	6.9	0.854964	Ambient
LEU-COMP-THERM-080	11	6.9	0.8001	Ambient
KRITZ-LWR-RESR-002	2	1.86	1.485	19.7/248.5

Table A-2 Critical Experiment Summary for MOX fuel

Description	Number of cases	Enrichment (%)		Pitch (cm)	Temperature (°C)
		²³⁹ Pu	²⁴⁰ Pu		
MIX-COMP-THERM-001	4	22	86.15	0.9525–1.905	Ambient
MIX-COMP-THERM-002	6	91.83	7.76	1.778–2.51447	Ambient
MIX-COMP-THERM-004	11	68	22	1.825–2.474	Ambient

Results: MG KENO and CE KENO calculated-to-expected (C/E) values for the LEU-COMP and MIX-COMP systems are presented in Figure A-1 and Figure A-2, respectively. Uncertainties in k_{eff} originating from experimental and MG data uncertainties are depicted as dotted lines in the figures. The data used in the figures are listed in Table A-3 and Table A-4. Average CE KENO C/E results for LEU and MIX-COMP are 0.99970 ± 0.00020 and 0.99931 ± 0.00087 , respectively.

A detailed explanation of uncertainties and discussion on individual experimental sets can be found in a recent paper by Marshall [24].

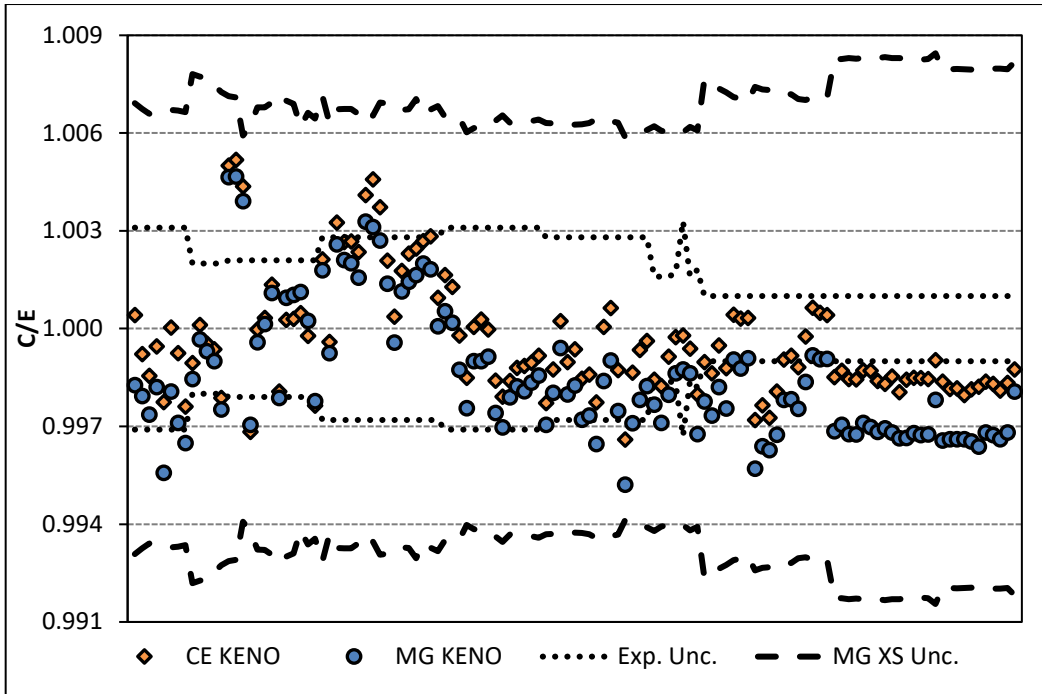


Figure A-1 C/E Values for LEU-COMP-THERM Systems Using SCALE 6.2 [24]

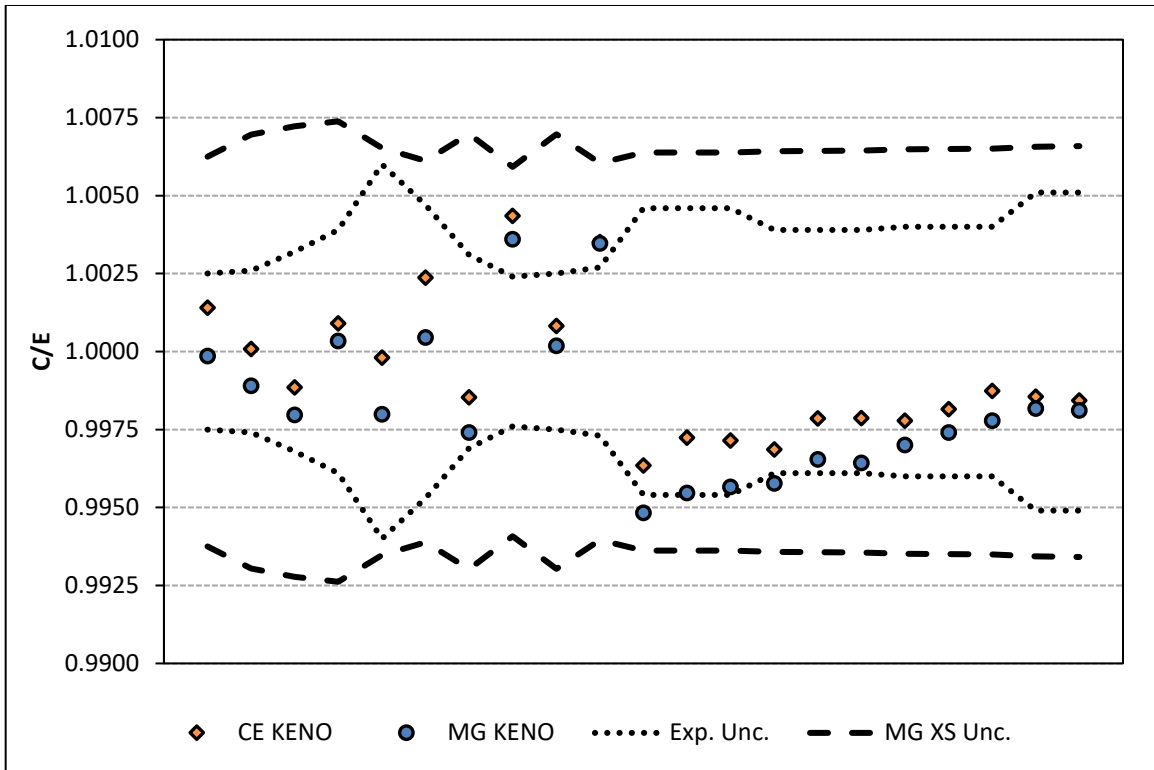


Figure A-2 C/E Values for MIX COMP-THERM Systems Using SCALE 6.2 [24]

Table A-3 Critical Experiment Comparison for UOX fuel

Category	252-group		Continuous energy	
	Average C/E	Uncertainty	Average C/E	Uncertainty
LEU-COMP-THERM-001	1.00285	0.00041	1.00197	0.00041
LEU-COMP-THERM-002	0.99719	0.00072	0.99805	0.00072
LEU-COMP-THERM-008	1.00566	0.00083	1.00293	0.00083
LEU-COMP-THERM-010	0.99915	0.00020	0.99970	0.00020
LEU-COMP-THERM-017	0.99724	0.00083	0.99777	0.00083
LEU-COMP-THERM-042	1.00730	0.00159	1.00241	0.00158
LEU-COMP-THERM-046	0.99870	0.00087	0.99931	0.00087
LEU-COMP-THERM-050	1.00147	0.00139	1.00128	0.00139
LEU-COMP-THERM-078	0.99985	0.00068	1.00025	0.00068
LEU-COMP-THERM-080	1.00232	0.00056	1.00307	0.00056
KRITZ-LWR-RESR-002	N/A	N/A	0.997352	0.0000995

Table A-4 Critical Experiment Comparison for MOX fuel

Category	252-group		Continuous energy	
	Average C/E	Uncertainty	Average C/E	Uncertainty
MIX-COMP-THERM-001	0.99927	0.00005	1.00031	0.00005
MIX-COMP-THERM-002	1.00328	0.00005	1.00433	0.00005
MIX-COMP-THERM-004	0.99665	0.00003	0.99773	0.00003

A.2 Pin Power Benchmarks

Purpose: Measured relative pin powers from six B&W-1810 [25] critical experiments that are applicable to LWRs, flux spectra, and fuel materials are modeled with CE KENO. The pin power RMS and maximum differences from these experiments provide a basis for the accuracy of the CE KENO pin power calculations.

Description: The range of soluble boron concentrations, fuel enrichments, and fuel lattice geometries are listed in Table A-5. Pin powers percent differences are shown in Figure A-3 through Figure A-8. Figure A-8 summarizes RMS and max differences observed in pin power comparisons. In general, the RMS error across the central quarter of the assembly ranges from 0.46 to 0.95%, while the most extreme departures range from -2.08 to 2.58%. In most cases, the regions of highest misprediction are directly adjacent to the water hole locations. Although pin powers are predicted accurately in general, there is a noticeable shift in the predictions, to an average of about -1.0% at approximately 20 cm from the center of the lattice. The increase in pin power differences trends as a function of distance from the center of the core (of -0.02% per cm). Similar trends are also observed in deterministic code CASMO-5 [26]. Maximum pin power differences with the measurements are also observed at the same pin locations for both codes. Since CASMO-5 and CE KENO have different transport solvers (deterministic vs MC) and nuclear data processing (Bondarenko based vs continuous energy), missing model descriptions or measurement errors are considered to be possible causes for large pin power differences with measurements at some locations.

Table A-5 Critical Experiment Summary for B&W 1810

Core configuration	2.46 wt% rods	4.02 wt% rods	UO ₂ -Gd ₂ O ₃ rods	Similar fuel design	Boron concentration (ppm)
1	4,808	0	0	B&W 15 × 15	1,337.9
5	4,780	0	20	B&W 15 × 15	1,208.0
7	3,920	888	0	B&W 15 × 15	1,899.3
14	3,920	860	20	B&W 15 × 15	1,653.8
18	3,676	944	0	CE 16 × 16	1,776.8
20	3,676	912	20	CE 16 × 16	1,499.8

N/A							
-0.40%	-0.02%						
-0.56%	-0.45%	N/A					
0.24%	0.44%	0.42%	0.86%				
0.43%	0.51%	-0.23%	0.03%	N/A			
-0.84%	-0.84%	N/A	-0.10%	-0.08%	-0.23%		
-0.21%	-1.37%	0.54%	0.23%	0.11%	0.49%	0.08%	
-0.21%	0.17%	0.27%	0.14%	0.08%	0.00%	-0.07%	0.18%

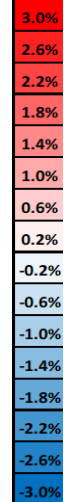


Figure A-3 B&W Core 1 Pin Power Differences for CE KENO

N/A							
-0.42%	0.59%						
0.18%	0.35%	N/A					
1.05%	-0.83%	-0.10%	0.35%				
-0.16%	0.34%	0.05%	-0.28%	N/A			
1.28%	-0.30%	N/A	0.49%	-0.96%	0.60%		
0.67%	0.24%	-0.32%	0.44%	0.02%	-0.47%	-0.15%	
1.01%	-0.14%	-0.32%	-0.23%	-0.38%	-0.38%	-0.06%	-0.23%

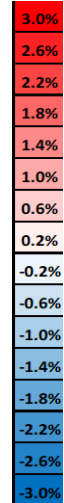


Figure A-4 B&W Core 5 Pin Power Differences for CE KENO

N/A								
-0.31%	-0.17%							
-0.35%	-0.82%	N/A						
0.42%	-0.06%	1.43%	0.39%					
-2.08%	-0.26%	0.39%	0.13%	N/A				
-0.75%	-0.02%	N/A	0.68%	-0.20%	1.05%			
-0.47%	-0.56%	1.52%	0.09%	0.22%	0.93%	-0.21%		
-0.42%	-0.43%	-1.32%	0.59%	0.04%	-0.62%	0.11%	-0.86%	

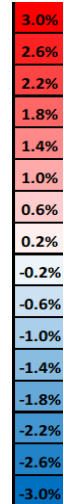


Figure A-5 B&W Core 12 Pin Power Differences for CE KENO

N/A								
-1.17%	-0.71%							
-0.47%	-0.95%	N/A						
-0.05%	-0.53%	0.79%	-0.05%					
-0.12%	-0.53%	0.88%	0.87%	N/A				
-0.64%	-1.17%	N/A	2.12%	0.11%	-0.01%			
0.47%	-1.81%	0.84%	0.90%	-0.26%	-0.40%	-0.36%		
-0.19%	0.27%	0.02%	0.88%	-0.24%	0.36%	-0.72%	0.17%	

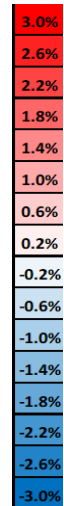


Figure A-6 B&W Core 14 Pin Power Differences for CE KENO

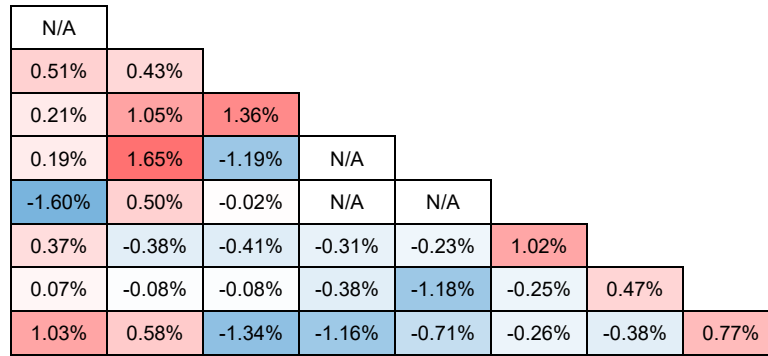


Figure A-7 B&W Core 18 Pin Power Differences for CE KENO

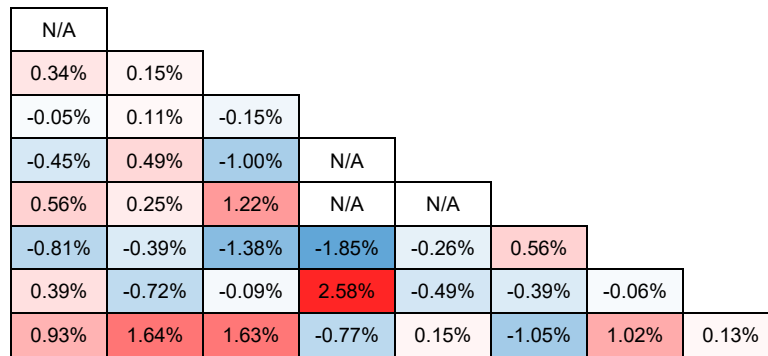


Figure A-8 B&W Core 20 Pin Power Differences for CE KENO

Table A-6 Critical Experiment Comparison for B&W 1810

Core	RMS Error	Max Error
1	0.46%	-1.37%
5	0.53%	1.28%
12	0.75%	-2.08%
14	0.80%	2.12%
18	0.78%	1.65%
20	0.95%	2.58%

A.3 Serpent k_{eff} Comparisons

Serpent MC code results are used in Test Suites 11 and 12 as reference solutions because of its extensive lattice physics edits. Both test suites employ nominal PWR and BWR lattices for testing. Table A-7 provides a comparison of k_{eff} results with CE KENO. As seen from the results, Serpent and CE KENO results agree well, less than 100 pcm for all cases except BWR 10×10 0% void (121 pcm).

Table A-7 Serpent and CE KENO k_{inf} Comparisons

Lattice	Nominal State	Serpent	sigma	CE KENO	sigma	Δk_{inf}
PWR 17×17	1300 ppm B	1.17253	4.70E-05	1.17289	9.90E-05	-36
BWR 10×10	0% Void	0.98326	7.20E-05	0.98205	9.90E-05	121
	40% Void	0.96260	7.40E-05	0.96181	9.90E-05	79
	70% Void	0.94200	7.40E-05	0.94147	9.90E-05	53
	90% Void	0.92732	7.20E-05	0.92688	1.00E-04	44

APPENDIX B 2D NUMERICAL BENCHMARK ASSESSMENT

B.1 Test Suite 1 – BOL LWR Assemblies Baseline

Purpose: Performance of the NEWT and Polaris lattice physics codes for common assembly designs is tested using BWR and PWR case matrices at BOL. The purpose of this test suite is to test code accuracies with respect to nominal operating state points for different lattice types. Pin powers and k_{inf} values are compared to CE KENO values.

Target Accuracy

- 200 pcm difference in k_{inf}
- 1% RMS and 1.5% max difference in pin power distribution for BWR lattices
- 0.5% RMS and 1.5% max difference in pin power distribution for PWR lattices

Acceptance Accuracy

- 400 pcm difference in k_{inf}
- 1.5% RMS and 2.5% max difference in pin power distribution for BWR and PWR lattices

B.1.1 BWR

Description: All assembly designs for different geometries and unique lattice types (e.g., axial natural enrichment blankets [NAT], dominant lattice [DOM], plenum lattice [PLE], vanished lattice [VAN], etc.) are listed in Table B-1. All assemblies are modeled with a wide gap on the north/west sides and a narrow gap on the south/east sides. OEM control blades are used for the assembly configurations with control blades. Different fuel assembly designs covered by this test suite are shown in Table B-1.

Table B-1 Test Suite BWR Assembly Geometries

Assembly design	Product line	Lattice type
8 × 8	GE9	DOM
9 × 9	GE11	DOM
10 × 10	GE14	DOM, VAN, PLE, NAT PSZ, N-V, N-T
10 × 10	SVEA-96	DOM
10 × 10	Atrium10	DOM

Each lattice type in Table B-1 is tested for configurations in which control blades are out (uncontrolled) and control blades are in (controlled) using the case matrix presented in Table B-2. State points in the case matrix are selected based on the branch cases used in cross section generation for PARCS/TRACE [27].

Table B-2 BWR Standard Case Matrix for Uncontrolled And Controlled Cases

Case number	TF (K) ¹	TC (K) ²	Void fraction (%)
1	293	293	0
2	500	293	0
3	950	293	0
4	500	560	0
5	500	560	40
6	500	560	70
7	500	560	90
8	950	560	0
9	950	560	40
10	950	560	70
11	950	560	90
12	1,500	560	0
13	1,500	560	40
14	1,500	560	70
15	1,500	560	90

¹ TF = fuel temperature

² TC = coolant temperature

Results: MG KENO, NEWT, and Polaris comparisons for uncontrolled and controlled cases are shown in Figure B-1 and Figure B-2, respectively. MG KENO cases were not run for 10 × 10 PSZ, N-V, and N-T cases.

The NEWT results are generally lower than the MG KENO results. MG KENO uses the same cross sections as NEWT, so the discrepancies between the MG KENO and NEWT results indicate a difference in the transport solutions. Mesh refinement studies show that NEWT results cannot be improved further by increasing spatial mesh. However, if angle mesh is refined beyond $S_n=16$ by using a product quadrature set, an improvement of more than 100 pcm is observed. Use of high-order product quadrature sets in current NEWT is not practical due to long run times.

Similar trends with respect to void fraction and coolant temperature (cases 1, 2, and 3) are observed across all lattice types. This bias is believed to be the result of insufficient treatment of MG cross sections in the unresolved resonance energy range.

Although there is a consistent bias between NEWT and Polaris results for uncontrolled cases, this bias diminishes for controlled cases except in natural enrichment zones (NAT, N-T, N-V).

Biases in k_{inf} with respect to coolant void fractions at different fuel temperatures (cases 4–15) can be seen in Figure B-3 for GE14-DOM lattice. Consistent void trend (0%, 40%, 70%, 90%) and control blade biases are observed for all fuel temperatures.

The results presented in Figure B-1 and Figure B-2 are summarized statistically in Table B-3 through Table B-5 for MG KENO, NEWT, and Polaris, respectively. The mean, min, and max differences in k_{inf} are presented for each lattice type. The mean results for NEWT are consistently low by ~100–200 pcm. The largest k_{inf} differences (~400 pcm low) are observed for the NEWT cases for uncontrolled GE14 NAT and 8×8 lattices at HFP conditions.

The general void trend and biases observed in natural enrichment zones are being investigated and are expected to be resolved with improvements in cross section processing.

NEWT and Polaris pin power distributions are compared to CE KENO reference pin power distributions for selected lattices at different void fractions. Differences between CE KENO pin powers and the other two codes are presented in Figure B-4 through Figure B-12. While the largest pin power differences occur at the wide-wide corner, gadolinia rods exhibit larger differences compared to the rest of the fuel rods. When control blades are inserted (Figure B-6), the largest pin power difference shifts to the narrow-narrow corner, and pin power differences are reduced overall. The Polaris maximum pin power difference (1.71%) for 10×10 DOM lattice exhibits the largest difference of all the sampled lattices. This value fails the target accuracy criteria, but it passes the acceptance accuracy criteria and will be investigated further.

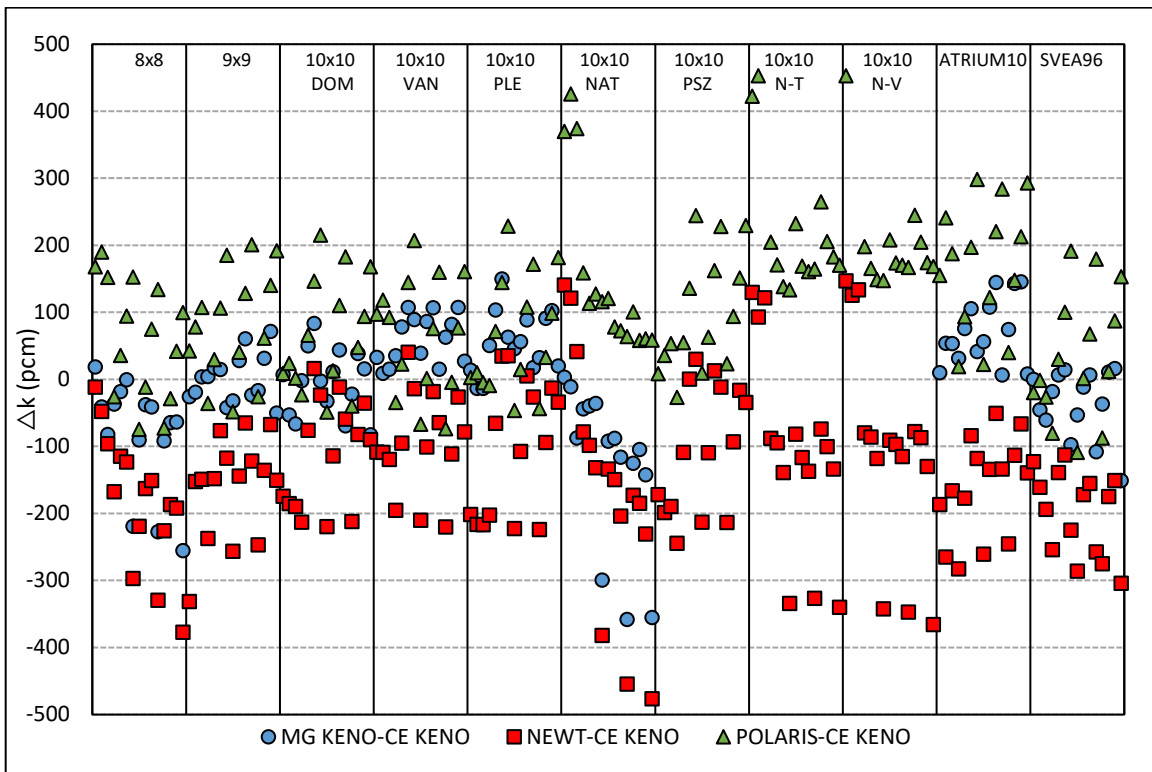


Figure B-1 Test Suite 1: BWR k_{inf} Comparisons for Uncontrolled Cases

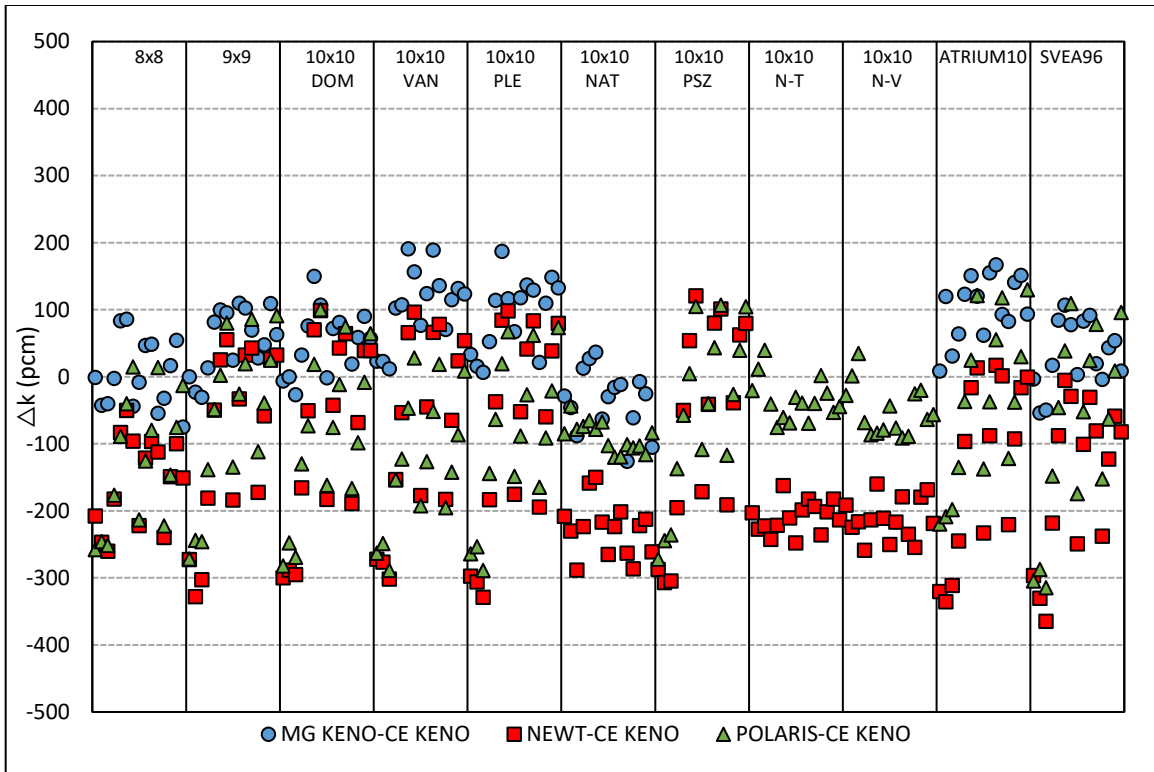


Figure B-2 Test Suite 1: BWR k_{inf} Comparisons for Controlled Cases

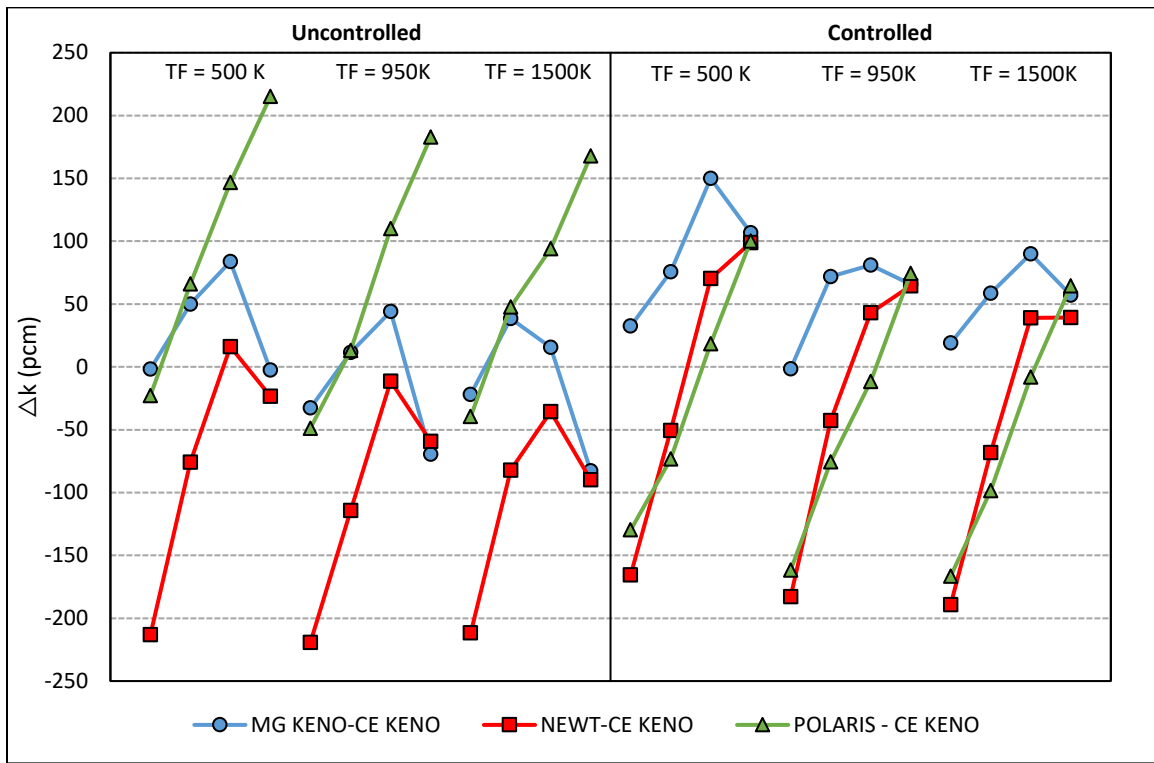


Figure B-3 Test Suite 1: Void Fraction Trend for GE14-DOM Lattice

Table B-3 BWR Standard Case Matrix MG KENO k_{inf} (pcm) Statistics

Lattice	Uncontrolled				Controlled			
	σ	mean	max	min	σ	mean	max	min
8 × 8	84	-83	19	-256	52	2	86	-75
9 × 9	36	2	72	-50	49	52	109	-31
10 × 10 - DOM	47	-3	84	-83	48	52	150	-27
10 × 10 - VAN	36	60	108	9	56	-35	16	-151
10 × 10 - PLE	47	54	150	-13	55	93	187	7
10 × 10 - NAT	118	-126	3	-358	47	-35	37	-126
ATRIUM10	49	71	145	7	48	104	167	9
SVEA-96	51	-35	16	-151	50	32	107	-54

Table B-4 BWR Standard Case Matrix NEWT Δk_{inf} (pcm) Statistics

Lattice	Uncontrolled				Controlled			
	σ	mean	max	min	σ	mean	max	min
8 × 8	100	-180	-12	-377	67	-155	-50	-260
9 × 9	76	-160	-65	-331	133	-89	55	-303
10 × 10 - DOM	80	-109	16	-219	144	-82	99	-300
10 × 10 - VAN	74	-95	41	-220	141	-199	-113	-304
10 × 10 - PLE	102	-103	35	-224	155	-81	98	-329
10 × 10 - NAT	182	-159	141	-476	41	-227	-150	-288
ATRIUM10	74	-161	-51	-282	133	-130	17	-336
SVEA-96	63	-199	-113	-304	119	-153	-6	-365

Table B-5 BWR Standard Case Matrix Polaris Δk_{inf} (pcm) Statistics

Lattice	Uncontrolled				Controlled			
	σ	mean	max	min	σ	mean	max	min
8 × 8	89	62	190	-75	98	-127	15	-258
9 × 9	81	80	201	-48	123	-64	91	-272
10 × 10 - DOM	84	65	215	-49	125	-84	100	-282
10 × 10 - VAN	87	65	207	-74	102	33	191	-109
10 × 10 - PLE	87	64	229	-46	121	-89	73	-289
10 × 10 - NAT	127	153	426	58	22	-90	-44	-120
ATRIUM10	121	239	510	134	32	-34	40	-76
SVEA-96	89	98	245	-27	128	-56	107	-272

NEWT 0% Void (RMS=0.40%, MAX=0.98%)

0.95%	0.83%	0.55%	0.36%	0.47%	0.20%	0.55%	0.32%	0.65%	0.98%
0.83%	0.16%	-0.30%	0.03%	-0.18%	-0.12%	-0.47%	-0.04%	-0.36%	0.30%
0.55%	-0.30%	-0.20%	-0.85%	-0.16%	-0.41%	-0.10%	-0.74%	-0.11%	-0.05%
0.36%	0.03%	-0.85%	-0.02%	-0.22%	N/A	N/A	-0.07%	-0.39%	0.07%
0.47%	-0.18%	-0.16%	-0.22%	0.61%	N/A	N/A	-0.16%	-0.27%	0.01%
0.20%	-0.12%	-0.41%	N/A	N/A	0.43%	-0.08%	-0.51%	-0.13%	0.02%
0.55%	-0.47%	-0.10%	N/A	N/A	-0.08%	-0.31%	-0.14%	-0.53%	-0.04%
0.32%	-0.04%	-0.74%	-0.07%	-0.16%	-0.51%	-0.14%	-0.62%	-0.07%	0.07%
0.65%	-0.36%	-0.11%	-0.39%	-0.27%	-0.13%	-0.53%	-0.07%	-0.17%	0.33%
0.98%	0.30%	-0.05%	0.07%	0.01%	0.02%	-0.04%	0.07%	0.33%	0.62%

2.0%
1.8%
1.6%
1.4%
1.2%
1.0%
0.8%
0.6%
0.4%
0.2%
0.0%
-0.2%
-0.4%
-0.6%
-0.8%
-1.0%
-1.2%
-1.4%
-1.6%
-1.8%
-2.0%

Polaris 0% Void (RMS=0.32%, MAX=1.07%)

1.07%	0.71%	0.14%	-0.25%	-0.31%	-0.48%	-0.15%	-0.10%	0.36%	1.00%
0.71%	0.39%	-0.01%	0.13%	0.00%	-0.11%	-0.29%	-0.02%	-0.06%	0.11%
0.14%	-0.01%	-0.12%	-0.38%	-0.16%	-0.21%	-0.11%	-0.49%	-0.07%	-0.15%
-0.25%	0.13%	-0.38%	0.01%	0.03%	N/A	N/A	0.10%	-0.12%	-0.10%
-0.31%	0.00%	-0.16%	0.03%	0.70%	N/A	N/A	0.04%	-0.08%	-0.16%
-0.48%	-0.11%	-0.21%	N/A	N/A	0.70%	0.11%	-0.27%	-0.11%	-0.12%
-0.14%	-0.29%	-0.11%	N/A	N/A	0.11%	0.10%	-0.10%	-0.21%	-0.19%
-0.10%	-0.02%	-0.49%	0.10%	0.04%	-0.27%	-0.10%	-0.24%	-0.05%	0.01%
0.36%	-0.06%	-0.06%	-0.11%	-0.08%	-0.11%	-0.21%	-0.05%	0.24%	0.32%
1.00%	0.11%	-0.14%	-0.10%	-0.16%	-0.12%	-0.19%	0.01%	0.32%	0.77%

2.0%
1.8%
1.6%
1.4%
1.2%
1.0%
0.8%
0.6%
0.4%
0.2%
0.0%
-0.2%
-0.4%
-0.6%
-0.8%
-1.0%
-1.2%
-1.4%
-1.6%
-1.8%
-2.0%

Figure B-4 Test Suite 1: 10 × 10 DOM Zone Pin Power Differences at 0% Void Fraction for NEWT and Polaris

NEWT 40% Void (RMS=0.37%, MAX=0.90%)

0.84%	0.90%	0.64%	0.51%	0.45%	0.30%	0.37%	0.21%	0.87%	0.78%
0.90%	0.30%	-0.05%	-0.02%	-0.31%	-0.08%	-0.23%	-0.02%	0.01%	0.35%
0.64%	-0.05%	-0.13%	-0.49%	-0.14%	-0.40%	-0.08%	-0.59%	-0.12%	0.06%
0.51%	-0.02%	-0.49%	-0.13%	-0.35%	N/A	N/A	-0.19%	-0.43%	0.08%
0.45%	-0.31%	-0.14%	-0.35%	0.04%	N/A	N/A	-0.37%	-0.22%	-0.12%
0.30%	-0.08%	-0.40%	N/A	N/A	-0.01%	-0.03%	-0.36%	-0.14%	-0.19%
0.37%	-0.23%	-0.08%	N/A	N/A	-0.03%	-0.44%	-0.20%	-0.43%	-0.23%
0.21%	-0.02%	-0.59%	-0.19%	-0.37%	-0.36%	-0.20%	-0.60%	-0.05%	0.03%
0.87%	0.01%	-0.12%	-0.43%	-0.22%	-0.14%	-0.43%	-0.05%	-0.26%	0.19%
0.78%	0.35%	0.06%	0.08%	-0.12%	-0.19%	-0.23%	0.03%	0.19%	0.52%

2.0%
1.8%
1.6%
1.4%
1.2%
1.0%
0.8%
0.6%
0.4%
0.2%
0.0%
-0.2%
-0.4%
-0.6%
-0.8%
-1.0%
-1.2%
-1.4%
-1.6%
-1.8%
-2.0%

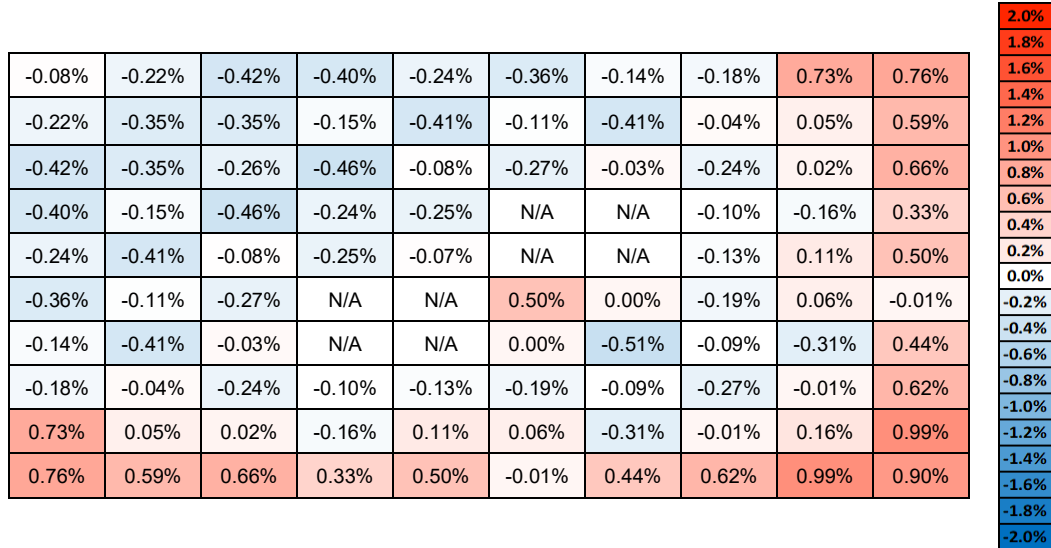
Polaris 40% Void (RMS=0.26 %, MAX=0.84%)

0.84%	0.67%	0.11%	-0.10%	-0.36%	-0.31%	-0.32%	-0.19%	0.51%	0.75%
0.67%	0.45%	0.18%	0.00%	-0.16%	-0.08%	-0.08%	-0.03%	0.23%	0.14%
0.11%	0.18%	-0.07%	-0.09%	-0.17%	-0.14%	-0.10%	-0.32%	-0.09%	-0.02%
-0.10%	0.00%	-0.09%	-0.10%	0.05%	N/A	N/A	0.00%	-0.17%	-0.01%
-0.36%	-0.16%	-0.16%	0.05%	0.17%	N/A	N/A	-0.09%	-0.10%	-0.18%
-0.30%	-0.08%	-0.14%	N/A	N/A	0.32%	0.19%	-0.08%	-0.13%	-0.22%
-0.32%	-0.08%	-0.10%	N/A	N/A	0.19%	0.04%	-0.16%	-0.13%	-0.31%
-0.18%	-0.03%	-0.31%	0.00%	-0.09%	-0.08%	-0.16%	-0.23%	-0.03%	0.05%
0.52%	0.24%	-0.09%	-0.17%	-0.10%	-0.13%	-0.13%	-0.03%	0.07%	0.18%
0.76%	0.15%	-0.02%	-0.01%	-0.18%	-0.22%	-0.31%	0.05%	0.18%	0.66%

2.0%
1.8%
1.6%
1.4%
1.2%
1.0%
0.8%
0.6%
0.4%
0.2%
0.0%
-0.2%
-0.4%
-0.6%
-0.8%
-1.0%
-1.2%
-1.4%
-1.6%
-1.8%
-2.0%

Figure B-5 Test Suite 1: 10 × 10 DOM Zone Pin Power Differences at 40% Void Fraction for NEWT and Polaris

NEWT 40% Void (Controlled, RMS=0.37%, MAX=0.99%)



Polaris 40% Void (Controlled, RMS=0.43%, MAX=1.71%)

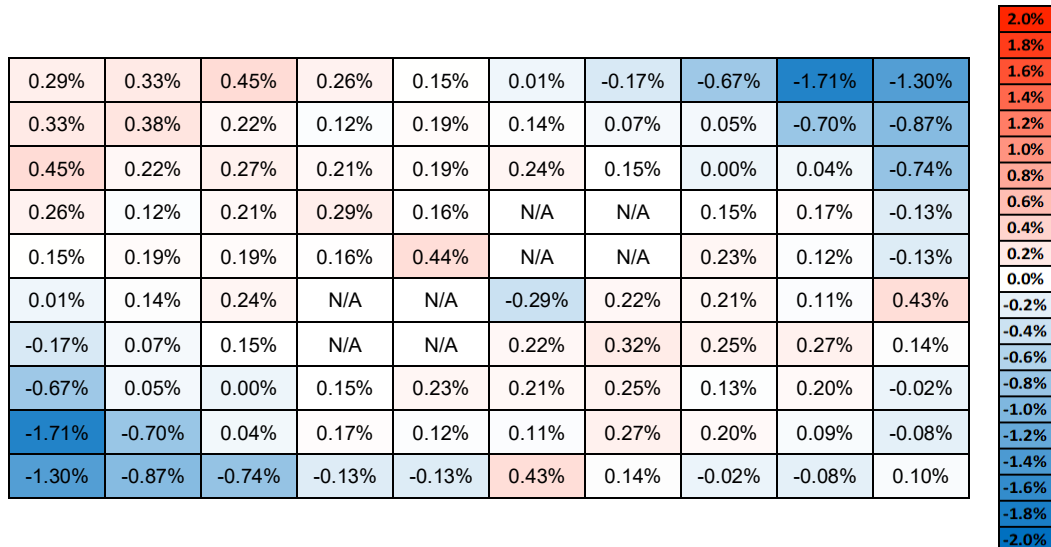
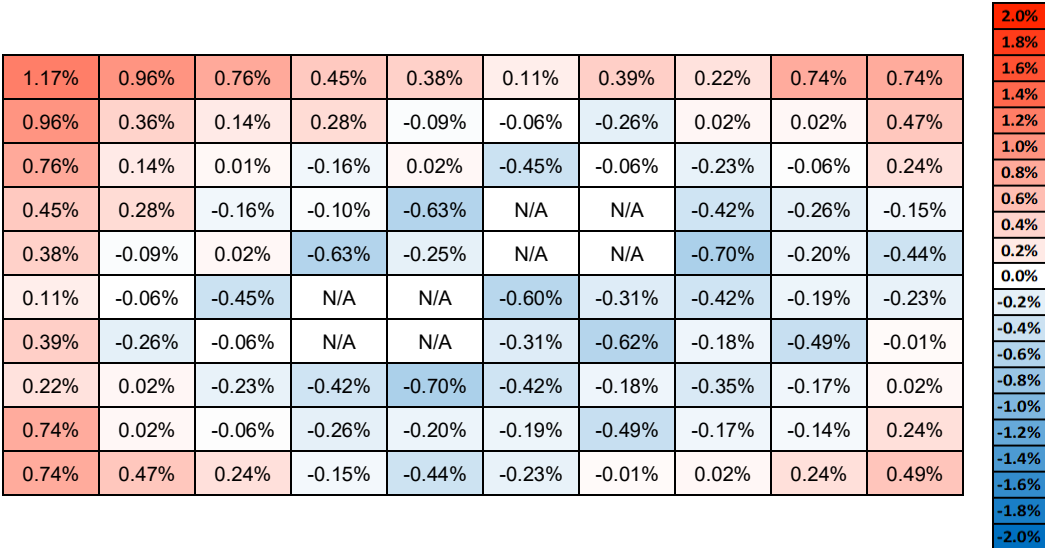


Figure B-6 Test Suite 1: 10 × 10 DOM Zone Pin Power Differences at 40% Void Fraction for NEWT and Polaris Controlled Cases

NEWT 70% Void (RMS=0.40%, MAX=1.17%)



Polaris 70% Void (RMS=0.23%, MAX=0.96%)

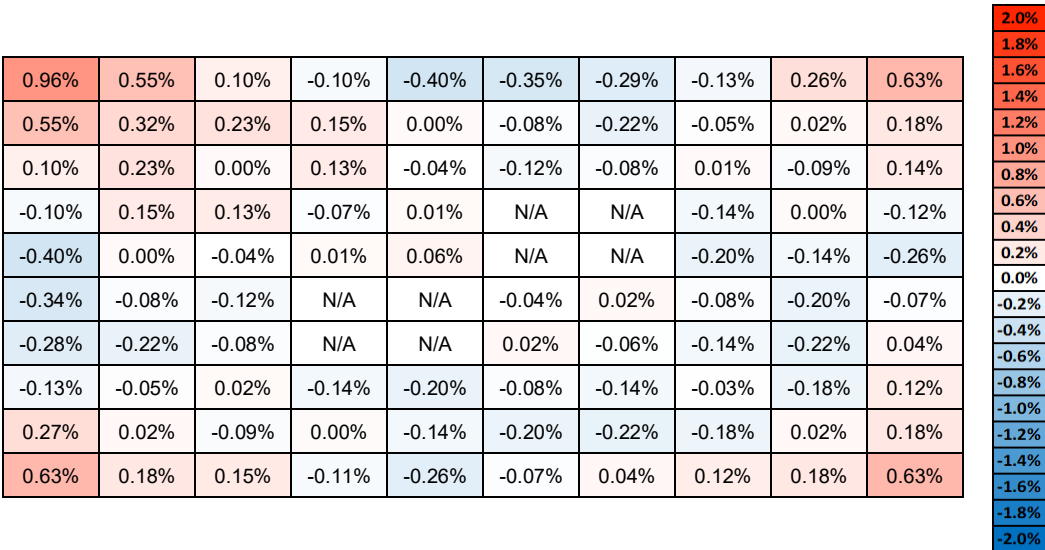


Figure B-7 Test Suite 1: 10 × 10 DOM Zone Pin Power Differences at 70% Void Fraction for NEWT and Polaris

NEWT 90% (RMS=0.54%, MAX=1.15%)

1.09%	1.15%	0.95%	0.36%	0.56%	-0.13%	0.32%	0.37%	0.95%	0.71%
1.15%	0.82%	0.34%	0.37%	-0.06%	-0.09%	-0.01%	0.10%	0.79%	0.96%
0.95%	0.34%	-0.07%	-0.14%	0.05%	-0.47%	-0.06%	-0.29%	0.07%	0.25%
0.36%	0.37%	-0.14%	-0.20%	-1.10%	N/A	N/A	-0.62%	-0.28%	-0.22%
0.56%	-0.06%	0.05%	-1.10%	-0.50%	N/A	N/A	-1.04%	-0.07%	-0.64%
-0.13%	-0.09%	-0.47%	N/A	N/A	-1.01%	-0.63%	-0.68%	-0.15%	-0.50%
0.32%	-0.01%	-0.06%	N/A	N/A	-0.63%	-0.73%	-0.25%	-0.35%	-0.35%
0.37%	0.10%	-0.29%	-0.62%	-1.04%	-0.68%	-0.25%	-0.40%	-0.10%	-0.25%
0.95%	0.79%	0.07%	-0.28%	-0.07%	-0.15%	-0.35%	-0.10%	0.22%	0.42%
0.71%	0.96%	0.25%	-0.22%	-0.64%	-0.50%	-0.35%	-0.25%	0.42%	0.36%

2.0%
1.8%
1.6%
1.4%
1.2%
1.0%
0.8%
0.6%
0.4%
0.2%
0.0%
-0.2%
-0.4%
-0.6%
-0.8%
-1.0%
-1.2%
-1.4%
-1.6%
-1.8%
-2.0%

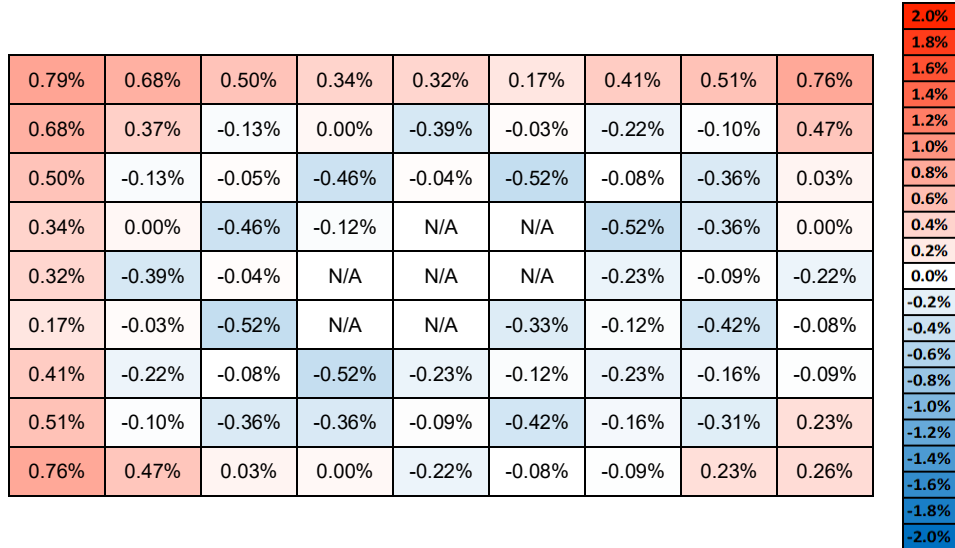
Polaris 90% (RMS=0.19%, MAX=0.57%)

0.57%	0.42%	0.12%	-0.05%	-0.09%	-0.26%	-0.29%	0.06%	0.24%	0.37%
0.42%	0.35%	0.22%	0.13%	0.03%	-0.18%	-0.07%	-0.15%	0.41%	0.37%
0.12%	0.22%	-0.21%	0.16%	-0.08%	0.05%	-0.14%	-0.04%	-0.09%	0.11%
-0.05%	0.13%	0.16%	-0.22%	-0.02%	N/A	N/A	-0.13%	0.02%	-0.01%
-0.09%	0.03%	-0.09%	-0.02%	0.12%	N/A	N/A	-0.17%	-0.04%	-0.07%
-0.26%	-0.18%	0.05%	N/A	N/A	-0.09%	-0.08%	-0.16%	-0.23%	-0.04%
-0.29%	-0.07%	-0.14%	N/A	N/A	-0.08%	-0.09%	-0.25%	-0.08%	-0.13%
0.06%	-0.15%	-0.04%	-0.14%	-0.17%	-0.16%	-0.25%	-0.14%	-0.22%	-0.08%
0.23%	0.40%	-0.10%	0.02%	-0.04%	-0.23%	-0.08%	-0.22%	0.06%	0.17%
0.37%	0.36%	0.10%	-0.02%	-0.07%	-0.04%	-0.13%	-0.08%	0.17%	0.32%

2.0%
1.8%
1.6%
1.4%
1.2%
1.0%
0.8%
0.6%
0.4%
0.2%
0.0%
-0.2%
-0.4%
-0.6%
-0.8%
-1.0%
-1.2%
-1.4%
-1.6%
-1.8%
-2.0%

Figure B-8 Test Suite 1: 10 × 10 DOM Zone Pin Power Differences at 90% Void Fraction for NEWT and Polaris

NEWT 40% (RMS= 0.34%, MAX=0.79%)



Polaris 40% (RMS= 0.13%, MAX=0.35%)

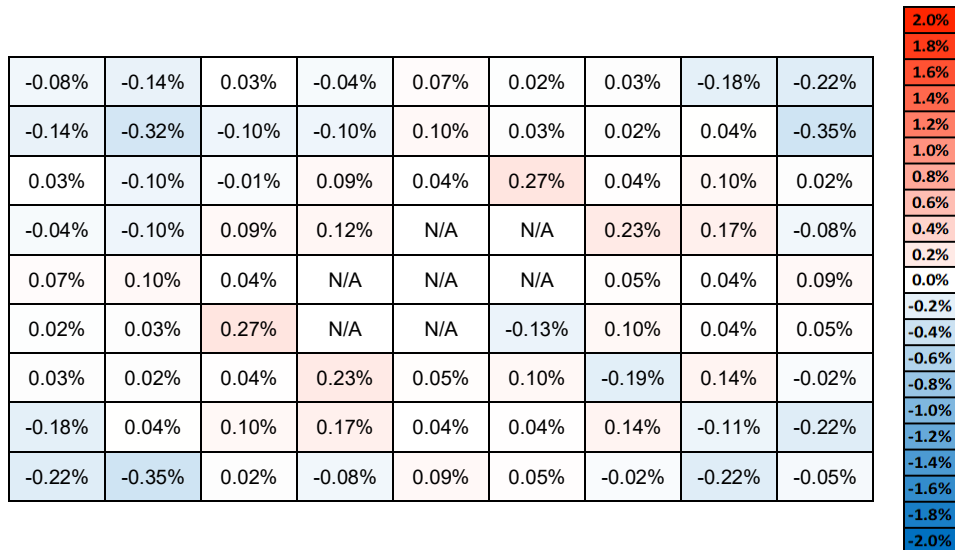


Figure B-9 Test Suite 1: 9 × 9 DOM Zone Pin Power Differences at 40% Void Fraction for NEWT and Polaris

NEWT 40% (RMS=0.37%, MAX=1.00%)

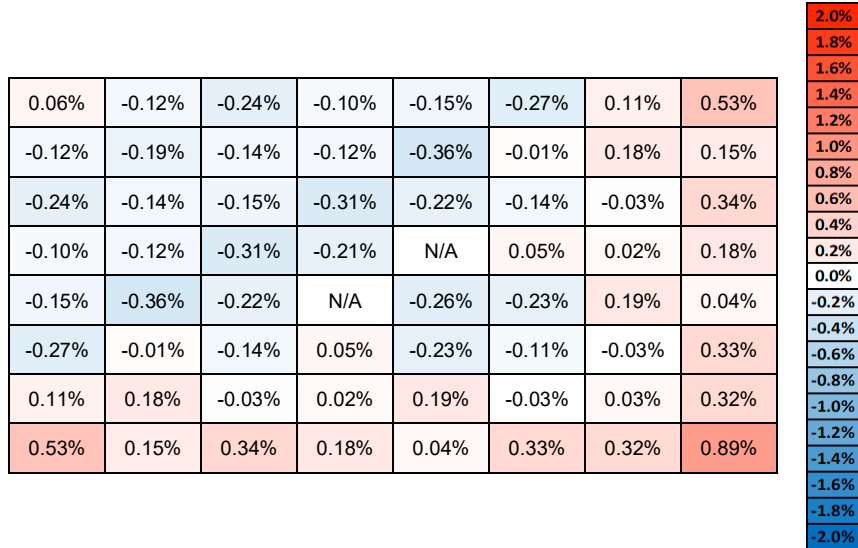


Polaris 40% (RMS=0.11%, MAX=0.28%)



Figure B-10 Test Suite 1: 8 × 8 DOM Zone Pin Power Differences at 40% Void Fraction for NEWT and Polaris

NEWT 40% (Controlled, RMS=0.24%, MAX=0.89%)



Polaris 40% (Controlled, RMS=0.34%, MAX=1.23%)

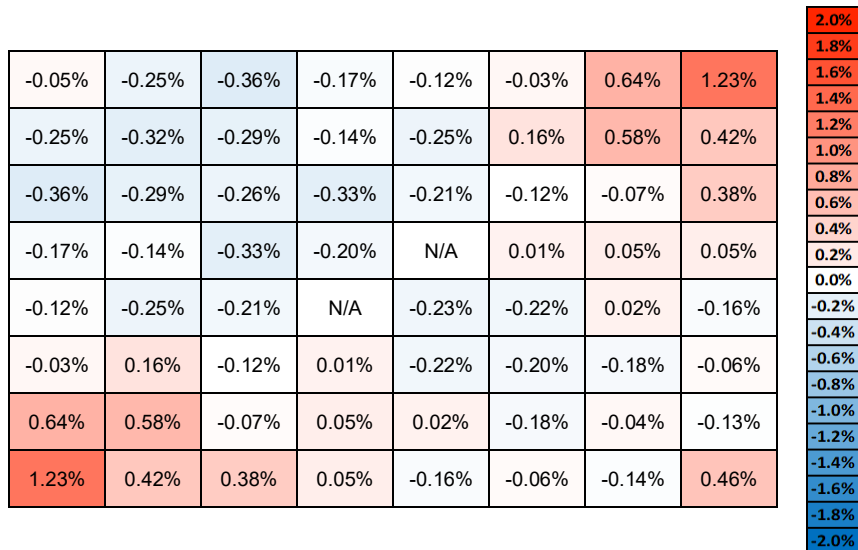
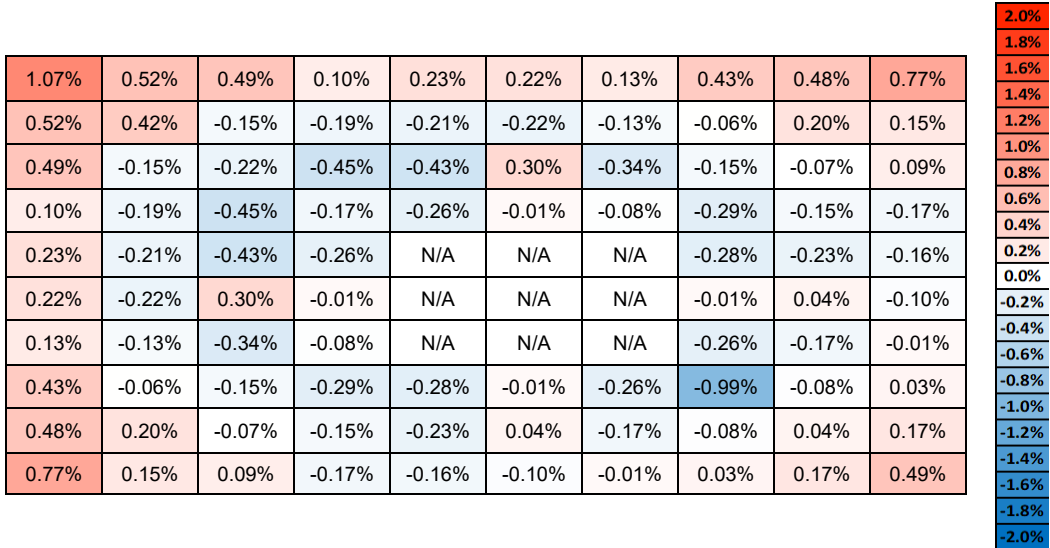


Figure B-11 Test Suite 1: 8 × 8 DOM Zone Pin Power Differences at 40% Void Fraction for NEWT and Polaris Controlled Cases

NEWT 40% (RMS= 0.31%, MAX=1.07%)



Polaris 40% (RMS= 0.18%, MAX=0.94%)

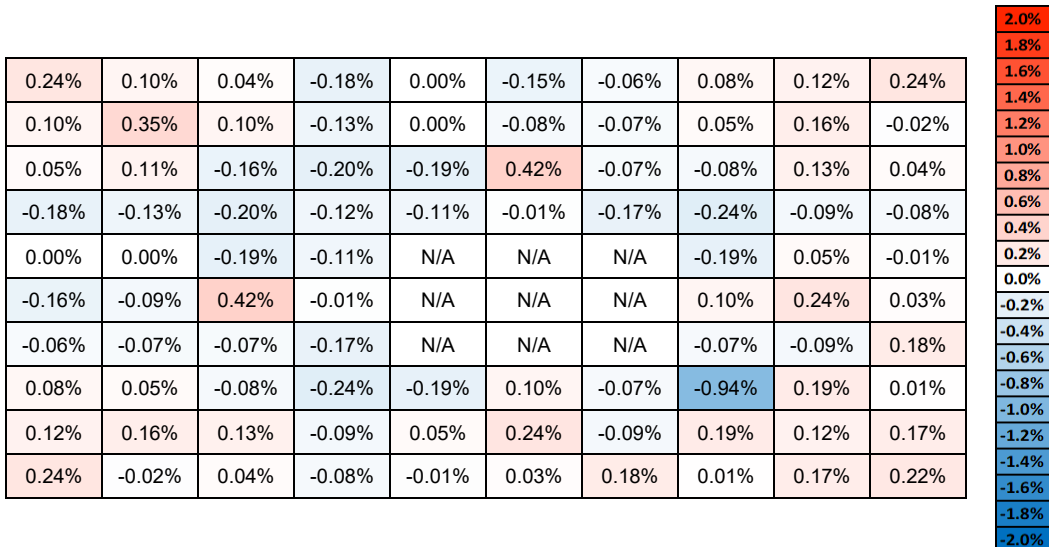


Figure B-12 Test Suite 1: ATRIUM10 DOM Zone Pin Power Differences at 40% void Fraction for NEWT

B.1.2 PWR

Description: PWR assembly designs for this test suite are selected based on their unique geometries and prevalence in industry. Each assembly design (Table B-6) is tested using the test matrix listed in Table B-7. The case matrix is intended to capture the effect of changes in moderator temperature, fuel temperature, and boron concentrations. To capture any biases or trends, case matrix values are selected beyond their expected ranges during regular reactor operations (e.g., TF = 1,773 K vs TF = 1,500 K for PWR case matrix used in cross section generation)

Table B-6 Test Suite 1: PWR Assembly Geometries

Assembly design	Product line
14 × 14	Westinghouse (WE) Standard
15 × 15	WE Standard
16 × 16	Combustion Engineering
17 × 17	WE Standard
17 × 17	WE OFA
18 × 18	Westinghouse

Table B-7 PWR Standard Case Matrix for Uncontrolled And Controlled Cases

Case number	TF (K)	TC (K)	PC (ppm)
1	293	293	0
2	293	293	1,000
3	293	293	1,300
4	293	293	2,000
5	293	293	2,500
6	560	560	0
7	560	560	1,000
8	560	560	1,300
9	560	560	2,000
10	560	560	2,500
11	900	550	1,300
12	900	560	1,300
13	900	600	1,300
14	1,773	560	1,300

Results: Comparison of MG KENO, NEWT and Polaris k_{inf} differences for uncontrolled cases are shown in Figure B-13 and are shown in Figure B-14 for controlled cases.

MG KENO results for 16×16 CE design display some outliers that are believed to be due to Dancoff factors. When the boron concentration is increased, it hardens the spectrum and changes the Dancoff factors around the large water rods. The MG KENO and NEWT results are consistent for uncontrolled cases in general, while Polaris results are higher. Trends are easily identifiable when both Polaris and NEWT are low for the controlled cases. Improvements are being made to MG cross section processing to help show the trends and biases observed in the PWR cases.

To show the effect of increasing boron concentration on k_{inf} differences, boron concentration variations for 293 K cold and 560 K hot zero power (HZP) cases (cases 1–5 and 6–10) are plotted in Figure B-15 and Figure B-16 for uncontrolled and controlled cases, respectively.

Statistics for MG KENO, NEWT, and Polaris k_{inf} differences are presented in Table B-8 through Table B-10. Polaris and NEWT results show similar means and standard deviations for the controlled cases. The largest k_{inf} differences are observed at zero boron concentration cases.

Pin power differences for each set of lattice types are presented in Figure B-17 through Figure B-22. While edge rods exhibit larger-than-average differences, the largest differences for the uncontrolled cases are observed around guide tubes for all lattice types. For the controlled case shown in Figure B-18, the largest differences are shifted to corner pins.

Based on the trend in k_{inf} differences, the largest pin power difference is expected in 16×16 CE lattice types due to the large guide tubes in the design. However, pin power differences are given below 1.5% for 16×16 CE lattice (Figure B-21).

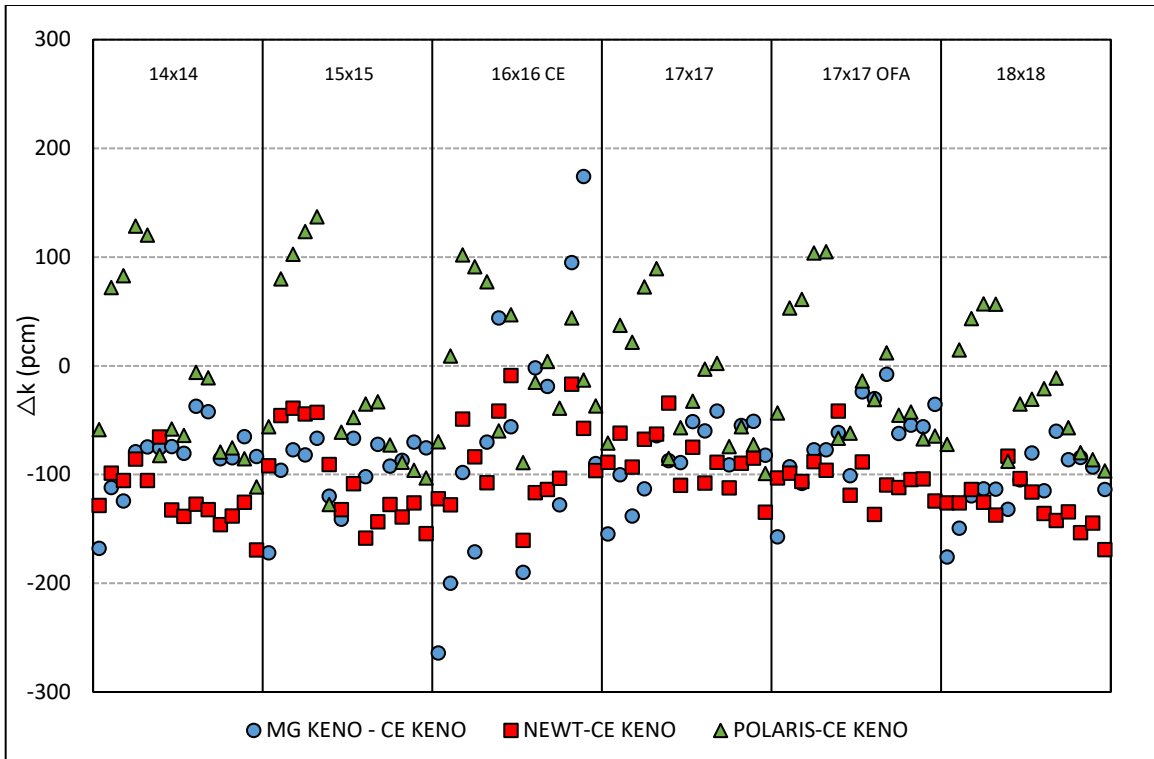


Figure B-13 Test Suite 1: PWR k_{inf} Comparisons for Uncontrolled Cases

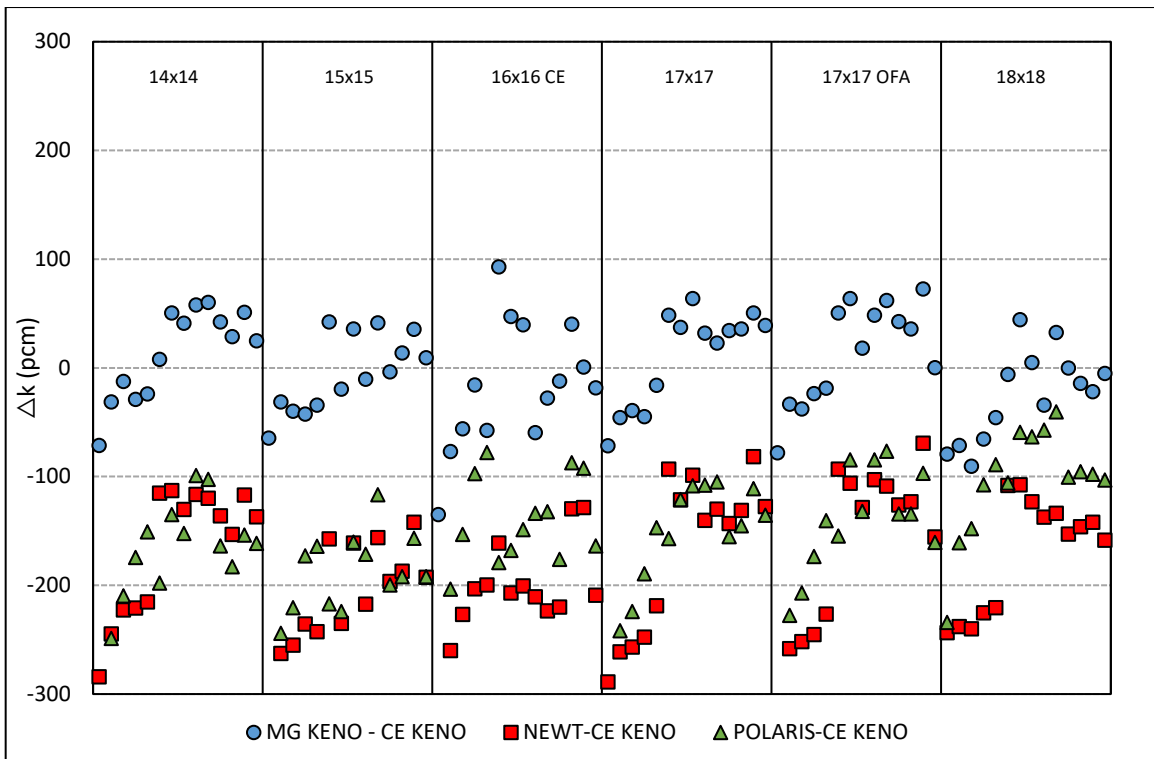


Figure B-14 Test Suite 1: PWR k_{inf} Comparisons for Controlled Cases

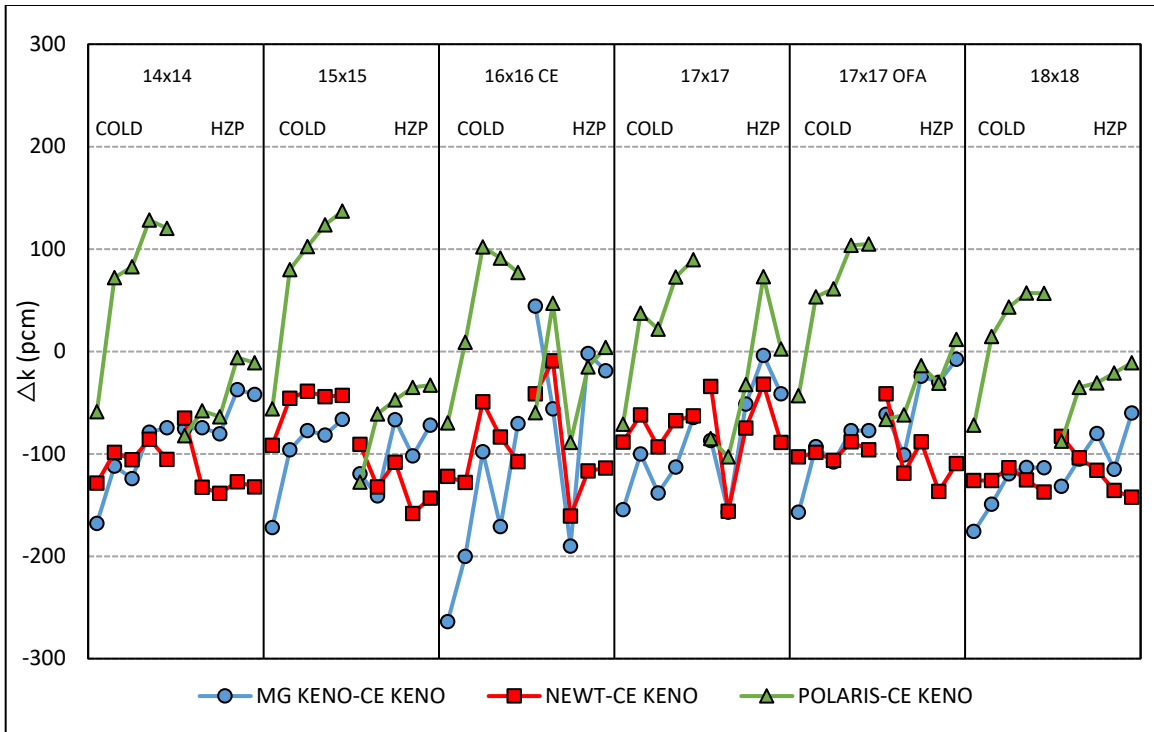


Figure B-15 Test Suite 1: Effect of Boron Concentration on k_{inf} Differences for Uncontrolled Cases

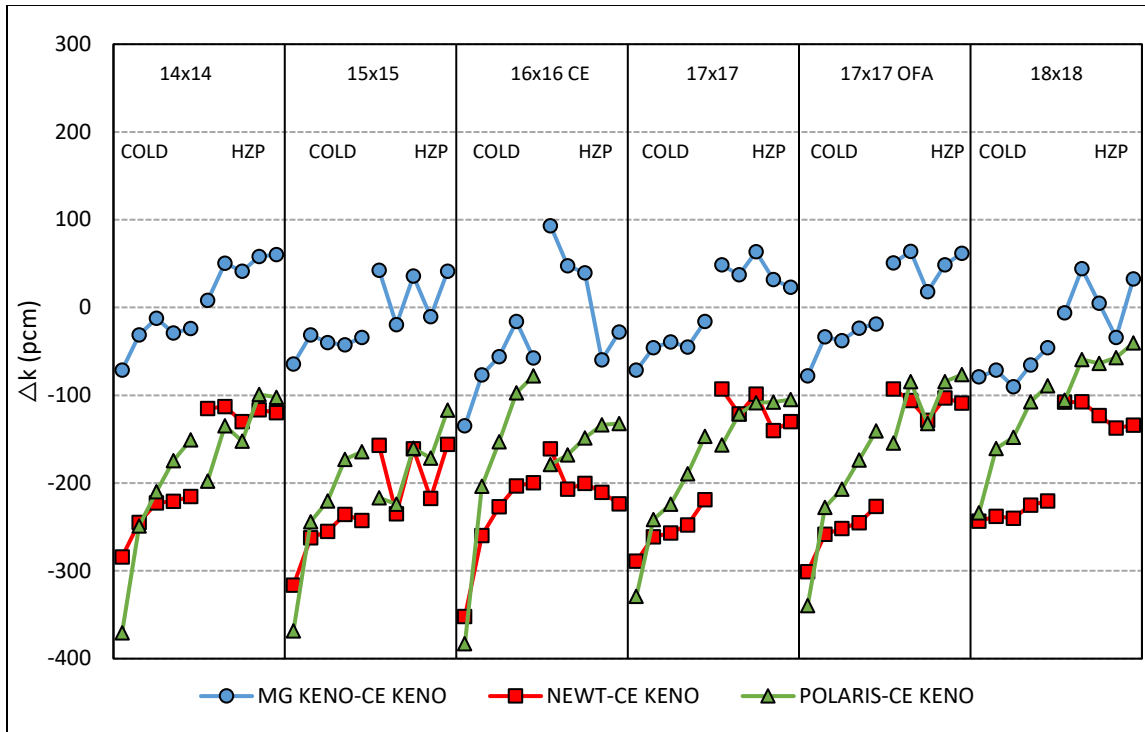


Figure B-16 Test Suite 1: Effect of Boron Concentration on k_{inf} Differences for Controlled Cases

Table B-8 PWR Standard Case Matrix MG KENO Δk_{inf} (pcm) Statistics

Lattice	Uncontrolled				Controlled			
	σ	mean	max	min	σ	mean	max	min
14 × 14	33	-85	-37	-168	41	14	60	-71
15 × 15	31	-94	-67	-172	35	-5	42	-65
16 × 16 CE	121	-70	174	-264	59	-17	93	-135
17 × 17	34	-84	-42	-155	44	10	64	-72
17 × 17 OFA	39	-68	-8	-157	47	14	73	-78
18 × 18	30	-110	-60	-176	41	-25	44	-90

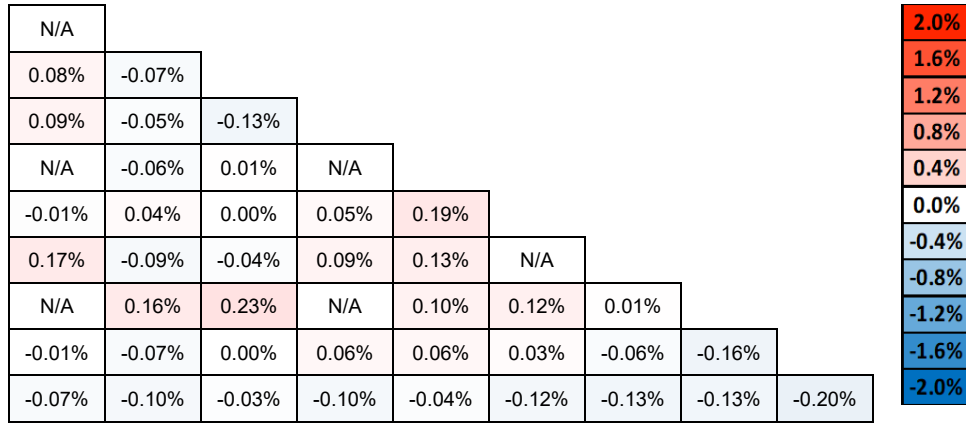
Table B-9 PWR Standard Case Matrix NEWT Δk_{inf} (pcm) Statistics

Lattice	Uncontrolled				Controlled			
	σ	mean	max	min	σ	mean	max	min
14 × 14	27	-121	-65	-169	58	-166	-113	-284
15 × 15	44	-103	-39	-158	50	-211	-142	-317
16 × 16 CE	45	-86	-9	-161	55	-209	-128	-352
17 × 17	25	-87	-34	-135	71	-167	-82	-289
17 × 17 OFA	22	-102	-42	-137	76	-164	-69	-301
18 × 18	21	-129	-83	-169	52	-170	-107	-244

Table B-10 PWR Standard Case Matrix Polaris Δk_{inf} (pcm) Statistics

Lattice	Uncontrolled				Controlled			
	σ	mean	max	min	σ	mean	max	min
14 × 14	83	-16	128	-111	68	-179	-99	-371
15 × 15	90	-20	137	-128	59	-200	-117	-369
16 × 16 CE	61	4	102	-89	76	-157	-78	-383
17 × 17	61	-23	90	-99	64	-163	-105	-329
17 × 17 OFA	63	-7	105	-67	70	-153	-77	-340
18 × 18	55	-29	57	-97	50	-104	-40	-234

NEWT (RMS= 0.10%, MAX=0.23%)



Polaris (RMS= 0.07%, MAX=0.19%)

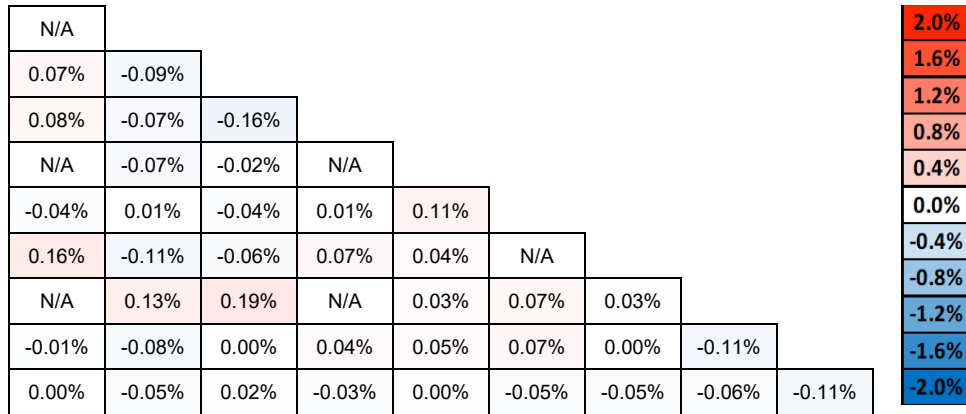


Figure B-17 Test Suite 1: 17 × 17 Lattice Pin Power Differences at Nominal Conditions for NEWT (top) and Polaris (bottom)

NEWT (Controlled, RMS=0.22%, MAX=0.54%)

N/A										2.0%
0.13%	-0.07%									1.6%
-0.14%	-0.03%	0.06%								1.2%
N/A	-0.10%	-0.27%	N/A							0.8%
-0.46%	-0.08%	-0.15%	-0.26%	-0.09%						0.4%
-0.05%	-0.16%	-0.12%	-0.36%	-0.10%	N/A					0.0%
N/A	-0.21%	-0.28%	N/A	-0.18%	-0.03%	0.20%				-0.4%
0.00%	-0.11%	-0.02%	-0.06%	0.23%	0.38%	0.29%	0.45%			-0.8%
0.07%	0.09%	0.12%	0.07%	0.01%	0.35%	0.27%	0.38%	0.54%		-1.2%
										-1.6%
										-2.0%

Polaris (Controlled, RMS=0.11%, MAX=0.27%)

N/A										2.0%
-0.03%	-0.07%									1.6%
-0.03%	0.08%	0.26%								1.2%
N/A	0.08%	-0.01%	N/A							0.8%
-0.27%	0.11%	0.10%	0.00%	0.20%						0.4%
0.08%	0.01%	0.04%	-0.20%	0.08%	N/A					0.0%
N/A	-0.10%	-0.19%	N/A	-0.11%	-0.07%	-0.02%				-0.4%
0.20%	-0.03%	0.02%	-0.10%	0.16%	0.19%	0.06%	0.01%			-0.8%
0.00%	0.05%	0.01%	-0.10%	-0.14%	0.03%	-0.07%	-0.07%	0.06%		-1.2%
										-1.6%
										-2.0%

Figure B-18 Test Suite 1: 17 × 17 Lattice Pin Power Differences at Nominal Controlled Conditions for NEWT (top) and Polaris (bottom)

NEWT (Controlled, RMS=0.58%, MAX=1.20%)

-1.10%	-0.67%	-0.50%	-0.59%	-0.52%	-0.30%	-0.50%	-0.78%	-0.37%	-0.33%	-0.46%	-0.79%	-0.74%	-1.00%	2.0%
-0.67%	-0.08%	0.31%	0.03%	0.04%	0.25%	0.10%	-0.05%	0.42%	0.02%	0.15%	0.10%	-0.32%	-0.86%	1.6%
-0.50%	0.31%	N/A	0.64%	0.80%	N/A	0.56%	0.45%	N/A	0.69%	0.90%	N/A	0.39%	-0.62%	1.2%
-0.59%	0.03%	0.64%	0.85%	1.20%	0.76%	0.05%	0.01%	0.78%	1.08%	1.04%	0.86%	0.18%	-0.39%	0.8%
-0.52%	0.04%	0.80%	1.20%	N/A	0.28%	-0.38%	-0.14%	0.27%	N/A	1.00%	0.79%	0.10%	-0.46%	0.4%
-0.30%	0.25%	N/A	0.76%	0.28%	-0.36%	-0.55%	-0.81%	-0.32%	0.16%	0.84%	N/A	0.29%	-0.16%	0.0%
-0.50%	0.10%	0.56%	0.05%	-0.38%	-0.55%	N/A	-0.84%	-0.86%	-0.28%	0.32%	0.52%	0.07%	-0.56%	-0.4%
-0.78%	-0.05%	0.45%	0.01%	-0.14%	-0.81%	-0.84%	-1.11%	-0.95%	-0.19%	0.17%	0.45%	0.06%	-0.48%	-0.8%
-0.37%	0.42%	N/A	0.78%	0.27%	-0.32%	-0.86%	-0.95%	-0.24%	0.33%	0.74%	N/A	0.31%	-0.37%	-1.2%
-0.33%	0.02%	0.69%	1.08%	N/A	0.16%	-0.28%	-0.19%	0.33%	N/A	1.00%	0.71%	0.08%	-0.26%	-1.6%
-0.46%	0.15%	0.90%	1.04%	1.00%	0.84%	0.32%	0.17%	0.74%	1.00%	1.10%	0.84%	-0.05%	-0.66%	-2.0%
-0.79%	0.10%	N/A	0.86%	0.79%	N/A	0.52%	0.45%	N/A	0.71%	0.84%	N/A	-0.08%	-0.65%	
-0.74%	-0.32%	0.39%	0.18%	0.10%	0.29%	0.07%	0.06%	0.31%	0.08%	-0.05%	-0.08%	-0.74%	-0.89%	
-1.00%	-0.86%	-0.62%	-0.39%	-0.46%	-0.16%	-0.56%	-0.48%	-0.37%	-0.26%	-0.66%	-0.65%	-0.89%	-1.08%	

Polaris (Controlled, RMS=0.71%, MAX=1.45%)

-1.30%	-0.81%	-0.66%	-0.69%	-0.58%	-0.44%	-0.55%	-0.85%	-0.50%	-0.40%	-0.55%	-0.95%	-0.89%	-1.21%	2.0%
-0.81%	-0.10%	0.31%	0.11%	0.14%	0.27%	0.20%	0.03%	0.44%	0.11%	0.24%	0.10%	-0.36%	-1.01%	1.6%
-0.66%	0.31%	N/A	0.73%	0.86%	N/A	0.62%	0.50%	N/A	0.75%	1.00%	N/A	0.39%	-0.78%	1.2%
-0.69%	0.11%	0.73%	1.17%	1.44%	0.94%	0.21%	0.18%	0.96%	1.32%	1.37%	0.95%	0.25%	-0.48%	0.8%
-0.58%	0.14%	0.86%	1.44%	N/A	0.28%	-0.47%	-0.24%	0.27%	N/A	1.24%	0.85%	0.19%	-0.53%	0.4%
-0.44%	0.27%	N/A	0.94%	0.28%	-0.52%	-0.84%	-1.06%	-0.35%	0.17%	1.02%	N/A	0.31%	-0.30%	0.0%
-0.55%	0.20%	0.62%	0.21%	-0.47%	-0.84%	N/A	-1.20%	-0.97%	-0.34%	0.49%	0.57%	0.16%	-0.62%	-0.4%
-0.85%	0.03%	0.50%	0.18%	-0.24%	-1.06%	-1.20%	-1.45%	-1.08%	-0.27%	0.33%	0.48%	0.13%	-0.54%	-0.8%
-0.50%	0.44%	N/A	0.96%	0.27%	-0.35%	-0.97%	-1.08%	-0.27%	0.34%	0.92%	N/A	0.34%	-0.51%	-1.2%
-0.40%	0.11%	0.75%	1.32%	N/A	0.17%	-0.34%	-0.27%	0.34%	N/A	1.23%	0.75%	0.16%	-0.33%	-1.6%
-0.55%	0.24%	1.00%	1.37%	1.24%	1.02%	0.49%	0.33%	0.92%	1.23%	1.42%	0.93%	0.03%	-0.76%	-2.0%
-0.95%	0.10%	N/A	0.95%	0.85%	N/A	0.57%	0.48%	N/A	0.75%	0.93%	N/A	-0.07%	-0.81%	
-0.89%	-0.36%	0.39%	0.25%	0.19%	0.31%	0.16%	0.13%	0.34%	0.16%	0.03%	-0.07%	-0.78%	-1.05%	
-1.21%	-1.01%	-0.78%	-0.48%	-0.53%	-0.30%	-0.62%	-0.54%	-0.51%	-0.33%	-0.76%	-0.81%	-1.05%	-1.29%	

Figure B-19 Test Suite 1: 14 × 14 Lattice Pin Power Differences at Cold Controlled Conditions for NEWT (top) and Polaris (bottom)

NEWT (RMS=0.11%, MAX=0.27%)

-0.13%	-0.06%	-0.02%	-0.08%	-0.27%	0.00%	-0.18%	0.03%	-0.09%	-0.03%	-0.08%	0.00%	0.05%	-0.05%	2.0%
-0.06%	0.09%	0.09%	-0.05%	0.01%	0.05%	0.03%	0.10%	-0.10%	0.03%	0.03%	-0.02%	-0.03%	-0.16%	1.6%
-0.02%	0.09%	N/A	0.07%	0.20%	N/A	-0.03%	-0.13%	N/A	-0.03%	0.18%	N/A	0.10%	-0.20%	1.2%
-0.08%	-0.05%	0.07%	0.16%	0.15%	0.03%	-0.16%	-0.15%	0.02%	0.02%	0.04%	0.15%	0.06%	0.02%	0.8%
-0.27%	0.01%	0.20%	0.15%	N/A	-0.16%	0.09%	0.05%	-0.07%	N/A	0.23%	-0.03%	-0.13%	-0.13%	0.4%
0.00%	0.05%	N/A	0.03%	-0.16%	-0.04%	-0.02%	0.05%	0.08%	0.21%	0.01%	N/A	-0.01%	-0.16%	0.0%
-0.18%	0.03%	-0.03%	-0.16%	0.09%	-0.02%	N/A	-0.03%	0.26%	-0.12%	-0.13%	0.20%	-0.11%	0.04%	-0.4%
0.03%	0.10%	-0.13%	-0.15%	0.05%	0.05%	-0.03%	0.06%	0.02%	-0.03%	-0.05%	-0.07%	-0.11%	-0.03%	-0.8%
-0.09%	-0.10%	N/A	0.02%	-0.07%	0.08%	0.26%	0.02%	0.09%	0.10%	0.22%	N/A	-0.08%	-0.02%	-1.2%
-0.03%	0.03%	-0.03%	0.02%	N/A	0.21%	-0.12%	-0.03%	0.10%	N/A	0.11%	0.04%	0.07%	-0.14%	-1.6%
-0.08%	0.03%	0.18%	0.04%	0.23%	0.01%	-0.13%	-0.05%	0.22%	0.11%	-0.05%	0.16%	0.10%	-0.06%	-2.0%
0.00%	-0.02%	N/A	0.15%	-0.03%	N/A	0.20%	-0.07%	N/A	0.04%	0.16%	N/A	0.00%	-0.10%	
0.05%	-0.03%	0.10%	0.06%	-0.13%	-0.01%	-0.11%	-0.11%	-0.08%	0.07%	0.10%	0.00%	0.04%	0.05%	
-0.05%	-0.16%	-0.20%	0.02%	-0.13%	-0.16%	0.04%	-0.03%	-0.02%	-0.14%	-0.06%	-0.10%	0.05%	0.07%	

Polaris (RMS=0.10%, MAX=0.30%)

-0.08%	-0.03%	0.05%	-0.07%	-0.22%	0.05%	-0.14%	0.06%	-0.03%	0.03%	-0.06%	0.06%	0.07%	-0.01%	2.0%
-0.03%	0.05%	0.09%	-0.09%	-0.01%	0.03%	0.01%	0.06%	-0.10%	0.01%	-0.01%	-0.02%	-0.07%	-0.13%	1.6%
0.05%	0.09%	N/A	0.06%	0.23%	N/A	-0.02%	-0.13%	N/A	0.00%	0.17%	N/A	0.10%	-0.15%	1.2%
-0.07%	-0.09%	0.06%	0.05%	0.08%	-0.02%	-0.18%	-0.18%	-0.03%	-0.05%	-0.07%	0.15%	0.01%	0.04%	0.8%
-0.22%	-0.01%	0.23%	0.08%	N/A	-0.17%	0.13%	0.08%	-0.07%	N/A	0.16%	-0.01%	-0.14%	-0.08%	0.4%
0.05%	0.03%	N/A	-0.02%	-0.17%	-0.09%	0.00%	0.05%	0.08%	0.22%	-0.04%	N/A	-0.03%	-0.13%	0.0%
-0.14%	0.01%	-0.02%	-0.18%	0.13%	0.00%	N/A	-0.04%	0.30%	-0.08%	-0.16%	0.20%	-0.13%	0.07%	-0.4%
0.06%	0.06%	-0.13%	-0.18%	0.08%	0.05%	-0.04%	0.04%	0.07%	0.01%	-0.09%	-0.08%	-0.15%	0.01%	-0.8%
-0.03%	-0.10%	N/A	-0.03%	-0.07%	0.08%	0.30%	0.07%	0.08%	0.10%	0.17%	N/A	-0.10%	0.03%	-1.2%
0.03%	0.01%	0.00%	-0.05%	N/A	0.22%	-0.08%	0.01%	0.10%	N/A	0.04%	0.06%	0.04%	-0.09%	-1.6%
-0.06%	-0.01%	0.17%	-0.07%	0.16%	-0.04%	-0.16%	-0.09%	0.17%	0.04%	-0.17%	0.15%	0.06%	-0.04%	-2.0%
0.06%	-0.02%	N/A	0.15%	-0.01%	N/A	0.20%	-0.08%	N/A	0.06%	0.15%	N/A	0.00%	-0.04%	
0.07%	-0.07%	0.10%	0.01%	-0.14%	-0.03%	-0.13%	-0.15%	-0.10%	0.04%	0.06%	0.00%	0.00%	0.08%	
-0.01%	-0.13%	-0.15%	0.04%	-0.08%	-0.13%	0.07%	0.01%	0.03%	-0.09%	-0.04%	-0.04%	0.08%	0.10%	

Figure B-20 Test Suite 1: 14 × 14 Lattice Pin Power Differences at Nominal Conditions for NEWT (top) and Polaris (bottom)

NEWT (RMS=0.69%, MAX=1.49%)

-0.72%	-0.64%	-0.58%	-0.44%	-0.41%	-0.56%	-0.71%	-0.79%	2.0%
-0.74%	-0.57%	-0.31%	-0.12%	-0.06%	-0.28%	-0.68%	-0.71%	1.6%
-0.50%	-0.23%	0.23%	1.21%	1.21%	0.41%	-0.28%	-0.56%	1.2%
-0.38%	-0.06%	1.34%	N/A	N/A	1.21%	-0.06%	-0.41%	0.8%
-0.16%	0.21%	1.38%	N/A	N/A	1.21%	-0.12%	-0.44%	0.4%
0.20%	0.20%	0.53%	1.38%	1.34%	0.23%	-0.31%	-0.58%	0.0%
1.49%	0.53%	0.20%	0.21%	-0.06%	-0.23%	-0.57%	-0.64%	-0.4%
N/A	1.49%	0.20%	-0.16%	-0.38%	-0.50%	-0.74%	-0.72%	-0.8%
								-1.2%
								-1.6%
								-2.0%

Polaris (RMS=0.08%, MAX=0.18%)

0.10%	0.11%	-0.04%	-0.07%	-0.04%	-0.03%	0.04%	0.03%	2.0%
0.00%	-0.05%	-0.06%	0.02%	0.07%	-0.03%	-0.16%	0.04%	1.6%
-0.03%	-0.03%	-0.02%	0.02%	0.03%	0.17%	-0.04%	-0.05%	1.2%
-0.13%	-0.03%	0.09%	N/A	N/A	0.01%	0.04%	-0.07%	0.8%
-0.10%	0.10%	0.04%	N/A	N/A	0.00%	-0.01%	-0.10%	0.4%
-0.03%	-0.08%	0.02%	0.05%	0.10%	-0.02%	-0.08%	-0.06%	0.0%
0.18%	-0.06%	-0.07%	0.12%	-0.01%	-0.01%	-0.05%	0.10%	-0.4%
N/A	0.18%	-0.03%	-0.08%	-0.11%	-0.01%	0.01%	0.10%	-0.8%
								-1.2%
								-1.6%
								-2.0%

Figure B-21 Test Suite 1: 16 × 16 CE Lattice Pin Power Differences at Nominal Conditions for NEWT (top) and Polaris (bottom)

NEWT (RMS=0.16%, MAX=0.45%)

-0.05%	0.07%	0.05%	-0.12%	0.02%	-0.13%	0.17%	0.01%	0.14%	0.02%	-0.05%	-0.08%	0.12%	-0.36%	-0.06%	-0.02%	-0.31%	0.26%
0.07%	-0.07%	0.31%	-0.09%	0.01%	0.10%	-0.02%	-0.21%	-0.09%	-0.08%	-0.08%	-0.21%	-0.27%	-0.12%	-0.03%	0.05%	-0.33%	-0.25%
-0.08%	0.06%	-0.11%	0.21%	-0.16%	-0.16%	N/A	0.27%	-0.16%	-0.08%	-0.10%	N/A	0.17%	-0.02%	-0.10%	0.21%	-0.01%	-0.15%
0.01%	-0.22%	0.21%	N/A	-0.02%	0.21%	0.09%	0.15%	0.04%	-0.05%	0.00%	0.21%	0.38%	0.07%	N/A	-0.04%	0.03%	0.07%
-0.43%	0.26%	-0.03%	-0.02%	0.05%	0.14%	0.05%	N/A	-0.04%	0.15%	N/A	0.17%	-0.09%	-0.09%	0.01%	-0.08%	-0.25%	-0.11%
-0.07%	0.17%	0.09%	0.21%	-0.24%	0.02%	0.04%	0.08%	-0.23%	0.00%	-0.10%	-0.10%	-0.01%	-0.01%	0.07%	-0.14%	0.05%	0.18%
-0.02%	0.36%	N/A	0.22%	0.31%	-0.09%	-0.09%	-0.07%	-0.16%	0.12%	-0.05%	0.17%	-0.04%	-0.09%	0.30%	N/A	-0.26%	-0.27%
0.08%	-0.02%	0.20%	0.02%	N/A	-0.11%	-0.07%	0.32%	0.03%	-0.05%	-0.22%	-0.05%	0.17%	N/A	-0.18%	0.44%	0.06%	-0.24%
-0.12%	0.10%	-0.03%	0.17%	0.27%	0.08%	-0.16%	0.03%	N/A	0.11%	-0.17%	-0.35%	-0.10%	0.10%	0.29%	-0.04%	-0.01%	0.02%
0.08%	0.04%	0.05%	0.01%	0.21%	0.00%	0.06%	-0.11%	0.24%	-0.04%	-0.21%	0.21%	-0.29%	0.45%	-0.20%	0.22%	0.19%	-0.10%
0.26%	0.11%	-0.04%	0.13%	N/A	0.09%	-0.05%	0.04%	-0.43%	0.04%	-0.33%	0.15%	-0.11%	N/A	0.40%	0.13%	-0.13%	-0.24%
-0.02%	-0.01%	N/A	0.08%	-0.09%	0.03%	-0.21%	-0.05%	-0.16%	0.21%	-0.04%	0.16%	-0.06%	0.34%	0.07%	N/A	0.25%	-0.15%
-0.13%	0.11%	0.04%	-0.13%	-0.21%	-0.01%	0.03%	-0.02%	0.22%	-0.10%	0.21%	0.01%	0.08%	-0.03%	0.15%	0.18%	0.30%	-0.01%
-0.17%	0.13%	0.11%	-0.05%	-0.03%	0.06%	-0.03%	N/A	0.04%	0.13%	N/A	0.02%	-0.29%	-0.25%	0.21%	-0.01%	0.13%	-0.11%
0.01%	0.03%	-0.04%	N/A	0.08%	0.01%	-0.01%	0.07%	-0.21%	-0.20%	-0.11%	0.45%	0.09%	0.09%	N/A	0.02%	-0.22%	0.00%
-0.15%	-0.27%	0.21%	0.15%	-0.02%	-0.01%	N/A	-0.13%	-0.10%	0.35%	0.06%	N/A	0.25%	-0.08%	0.09%	0.08%	0.05%	-0.16%
-0.25%	-0.20%	-0.14%	-0.03%	-0.12%	-0.14%	0.12%	-0.19%	-0.20%	0.00%	-0.13%	-0.13%	0.17%	0.01%	-0.03%	-0.21%	-0.02%	-0.07%
0.07%	0.07%	0.10%	0.01%	-0.11%	-0.20%	0.11%	0.08%	0.15%	-0.04%	-0.11%	0.11%	-0.33%	-0.05%	-0.19%	-0.09%	-0.13%	0.00%

-2.0%	-1.8%	-1.6%	-1.4%	-1.2%	-1.0%	-0.8%	-0.6%	-0.4%	-0.2%	0.0%	0.2%	0.4%	0.6%	0.8%	1.0%	1.2%	1.4%	1.6%	1.8%	2.0%
-------	-------	-------	-------	-------	-------	-------	-------	-------	-------	------	------	------	------	------	------	------	------	------	------	------

Polaris (RMS= 0.15%, MAX=0.43%)

-0.02%	0.12%	0.09%	-0.08%	0.05%	-0.09%	0.21%	0.05%	0.18%	0.06%	-0.02%	-0.05%	0.16%	-0.33%	-0.02%	0.03%	-0.27%	0.30%
0.12%	-0.04%	0.34%	-0.08%	0.02%	0.06%	-0.04%	-0.21%	-0.05%	-0.05%	-0.08%	-0.23%	-0.31%	-0.10%	-0.02%	0.08%	-0.30%	-0.21%
-0.04%	0.08%	-0.13%	0.17%	-0.17%	-0.21%	N/A	0.26%	-0.14%	-0.07%	-0.11%	N/A	0.13%	-0.03%	-0.15%	0.18%	0.01%	-0.10%
0.04%	-0.21%	0.16%	N/A	-0.04%	0.18%	0.02%	0.09%	0.03%	-0.08%	-0.06%	0.14%	0.35%	0.04%	N/A	-0.08%	0.04%	0.10%
-0.40%	0.28%	-0.04%	-0.04%	0.03%	0.16%	0.04%	N/A	-0.07%	0.12%	N/A	0.15%	-0.07%	-0.10%	-0.01%	-0.10%	-0.23%	-0.08%
-0.04%	0.12%	0.05%	0.18%	-0.22%	0.03%	0.03%	0.04%	-0.26%	-0.02%	-0.13%	-0.12%	0.00%	0.00%	0.04%	-0.18%	0.00%	0.21%
0.02%	0.34%	N/A	0.15%	0.29%	-0.10%	-0.09%	-0.04%	-0.13%	0.16%	-0.01%	0.19%	-0.06%	-0.11%	0.23%	N/A	-0.29%	-0.24%
0.11%	-0.02%	0.19%	-0.04%	N/A	-0.15%	-0.04%	0.31%	0.01%	-0.06%	-0.18%	-0.01%	0.13%	N/A	-0.25%	0.43%	0.07%	-0.21%
-0.07%	0.14%	-0.02%	0.16%	0.25%	0.06%	-0.13%	0.01%	N/A	0.08%	-0.14%	-0.30%	-0.12%	0.07%	0.28%	-0.02%	0.03%	0.06%
0.12%	0.07%	0.06%	-0.02%	0.18%	-0.02%	0.09%	-0.13%	0.21%	-0.06%	-0.18%	0.25%	-0.32%	0.42%	-0.22%	0.24%	0.22%	-0.07%
0.30%	0.11%	-0.04%	0.06%	N/A	0.06%	-0.01%	0.07%	-0.38%	0.08%	-0.28%	0.20%	-0.15%	N/A	0.33%	0.12%	-0.12%	-0.21%
0.02%	-0.04%	N/A	0.01%	-0.10%	0.01%	-0.19%	-0.01%	-0.11%	0.25%	0.01%	0.18%	-0.07%	0.32%	0.00%	N/A	0.22%	-0.11%
-0.09%	0.07%	0.00%	-0.16%	-0.20%	0.00%	0.01%	-0.06%	0.19%	-0.13%	0.17%	-0.01%	0.08%	-0.02%	0.13%	0.15%	0.26%	0.02%
-0.14%	0.15%	0.09%	-0.09%	-0.04%	0.07%	-0.04%	N/A	0.01%	0.09%	N/A	0.01%	-0.27%	-0.28%	0.19%	-0.03%	0.15%	-0.09%
0.04%	0.04%	-0.08%	N/A	0.05%	-0.02%	-0.08%	0.01%	-0.23%	-0.22%	-0.17%	0.39%	0.06%	0.05%	N/A	-0.02%	-0.21%	0.03%
-0.10%	-0.23%	0.18%	0.11%	-0.03%	-0.06%	N/A	-0.15%	-0.09%	0.36%	0.05%	N/A	0.20%	-0.10%	0.04%	0.05%	0.07%	-0.11%
-0.21%	-0.18%	-0.11%	-0.01%	-0.10%	-0.19%	0.10%	-0.19%	-0.16%	0.03%	-0.12%	-0.16%	0.13%	0.02%	-0.02%	-0.18%	0.00%	-0.02%
0.11%	0.11%	0.15%	0.04%	-0.08%	-0.16%	0.14%	0.12%	0.18%	-0.01%	-0.08%	0.14%	-0.29%	-0.02%	-0.16%	-0.05%	-0.08%	0.04%

-2.0%	-1.8%	-1.6%	-1.4%	-1.2%	-1.0%	-0.8%	-0.6%	-0.4%	-0.2%	0.0%	0.2%	0.4%	0.6%	0.8%	1.0%	1.2%	1.4%	1.6%	1.8%	2.0%
-------	-------	-------	-------	-------	-------	-------	-------	-------	-------	------	------	------	------	------	------	------	------	------	------	------

Figure B-22 Test Suite 1: 18 × 18 Lattice Pin Power Differences at Nominal Conditions for NEWT (top) and Polaris (bottom)

B.2 Test Suite 2 – Control Elements

Purpose: Performance of the lattice physics calculations with respect to different control element designs is tested for the nominal BWR and PWR lattice configurations.

Target Accuracy:

- 200 pcm difference in k_{inf}
- 1% RMS and 1.5% max difference in pin power distribution for BWR lattices
- 0.5% RMS and 1.5% max difference in pin power distribution for PWR lattices

Acceptance Accuracy:

- 400 pcm difference in k_{inf}
- 1.5% RMS and 2.5% max difference in pin power distribution for BWR and PWR lattices

B.2.1 BWR

Description: Common control blade geometries and poison materials are tested for the nominal 10×10 GE14-DOM lattice at nominal conditions for different void fractions. The test matrix is given in Table B-11.

Table B-11 Test Suite 2: BWR Case Matrix

Case number	TF (K)	TC (K)	Void fraction (%)	Control blade
1	950	560	0	OEM (B ₄ C)
2	950	560	40	OEM (B ₄ C)
3	950	560	70	OEM (B ₄ C)
4	950	560	90	OEM (B ₄ C)
5	950	560	0	Marathon (B ₄ C)
6	950	560	40	Marathon (B ₄ C)
7	950	560	70	Marathon (B ₄ C)
8	950	560	90	Marathon (B ₄ C)
9	950	560	0	Hafnium
10	950	560	40	Hafnium
11	950	560	70	Hafnium
12	950	560	90	Hafnium

Results: Comparison of k_{inf} differences for different control blade material types are plotted in Figure B-23 for NEWT and in Figure B-24 for Polaris. Both plots also include MG KENO results for comparison. There is a spread of ~100 pcm in NEWT results at 0% void that narrows to <50 pcm at 90% void. Although k_{inf} differences exhibit the same sensitivity to changes in void fraction, hafnium blades are more positive than the B₄C results.

As in NEWT results, there is a spread of ~100 pcm in Polaris results at 0% void. However, this spread stays the same for all void fractions. Hafnium and Marathon blades show the same bias compared to B₄C blades. Since Marathon blades only differ in geometry when compared to B₄C blades, this bias requires further investigation.

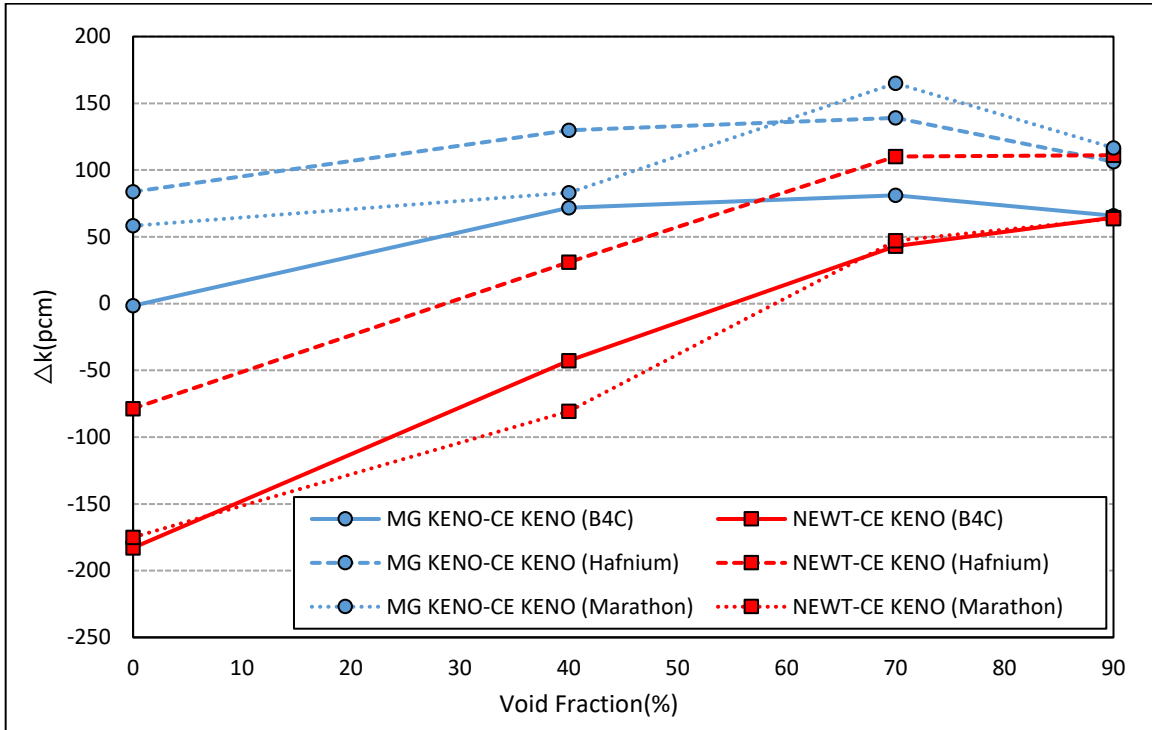


Figure B-23 Test Suite 2: MG KENO and NEWT k_{inf} Void Fraction Trends for Different Control Blade Types

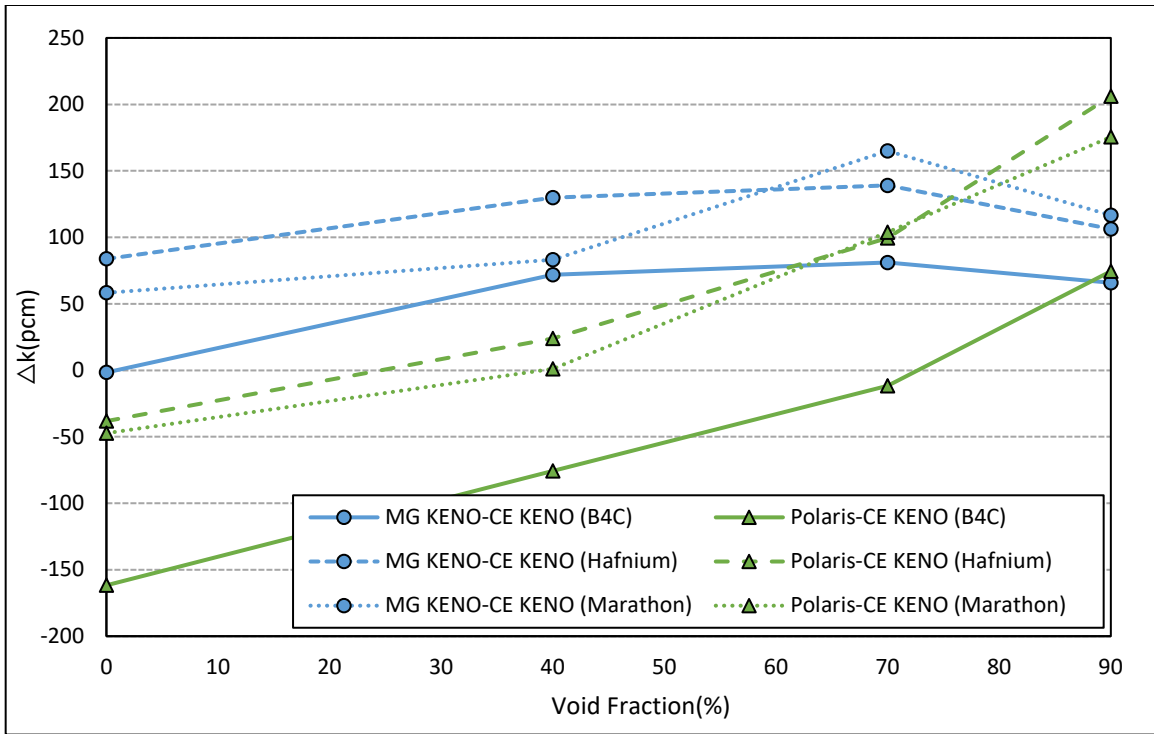


Figure B-24 Test Suite 2: k_{inf} MG KENO and Polaris Void Fraction Trends for Different Control Blade Types

B.2.2 PWR

Description: The control rod types given in Table B-12 are tested for the nominal 17×17 WE lattice design at 0 ppm and 1,300 ppm boron concentrations at HFP conditions.

Table B-12 Test Suite 2: PWR Case Matrix

Case number	TF (K)	TC (K)	PC ^a (ppm)	Control rod
1	900	560	0	B ₄ C
2	900	560	0	AIC
3	900	560	0	Inconel
4	900	560	1,300	B ₄ C
5	900	560	1,300	AIC
6	900	560	1,300	Inconel

^a PC = soluble boron concentration

Results: The k_{inf} differences for different control rod types are compared in Figure B-25. Change in boron concentration has an effect of less than 50 pcm on the accuracy of k_{inf} for most cases. The boron trend is negligible for all control rod types. Each control rod type shows a different bias in the results with each MG code. For instance, the AIC rods are approximately 50 pcm high in MG KENO, while they are approximately 150 pcm low in Polaris. However, the results are all within the 200 pcm acceptance criteria.

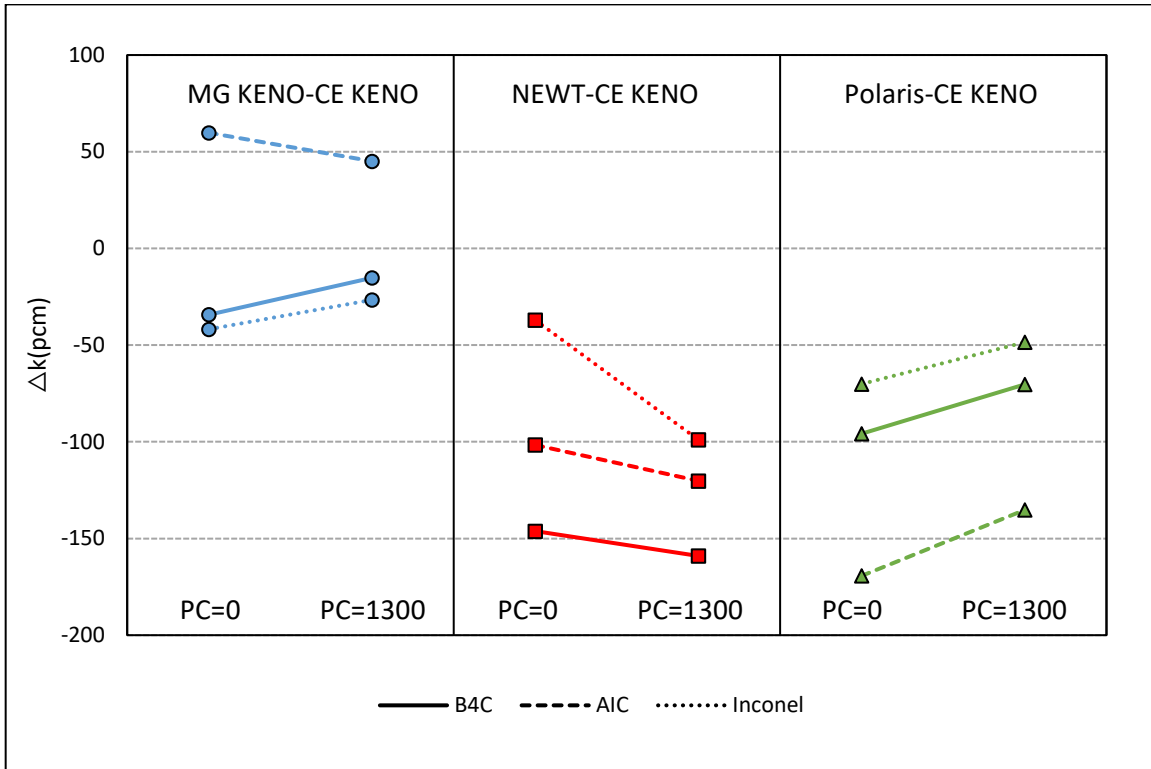


Figure B-25 Test Suite 2: k_{inf} Boron Trends for Different Control Rod Types

B.3 Test Suite 3 – MOX Fuel

Purpose: The performance of the lattice physics calculations for weapons- and recycle-grade MOX fuel for different lattice geometries is tested. The same test matrix used in Test Suite 1 is also used in this test suite. In order to use a realistic plutonium enrichment pattern, available MOX lattice designs from open literature are used instead of the nominal lattice types.

Target Accuracy:

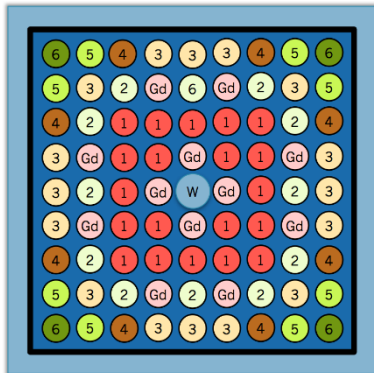
- 200 pcm difference in k_{inf}
- 1% RMS and 1.5% max difference in pin power distribution for BWR lattices
- 0.5% RMS and 1.5% max difference in pin power distribution for PWR lattices

Acceptance Accuracy:

- 400 pcm difference in k_{inf}
- 1.5% RMS and 2.5% max difference in pin power distribution for BWR and PWR lattices

B.3.1 BWR

Description: A 9×9 (GE11) lattice design (shown in Figure B-26) [13] is tested using the BWR standard case matrix presented in Table B-13.



^{235}U 0.26 wt%
 Average Pu^{tot} 8.12 wt%
 Average Pu^{fiss} 5.52 wt%
 ^{239}Pu 59.7 wt%

Figure B-26 BWR MOX Lattice Design [13]

Table B-13 Test Suite 3: BWR Case Matrix

Case number	TF (K)	TC (K)	Void fraction (%)
1	293	293	Cold
2	293	293	Cold
3	293	293	Cold
4	500	560	0
5	500	560	40
6	500	560	70
7	500	560	90
8	950	560	0
9	950	560	40
10	950	560	70
11	950	560	90
12	1,500	560	0
13	1,500	560	40
14	1,500	560	70
15	1,500	560	90

Results: Comparisons of k_{inf} differences are plotted for uncontrolled cases in Figure B-27 and uncontrolled cases in Figure B-28. Cold cases 1, 2, and 3 do not show any trends with respect to increasing fuel temperature (293 K, 500 K, 950 K), but Polaris results are approximately 300 pcm higher than MG KENO. Hot cases (4–15) show consistent trends vs void fraction for each code. The Polaris results are approximately 200 pcm higher and show a different trend from the other MG codes. As observed in the UOX lattices in test suite 2, control blade insertion introduces a bias to the results. The MG KENO and NEWT show consistent trends vs void fraction for the hot cases, and the largest differences are observed at 90% void fractions. Statistics for MG KENO, NEWT, and Polaris k_{inf} differences are presented in Table B-14. The poor MG KENO and NEWT results are likely due to inadequacies in the resonance self-shielding using 1D unit cells that assume a uniform lattice.

Pin power differences with the CE KENO reference distributions are presented in Figure B-29 and Figure B-30. NEWT results exhibit large differences around the water rod and at gadolinium rod locations. The largest difference is in a gadolinium rod, and it increases with increasing void fraction (1.13% vs 1.66%). On the other hand, Polaris results are consistent with test suite 1 results. No significant bias is observed in gadolinium rod locations or around the water rod. The largest differences are at wide-wide NW corner pins (1.67% at 40% void and 1.28% at 90% void). Results for both codes exceed the desired target accuracy. Model improvements for the gadolinia rods are being investigated for NEWT solutions, including the resonance self-shielding models.

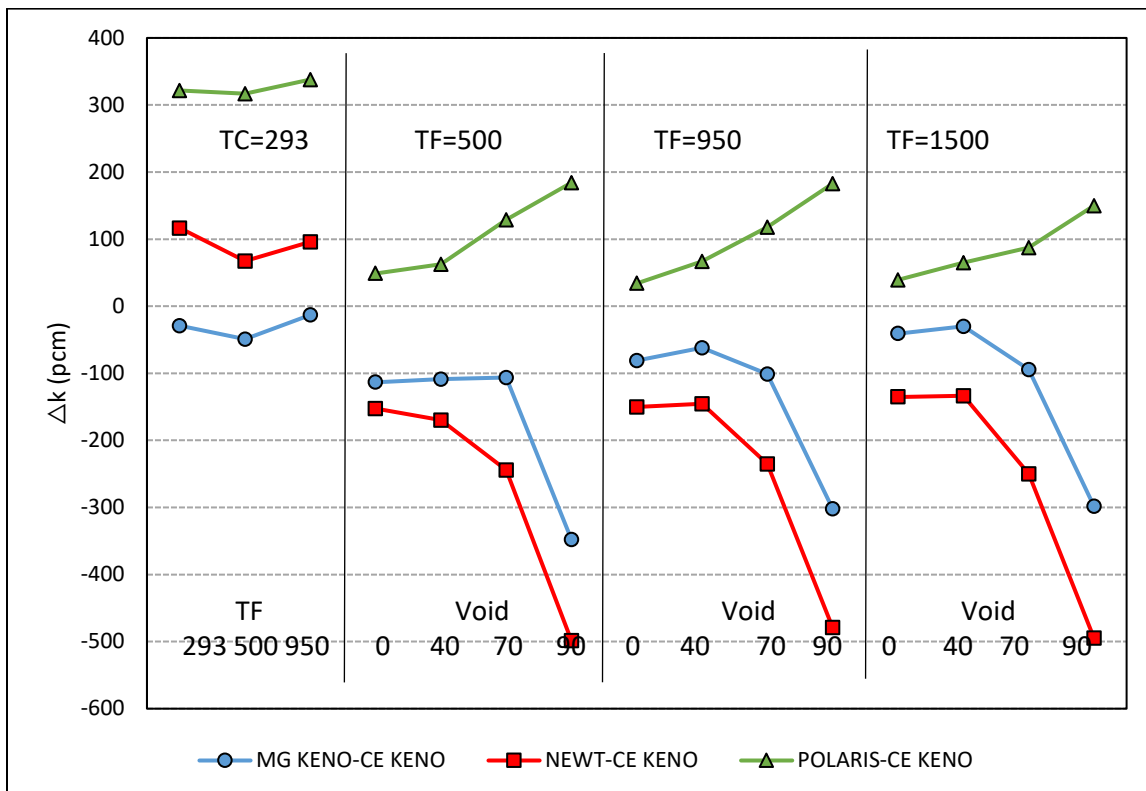


Figure B-27 Test Suite 3: MOX BWR k_{inf} Differences for Uncontrolled Cases

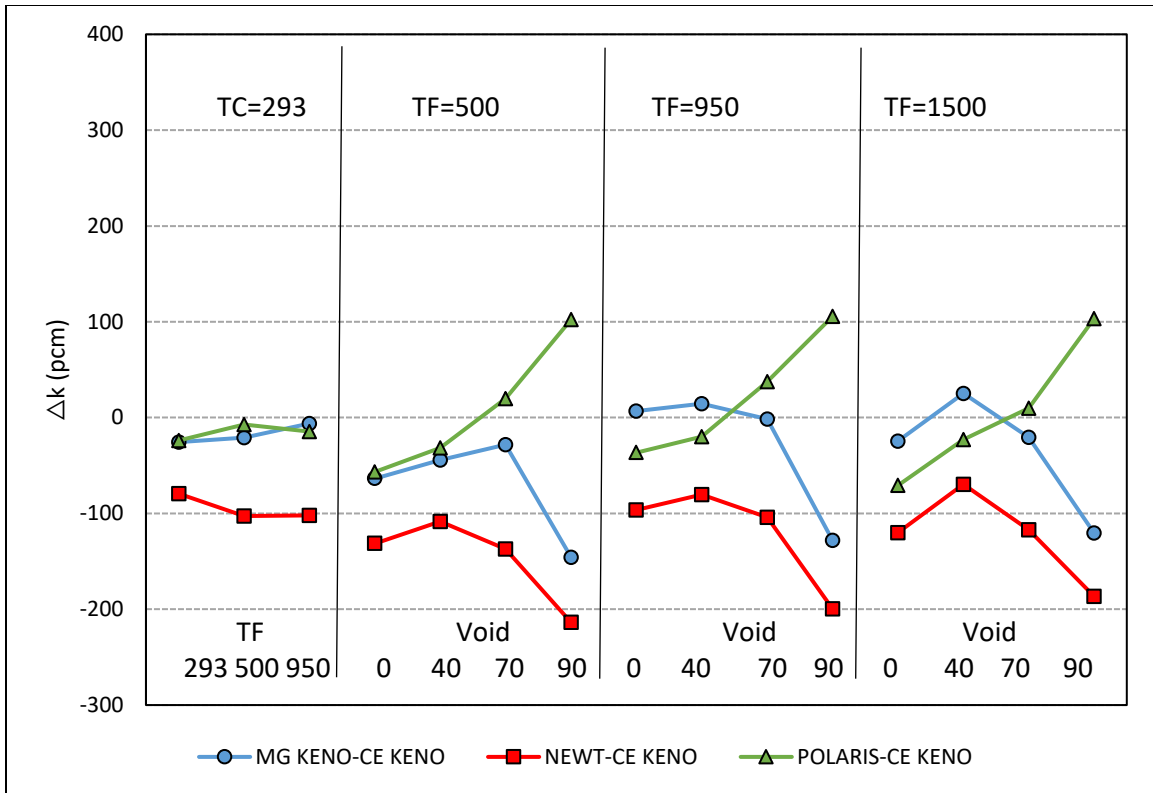


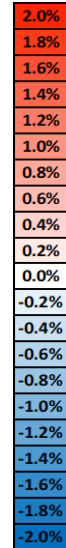
Figure B-28 Test Suite 3: MOX BWR k_{inf} Differences for Controlled Cases

Table B-14 BWR 9 × 9-1 Lattice MOX k_{inf} (pcm) Statistics

Code	Uncontrolled				Controlled			
	σ	mean	max	min	σ	mean	max	min
MG KENO	108	-118	-13	-348	53	-39	25	-146
NEWT	195	-187	117	-499	44	-123	-70	-214
Polaris	106	143	338	34	57	6	106	-71

NEWT (RMS= 0.61 % max=1.13 ± 0.09 %)

1.13%	0.63%	0.47%	0.22%	0.14%	0.18%	0.30%	0.47%	0.76%
0.63%	-0.07%	-0.56%	1.13%	-0.69%	1.09%	-0.57%	-0.18%	0.19%
0.47%	-0.56%	-0.95%	-0.71%	-0.68%	-0.68%	-0.69%	-0.45%	0.11%
0.22%	1.13%	-0.71%	-0.84%	0.85%	-0.54%	-0.70%	1.04%	-0.16%
0.14%	-0.69%	-0.68%	0.85%	N/A	0.89%	-0.55%	-0.55%	-0.06%
0.18%	1.09%	-0.68%	-0.54%	0.89%	-0.60%	-0.57%	1.11%	-0.14%
0.30%	-0.57%	-0.69%	-0.70%	-0.55%	-0.57%	-0.64%	-0.40%	0.18%
0.47%	-0.18%	-0.45%	1.04%	-0.55%	1.11%	-0.40%	-0.29%	0.05%
0.76%	0.19%	0.11%	-0.16%	-0.06%	-0.14%	0.18%	0.05%	0.46%



Polaris (RMS= 0.17 % max=0.5 ± 0.09 %)

0.50%	0.25%	0.37%	0.02%	0.00%	0.09%	0.03%	0.25%	0.28%
0.25%	0.19%	-0.12%	0.03%	-0.27%	0.03%	-0.18%	0.07%	0.11%
0.37%	-0.12%	-0.29%	-0.11%	-0.28%	-0.15%	-0.21%	-0.02%	0.14%
0.02%	0.03%	-0.11%	-0.22%	0.01%	-0.11%	-0.28%	0.06%	-0.03%
0.00%	-0.27%	-0.28%	0.01%	N/A	0.05%	-0.12%	-0.24%	0.12%
0.09%	0.03%	-0.15%	-0.11%	0.05%	-0.08%	-0.20%	0.14%	-0.05%
0.04%	-0.18%	-0.21%	-0.28%	-0.12%	-0.20%	-0.13%	-0.02%	0.25%
0.25%	0.07%	-0.02%	0.06%	-0.24%	0.14%	-0.02%	-0.04%	0.00%
0.28%	0.11%	0.14%	-0.03%	0.12%	-0.05%	0.25%	0.00%	0.26%

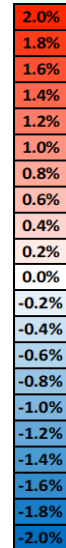


Figure B-29 Test Suite 3 MOX BWR Pin Power Differences at 40% Void

NEWT (RMS=0.83%, MAX=1.76%)

1.09%	0.89%	0.27%	-0.50%	-0.41%	-0.28%	0.36%	0.49%	0.90%
0.89%	0.90%	0.22%	1.61%	-0.44%	1.66%	0.33%	0.53%	0.42%
0.27%	0.22%	-0.66%	-1.16%	-1.22%	-0.89%	-0.30%	-0.27%	0.09%
-0.50%	1.61%	-1.16%	-1.76%	0.85%	-1.50%	-0.95%	1.37%	-0.48%
-0.41%	-0.44%	-1.22%	0.85%	N/A	0.84%	-0.95%	-0.54%	-0.58%
-0.28%	1.66%	-0.89%	-1.50%	0.84%	-1.31%	-0.60%	1.39%	-0.54%
0.36%	0.33%	-0.30%	-0.95%	-0.95%	-0.60%	-0.62%	-0.02%	-0.06%
0.49%	0.53%	-0.27%	1.37%	-0.54%	1.39%	-0.02%	0.22%	0.21%
0.90%	0.42%	0.09%	-0.48%	-0.58%	-0.54%	-0.06%	0.21%	0.59%

2.0%
1.8%
1.6%
1.4%
1.2%
1.0%
0.8%
0.6%
0.4%
0.2%
0.0%
-0.2%
-0.4%
-0.6%
-0.8%
-1.0%
-1.2%
-1.4%
-1.6%
-1.8%
-2.0%

Polaris (RMS=0.19%, MAX=0.37%)

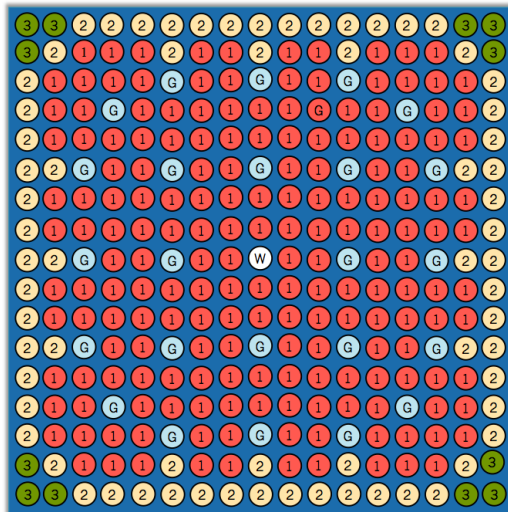
0.30%	0.28%	0.18%	-0.36%	-0.09%	-0.03%	0.07%	0.11%	0.27%
0.28%	0.37%	0.15%	0.18%	-0.06%	0.26%	0.12%	0.11%	0.13%
0.18%	0.15%	-0.03%	-0.11%	-0.26%	-0.11%	0.00%	-0.19%	0.14%
-0.36%	0.18%	-0.11%	-0.25%	0.13%	-0.30%	-0.33%	0.20%	0.02%
-0.09%	-0.06%	-0.26%	0.13%	N/A	0.11%	-0.16%	-0.17%	0.00%
-0.03%	0.26%	-0.11%	-0.30%	0.11%	-0.24%	-0.29%	0.22%	-0.12%
0.07%	0.12%	0.00%	-0.33%	-0.16%	-0.29%	-0.36%	-0.11%	0.02%
0.11%	0.11%	-0.20%	0.20%	-0.17%	0.22%	-0.11%	-0.07%	0.02%
0.27%	0.12%	0.14%	0.02%	0.00%	-0.12%	0.02%	0.02%	0.25%

2.0%
1.8%
1.6%
1.4%
1.2%
1.0%
0.8%
0.6%
0.4%
0.2%
0.0%
-0.2%
-0.4%
-0.6%
-0.8%
-1.0%
-1.2%
-1.4%
-1.6%
-1.8%
-2.0%

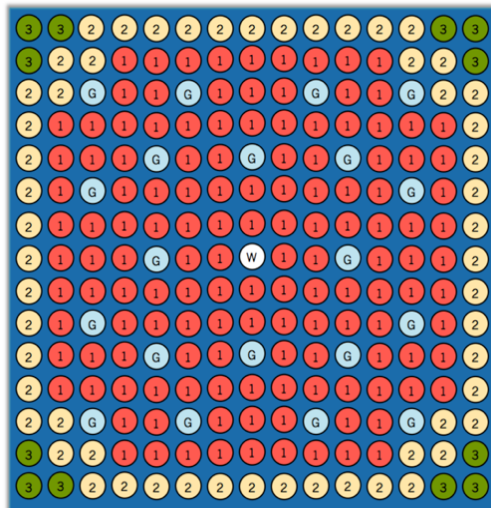
Figure B-30 Test Suite 3 MOX BWR Pin Power Differences at 90% Void

B.3.2 PWR

Description: The 17×17 and 15×15 PWR lattices are modeled for this test suite. Enrichment zonings and lattice average enrichments are shown in Figure B-31. Weapons-grade plutonium vector is used in the 17×17 lattice fuel pins, while recycle-grade plutonium vector is used in the 15×15 lattice fuel pins.



^{235}U	0.23 wt%
Average Pu^{tot}	3.95 wt%
Average Pu^{fiss}	3.709 wt%
^{239}Pu	93.6 wt%



^{235}U	0.27 wt%
Average Pu^{tot}	8.13 wt%
Average Pu^{fiss}	5.51 wt%
^{239}Pu	59.21 wt%

Figure B-31 Test Suite 3: PWR MOX Lattice Designs

Results: The calculated k_{inf} differences for 17×17 lattice design for uncontrolled cases are shown in Figure B-32 and controlled cases in Figure B-33. The calculated k_{inf} differences for 15×15 lattice design are shown in Figure B-34 for uncontrolled cases and in Figure B-35 for controlled cases.

Changes in k_{inf} differences with increasing boron concentrations for 293 K cold cases (1–5) and 560 K hot zero power cases (6–10) can be seen in Figure B-32 through Figure B-35.

Although lattice size and plutonium vectors are different, similar trends are observed in the 17×17 and 15×15 lattice designs. Changes in moderator temperature at HFP conditions (cases 11, 12, and 13) do not show significant trends or biases. Polaris results for the uncontrolled cases are typically higher than the other MG codes. Statistics for MG KENO, NEWT and Polaris k_{inf} differences are presented in Table B-15.

Pin power differences vs the CE KENO reference distributions are presented in Figure B-36 and Figure B-37 for uncontrolled and controlled cases for NEWT and Polaris codes, respectively. Both codes show good agreement with CE KENO results. The largest pin power difference is less than 0.51% for all cases.

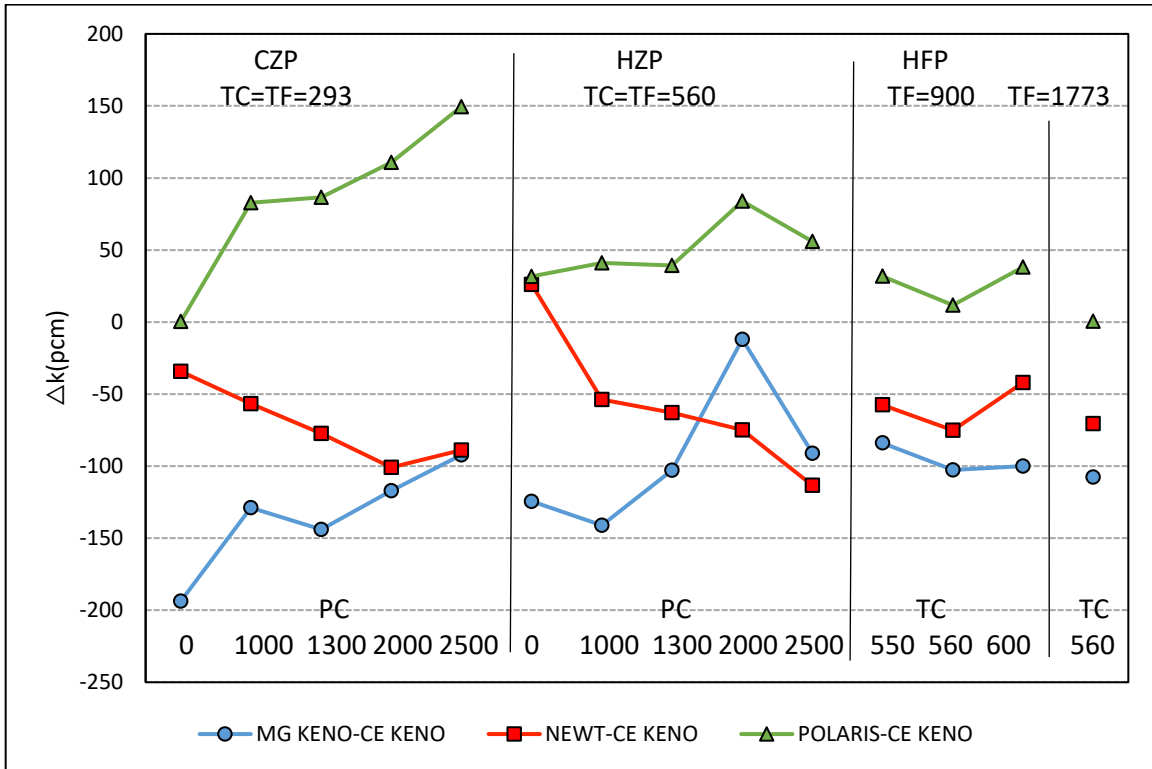


Figure B-32 Test suite 3 17×17 MOX PWR Lattice k_{inf} Differences for Uncontrolled Cases

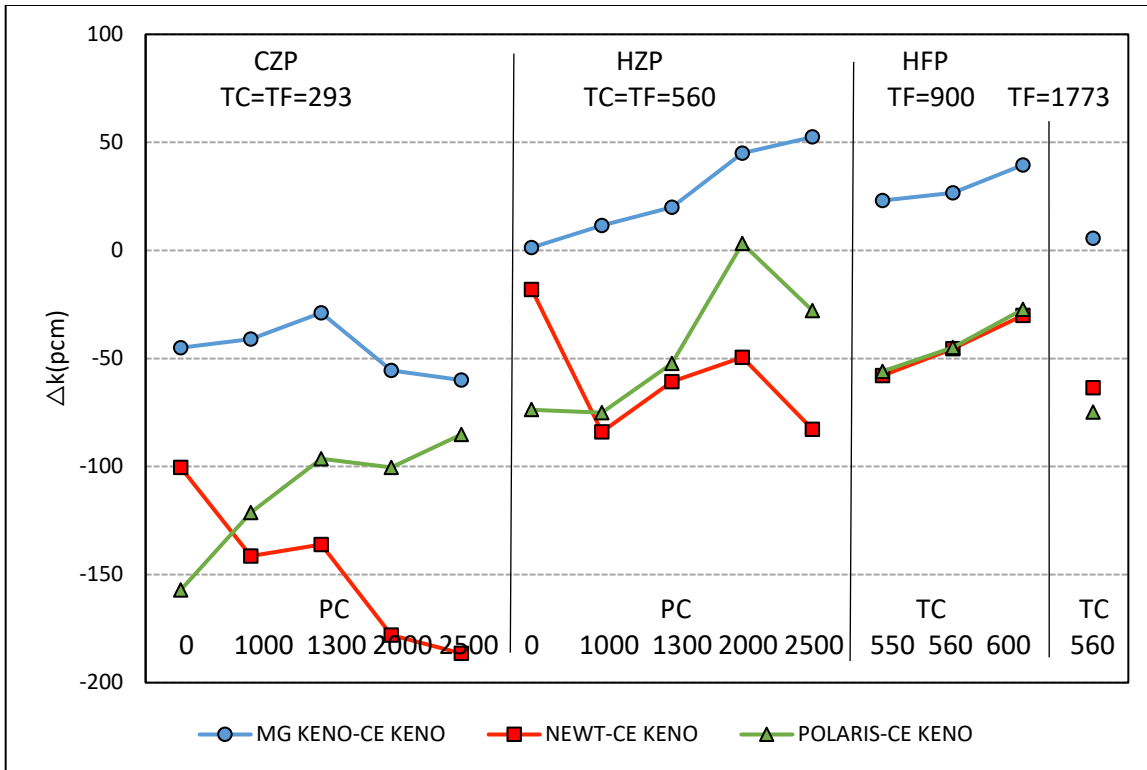


Figure B-33 Test suite 3 17 × 17 MOX PWR Lattice k_{inf} Differences for Controlled Cases

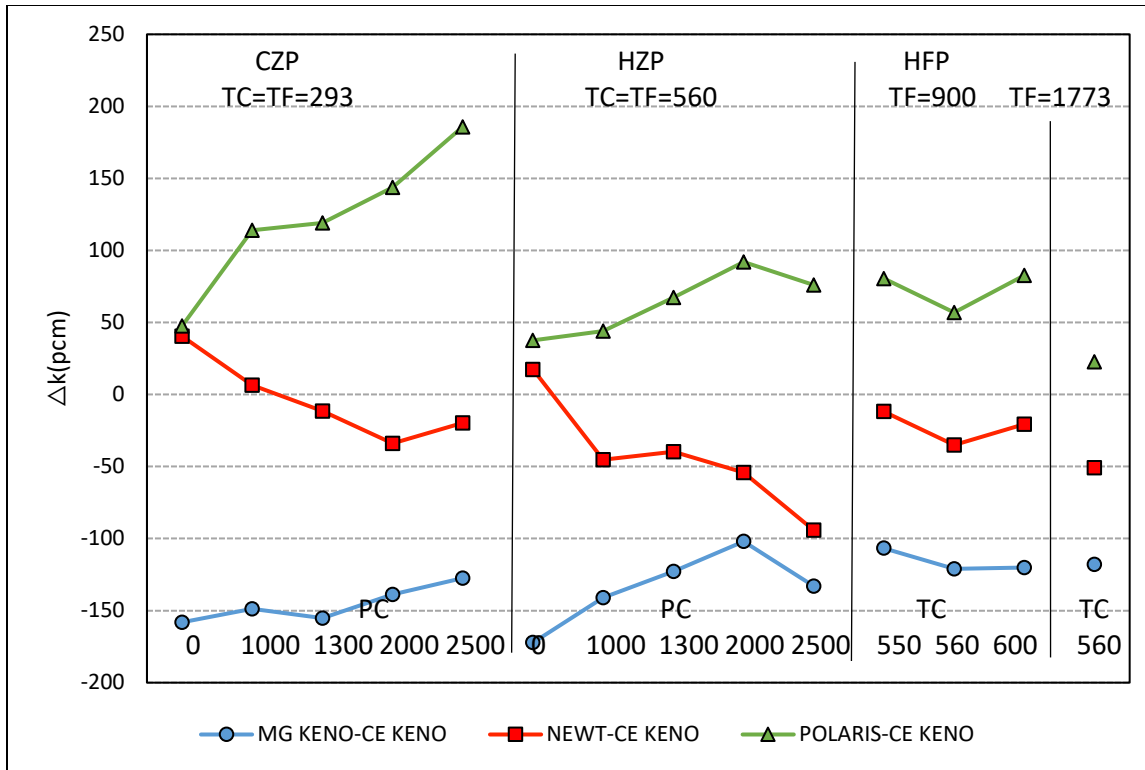


Figure B-34 Test Suite 3: 15 × 15 MOX PWR Lattice k_{inf} Differences for ncontrolled Cases

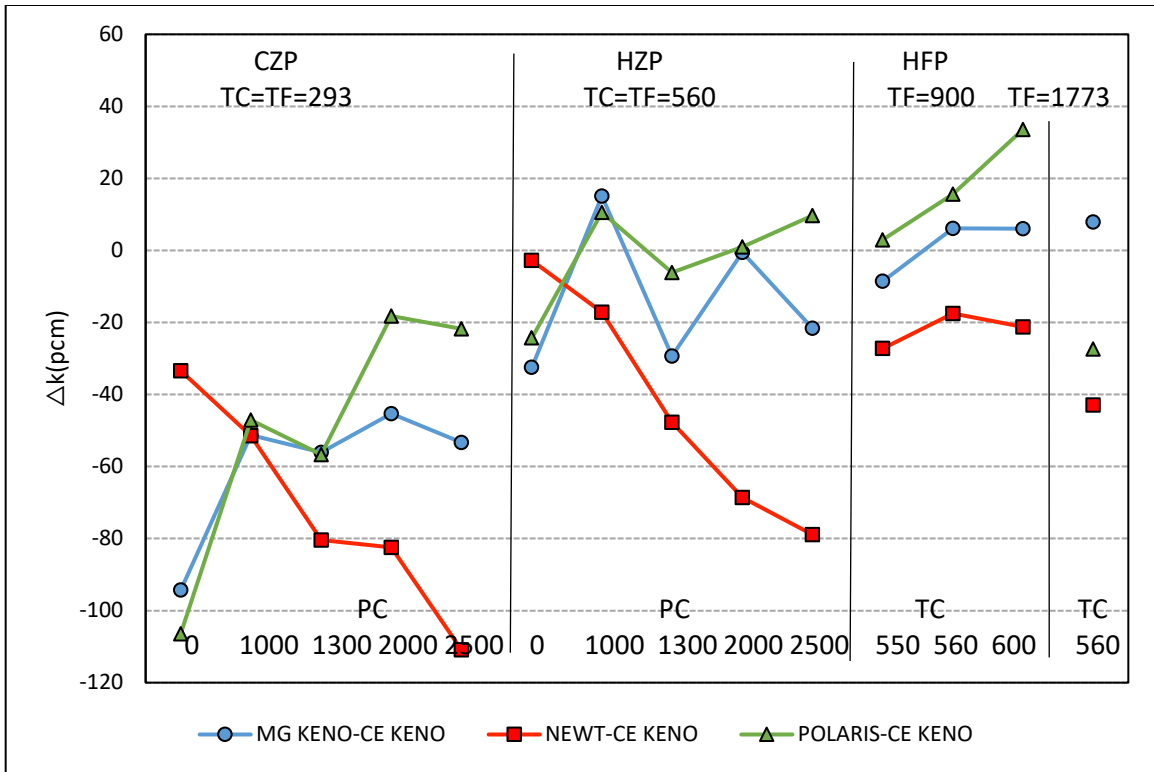


Figure B-35 Test suite 3 15 × 15 MOX PWR Lattice k_{inf} Differences for Controlled Cases

Table B-15 PWR MOX k_{inf} (pcm) Statistics

Code	Lattice	Uncontrolled				Controlled			
		σ	mean	max	min	σ	mean	max	min
MG KENO	15 × 15	20	-133	-102	-172	20	-133	-102	-172
	17 × 17	42	-110	-12	-194	39	0	52	-60
NEWT	15 × 15	33	-78	15	-133	31	-49	-3	-111
	17 × 17	33	-61	1	-108	53	-88	-18	-186
Polaris	15 × 15	45	-20	15	-56	36	-17	34	-106
	17 × 17	43	3	52	-60	41	-71	3	-157

NEWT (RMS=0.10%, MAX=0.31%)

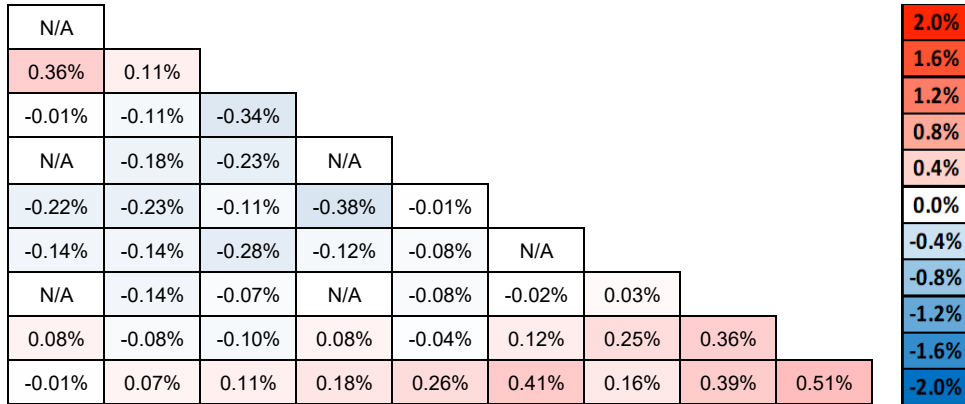
N/A										2.0%
0.00%	-0.07%									1.6%
-0.11%	-0.04%	-0.01%								1.2%
N/A	0.01%	-0.05%	N/A							0.8%
0.07%	0.07%	-0.02%	0.03%	-0.18%						0.4%
-0.10%	-0.19%	-0.11%	-0.02%	0.18%	N/A					0.0%
N/A	0.00%	0.12%	N/A	0.02%	0.10%	-0.23%				-0.4%
-0.03%	0.05%	-0.13%	0.17%	-0.05%	-0.03%	-0.17%	0.00%			-0.8%
-0.05%	0.01%	-0.06%	0.03%	0.02%	0.07%	0.04%	0.16%	0.31%		-1.2%
										-1.6%
										-2.0%

Polaris (RMS=0.09%, MAX=0.24%)

N/A										2.0%
0.04%	-0.05%									1.6%
-0.06%	-0.05%	-0.02%								1.2%
N/A	0.05%	0.00%	N/A							0.8%
0.10%	0.06%	-0.03%	0.03%	-0.23%						0.4%
-0.05%	-0.18%	-0.11%	0.01%	0.13%	N/A					0.0%
N/A	0.02%	0.11%	N/A	-0.01%	0.10%	-0.18%				-0.4%
-0.05%	0.04%	-0.12%	0.14%	-0.07%	0.00%	-0.13%	-0.03%			-0.8%
-0.02%	-0.01%	-0.08%	0.06%	-0.01%	0.08%	0.05%	0.09%	0.24%		-1.2%
										-1.6%
										-2.0%

Figure B-36 Test Suite 3: 17 × 17 lattice Pin Power Differences at Nominal Conditions for NEWT (Top) and Polaris (Bottom)

NEWT (RMS=0.20%, MAX=0.51%)



Polaris (RMS=0.10%, MAX=0.28%)

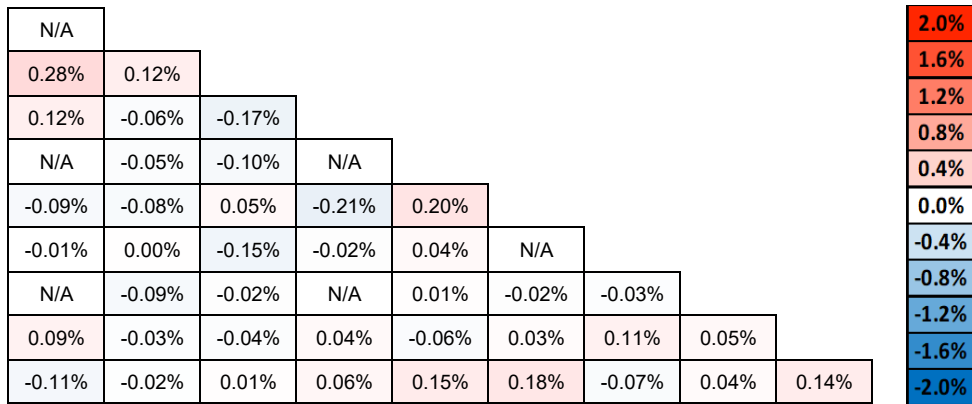


Figure B-37 Test suite 3 17x17 Lattice Pin Power Differences at Nominal Controlled Conditions for NEWT (Top) and Polaris (Bottom)

B.4 Test Suite 4 – Reactivity Worth of Depleted Fuel

Purpose: The reactivity worth of fission products and actinides in depleted UOX and MOX fuels is tested for middle of life (MOL) at 40 GWd/MTU and end of life (EOL) at 80 GWd/MTU burnup values. The nuclide density distributions at 40 GWd/MTU and 80 GWd/MTU are obtained from TRITON/NEWT depletion calculations.

Target Accuracy:

- 200 pcm difference in k_{inf}
- 1% RMS and 1.5% max difference in pin power distribution for BWR lattices
- 0.5% RMS and 1.5% max difference in pin power distribution for PWR lattices

Acceptance Accuracy:

- 400 pcm difference in k_{inf}
- 1.5% RMS and 2.5% max difference in pin power distribution for BWR and PWR lattices

B.4.1 BWR

Description: The nominal uncontrolled 10 × 10 GE14 lattice is tested using the case matrix listed in Table B-16.

Table B-16 Test Suite 4: BWR Case Matrix

Case number	Burnup (GWd/MTU)	TF (K)	TC (K)	Void fraction (%)
1	0	950	560	0
2	0	950	560	40
3	0	950	560	70
4	0	950	560	90
5	40	950	560	0
6	40	950	560	40
7	40	950	560	70
8	40	950	560	90
9	80	950	560	0
10	80	950	560	40
11	80	950	560	70
12	80	950	560	90

Results: Figure B-38 shows the change in void trend with depletion. Although fresh fuel exhibits a different void trend, there is no significant k_{inf} bias between results of the isotopic configurations at 40 GWd/MTU and 80 GWd/MTU. The 90% void cases display the greatest bias for depleted fuel, with Polaris >250 pcm high and MG KENO and NEWT ~200 pcm low.

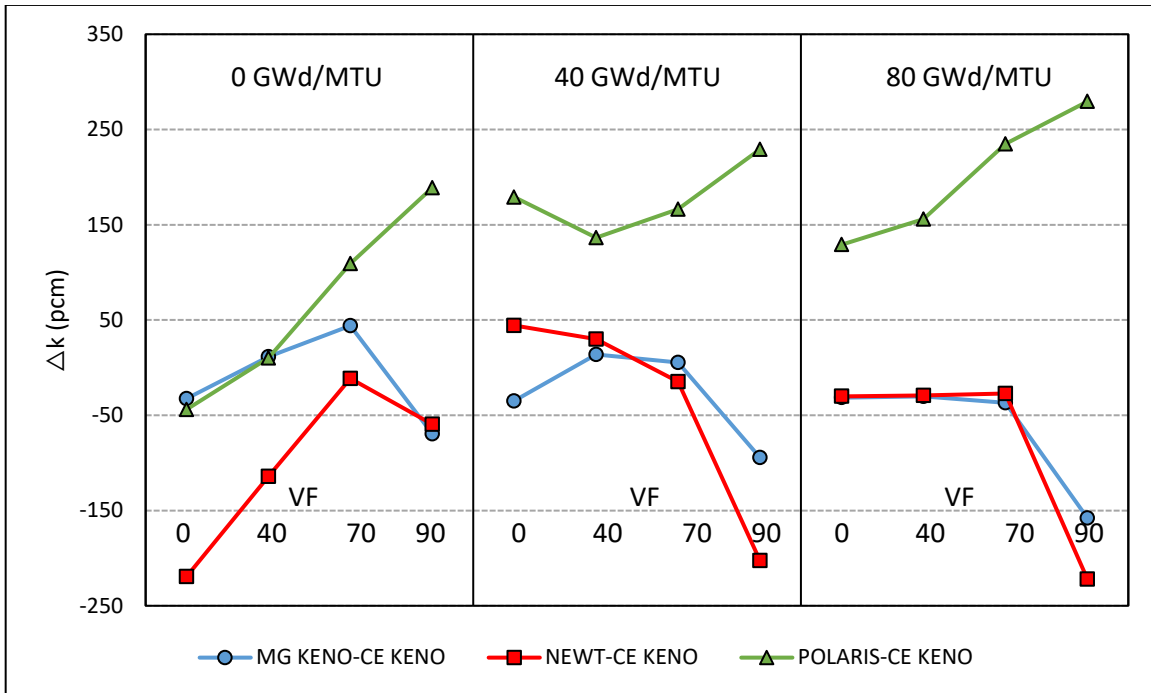


Figure B-38 Test Suite 4: 10 × 10 BWR Lattice k_{inf} Differences

B.4.2 PWR

Description: The nominal uncontrolled 17 × 17 WE lattice is tested using the case matrix listed in Table B-17.

Table B-17 Test Suite 4: PWR Case Matrix

Case number	Burnup (GWd/MTU)	TF (K)	TC (K)	PC (ppm)
1	0	900	560	0
2	40	900	560	0
3	80	900	560	0

Results: No significant biases are shown in Figure B-39. The Polaris results are approximately 100 pcm higher than the other MG codes.

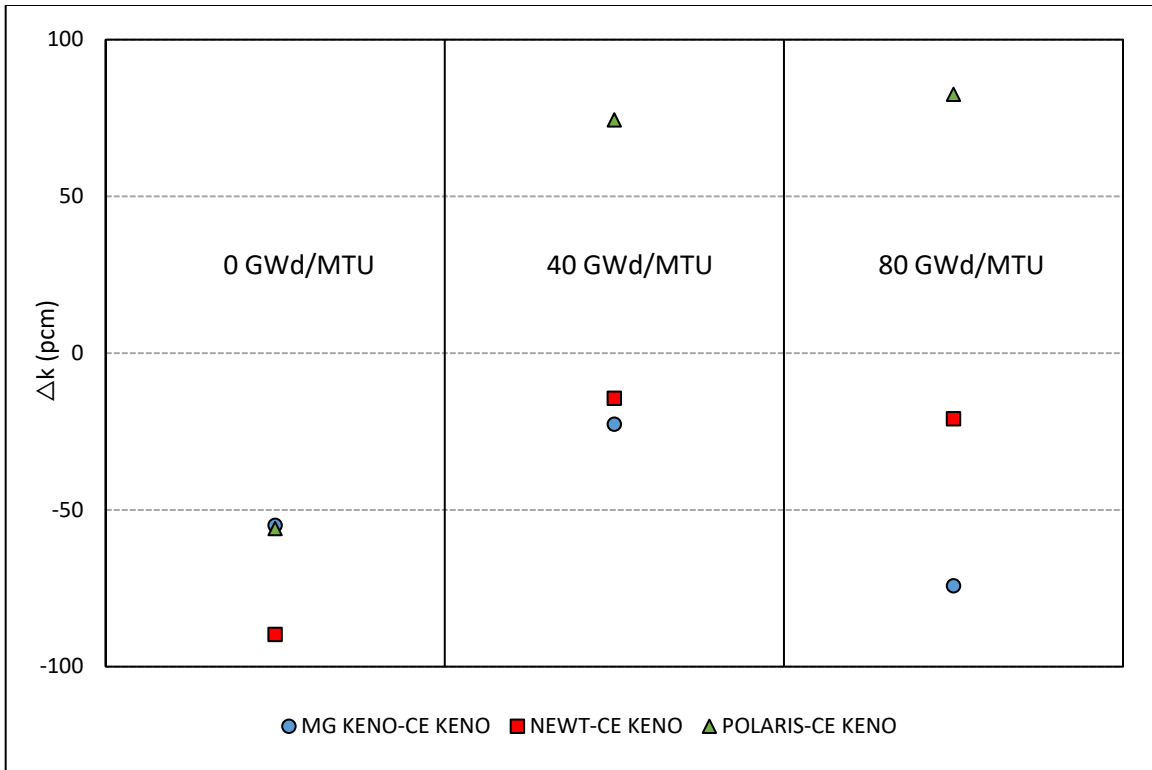


Figure B-39 Test Suite 4: 17 × 17 PWR Lattice k_{inf} Differences

B.5 Test Suite 5 – Depletion Calculations

Purpose: Performance of the depletion calculations is tested in this suite. UOX assemblies are depleted up to 15 GWd/MTU for BWR and up to 80 GWd/MTU for PWR assemblies using CE KENO, NEWT, and Polaris codes. The BWR assembly specifications and operating conditions are adapted from EGUNF Phase II benchmark, which focuses on gadolinium depletion in the first cycle (geometry details provided in the Expert Group on Burn-Up Credit (EGBUC) Phase IIIC benchmark [28]). The nominal PWR assembly is used for PWR depletion. Eigenvalues (at every depletion step) and U/Pu vectors are compared for the three codes.

Target Accuracy:

- 200 pcm difference in k_{inf}
- 1% relative difference in major in U/Pu vectors

Acceptance Accuracy:

- 400 pcm difference in k_{inf} and
- 2% relative difference in U/Pu vectors

B.5.1 BWR

Description: UOX fuel is tested using an 8 × 8 ATRIUM lattice design. The case matrix for this test suite is provided in Table B-18.

Table B-18 Test Suite 5: BWR Case Matrix

Case number	TF (K)	TC (K)	Void fraction (%)
1	900	559	0
2	900	559	40
3	900	559	70

Results: Figure B-40 shows evaluation of the k_{inf} difference between NEWT and CE KENO calculations at different void fractions. Depletion calculations for all void fractions exhibit similar trends with depletion. As in the void fraction trend seen at BOL, 0% and 70% void fraction results are close (-279 and -311 pcm), while k_{inf} differences at 40% void fraction show only -58 pcm bias at 15 GWd/MTU. Polaris results (shown in Figure B-41) exhibit smaller k_{inf} differences for all void fractions. The maximum difference is observed at 9 GWd/MTU as -173 pcm for 70% void fraction.

Relative differences in U/Pu vectors are listed in Table B-19 and Table B-20 at 8 GWd/MTU and 14 GWd/MTU burnup values, respectively. Overall, both U and Pu concentrations show good agreement. The highest differences are observed in ^{238}Pu concentrations for Polaris (2.1%) and NEWT (1.9%).

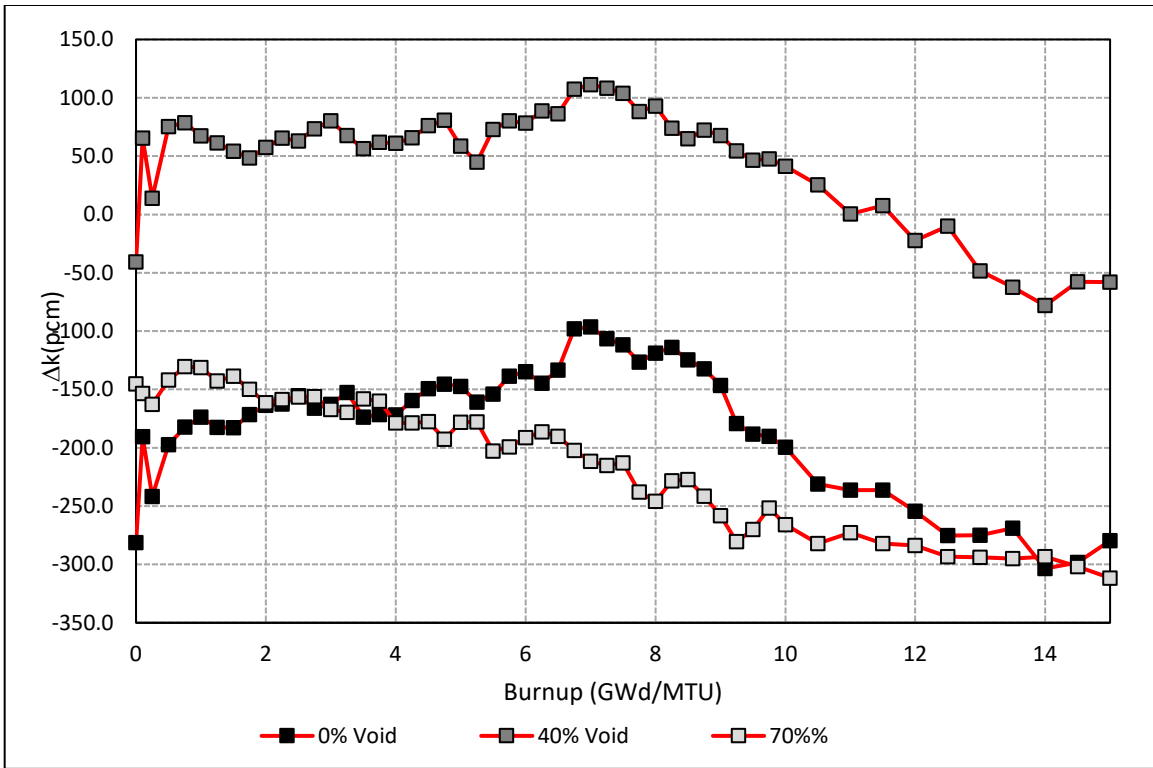


Figure B-40 Test Suite 5: 8 × 8 BWR Lattice NEWT k_{inf} Differences

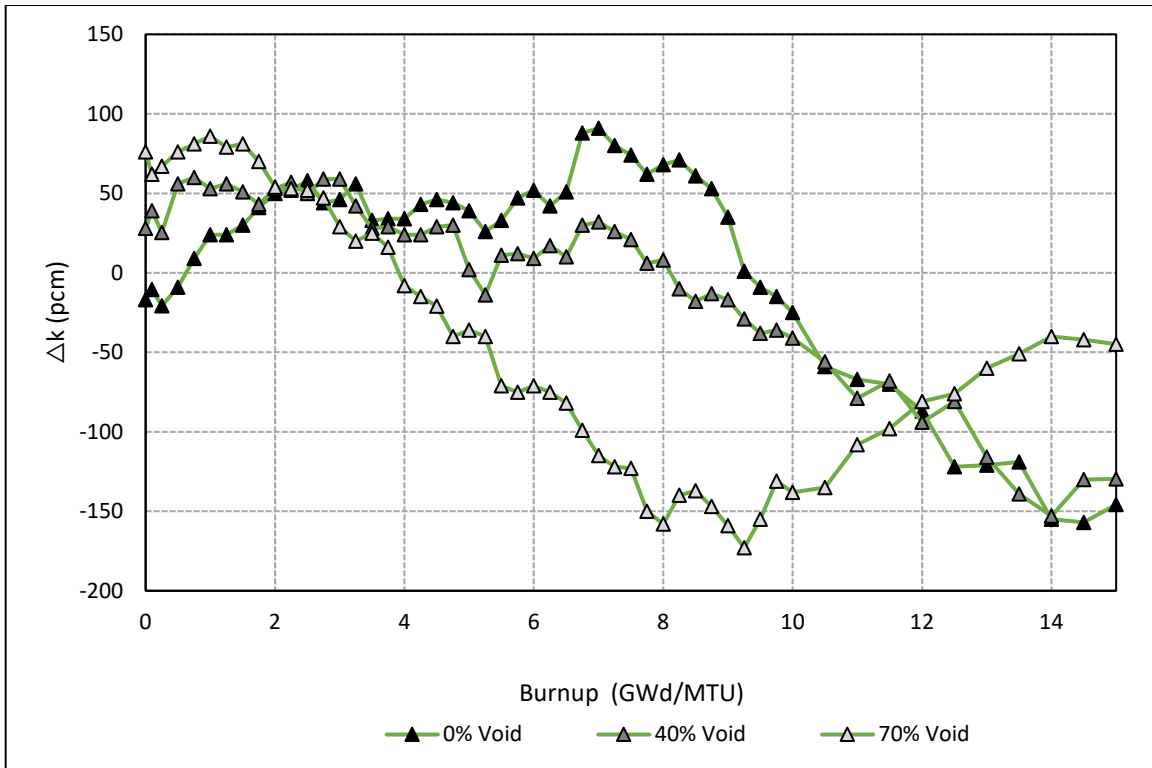


Figure B-41 Test suite 5 8 × 8 BWR Lattice Polaris k_{inf} Differences

Table B-19 Test Suite 5: BWR Relative Differences in Major Actinide Concentrations at 8 GWd/MTU

Isotope/void fraction	0%		40%		70%	
	NEWT (%)	Polaris (%)	NEWT (%)	Polaris (%)	NEWT (%)	Polaris (%)
^{234}U	0.2	0.2	0.1	0.3	0.2	0.3
^{235}U	-0.1	-0.1	-0.1	-0.1	0.0	0.0
^{236}U	0.3	0.3	0.2	0.3	0.2	0.3
^{238}U	0.0	0.0	0.0	0.0	0.0	0.0
^{238}Pu	-1.7	-2.0	-1.8	-2.1	-1.3	-2.1
^{239}Pu	-1.2	-1.3	-1.8	-1.1	0.9	-0.9
^{240}Pu	-1.0	-1.9	-1.5	-1.6	0.6	-1.5
^{241}Pu	-0.7	-1.6	-0.9	-1.4	0.8	-1.2
^{242}Pu	-0.9	-2.0	-0.6	-1.8	0.4	-1.8
^{241}Am	-1.0	-1.7	-1.0	-1.5	0.7	-1.3

Table B-20 Test Suite 5: BWR Relative Differences in Major Actinide Concentrations at 14 GWd/MTU

Isotope/void fraction	0%		40%		70%	
	NEWT (%)	Polaris (%)	NEWT (%)	Polaris (%)	NEWT (%)	Polaris (%)
²³⁴ U	0.1	0.4	0.1	0.5	0.3	0.6
²³⁵ U	-0.1	-0.2	-0.2	-0.1	0.0	-0.1
²³⁶ U	0.3	0.3	0.3	0.3	0.1	0.3
²³⁸ U	0.0	0.0	0.0	0.0	0.0	0.0
²³⁸ Pu	-1.7	-1.9	-2.0	-1.9	-1.1	-2.0
²³⁹ Pu	-1.2	-1.3	-1.9	-1.1	1.1	-0.9
²⁴⁰ Pu	-1.3	-1.8	-1.6	-1.6	0.6	-1.5
²⁴¹ Pu	-0.8	-1.3	-0.8	-1.0	0.9	-0.8
²⁴² Pu	-0.5	-1.6	-0.4	-1.4	0.4	-1.3
²⁴¹ Am	-0.5	-1.5	-1.0	-1.2	0.9	-1.0

B.5.2 PWR

Description: UOX fuel is tested using the nominal 17 × 17 lattice design from test suite 1 at nominal core conditions (TF = 900 K, TC = 560 K, and PC=1300 ppm).

Results: Changes in Δk_{inf} between NEWT, Polaris, MG KENO and CE KENO with increasing burnup are shown in Figure B-42. A good agreement is seen between NEWT and Polaris results up to 30 GWd/MTU. Differences in Δk_{inf} increase with burnup and reach 200 pcm at 80 GWd/MTU.

All codes pass acceptance criteria for this test suite. While Polaris results also pass target criteria, NEWT results fail target criteria after 50 GWd/MTU.

Relative differences in isotopic density distributions for NEWT and Polaris codes are provided in Table B-21. Both codes pass acceptance criteria at 30 GWd/MTU. The relative difference in U isotopes increases considerably at 80 GWd/MTU. Similar to low burnup BWR depletion, relative differences in ²³⁸Pu concentrations are high. However, the largest differences are observed in U isotopes at 80 GWd/MTU.

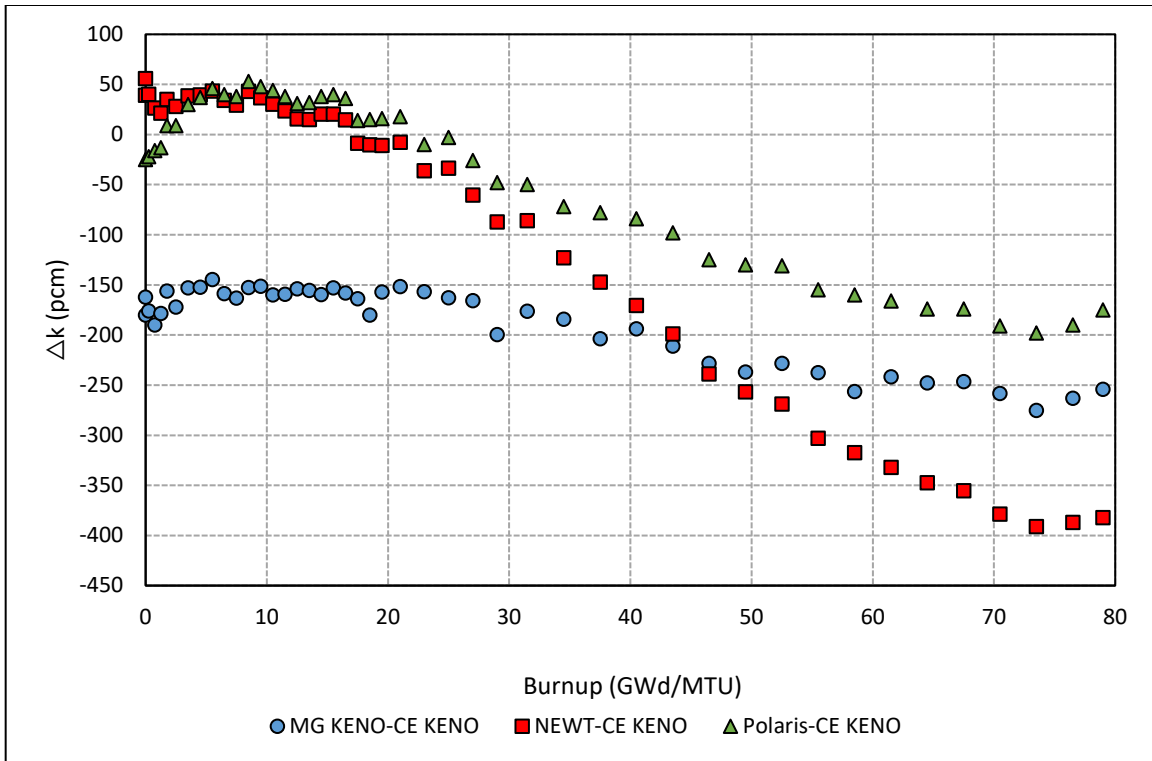


Figure B-42 Test Suite 5: 17 × 17 PWR Lattice k_{inf} Differences

Table B-21 Test Suite 5: PWR Relative Differences in Major Actinide Concentrations at 30 GWd/MTU and 80 GWd/MTU

Burnup Isotope/code	30 GWd/MTU		80 GWd/MTU	
	NEWT (%)	Polaris (%)	NEWT (%)	Polaris (%)
²³⁴ U	0.5	1.4	0.5	3.9
²³⁵ U	-0.5	-0.3	-4.6	-3.7
²³⁶ U	0.3	0.2	0.5	0.5
²³⁸ U	0.0	0.0	0.0	0.0
²³⁸ Pu	-1.7	-1.2	-2.0	-2.0
²³⁹ Pu	-1.3	-1.2	-2.2	-1.7
²⁴⁰ Pu	-0.7	-1.2	-1.0	-1.6
²⁴¹ Pu	-1.2	-1.1	-1.9	-1.8
²⁴² Pu	-0.6	0.1	0.3	-0.3

B.6 Test Suite 6 – Boron Injection

Purpose: Performance of the lattice physics calculations with respect to variations in the moderator boron concentrations is tested. Since soluble boron is used as part of the regular operation in PWR reactors, boron variations at cold, hot zero, and HFP cases are covered by this test suite. Unlike PWRs, boron injection is considered an accident condition for BWRs. Therefore, as limiting conditions, only cold and HZP cases are tested for BWR lattices.

Target Accuracy:

- 200 pcm difference in k_{inf}
- 1% RMS and 1.5% max difference in pin power distribution for BWR lattices
- 0.5% RMS and 1.5% max difference in pin power distribution for PWR lattices

Acceptance Accuracy:

- 400 pcm difference in k_{inf}
- 1.5% RMS and 2.5% max difference in pin power distribution for BWR and PWR lattices

B.6.1 BWR

Description: The nominal uncontrolled 10 × 10 GE14 lattice is tested using the case matrix listed in Table B-22.

Table B-22 Test Suite 6: BWR Case Matrix

Case number	TF (K)	TC (K)	PC (ppm)
1	293	293	0
2	293	293	1,000
3	293	293	2,000
4	560	560	0
5	560	560	1,000
6	560	560	2,000

Results: The k_{inf} differences are shown in Figure B-43. The cold NEWT and Polaris results show a bias vs boron concentration. The Polaris results are high at cold conditions but are nearly zero at HZP.

Pin power differences with the CE KENO reference distribution are presented in Figure B-44 for the HZP 2,000 ppm boron calculation (i.e., case 6 in Table B-22). The pin power differences pass the target accuracy criteria for both NEWT and Polaris.

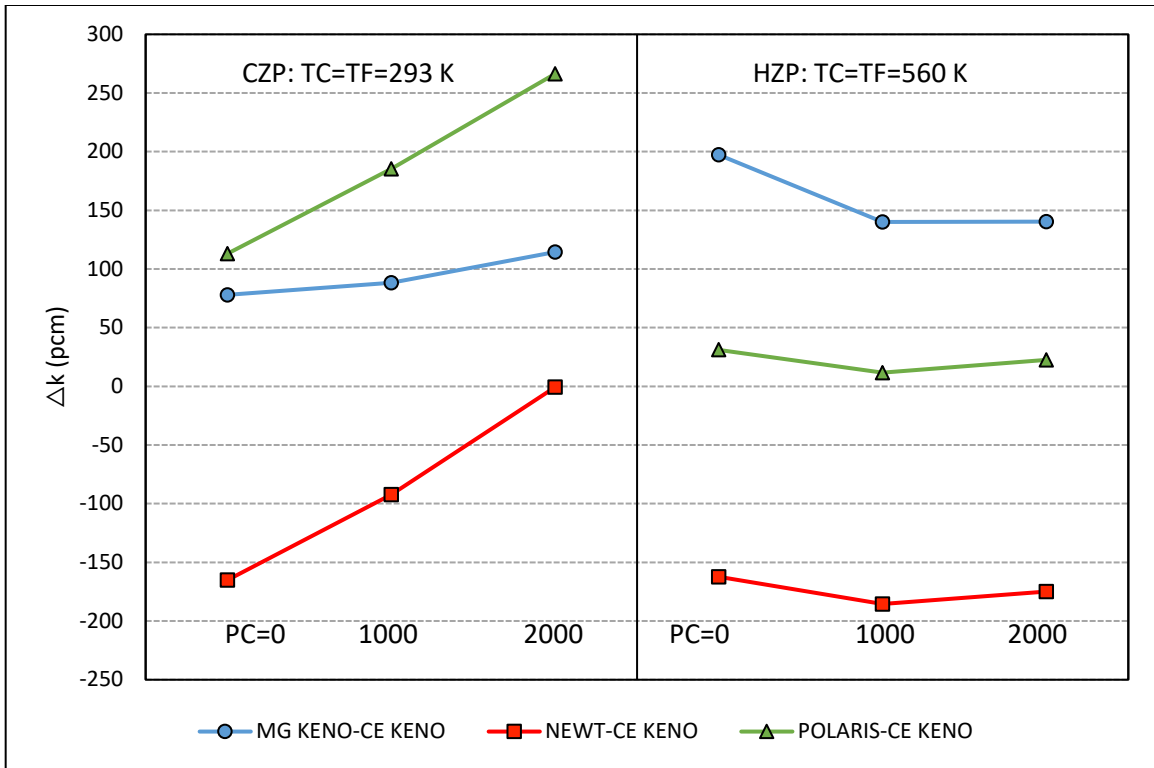


Figure B-43 Test Suite 6: BWR Lattice k_{inf} Differences for Boron Variations

NEWT (RMS=0.36%, MAX=0.98%)

0.98%	0.61%	0.36%	0.39%	0.45%	0.42%	0.42%	0.51%	0.64%	0.62%
0.61%	-0.20%	-0.33%	-0.18%	-0.27%	0.02%	-0.46%	0.16%	-0.18%	0.31%
0.36%	-0.33%	0.06%	-0.61%	0.05%	-0.42%	0.11%	-0.51%	-0.02%	0.03%
0.39%	-0.18%	-0.61%	-0.08%	-0.34%	N/A	N/A	-0.27%	-0.38%	-0.12%
0.45%	-0.27%	0.05%	-0.34%	0.18%	N/A	N/A	-0.24%	-0.26%	-0.06%
0.42%	0.02%	-0.42%	N/A	N/A	0.34%	-0.05%	-0.48%	0.02%	0.19%
0.42%	-0.46%	0.11%	N/A	N/A	-0.05%	-0.40%	-0.02%	-0.63%	0.16%
0.51%	0.16%	-0.51%	-0.27%	-0.24%	-0.48%	-0.02%	-0.54%	0.03%	-0.01%
0.64%	-0.18%	-0.02%	-0.38%	-0.26%	0.02%	-0.63%	0.03%	-0.32%	0.08%
0.62%	0.31%	0.03%	-0.12%	-0.06%	0.19%	0.16%	-0.01%	0.08%	0.50%

2.0%
1.8%
1.6%
1.4%
1.2%
1.0%
0.8%
0.6%
0.4%
0.2%
0.0%
-0.2%
-0.4%
-0.6%
-0.8%
-1.0%
-1.2%
-1.4%
-1.6%
-1.8%
-2.0%

Polaris (RMS=0.12%, MAX=0.37%)

0.30%	0.07%	-0.08%	0.00%	-0.01%	0.10%	0.01%	0.21%	0.13%	0.04%
0.07%	-0.21%	-0.10%	-0.05%	0.07%	0.02%	-0.14%	0.19%	0.12%	0.06%
-0.08%	-0.10%	0.15%	-0.04%	0.05%	-0.12%	0.10%	-0.04%	0.03%	0.05%
0.00%	-0.05%	-0.04%	-0.06%	-0.05%	N/A	N/A	-0.14%	-0.10%	-0.16%
-0.01%	0.07%	0.05%	-0.05%	0.10%	N/A	N/A	-0.12%	-0.10%	-0.13%
0.10%	0.02%	-0.12%	N/A	N/A	0.37%	0.02%	-0.20%	0.05%	0.15%
0.01%	-0.14%	0.10%	N/A	N/A	0.02%	-0.05%	0.01%	-0.27%	0.09%
0.21%	0.19%	-0.04%	-0.14%	-0.12%	-0.20%	0.01%	-0.13%	0.06%	-0.05%
0.13%	0.12%	0.03%	-0.10%	-0.10%	0.05%	-0.27%	0.06%	0.01%	-0.07%
0.04%	0.06%	0.05%	-0.16%	-0.13%	0.15%	0.09%	-0.05%	-0.07%	0.16%

2.0%
1.8%
1.6%
1.4%
1.2%
1.0%
0.8%
0.6%
0.4%
0.2%
0.0%
-0.2%
-0.4%
-0.6%
-0.8%
-1.0%
-1.2%
-1.4%
-1.6%
-1.8%
-2.0%

Figure B-44 Test Suite 6 10 × 10 DOM Zone Pin Power Differences at HZP Conditions at 2,000 ppm Boron Concentration

B.6.2 PWR

Description: The nominal uncontrolled 17×17 WE lattice is tested using the case matrix listed in Table B-23.

Table B-23 Test Suite 6: PWR Case Matrix

Case number	TF (K)	TC (K)	PC (ppm)
1	293	293	0
2	293	293	1,000
3	293	293	1,300
4	293	293	2,000
5	293	293	2,500
6	560	560	0
7	560	560	1,000
8	560	560	1,300
9	560	560	2,000
10	560	560	2,500
11	560	900	0
12	560	900	1,000
13	560	900	1,300
14	560	900	2,000
15	560	900	2,500

Results: Comparison of MG KENO, NEWT, and Polaris results are plotted in Figure B-45. With the exception of Polaris results at cold (293 K), all codes exhibit similar results.

Pin power differences with the CE KENO reference distribution are presented in Figure B-46 for the HFP, 0 ppm boron calculation (i.e., case 11 in Table B-23). The pin power differences pass the target accuracy criteria for both NEWT and Polaris.

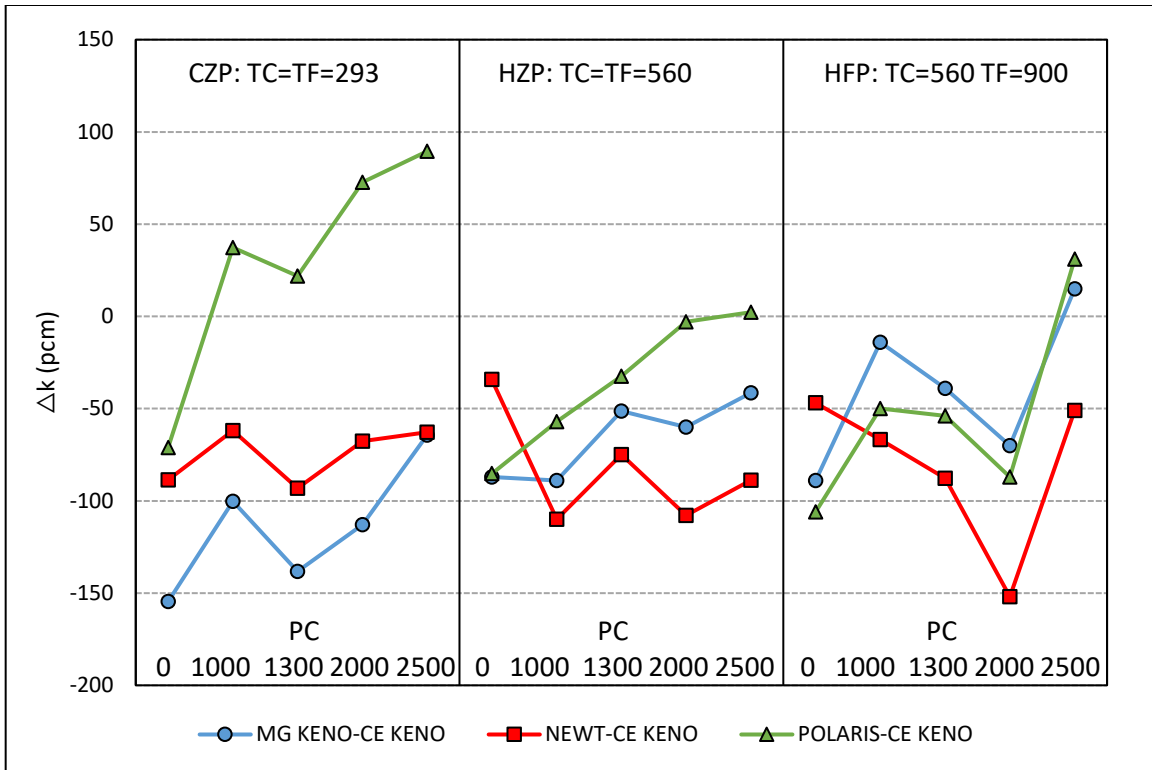
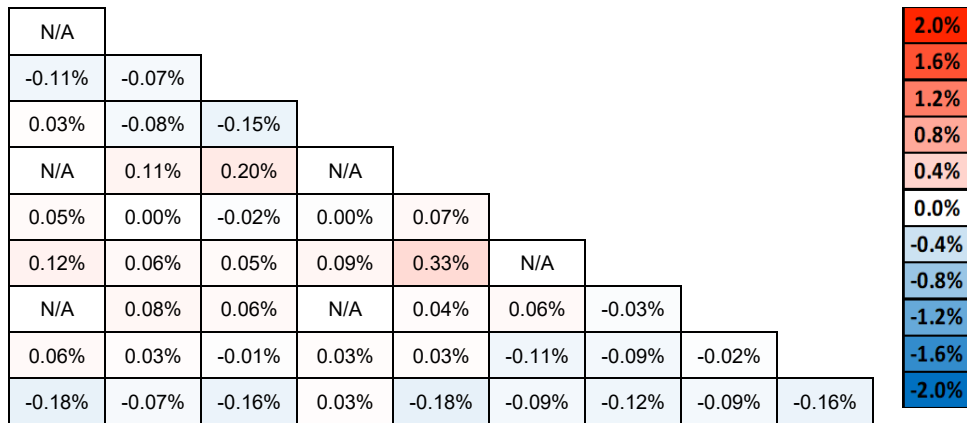


Figure B-45 Test Suite 6: PWR Lattice k_{inf} Differences for Boron Variations

NEWT (RMS= 0.11%, MAX=0.33%)



Polaris (RMS= 0.08%, MAX=0.23%)

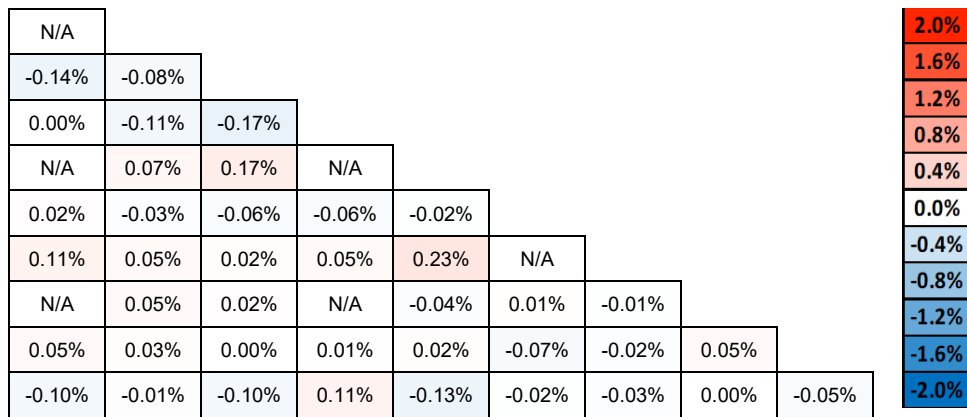


Figure B-46 Test Suite 6 17 × 17 Lattice Pin Power Differences at HFP Conditions at 0 ppm Boron Concentration

B.7 Test Suite 7 – Enrichment

Purpose: Performance of the lattice physics calculations with respect to increasing ^{235}U enrichments is tested. The enrichments of ^{235}U vary from 2–10 wt% in 2% increments for uncontrolled and controlled configurations.

Target Accuracy:

- 200 pcm difference in k_{inf}
- 1% RMS and 1.5% max difference in pin power distribution for BWR lattices
- 0.5% RMS and 1.5% max difference in pin power distribution for PWR lattices

Acceptance Accuracy:

- 400 pcm difference in k_{inf}
- 1.5% RMS and 2.5% max difference in pin power distribution for BWR and PWR lattices

B.7.1 BWR

Description: The nominal 10×10 GE14 lattice geometry is tested for the case matrix listed in Table B-24. The BWR lattice used in this test suite is shown in Figure B-47. Since this test suite requires fuel pin enrichments to be modified, uniform fuel enrichment is used instead of the enrichment zoning defined in test suite 1. The same gadolinia pin locations and gadolinia enrichments from the nominal configuration are preserved (light and dark pink colored fuel pins).

Table B-24 Test Suite 7: BWR Case Matrix

Case number	TF (K)	TC (K)	Void fraction (%)	Enrichment (wt%)
1	950	560	0	2
2	950	560	40	2
3	950	560	70	2
4	950	560	90	2
5	950	560	0	4
6	950	560	40	4
7	950	560	70	4
8	950	560	90	4
9	950	560	0	6
10	950	560	40	6
11	950	560	70	6
12	950	560	90	6
13	950	560	0	8
14	950	560	40	8
15	950	560	70	8
16	950	560	90	8
17	950	560	0	10
18	950	560	40	10
19	950	560	70	10
20	950	560	90	10

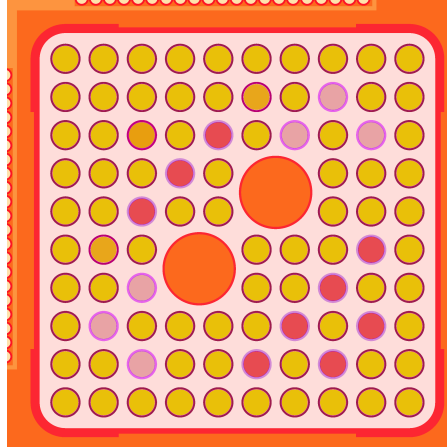


Figure B-47 Test Suite 7: BWR Lattice Design

Results: The Δk_{inf} values for uncontrolled and controlled cases based on the case matrix are plotted in Figure B-48 and Figure B-49, respectively.

In general, the same void trends with different biases are observed across all fuel enrichments. Polaris results show increasing positive bias vs void and enrichment, while NEWT results show larger negative bias at low enrichments. The bias introduced by control blade insertion is also similar to the biases seen in Test Suite 1. The Polaris results need further investigation.

Pin power differences with the CE KENO reference distribution are presented in Figure B-50 for the HFP, 40% void fraction 10% enrichment calculation (i.e., case 18 in Table B-24). The pin power differences pass the target accuracy criteria for both NEWT and Polaris.

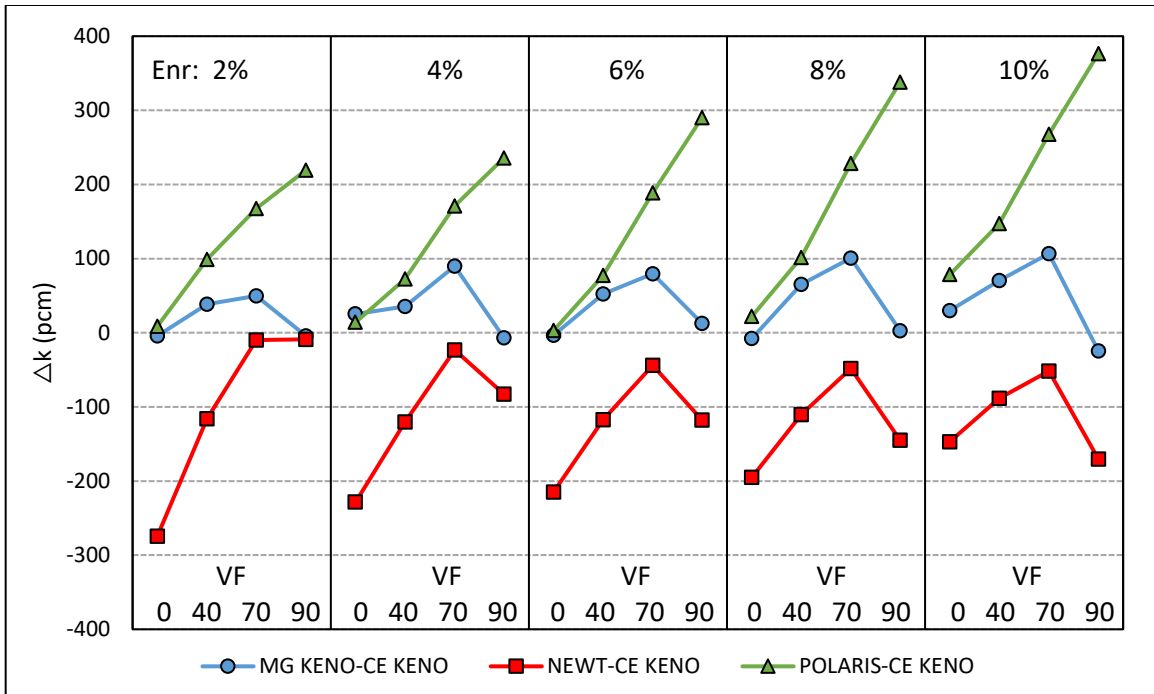


Figure B-48 Test Suite 7: k_{inf} Differences for Uncontrolled BWR Cases

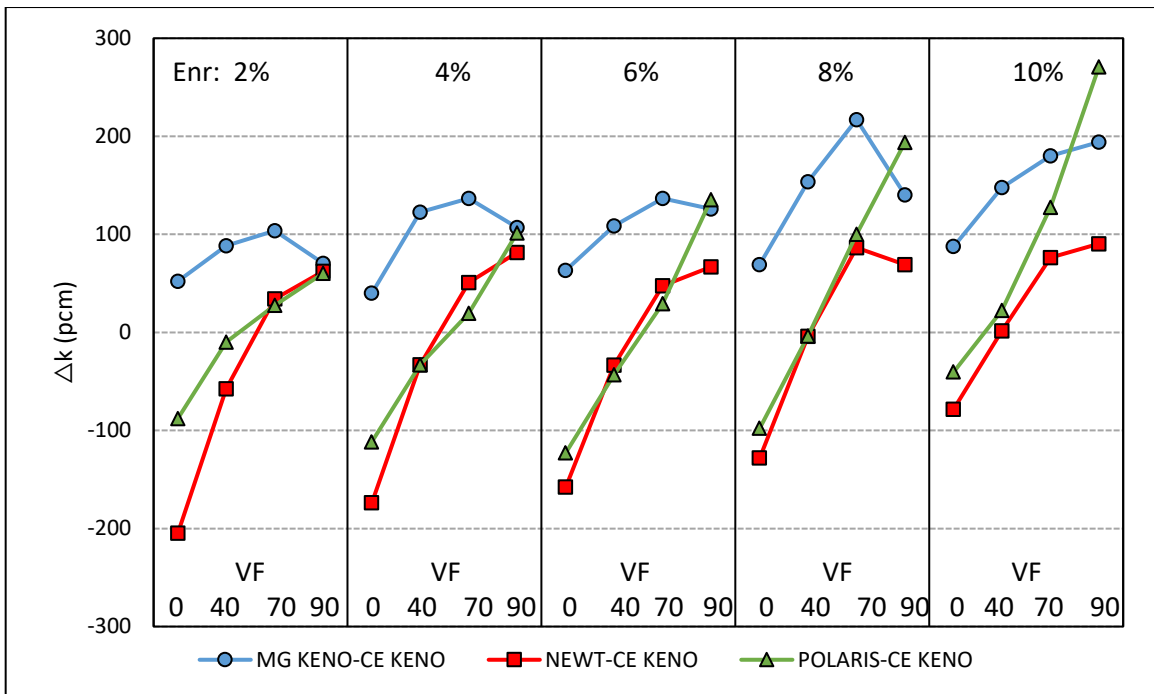


Figure B-49 Test Suite 7: k_{inf} Differences for Controlled BWR Cases

NEWT (RMS=0.43%, MAX=1.81%)

1.81%	0.98%	0.69%	0.21%	0.46%	0.35%	0.52%	0.30%	0.66%	1.23%	2.0%
0.98%	0.10%	-0.38%	-0.19%	-0.25%	-0.15%	-0.37%	-0.06%	-0.10%	0.28%	1.8%
0.69%	-0.38%	-0.23%	-0.50%	-0.08%	-0.41%	-0.03%	-0.51%	-0.14%	-0.11%	1.6%
0.21%	-0.19%	-0.50%	-0.15%	-0.40%	N/A	N/A	-0.38%	-0.26%	0.01%	1.4%
0.46%	-0.25%	-0.08%	-0.40%	0.13%	N/A	N/A	-0.27%	-0.28%	0.02%	1.2%
0.35%	-0.15%	-0.41%	N/A	N/A	-0.19%	-0.15%	-0.41%	-0.09%	-0.07%	1.0%
0.52%	-0.37%	-0.03%	N/A	N/A	-0.15%	-0.54%	-0.14%	-0.30%	0.02%	0.8%
0.30%	-0.06%	-0.51%	-0.38%	-0.27%	-0.41%	-0.14%	-0.46%	-0.14%	0.23%	0.6%
0.66%	-0.10%	-0.14%	-0.26%	-0.28%	-0.09%	-0.30%	-0.14%	-0.39%	0.01%	0.4%
1.23%	0.28%	-0.11%	0.01%	0.02%	-0.07%	0.02%	0.23%	0.01%	0.32%	0.2%
										0.0%
										-0.2%
										-0.4%
										-0.6%
										-0.8%
										-1.0%
										-1.2%
										-1.4%
										-1.6%
										-1.8%
										-2.0%

Polaris (RMS=0.21%, MAX=0.79%)

0.77%	0.57%	0.33%	-0.09%	0.02%	0.01%	0.13%	0.03%	0.20%	0.79%	2.0%
0.57%	0.14%	-0.09%	-0.03%	-0.01%	-0.18%	-0.19%	-0.08%	0.07%	0.09%	1.8%
0.33%	-0.09%	-0.18%	-0.11%	-0.11%	-0.08%	-0.08%	-0.22%	-0.15%	-0.07%	1.6%
-0.09%	-0.03%	-0.11%	-0.14%	-0.07%	N/A	N/A	-0.18%	-0.07%	0.04%	1.4%
0.02%	-0.01%	-0.11%	-0.07%	0.26%	N/A	N/A	-0.07%	-0.20%	0.04%	1.2%
0.01%	-0.18%	-0.08%	N/A	N/A	0.03%	0.00%	-0.27%	-0.08%	-0.03%	1.0%
0.13%	-0.19%	-0.08%	N/A	N/A	0.00%	-0.24%	-0.13%	-0.01%	0.03%	0.8%
0.03%	-0.08%	-0.22%	-0.18%	-0.07%	-0.27%	-0.13%	-0.15%	-0.13%	0.26%	0.6%
0.20%	0.07%	-0.15%	-0.07%	-0.20%	-0.08%	-0.01%	-0.13%	-0.25%	-0.08%	0.4%
0.79%	0.09%	-0.07%	0.04%	0.04%	-0.03%	0.03%	0.26%	-0.08%	0.19%	0.2%
										0.0%
										-0.2%
										-0.4%
										-0.6%
										-0.8%
										-1.0%
										-1.2%
										-1.4%
										-1.6%
										-1.8%
										-2.0%

Figure B-50 Test Suite 7: 10 × 10 DOM Zone Pin Power Differences at HFP Conditions, 40% Void Fraction, and 10% ²³⁵U Enrichment

B.7.2 PWR

Description: The nominal 17×17 WE lattice design is used for testing k_{inf} differences with respect to variations in fuel enrichments at HFP conditions. The case matrix is presented in Table B-25.

Table B-25 Test Suite 7: PWR Case Matrix

Case number	TF (K)	TC (K)	PC (ppm)	Enrichment (wt %)	Control rod
1	900	560	1,300	2	Out
2	900	560	1,300	4	Out
3	900	560	1,300	6	Out
4	900	560	1,300	8	Out
5	900	560	1,300	10	Out
6	900	560	1,300	2	In
7	900	560	1,300	4	In
8	900	560	1,300	6	In
9	900	560	1,300	8	In
10	900	560	1,300	10	In

Results: MG KENO, NEWT, and Polaris results are compared in Figure B-51 for uncontrolled and controlled configurations. Although no significant trend is observed with respect to increasing fuel enrichments, control rod biases are noticeable. Polaris is approximately 150 pcm low, NEWT is approximately 100 pcm low, and MG KENO is approximately 50 pcm high.

Pin power differences with the CE KENO reference distribution are presented in Figure B-52 for the HFP 10% enrichment calculation (i.e., case 5 in Table B-25). The pin power differences pass the target accuracy criteria for both NEWT and Polaris.

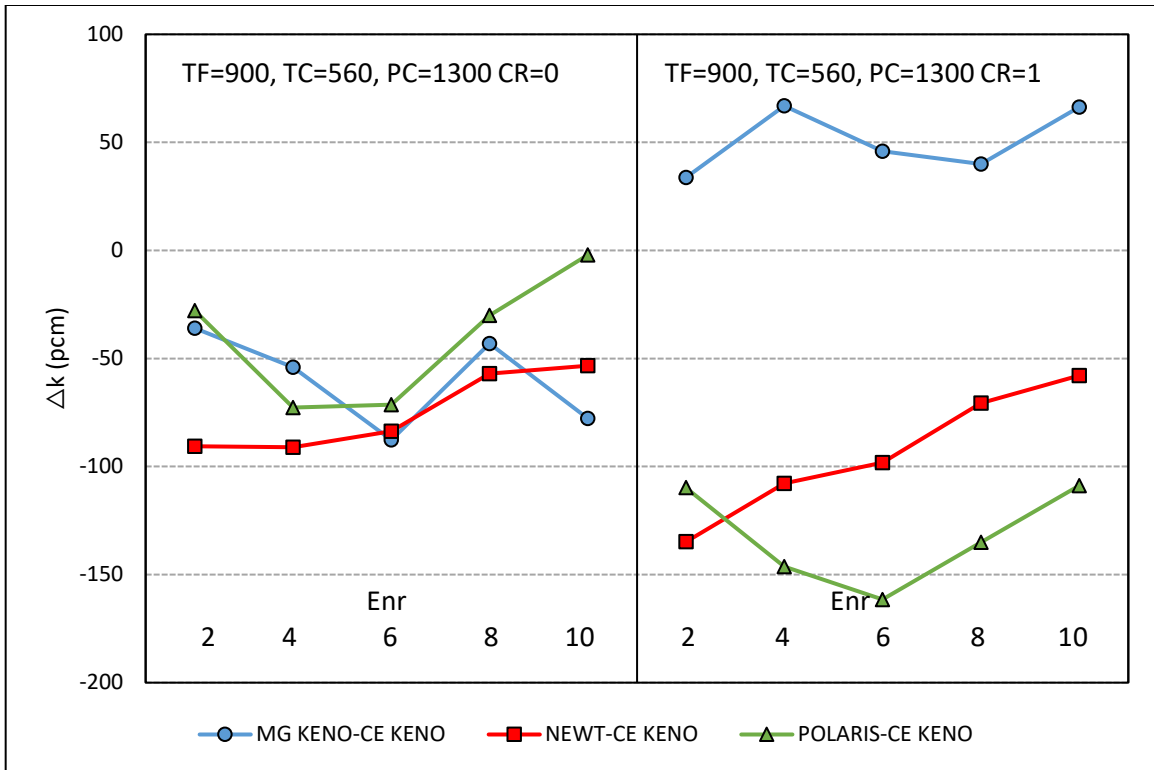
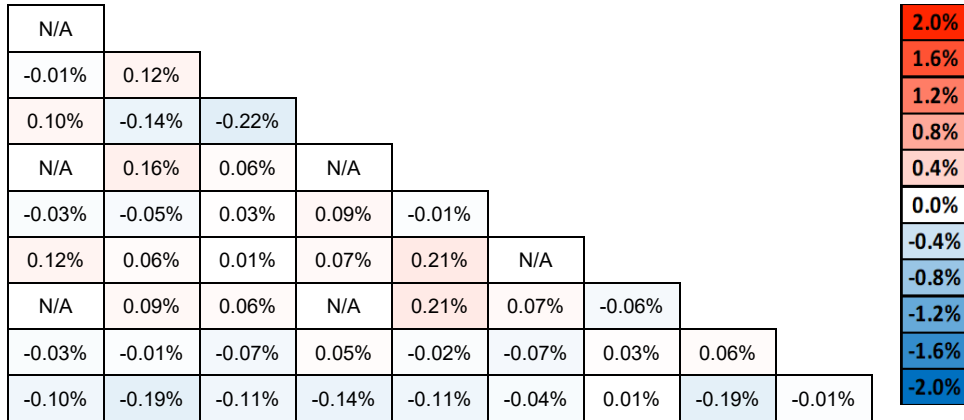
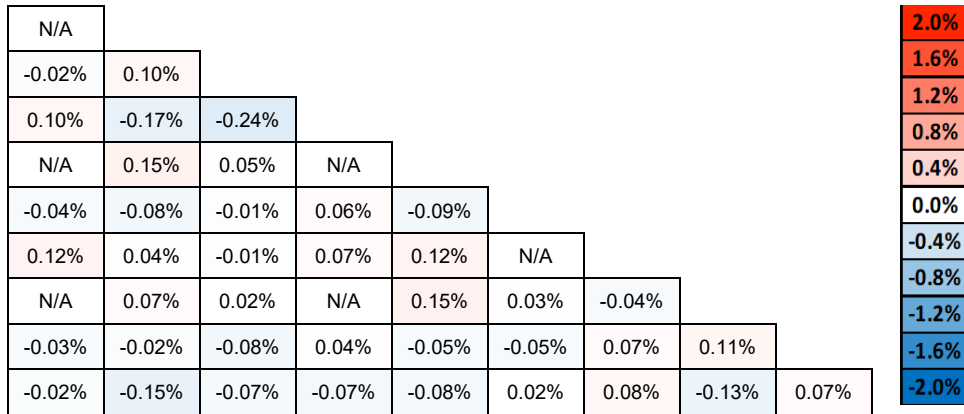


Figure B-51 Test Suite 7: k_{inf} Differences for Uncontrolled and Controlled PWR Cases

NEWT (RMS= 0.10%, MAX=0.22%)



Polaris (RMS= 0.09%, MAX=0.24%)



**Figure B-52 Test Suite 7: 17 × 17 Lattice Pin Power Differences at HFP Conditions
²³⁵U Enrichment**

B.8 Test Suite 8 – Fuel Temperature

Purpose: Performance of the lattice physics calculations with respect to varying fuel temperature is tested for the nominal BWR and PWR lattices at nominal uncontrolled configurations.

Target Accuracy:

- 200 pcm difference in k_{inf}
- 1% RMS and 1.5% max difference in pin power distribution for BWR lattices
- 0.5% RMS and 1.5% max difference in pin power distribution for PWR lattices

Acceptance Accuracy:

- 400 pcm difference in k_{inf}
- 1.5% RMS and 2.5% max difference in pin power distribution for BWR and PWR lattices

B.8.1 BWR

Description: The nominal uncontrolled 10 × 10 GE14 lattice is tested using the case matrix listed in Table B-26. Fuel temperature is varied from 500–3,000 K (approximate UOX melting temperature [29,30]).

Table B-26 Test Suite 8: BWR Case Matrix

Case number	TF (K)	TC (K)	Void fraction (%)
1	500	560	0
2	500	560	40
3	500	560	70
4	500	560	90
5	950	560	0
6	950	560	40
7	950	560	70
8	950	560	90
9	1,500	560	0
10	1,500	560	40
11	1,500	560	70
12	1,500	560	90
13	3,000	560	0
14	3,000	560	40
15	3,000	560	70
16	3,000	560	90

Results: The k_{inf} differences are plotted in Figure B-53. MG KENO and NEWT results vs void fraction are similar in shape to results in test suite 1. MG KENO shows no bias. NEWT results show a bias of -200–0 pcm vs void fraction, and Polaris results show a bias of 0–200 pcm. However, none of the codes shows a bias vs fuel temperature.

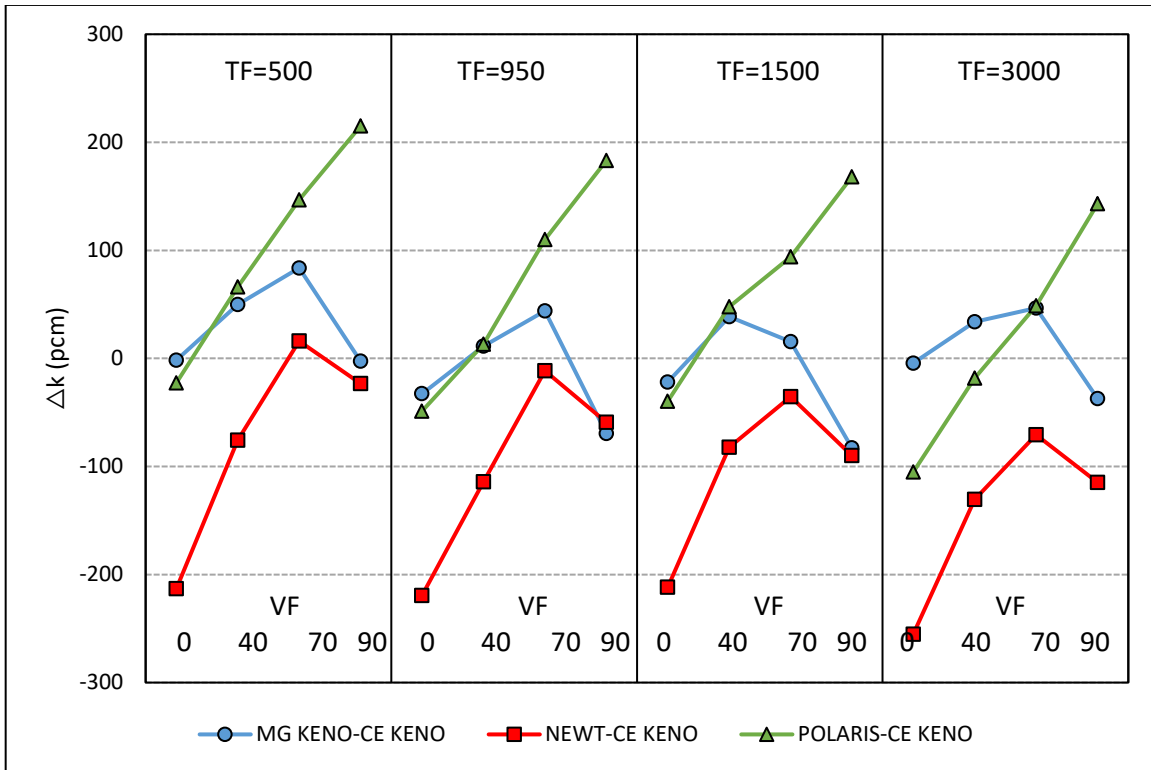


Figure B-53 Test Suite 8: k_{inf} Differences for Uncontrolled BWR Cases

B.8.2 PWR

Description: The nominal uncontrolled 17×17 WE lattice design is tested using the case matrix listed in Table B-27. Fuel temperature is varied from 560–3,000 K UOX melting temperature.

Table B-27 Test Suite 8: PWR Case Matrix

Case number	TF (K)	TC (K)	PC (ppm)
1	560	560	1,300
2	900	560	1,300
3	1,773	560	1,300
4	3,000	560	1,300

Results: The k_{inf} differences are plotted in Figure B-54. The MG KENO bias varies from -75–25 pcm. NEWT results show a bias of -200 to -100 pcm. Polaris results show a bias of -125 to -50 pcm.

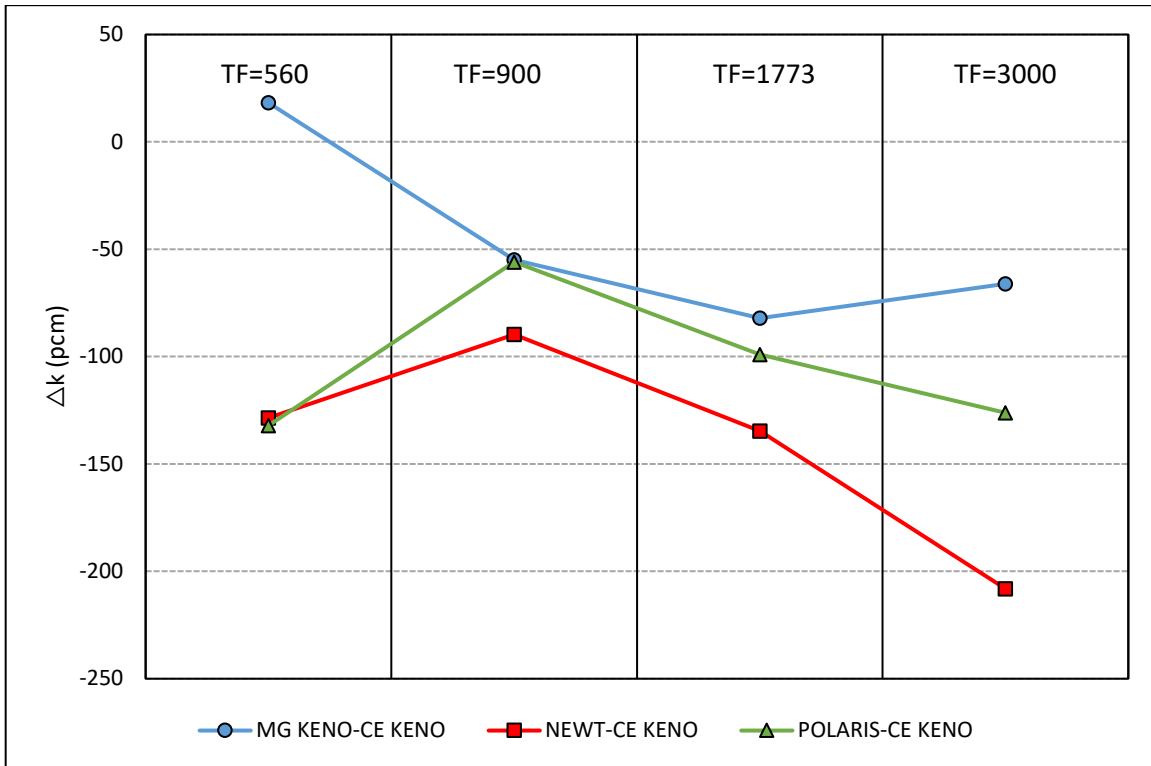


Figure B-54 Test Suite 8: k_{inf} Differences for Uncontrolled PWR Cases

B.9 Test Suite 9 – Burnable Poison Loading

Purpose: Performance of the lattice physics calculations with respect to varying BP concentrations is tested at nominal uncontrolled configurations.

Target Accuracy:

- 200 pcm difference in k_{inf}
- 1% RMS and 1.5% max difference in pin power distribution for BWR lattices
- 0.5% RMS and 1.5% max difference in pin power distribution for PWR lattices

Acceptance Accuracy:

- 400 pcm difference in k_{inf}
- 1.5% RMS and 2.5% max difference in pin power distribution for BWR and PWR lattices

B.9.1 BWR

Description: The nominal uncontrolled 10×10 GE14 lattice is used for testing gadolinia loadings up to 10 wt% in Gd_2O_3 - UO_2 pins. The test matrix used in this test suite is listed in Table B-28.

Table B-28 Test Suite 9: BWR Case Matrix

Case number	Gd (wt%)	Void fraction (%)
1	0	0
2	0	40
3	0	70
4	0	90
5	6	0
6	6	40
7	6	70
8	6	90
9	10	0
10	10	40
11	10	70
12	10	90

Results: The k_{inf} differences for increasing gadolinia loadings are plotted in Figure B-55. MG KENO and NEWT show a large bias of -400 pcm for no gadolinia and 90% void. The 6% and 10% gadolinia cases look much better, with a MG KENO bias of 0–100 pcm and a NEWT bias of -200–0 pcm. Polaris results range from 0–100 pcm except for 90% void cases that show 200–250 pcm bias.

Pin power differences with the CE KENO reference distribution are presented in Figure B-56 for the HFP, 40% void fraction, and 10% gadolinia calculation (i.e., case 10 in Table B-28). The pin power differences pass the target accuracy criteria for both NEWT and Polaris.

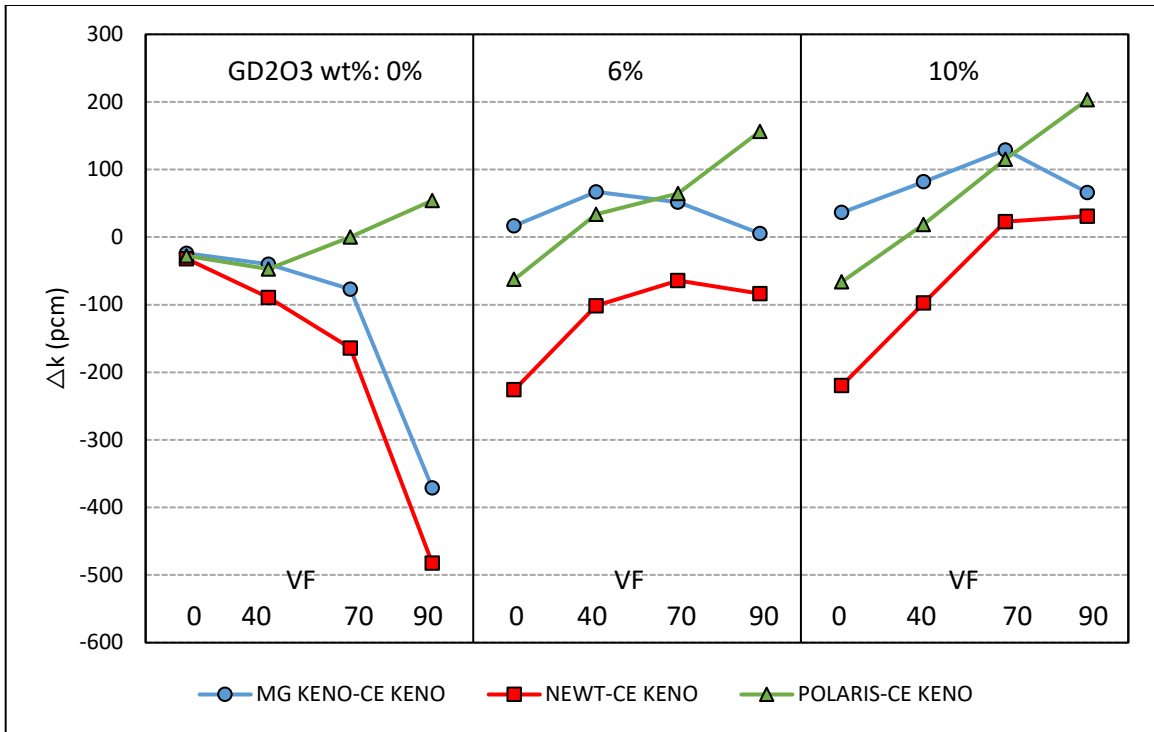


Figure B-55 Test suite 9: k_{inf} Differences for Uncontrolled BWR Cases

NEWT (RMS=0.39%, MAX=1.18%)

1.18%	0.89%	0.59%	0.43%	0.49%	0.19%	0.51%	0.26%	0.94%	0.74%	2.0%
0.89%	0.28%	0.12%	0.15%	-0.14%	-0.14%	-0.27%	-0.11%	-0.18%	0.56%	1.8%
0.59%	0.12%	-0.13%	-0.47%	-0.14%	-0.47%	-0.08%	-0.39%	-0.07%	0.00%	1.6%
0.43%	0.15%	-0.47%	-0.15%	-0.53%	N/A	N/A	-0.40%	-0.40%	-0.05%	1.4%
0.49%	-0.14%	-0.14%	-0.53%	-0.02%	N/A	N/A	-0.35%	-0.35%	-0.06%	1.2%
0.19%	-0.14%	-0.47%	N/A	N/A	-0.36%	-0.31%	-0.38%	-0.11%	-0.13%	1.0%
0.51%	-0.27%	-0.08%	N/A	N/A	-0.31%	-0.58%	-0.21%	-0.38%	-0.02%	0.8%
0.26%	-0.11%	-0.39%	-0.40%	-0.35%	-0.38%	-0.21%	-0.40%	-0.18%	-0.06%	0.6%
0.94%	-0.18%	-0.07%	-0.40%	-0.35%	-0.11%	-0.38%	-0.18%	0.01%	0.36%	0.4%
0.74%	0.56%	0.00%	-0.05%	-0.06%	-0.13%	-0.02%	-0.06%	0.36%	0.45%	0.2%
										0.0%
										-0.2%
										-0.4%
										-0.6%
										-0.8%
										-1.0%
										-1.2%
										-1.4%
										-1.6%
										-1.8%
										-2.0%

Polaris (RMS=0.13%, MAX=0.33%)

0.28%	0.16%	-0.02%	-0.02%	-0.03%	-0.10%	0.04%	-0.03%	0.33%	0.07%	2.0%
0.16%	0.12%	0.26%	0.19%	0.18%	-0.13%	-0.06%	-0.07%	0.01%	0.22%	1.8%
-0.02%	0.26%	-0.05%	0.02%	-0.12%	-0.08%	-0.06%	0.07%	-0.02%	0.00%	1.6%
-0.02%	0.19%	0.02%	-0.11%	-0.05%	N/A	N/A	-0.18%	-0.12%	-0.02%	1.4%
-0.03%	0.18%	-0.12%	-0.05%	0.10%	N/A	N/A	-0.07%	-0.23%	0.00%	1.2%
-0.10%	-0.13%	-0.08%	N/A	N/A	-0.11%	-0.13%	-0.03%	-0.06%	-0.06%	1.0%
0.04%	-0.06%	-0.06%	N/A	N/A	-0.13%	-0.12%	-0.14%	-0.03%	-0.01%	0.8%
-0.03%	-0.07%	0.07%	-0.18%	-0.07%	-0.03%	-0.14%	0.00%	-0.13%	-0.03%	0.6%
0.33%	0.01%	-0.02%	-0.12%	-0.23%	-0.06%	-0.03%	-0.13%	0.24%	0.23%	0.4%
0.07%	0.22%	0.00%	-0.02%	0.00%	-0.06%	-0.01%	-0.03%	0.23%	0.16%	0.2%
										0.0%
										-0.2%
										-0.4%
										-0.6%
										-0.8%
										-1.0%
										-1.2%
										-1.4%
										-1.6%
										-1.8%
										-2.0%

Figure B-56 Test suite 9: 10 × 10 DOM Zone Pin Power Differences at HFP Conditions, 40% Void Fraction, and 10% Gadolinia Loading

B.9.2 PWR

Description: The nominal uncontrolled 17×17 WE lattice is used for testing different B_4C , gadolinium, and IFBA BP enrichments for the nominal HFP conditions. Tested BP enrichments are listed in Table B-29.

Table B-29 Test Suite 9: PWR Case Matrix

Case number	PC (ppm)	B_4C (g/cm^3)	Gd (wt %)	IFBA ($mg^{10}B/in$)
1	1,300	1	0	0
2	1,300	2	0	0
3	1,300	4	0	0
4	1,300	0	6	0
5	1,300	0	10	0
6	1,300	0	0	4
7	1,300	0	0	15

Results: The k_{inf} differences with respect to variations in BP loadings are plotted in Figure B-57. MG KENO shows almost no bias except for IFBA (approximately -100 pcm). Polaris shows a bias for B_4C loadings (-200 to -75 pcm). NEWT shows large negative biases of approximately -125 pcm for B_4C , -200 pcm for gadolinium, and -300 to -200 pcm for IFBA. The larger bias for IFBA is likely due to the difficulty in modeling the thin burnable absorber layer in NEWT's arbitrary mesh structure that can only approximate cylinders.

Pin power differences with the CE KENO reference distribution are presented in Figure B-58 for the HFP 1,300 ppm boron $4 g/cm^3 B_4C$ calculation (i.e., case 3 in Table B-29). The pin power differences pass the target accuracy criteria for both NEWT and Polaris.

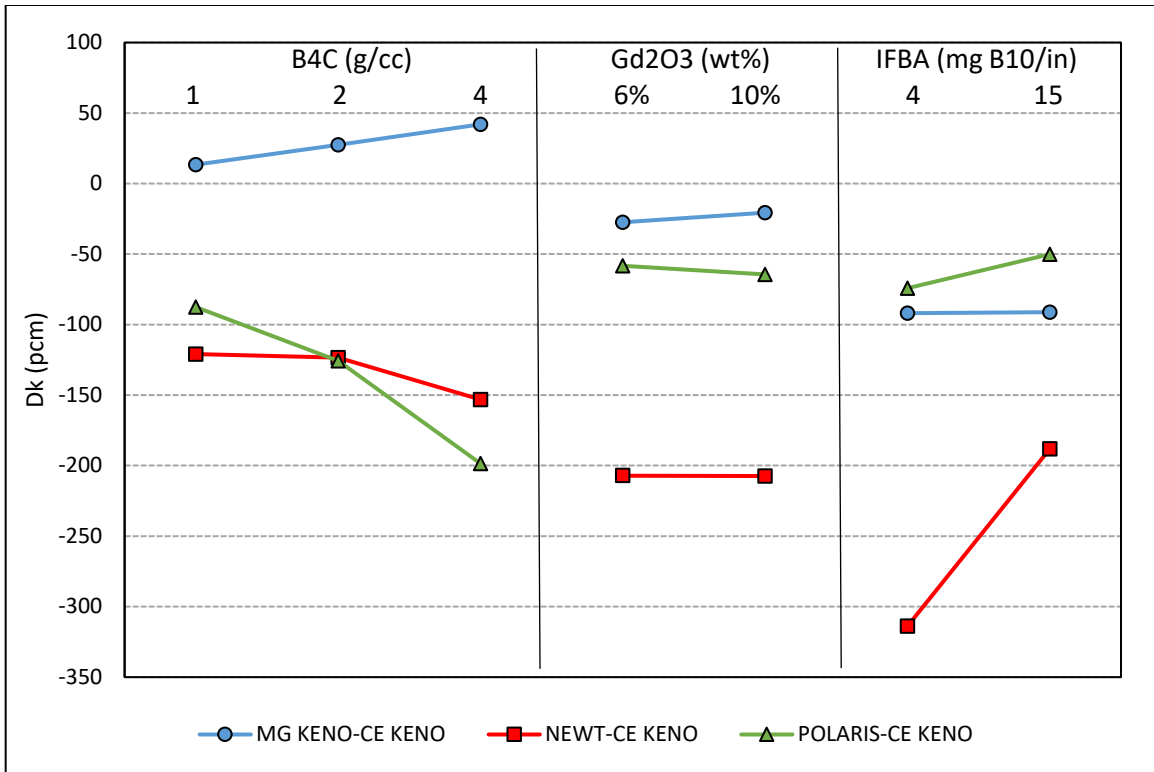
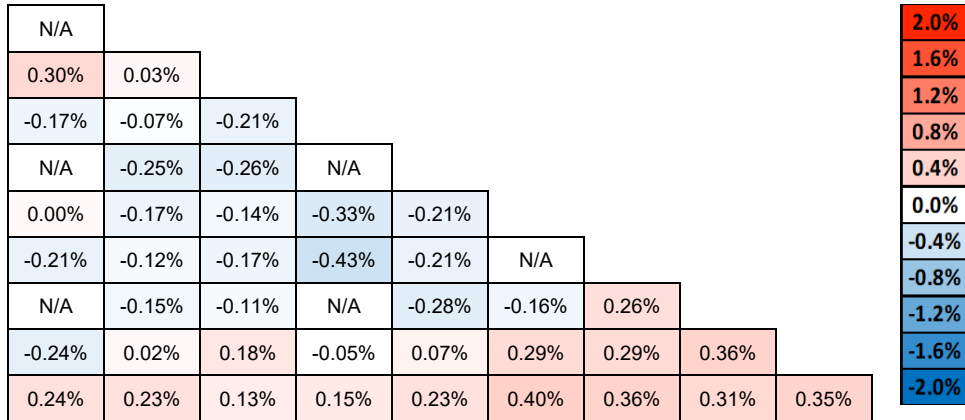


Figure B-57 Test Suite 9: k_{inf} Differences for Uncontrolled PWR Cases

NEWT (RMS= 0.23%, MAX=0.43%)



Polaris (RMS= 0.10%, MAX=0.28%)

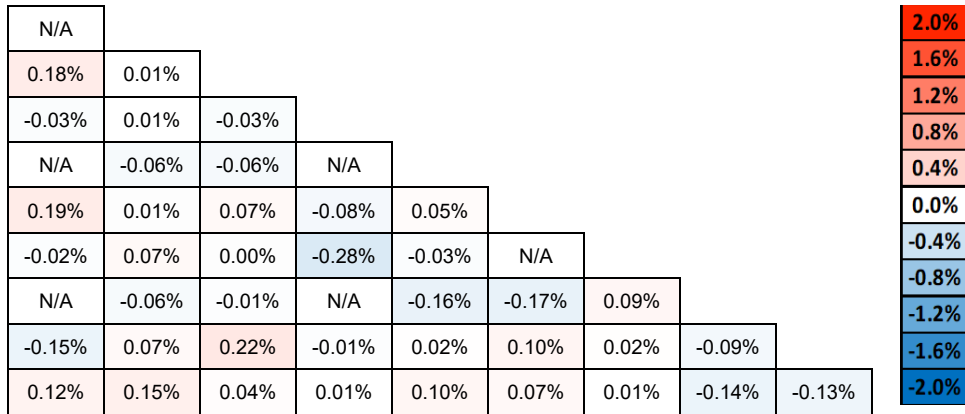


Figure B-58 Test Suite 9: 17 × 17 Lattice Pin Power Differences at HFP, 1,300 ppm Boron, and 4 g/cm³ B₄C Conditions

B.10 Test Suite 10 – Burnable Poison Spatial Variations

Purpose: Performance of the lattice physics calculations is tested for different numbers or patterns of BP loadings at nominal uncontrolled configurations.

Target Accuracy:

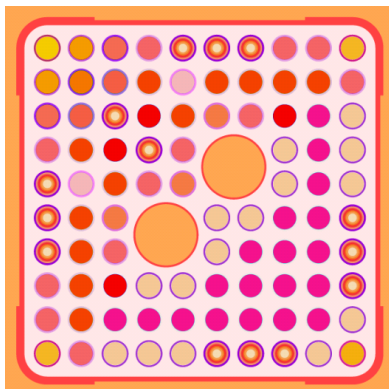
- 200 pcm difference in k_{inf}
- 1% RMS and 1.5% max difference in pin power distribution for BWR lattices
- 0.5% RMS and 1.5% max difference in pin power distribution for PWR lattices

Acceptance Accuracy:

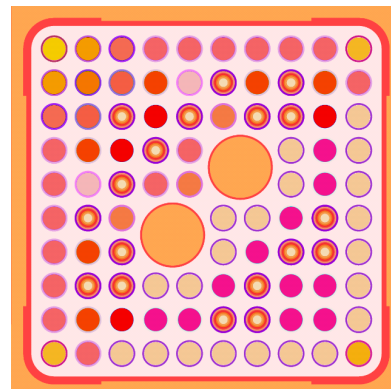
- 400 pcm difference in k_{inf}
- 1.5% RMS and 2.5% max difference in pin power distribution for BWR and PWR lattices

B.10.1 BWR

Description: The nominal 10×10 GE14 DOM lattice type is tested for edge and internal lumped (i.e., one or more neighboring) gadolinia rods. Gadolinia rod placement patterns are shown in Figure B-59. The case matrix for this test suite is listed in Table B-30. All cases use HFP conditions.



Edge d rod lumping



Internal Gd rod lumping

Figure B-59 Test Suite 10: Gadolinia Rod Patterns

Table B-30 Test Suite 10: BWR Case Matrix

Case number	Void fraction (%)	Location
1	0	Edge
2	40	Edge
3	70	Edge
4	90	Edge
5	0	Internal
6	40	Internal
7	70	Internal
8	90	Internal

Results: The k_{inf} differences with changing gadolinia rod patterns are plotted in Figure B-60 and Figure B-61 for uncontrolled and controlled configurations, respectively. MG KENO has a bias of 50–150 pcm. Polaris results vary from -150–200 pcm (internal pins are higher than edge pins by ~100 pcm). NEWT results vary from -250–0 pcm (internal pins are lower than edge pins by ~100 pcm).

Pin power differences with the CE KENO reference distribution are presented in Figure B-62 for the HFP 40% void fraction edge location calculation (i.e., case 2 in Table B-30). The pin power differences pass the target accuracy criteria for both NEWT and Polaris.

Pin power differences with the CE KENO reference distribution are presented in Figure B-63 for the HFP 40% void fraction internal location calculation (i.e., case 6 in Table B-30). The pin power differences pass the target accuracy criteria for both NEWT and Polaris.

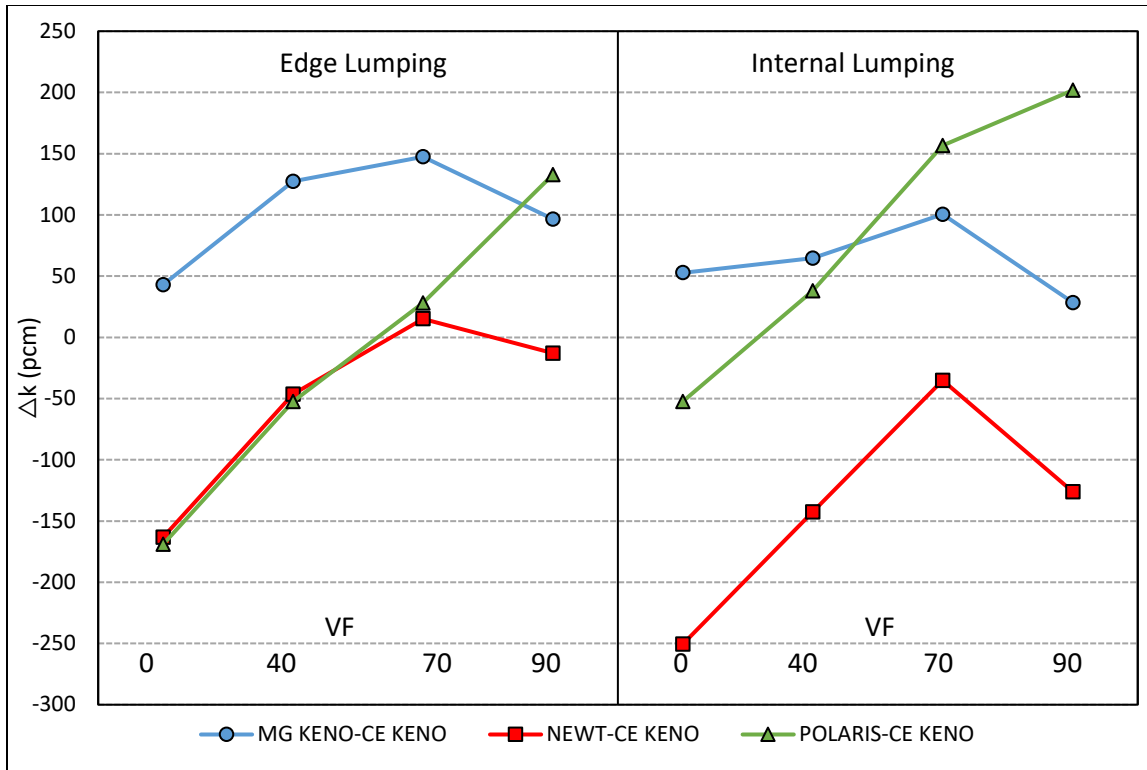


Figure B-60 Test Suite 10: k_{inf} Differences for BWR Uncontrolled Cases

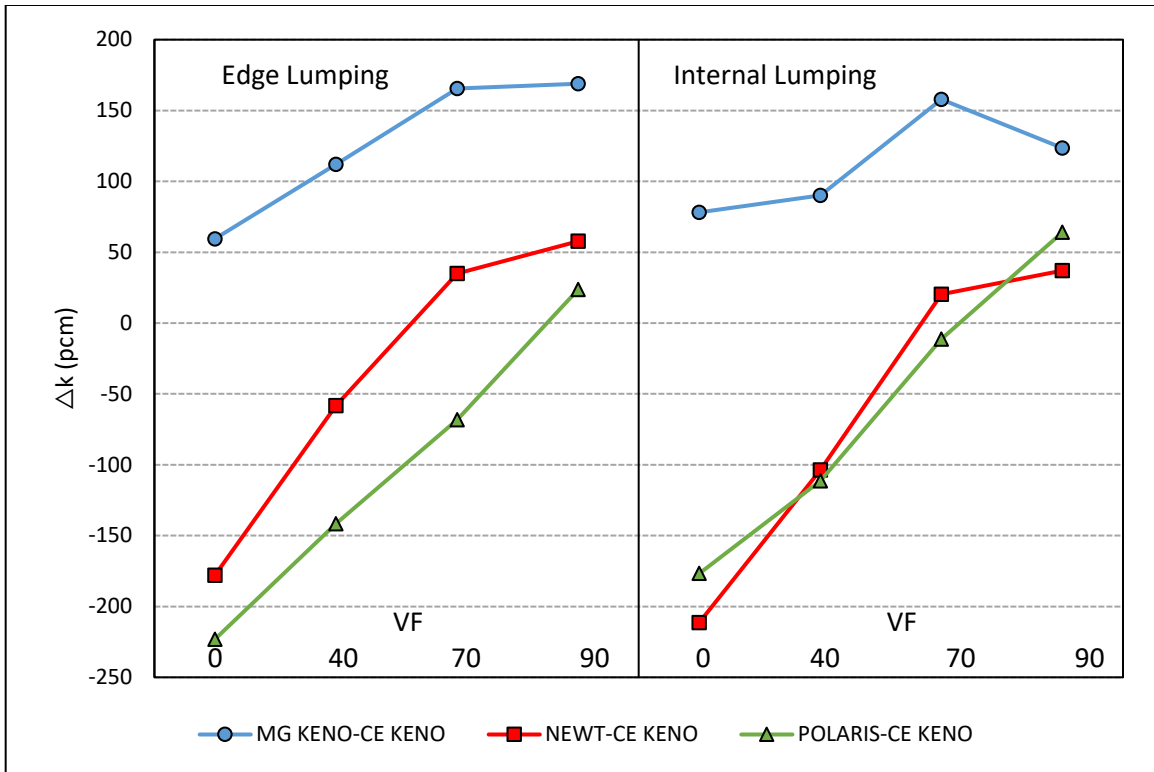


Figure B-61 Test Suite 10: k_{inf} Differences for BWR Controlled Cases

NEWT (RMS=0.34%, MAX=1.04%)

0.73%	0.77%	0.44%	0.06%	0.09%	0.01%	0.03%	0.42%	0.84%	1.04%	2.0%
0.77%	0.13%	-0.10%	-0.02%	-0.21%	-0.06%	-0.25%	-0.14%	0.14%	0.66%	1.8%
0.44%	-0.10%	-0.19%	-0.41%	-0.15%	-0.35%	-0.22%	-0.11%	0.10%	0.20%	1.6%
0.06%	-0.02%	-0.41%	-0.30%	-0.37%	N/A	N/A	-0.10%	-0.32%	-0.04%	1.4%
0.09%	-0.21%	-0.15%	-0.37%	0.12%	N/A	N/A	-0.18%	-0.31%	-0.08%	1.2%
0.01%	-0.06%	-0.35%	N/A	N/A	0.20%	-0.15%	-0.15%	-0.22%	-0.02%	1.0%
0.03%	-0.25%	-0.22%	N/A	N/A	-0.15%	-0.28%	-0.44%	-0.28%	-0.09%	0.8%
0.42%	-0.14%	-0.11%	-0.10%	-0.18%	-0.15%	-0.44%	-0.32%	-0.33%	0.03%	0.6%
0.84%	0.14%	0.10%	-0.32%	-0.31%	-0.22%	-0.28%	-0.33%	-0.16%	0.07%	0.4%
1.04%	0.66%	0.20%	-0.04%	-0.08%	-0.02%	-0.09%	0.03%	0.07%	0.46%	0.2%
										0.0%
										-0.2%
										-0.4%
										-0.6%
										-0.8%
										-1.0%
										-1.2%
										-1.4%
										-1.6%
										-1.8%
										-2.0%

Polaris (RMS=0.13%, MAX=0.35%)

-0.05%	0.10%	-0.08%	-0.18%	0.01%	-0.07%	-0.02%	0.16%	0.24%	0.35%	2.0%
0.10%	-0.02%	0.10%	0.11%	0.09%	0.04%	-0.04%	-0.01%	0.20%	0.31%	1.8%
-0.08%	0.10%	-0.13%	-0.07%	-0.10%	-0.15%	-0.11%	0.05%	0.18%	0.06%	1.6%
-0.18%	0.11%	-0.07%	-0.24%	-0.16%	N/A	N/A	-0.01%	-0.14%	-0.11%	1.4%
0.01%	0.09%	-0.10%	-0.16%	0.13%	N/A	N/A	-0.09%	-0.15%	-0.02%	1.2%
-0.07%	0.04%	-0.15%	N/A	N/A	0.13%	-0.08%	-0.10%	-0.01%	-0.04%	1.0%
-0.02%	-0.04%	-0.11%	N/A	N/A	-0.08%	-0.01%	-0.15%	-0.05%	-0.06%	0.8%
0.16%	-0.01%	0.05%	-0.01%	-0.09%	-0.10%	-0.15%	-0.14%	-0.14%	0.02%	0.6%
0.24%	0.20%	0.18%	-0.14%	-0.15%	-0.01%	-0.05%	-0.14%	0.04%	0.17%	0.4%
0.35%	0.31%	0.06%	-0.11%	-0.02%	-0.04%	-0.06%	0.02%	0.17%	0.20%	0.2%
										0.0%
										-0.2%
										-0.4%
										-0.6%
										-0.8%
										-1.0%
										-1.2%
										-1.4%
										-1.6%
										-1.8%
										-2.0%

Figure B-62 Test Suite 10: 10 × 10 DOM Zone Pin Power Differences at HFP Conditions, 40% Void Fraction, Edge Gadolinia Loading

NEWT (RMS=0.32%, MAX=0.95%)

0.95%	0.77%	0.46%	0.33%	0.48%	0.05%	0.30%	0.30%	0.68%	0.72%	2.0%
0.77%	0.58%	-0.17%	0.08%	-0.43%	-0.01%	-0.32%	-0.12%	-0.01%	0.24%	1.8%
0.46%	-0.17%	-0.15%	-0.45%	-0.14%	-0.32%	-0.09%	-0.23%	-0.13%	-0.11%	1.6%
0.33%	0.08%	-0.45%	-0.14%	-0.41%	N/A	N/A	-0.29%	-0.16%	0.10%	1.4%
0.48%	-0.43%	-0.14%	-0.41%	-0.06%	N/A	N/A	-0.25%	-0.26%	-0.05%	1.2%
0.05%	-0.01%	-0.32%	N/A	N/A	-0.03%	-0.26%	-0.27%	-0.17%	-0.15%	1.0%
0.30%	-0.32%	-0.09%	N/A	N/A	-0.26%	-0.35%	-0.27%	-0.14%	0.05%	0.8%
0.30%	-0.12%	-0.23%	-0.29%	-0.25%	-0.27%	-0.27%	-0.17%	-0.21%	0.02%	0.6%
0.68%	-0.01%	-0.13%	-0.16%	-0.26%	-0.17%	-0.14%	-0.21%	-0.07%	0.33%	0.4%
0.72%	0.24%	-0.11%	0.10%	-0.05%	-0.15%	0.05%	0.02%	0.33%	0.49%	0.2%
										0.0%
										-0.2%
										-0.4%
										-0.6%
										-0.8%
										-1.0%
										-1.2%
										-1.4%
										-1.6%
										-1.8%
										-2.0%

Polaris (RMS=0.12%, MAX=0.48%)

0.14%	0.15%	-0.06%	-0.03%	0.03%	-0.22%	-0.07%	0.06%	0.17%	0.12%	2.0%
0.15%	0.48%	0.02%	0.16%	-0.09%	-0.02%	-0.11%	-0.09%	0.15%	-0.04%	1.8%
-0.06%	0.02%	-0.08%	0.07%	-0.13%	0.05%	-0.06%	-0.14%	-0.07%	-0.08%	1.6%
-0.03%	0.16%	0.07%	-0.10%	0.05%	N/A	N/A	-0.09%	0.09%	0.17%	1.4%
0.03%	-0.09%	-0.13%	0.05%	0.03%	N/A	N/A	-0.05%	-0.11%	0.02%	1.2%
-0.22%	-0.02%	0.05%	N/A	N/A	0.18%	-0.11%	-0.06%	-0.12%	-0.15%	1.0%
-0.07%	-0.11%	-0.06%	N/A	N/A	-0.11%	0.00%	-0.19%	-0.05%	0.13%	0.8%
0.06%	-0.09%	-0.14%	-0.09%	-0.05%	-0.06%	-0.19%	0.12%	-0.04%	0.00%	0.6%
0.17%	0.15%	-0.07%	0.09%	-0.11%	-0.12%	-0.05%	-0.04%	0.05%	0.22%	0.4%
0.12%	-0.04%	-0.08%	0.17%	0.02%	-0.15%	0.13%	0.00%	0.22%	0.16%	0.2%
										0.0%
										-0.2%
										-0.4%
										-0.6%
										-0.8%
										-1.0%
										-1.2%
										-1.4%
										-1.6%
										-1.8%
										-2.0%

Figure B-63 Test Suite 10: 10 × 10 DOM Zone Pin Power Differences at HFP Conditions, 40% Void Fraction, Internal Gadolinia Loading

B.10.2 PWR

Description: The nominal 17×17 WE lattice type is tested for different loading patterns of five different BP types (B_4C , Pyrex, gadolinium, IFBA and WABA). Figure B-64 shows B_4C , Pyrex, and WABA loading patterns used in this test suite. Since loading patterns are identical for these three BP types, only representative B_4C patterns and samples from other BP models are shown. Integral BP (IFBA, gadolinium) patterns are shown in Figure B-65. The case matrix used in this test suite and the nominal loadings for each BP type are shown in Table B-31 and Table B-32. All cases were run at HFP conditions and 1,300 ppm soluble boron.

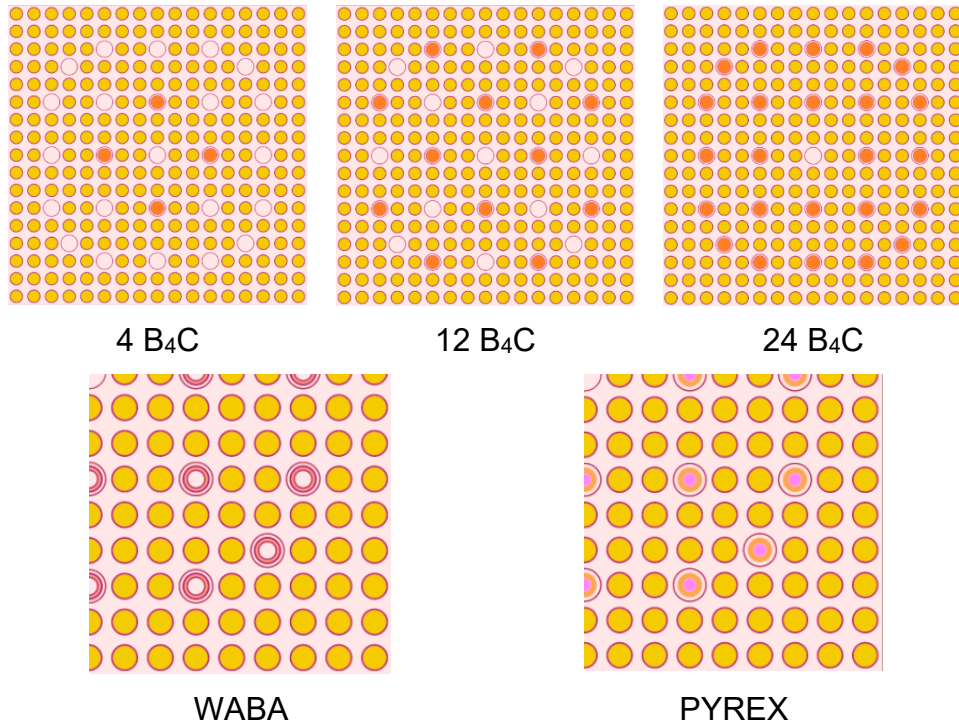


Figure B-64 Test Suite 10: PWR BP Loading Patterns

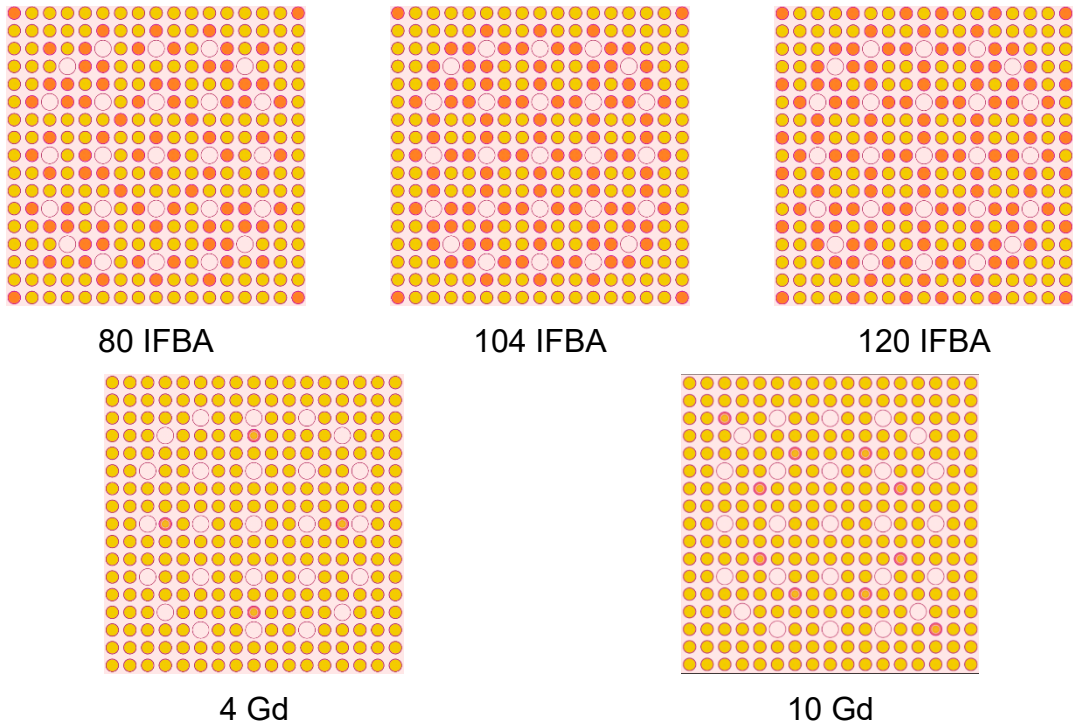


Figure B-65 Test Suite 10: PWR Integral BP Loading Patterns

Table B-31 Test Suite 10: PWR Case Matrix

Case number	BP type	Number of BPs
1	B ₄ C	4
2	B ₄ C	12
3	B ₄ C	24
4	Pyrex	4
5	Pyrex	12
6	Pyrex	24
7	Gd	4
8	Gd	12
9	IFBA	80
10	IFBA	104
11	IFBA	120
12	WABA	4
13	WABA	12
14	WABA	24

Table B-32 Test Suite 10: PWR Variations in Number of bp Rods

Burnable poison	Poison loading	Number of rods
Gadolinia	4 wt% Gd ₂ O ₃	4, 12
WABA	14 wt% B ₄ C	4, 12, 24
B ₄ C	4 wt% B ₄ C	4, 12, 24
Pyrex	12.5 wt% B ₂ O ₃	4, 12, 24
IFBA	3 mg ¹⁰ B/in.	80, 104, 120

Results: The k_{inf} differences based on the case matrix are plotted in Figure B-66. While no significant trend is observed with respect to BP loading patterns, a significant bias is observed in NEWT results for IFBA loadings. As noted previously, this is probably due to difficulty in modeling the thin burnable absorber layer in NEWT's arbitrary mesh structure that can only approximate cylinders.

MG KENO and Polaris results agree well and are within -100 to 0 pcm for all BP types except for B₄C, which is still within the target accuracy.

Pin power differences with the CE KENO reference distribution are presented in Figure B-67 for the HFP 1,300 ppm boron 4 B₄C rods calculation (i.e., case 1 in Table B-31). The pin power differences pass the target accuracy criteria for both NEWT and Polaris.

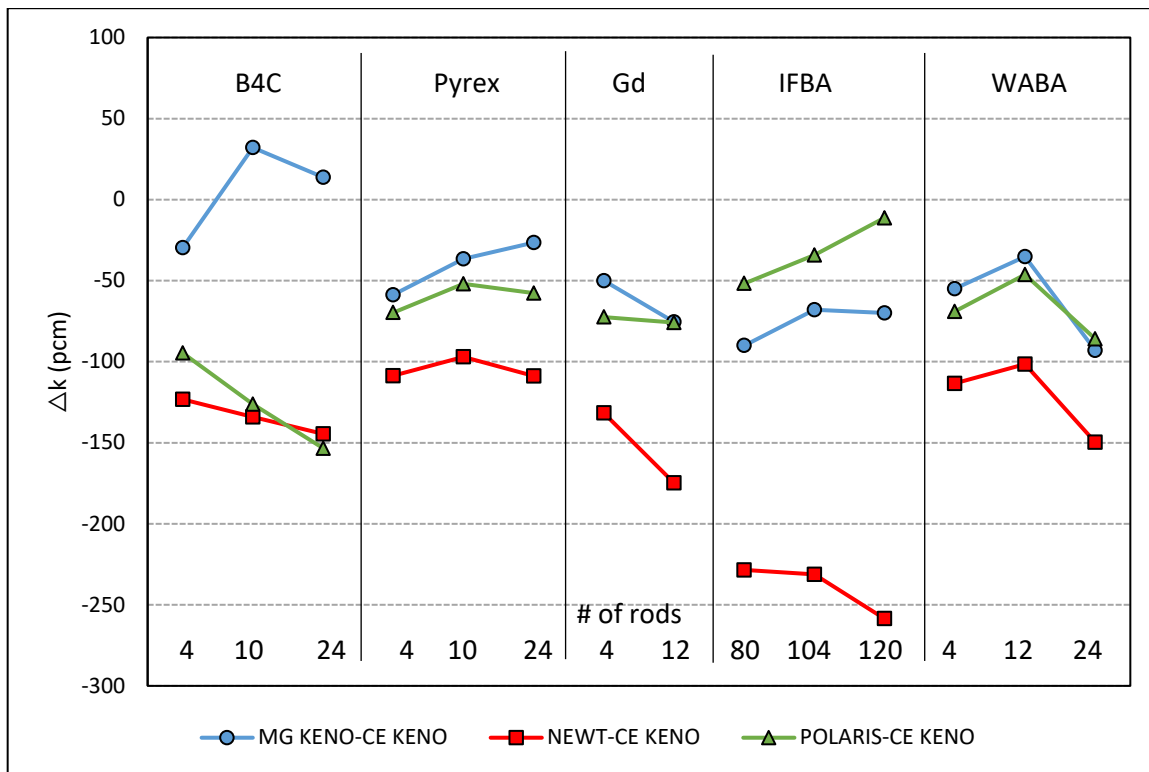
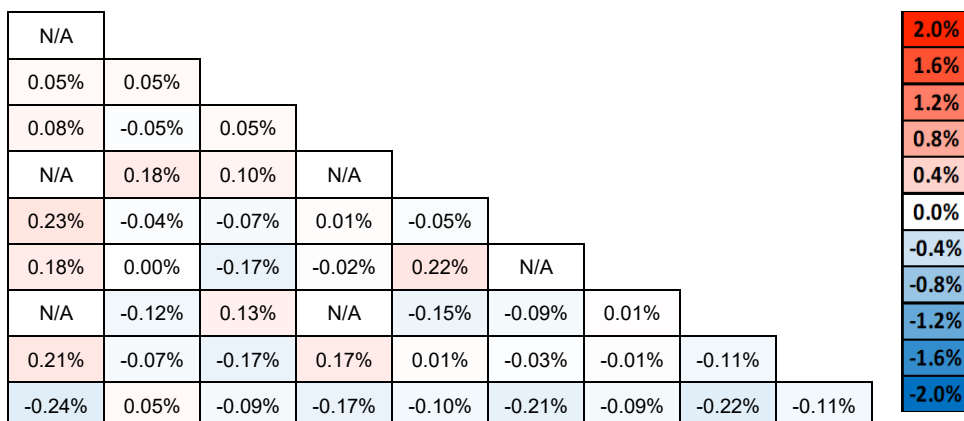


Figure B-66 Test Suite 10: PWR k_{inf} Differences

NEWT (RMS= 0.12%, MAX=0.24%)



Polaris (RMS= 0.12%, MAX=0.27%)

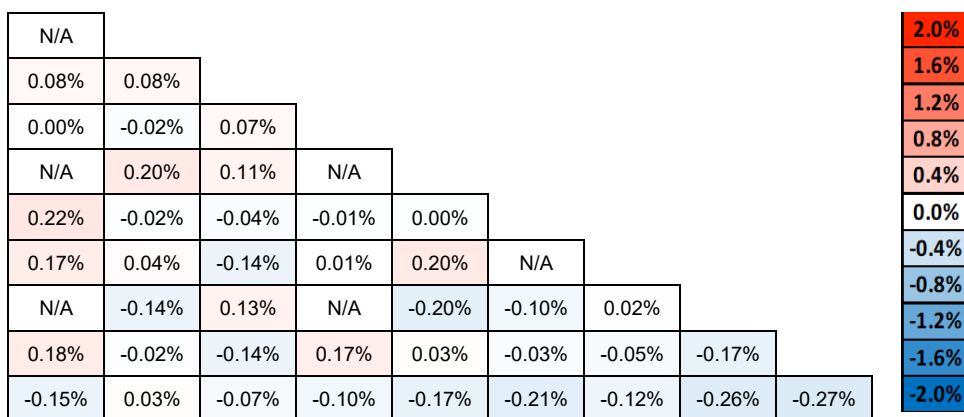


Figure B-67 Test Suite 10: 17 × 17 Lattice Pin Power Differences at HFP, 1,300 ppm boron, and 4 B₄C Rods

B.11 Test Suite 11 – PARCS Parameters for Fuel-Only Model

Purpose: The purpose of this test suite is to assess the accuracy of few-group homogenized cross section edits in NEWT and Polaris. While other test suites assess the accuracy of the underlying physics via comparison of pin powers and k_{inf} values for a wide range of conditions, this test suite focuses on the accuracy of post-processing the cross sections and flux distribution into parameters used in PARCS calculations. Few-group homogenized cross sections are compared with Serpent [20], a CE MC code with few-group homogenized cross section edits available at the time of this report.

Serpent Calculations: The following list summarizes important user options for generating and comparing few-group homogenized cross sections between SCALE and Serpent. The list also highlights important calculation differences and the impact these differences have on defining target and acceptance accuracy criteria.

- **Critical spectrum:** Both SCALE and Serpent have multiple options for performing critical spectrum calculations. ***For this report, the critical spectrum calculation in both codes is disabled.***
- **Reactivity cross sections:** The nu-fission, absorption, downscatter, and upscatter cross sections can be used to derive 4-factor formula quantities (ηf , p , and ϵ) and the fast-to-thermal flux ratio. As the results show below, SCALE and Serpent are in good agreement for the 4-factor formula terms and the fast-to-flux ratio. The individual cross sections are also in good agreement with the exception of the upscatter cross section. However, differences in the upscatter cross section do not lead to significant differences in k_{inf} . ***For this report, nu-fission, absorption, and downscatter are compared with tighter accuracy criteria as compared to the upscatter cross section.***
- **Transport cross sections:** Both NEWT and Serpent compute transport cross sections using the outscatter approximation. Polaris also used the outscatter approximation in its initial release in SCALE 6.2.0. With SCALE 6.2.1, Polaris was updated to include internal transport-to-total correction factors for hydrogen transport cross sections based on the procedure outlined by Herman [31]. Additional details on the transport cross section calculation and impact on Polaris/PARCS core calculations are provided by Xu [32]. ***For this report, transport cross sections are only be compared between Serpent and NEWT.*** A separate calculation is performed with Polaris for a single lattice configuration to demonstrate consistent transport cross sections among Serpent, NEWT, and Polaris using the outscatter approximation.
- **Kinetics parameters:** Both SCALE and Serpent calculations have options for forward-weighted and adjoint-weighted kinetics parameters. ***Forward-weighted kinetics parameters are compared in this report.*** Serpent also reports a precursor-averaged decay constant that is the beta-weighted sum of the group decay constants. For consistent comparison with SCALE, the precursor-average decay constant is recomputed from the Serpent data using the conventional formula: that is, the reciprocal of the beta-weighted sum of the group mean lifetime. Serpent calculations are performed with ENDF/B VII.0 nuclear data libraries, including delayed neutron data. SCALE uses ENDF/B VII.1 nuclear data libraries with internal delayed neutron data. The differences between ^{235}U and ^{238}U kinetics parameters are provided in Table B-41. The differences in kinetic parameters lead to large differences in the homogenized kinetic parameters. ***For this report, relative differences between kinetics parameters are provided, but no target or acceptance criteria are applied.*** A separate calculation is performed with Polaris for a single lattice configuration to demonstrate consistent homogenized kinetic parameters in Serpent and Polaris using ENDF/B VII.0 kinetics parameters for ^{235}U and ^{238}U .
- **Fission product yields:** As shown below, SCALE and Serpent fission product yields for I-135, ^{135}Xe , and ^{149}Pm have large differences. The NEWT ^{149}Pm yield is 100 times smaller than predictions from Serpent and Polaris. The ^{135}Xe yield is ~2 times larger than Serpent and NEWT. ***For this report, relative differences between fission product yields are provided, but target or acceptance criteria are not applied while the differences remain under investigation.***
- **Kappa values:** Serpent and SCALE have different energy deposition models. SCALE calculates kappa-absorption—the sum of kappa-fission and kappa-capture—for each material in the problem. To minimize tally computation, Serpent only calculates kappa-

fission reactions in the fuel materials. Serpent uses effective kappa-fission values to approximate the energy-release by capture. Although SCALE uses kappa-absorption for power normalization necessary for accurate depletion calculation, only the kappa-fission value is edited to the T16 file used by PARCS. ***For the next release of SCALE, the T16 file will contain the kappa-absorption value. For this report, Serpent kappa values are compared and assessed using the Polaris ratio of kappa absorption to fission. Because the NEWT output file does not provide the kappa absorption value, the NEWT kappa fission values are reported without target or accepted criteria applied.***

Target Accuracy:

- **Reactivity QOIs:** 200 pcm difference in k_{inf} and 4-factor terms (ηf , p , and ϵ); 1.5% relative difference in nu-fission, absorption, downscatter, and fast-to-thermal flux ratio; and 5% relative difference in upscatter cross sections
- **Other cross section QOIs:** 1.5% relative difference in kappa values (Polaris only), 1.5% relative difference in transport cross sections (NEWT only), and 1.5% relative difference in ADFs
- **Fission product yields:** No target accuracy provided
- **Kinetics parameters:** No target accuracy provided

Acceptance Accuracy:

- **Reactivity QOIs:** 400 pcm difference in k_{inf} and 4-factor terms (ηf , p , and ϵ); 3% relative difference in nu-fission, absorption, downscatter, and fast-to-thermal flux ratio; and 10% relative difference in upscatter cross sections
- **Other cross section QOIs:** 3% relative difference in kappa values (Polaris only), 3% relative difference in transport cross sections (NEWT only), and 3% relative difference in ADFs
- **Fission product yields:** No acceptance accuracy provided
- **Kinetics parameters:** No acceptance accuracy provided

B.11.1 BWR

Results: Comparisons of cross sections for a BOL GE14 DOM lattice at different void fractions are provided in Table B-33 through Table B-36.

For Polaris, 60 of 68 QOIs are within the target accuracy, and 67 of 68 are within the acceptance accuracy. The pcm difference in the fast fission factor at 90% void fraction is 421 pcm, indicating potential differences in the unresolved and fast energy range. Notable QOIs outside target accuracy include the fast fission factor for 40% void and 70% void fraction, and the fast group kappa value is approximately 2% higher than the Serpent for all void conditions.

For NEWT, 52 of 68 QOIs are within target accuracy, and 61 of 68 are within acceptance accuracy. Although NEWT demonstrates accurate k_{inf} agreement, it tends to overestimate ϵ and

underestimate ηf and p . The largest cancellation of error is exhibited at 90% void fraction, where pcm differences are -145 (k_{inf}), -217 (ηf), -314 (p), and 1,194 (ϵ). In relative percent differences, these values are -0.15% (k_{inf}), -0.20% (ηf), -0.63% (p), and 0.69% (ϵ). In other words, the differences in resonance escape probability and fast fission factor are 4 times larger in magnitude in k_{inf} , but they are in the opposite direction and cancel out. As mentioned earlier in the report, the NEWT calculations could be improved with product quadrature sets, but the runtime is not practical using SCALE 6.2. NEWT also exhibits an overprediction of the upscatter cross section, indicating potential issues in the thermal scattering convergence criteria.

Comparisons of fission product yield and kinetics parameters are provided in Table B-37 through Table B-40. Serpent calculations are performed with ENDF/B VII.0 nuclear data and kinetics parameters. Comparison of ^{235}U and ^{238}U kinetics parameters are provided in Table B-41, revealing large differences across ENDF/B VII.0, VII.1, and internal SCALE values. A separate Polaris calculation is performed at 40% void fraction with the ENDF/B VII.0 ^{235}U and ^{238}U kinetics parameters to demonstrate the impact on the homogenized kinetic parameters computed by each code. The new results reveal improved agreement in beta and lambda values compared to the original calculations shown in Table B-42.

The modified calculation also disables the specialized treatment for the hydrogen transport cross section in Polaris. The transport cross sections for the modified calculation are in consistent agreement with Serpent and NEWT when all three codes use the outscatter approximation for all isotopes.

**Table B-33 Test Suite 11: Cross Section Comparison for GE14 10 × 10
DOM Lattice at 0% Void Fraction**

QOI	Serpent	Polaris	Diff	NEWT	Diff
Reactivity edits					
k	0.98326	0.98184	-142 pcm	0.97934	-392 pcm
NUFISS(1)	6.60E-03	6.59E-03	-0.1%	6.61E-03	0.2%
NUFISS(2)	9.28E-02	9.31E-02	0.4%	9.29E-02	0.2%
ABS(1)*	9.03E-03	9.01E-03	-0.2%	9.04E-03	0.1%
ABS(2)*	8.38E-02	8.43E-02	0.6%	8.44E-02	0.7%
SCAT(1,2)	1.88E-02	1.87E-02	-0.3%	1.87E-02	-0.3%
SCAT(2,1)	1.34E-03	1.38E-03	2.7%	1.50E-03	11.6%
Derived reactivity quantities					
eta*f	1.10657	1.10434	-223 pcm	1.10110	-547 pcm
p	0.67177	0.67133	-44 pcm	0.67055	-122 pcm
eps	1.32274	1.32434	161 pcm	1.32647	373 pcm
PHI(1)/PHI(2)	4.54	4.58	1.0%	4.59	1.1%
Other XS					
KAPPA(1)	203	195	-4.0%	195	-4.0%
KAPPA(2)	202	194	-4.0%	194	-4.0%
TRANSPORT(1)	0.217	0.228	4.9%	0.216	-0.7%
TRANSPORT(2)	0.985	0.961	-2.4%	0.987	0.2%
ADF1(1)	0.978	0.975	-0.3%	0.979	0.1%
ADF1(2)	1.359	1.349	-0.7%	1.348	-0.8%
ADF2(1)	0.922	0.921	-0.2%	0.921	-0.1%
ADF2(2)	2.132	2.109	-1.1%	2.114	-0.9%
*Absorption cross sections are reduced due to neutron-producing non-fission reactions such as n2n and n3n					

Table B-34 Test Suite 11: Cross Section Comparison for GE14 10 × 10 DOM Lattice at 40% Void Fraction

QOI	Serpent	Polaris	Diff	NEWT	Diff
Reactivity edits					
k	0.96260	0.96215	-45 pcm	0.96018	-242 pcm
NUFISS(1)	6.29E-03	6.29E-03	0.0%	6.31E-03	0.3%
NUFISS(2)	8.93E-02	8.95E-02	0.2%	8.94E-02	0.1%
ABS(1)*	8.50E-03	8.47E-03	-0.3%	8.50E-03	0.0%
ABS(2)*	8.08E-02	8.12E-02	0.4%	8.12E-02	0.5%
SCAT(1,2)	1.35E-02	1.35E-02	-0.3%	1.35E-02	-0.4%
SCAT(2,1)	1.38E-03	1.41E-03	2.3%	1.52E-03	10.6%
Derived reactivity quantities					
eta*f	1.10474	1.10302	-172 pcm	1.10038	-435 pcm
p	0.61004	0.60980	-24 pcm	0.60868	-136 pcm
eps	1.42831	1.43050	218 pcm	1.43369	538 pcm
PHI(1)/PHI(2)	6.08	6.13	0.8%	6.15	1.0%
Other					
KAPPA(1)	203	207	2.1%	195	-4.0%
KAPPA(2)	202	200	-1.0%	194	-4.0%
TRANSPORT(1)	0.192	0.199	3.4%	0.191	-0.8%
TRANSPORT(2)	0.814	0.793	-2.5%	0.817	0.3%
ADF1(1)	0.980	0.976	-0.3%	0.981	0.1%
ADF1(2)	1.319	1.311	-0.6%	1.311	-0.6%
ADF2(1)	0.931	0.929	-0.2%	0.929	-0.2%
ADF2(2)	2.241	2.217	-1.1%	2.223	-0.8%
*Absorption cross sections are reduced due to neutron-producing non-fission reactions such as n2n and n3n					

Table B-35 Test Suite 11: Cross Section Comparison for GE14 10 × 10 DOM Lattice at 70% Void Fraction

QOI	Serpent	Polaris	Diff	NEWT	Diff
Reactivity edits					
k	0.94200	0.94279	79 pcm	0.94091	-109 pcm
NUFISS(1)	5.93E-03	5.94E-03	0.0%	5.96E-03	0.4%
NUFISS(2)	8.57E-02	8.59E-02	0.2%	8.59E-02	0.2%
ABS(1)*	7.88E-03	7.85E-03	-0.4%	7.88E-03	0.0%
ABS(2)*	7.80E-02	7.83E-02	0.3%	7.84E-02	0.5%
SCAT(1,2)	9.69E-03	9.66E-03	-0.4%	9.64E-03	-0.5%
SCAT(2,1)	1.43E-03	1.46E-03	1.8%	1.57E-03	9.6%
Derived reactivity quantities					
eta*f	1.09842	1.09722	-121 pcm	1.09536	-306 pcm
p	0.54714	0.54716	2 pcm	0.54540	-174 pcm
eps	1.56741	1.57042	301 pcm	1.57516	775 pcm
PHI(1)/PHI(2)	8.20	8.25	0.7%	8.30	1.2%
Other XS					
KAPPA(1)	203	207	2.0%	195	-4.0%
KAPPA(2)	202	200	-1.0%	194	-4.0%
TRANSPORT(1)	0.174	0.177	2.0%	0.172	-0.9%
TRANSPORT(2)	0.690	0.672	-2.6%	0.694	0.5%
ADF1(1)	0.982	0.979	-0.3%	0.983	0.1%
ADF1(2)	1.279	1.272	-0.5%	1.273	-0.4%
ADF2(1)	0.938	0.935	-0.3%	0.935	-0.2%
ADF2(2)	2.363	2.336	-1.1%	2.344	-0.8%
*Absorption cross sections are reduced due to neutron-producing non-fission reactions such as n2n and n3n					

Table B-36 Test Suite 11: Cross Section Comparison for GE14 10 × 10 DOM Lattice at 90% Void Fraction

QOI	Serpent	Polaris	Diff	NEWT	Diff
Reactivity edits					
k	0.92732	0.92898	166 pcm	0.92587	-145 pcm
NUFISS(1)	5.59E-03	5.59E-03	0.1%	5.61E-03	0.4%
NUFISS(2)	8.27E-02	8.29E-02	0.2%	8.32E-02	0.6%
ABS(1)*	7.27E-03	7.24E-03	-0.5%	7.29E-03	0.2%
ABS(2)*	7.59E-02	7.62E-02	0.4%	7.65E-02	0.8%
SCAT(1,2)	7.27E-03	7.24E-03	-0.4%	7.20E-03	-0.9%
SCAT(2,1)	1.48E-03	1.51E-03	1.5%	1.62E-03	9.1%
Derived reactivity quantities					
eta*f	1.08991	1.08877	-114 pcm	1.08774	-217 pcm
p	0.49495	0.49511	16 pcm	0.49181	-314 pcm
eps	1.71903	1.72323	421 pcm	1.73097	1,194 pcm
PHI(1)/PHI(2)	10.65	10.73	0.8%	10.84	1.9%
Other XS					
KAPPA(1)	203	207	1.8%	195	-4.0%
KAPPA(2)	202	200	-0.9%	194	-4.0%
TRANSPORT(1)	0.161	0.162	1.0%	0.159	-0.9%
TRANSPORT(2)	0.612	0.595	-2.7%	0.617	0.8%
ADF1(1)	0.984	0.980	-0.4%	0.985	0.1%
ADF1(2)	1.248	1.242	-0.5%	1.244	-0.4%
ADF2(1)	0.942	0.940	-0.3%	0.940	-0.2%
ADF2(2)	2.478	2.446	-1.3%	2.461	-0.7%
*Absorption cross sections are reduced due to neutron-producing non-fission reactions such as n2n and n3n					

Table B-37 Test Suite 11: Fission Product Yield and Kinetics Parameter Comparison for GE14 10 × 10 DOM Lattice at 0% Void Fraction

QOI	Serpent	Polaris	Diff (%)	NEWT	Diff (%)
Fission product yields					
¹³⁵ I	6.32E-02	6.05E-02	-4.3	6.29E-02	-0.5
¹³⁵ Xe	2.43E-03	4.96E-03	104.1	2.57E-03	5.6
¹⁴⁹ Pm	1.11E-02	8.99E-03	-19.3	6.81E-05	-99.4
Kinetics parameters					
INVVEL(1)	5.82E-08	5.79E-08	-0.6	5.91E-08	1.5
INVVEL(2)	2.55E-06	2.55E-06	0.0	2.56E-06	0.2
BETA(1)	2.09E-04	2.19E-04	4.8	2.08E-04	-0.3
BETA(2)	1.15E-03	1.46E-03	27.3	1.40E-03	21.9
BETA(3)	1.13E-03	1.35E-03	19.1	1.29E-03	14.1
BETA(4)	3.32E-03	2.81E-03	-15.2	2.68E-03	-19.1
BETA(5)	1.07E-03	9.46E-04	-11.8	9.00E-04	-16.1
BETA(6)	3.56E-04	3.14E-04	-11.7	3.04E-04	-14.5
BETA(Total)	7.24E-03	7.10E-03	-1.8	6.79E-03	-6.2
LAMBDA(1)	1.25E-02	1.25E-02	0.1	1.25E-02	0.0
LAMBDA(2)	3.17E-02	3.09E-02	-2.5	3.08E-02	-2.7
LAMBDA(3)	1.10E-01	1.15E-01	4.5	1.15E-01	4.4
LAMBDA(4)	3.20E-01	3.11E-01	-3.0	3.10E-01	-3.1
LAMBDA(5)	1.35E+00	1.25E+00	-7.3	1.24E+00	-8.1
LAMBDA(6)	8.87E+00	3.34E+00	-62.3	3.32E+00	-62.6
LAMBDA(Total)	9.72E-02	8.21E-02	-15.5	8.20E-02	-15.6

Table B-38 Test Suite 11: Fission Product Yield and Kinetics Parameter Comparison for GE14 10 × 10 DOM Lattice at 40% Void Fraction

QOI	Serpent	Polaris	Diff (%)	NEWT	Diff (%)
Fission product yields					
¹³⁵ I	6.32E-02	6.05E-02	-4.3	6.29E-02	-0.5
¹³⁵ Xe	2.43E-03	4.96E-03	104.1	2.57E-03	5.6
¹⁴⁹ Pm	1.11E-02	8.99E-03	-19.3	6.81E-05	-99.4
Kinetics parameters					
INVVEL(1)	5.53E-08	5.50E-08	-0.6	5.61E-08	1.4
INVVEL(2)	2.48E-06	2.48E-06	0.1	2.49E-06	0.3
BETA(1)	2.14E-04	2.19E-04	2.5	2.08E-04	-2.6
BETA(2)	1.18E-03	1.46E-03	23.5	1.40E-03	18.3
BETA(3)	1.17E-03	1.35E-03	14.9	1.29E-03	10.0
BETA(4)	3.44E-03	2.81E-03	-18.2	2.68E-03	-21.9
BETA(5)	1.13E-03	9.46E-04	-16.6	9.00E-04	-20.6
BETA(6)	3.76E-04	3.14E-04	-16.4	3.04E-04	-19.0
BETA(Total)	7.52E-03	7.10E-03	-5.5	6.79E-03	-9.7
LAMBDA(1)	1.25E-02	1.25E-02	0.1	1.25E-02	0.0
LAMBDA(2)	3.16E-02	3.09E-02	-2.4	3.08E-02	-2.6
LAMBDA(3)	1.10E-01	1.15E-01	4.4	1.15E-01	4.2
LAMBDA(4)	3.21E-01	3.11E-01	-3.2	3.10E-01	-3.4
LAMBDA(5)	1.34E+00	1.25E+00	-7.2	1.24E+00	-8.0
LAMBDA(6)	8.92E+00	3.34E+00	-62.5	3.32E+00	-62.8
LAMBDA(Total)	9.79E-02	8.21E-02	-16.2	8.19E-02	-16.3

Table B-39 Test Suite 11: Fission Product Yield and Kinetics Parameter Comparison for GE14 10 × 10 DOM Lattice at 70% Void Fraction

QOI	Serpent	Polaris	Diff (%)	NEWT	Diff (%)
Fission product yields					
¹³⁵ I	6.34E-02	6.07E-02	-4.2	6.29E-02	-0.8
¹³⁵ Xe	2.37E-03	4.85E-03	104.5	2.57E-03	8.2
¹⁴⁹ Pm	1.13E-02	9.22E-03	-18.3	6.81E-05	-99.4
Kinetics parameters					
INVVEL(1)	5.18E-08	5.15E-08	-0.6	5.24E-08	1.2
INVVEL(2)	2.40E-06	2.41E-06	0.2	2.42E-06	0.5
BETA(1)	2.18E-04	2.22E-04	1.8	2.06E-04	-5.7
BETA(2)	1.23E-03	1.48E-03	20.6	1.39E-03	12.9
BETA(3)	1.21E-03	1.38E-03	13.7	1.29E-03	6.4
BETA(4)	3.58E-03	2.92E-03	-18.5	2.72E-03	-24.0
BETA(5)	1.20E-03	1.03E-03	-13.8	9.60E-04	-20.0
BETA(6)	3.93E-04	3.31E-04	-15.8	3.15E-04	-19.9
BETA(Total)	7.83E-03	7.36E-03	-6.0	6.88E-03	-12.2
LAMBDA(1)	1.25E-02	1.26E-02	0.5	1.25E-02	0.4
LAMBDA(2)	3.16E-02	3.10E-02	-1.8	3.10E-02	-2.0
LAMBDA(3)	1.10E-01	1.17E-01	5.8	1.17E-01	5.6
LAMBDA(4)	3.22E-01	3.15E-01	-2.2	3.14E-01	-2.4
LAMBDA(5)	1.34E+00	1.28E+00	-4.5	1.27E+00	-5.4
LAMBDA(6)	8.96E+00	3.47E+00	-61.3	3.43E+00	-61.7
LAMBDA(Total)	9.87E-02	8.43E-02	-14.6	8.42E-02	-14.8

Table B-40 Test Suite 11: Fission Product Yield and Kinetics Parameter Comparison for GE14 10 × 10 DOM Lattice at 90% Void Fraction

QOI	Serpent	Polaris	Diff (%)	NEWT	Diff (%)
Fission product yields					
¹³⁵ I	6.35E-02	6.08E-02	-4.1	6.29E-02	-0.9
¹³⁵ Xe	2.34E-03	4.80E-03	104.7	2.57E-03	9.5
¹⁴⁹ Pm	1.13E-02	9.33E-03	-17.8	6.81E-05	-99.4
Kinetics parameters					
INVVEL(1)	4.84E-08	4.81E-08	-0.6	4.88E-08	0.8
INVVEL(2)	2.34E-06	2.34E-06	0.2	2.35E-06	0.7
BETA(1)	2.16E-04	2.23E-04	3.2	2.06E-04	-4.9
BETA(2)	1.26E-03	1.49E-03	18.6	1.39E-03	10.4
BETA(3)	1.25E-03	1.39E-03	11.6	1.29E-03	3.3
BETA(4)	3.70E-03	2.97E-03	-19.7	2.72E-03	-26.4
BETA(5)	1.26E-03	1.08E-03	-14.8	9.60E-04	-24.0
BETA(6)	4.09E-04	3.39E-04	-17.1	3.15E-04	-23.0
BETA(Total)	8.09E-03	7.49E-03	-7.4	6.88E-03	-15.0
LAMBDA(1)	1.25E-02	1.26E-02	0.7	1.25E-02	0.4
LAMBDA(2)	3.16E-02	3.11E-02	-1.6	3.10E-02	-2.0
LAMBDA(3)	1.10E-01	1.18E-01	6.5	1.17E-01	5.6
LAMBDA(4)	3.22E-01	3.16E-01	-1.7	3.14E-01	-2.4
LAMBDA(5)	1.34E+00	1.30E+00	-3.3	1.27E+00	-5.4
LAMBDA(6)	8.96E+00	3.52E+00	-60.7	3.43E+00	-61.7
LAMBDA(Total)	1.00E-01	8.54E-02	-14.7	8.42E-02	-15.9

Table B-41 ^{235}U and ^{238}U Kinetics Parameters

Precursor group	^{235}U lambda			^{238}U lambda		
	VII.0	VII.1	SCALE	VII.0	VII.1	SCALE
1	1.25E-02	1.33E-02	1.24E-02	1.25E-02	1.36E-02	1.32E-02
2	3.18E-02	3.27E-02	3.05E-02	3.03E-02	3.13E-02	3.21E-02
3	1.09E-01	1.21E-01	1.11E-01	1.16E-01	1.23E-01	1.39E-01
4	3.17E-01	3.03E-01	3.01E-01	3.41E-01	3.24E-01	3.58E-01
5	1.35E+00	8.49E-01	1.14E+00	1.32E+00	9.06E-01	1.41E+00
6	8.64E+00	2.85E+00	3.01E+00	9.98E+00	3.05E+00	4.02E+00
Precursor group	^{235}U delayed neutron fraction			^{238}U delayed neutron fraction		
	VII.0	VII.1	SCALE	VII.0	VII.1	SCALE
1	0.032	0.035	0.033	0.010	0.014	0.013
2	0.166	0.181	0.219	0.115	0.113	0.137
3	0.161	0.173	0.196	0.128	0.131	0.162
4	0.460	0.387	0.395	0.452	0.385	0.388
5	0.133	0.159	0.115	0.234	0.254	0.225
6	0.047	0.066	0.042	0.062	0.103	0.075

Table B-42 Comparison of Serpent and Polaris for GE14 10 × 10 DOM Lattice at 40% Void Fraction

QOI	Serpent	Polaris	Diff	Modified polaris	Diff
TRANSPORT(1)	0.192	0.199	3.4	0.190	-1.4
TRANSPORT(2)	0.814	0.793	-2.5	0.811	-0.4
BETA(1)	2.14E-04	2.19E-04	2.5	2.04E-04	-4.7
BETA(2)	1.18E-03	1.46E-03	23.5	1.14E-03	-4.0
BETA(3)	1.17E-03	1.35E-03	14.9	1.12E-03	-4.2
BETA(4)	3.44E-03	2.81E-03	-18.2	3.31E-03	-3.7
BETA(5)	1.13E-03	9.46E-04	-16.6	1.09E-03	-3.9
BETA(6)	3.76E-04	3.14E-04	-16.4	3.59E-04	-4.4
BETA(Total)	7.52E-03	7.10E-03	-5.5	7.22E-03	-3.9
LAMBDA(1)	1.25E-02	1.25E-02	0.1	1.25E-02	0.0
LAMBDA(2)	3.16E-02	3.09E-02	-2.4	3.16E-02	0.0
LAMBDA(3)	1.10E-01	1.15E-01	4.4	1.10E-01	0.0
LAMBDA(4)	3.21E-01	3.11E-01	-3.2	3.21E-01	0.0
LAMBDA(5)	1.34E+00	1.25E+00	-7.2	1.34E+00	0.0
LAMBDA(6)	8.92E+00	3.34E+00	-62.5	8.93E+00	0.1
LAMBDA(Total)	9.79E-02	8.21E-02	-16.2	9.81E-02	0.2

B.11.2 PWR

Results: Comparisons of cross sections for a BOL Westinghouse 17 × 17 lattice are provided in Table B-43 and Table B-44.

For Polaris, 13 of 15 QOIs are within the target accuracy, and all 15 are within the acceptance accuracy. The Polaris kappa values are 2.5% higher than for Serpent.

For NEWT, 14 of 15 QOIs are within the target acceptance accuracy with the exception the upscatter cross section which is 10.8% higher than for Serpent. The upscatter cross section discrepancy does not have a significant impact on the reactivity balance as shown in the 4-factor comparisons.

Table B-43 Test Suite 11: Cross Section Comparison for 17 × 17 WE Lattice

QOI	Serpent	Polaris	Diff (%)	NEWT	Diff (%)
Reactivity edits					
k	1.17253	1.17240	-13 pcm	1.17157	-96 pcm
NUFISS(1)	6.88E-03	6.87E-03	-0.1	6.89E-03	0.2
NUFISS(2)	1.37E-01	1.37E-01	0.0	1.37E-01	-0.1
ABS(1)*	9.93E-03	9.92E-03	-0.1	9.94E-03	0.1
ABS(2)*	9.48E-02	9.47E-02	-0.1	9.48E-02	-0.1
SCAT(1,2)	1.79E-02	1.78E-02	-0.4	1.79E-02	-0.1
SCAT(2,1)	1.61E-03	1.64E-03	2.0	1.78E-03	10.8
Derived reactivity quantities					
eta*f	1.44290	1.44410	121 pcm	1.44206	-84 pcm
p	0.63948	0.63867	-81 pcm	0.63856	-92 pcm
eps	1.27072	1.27129	56 pcm	1.27228	155 pcm
PHI(1)/PHI(2)	5.39	5.40	0.3	5.40	0.2
Other XS					
KAPPA(1)	203	209	2.5	195	-4.0
KAPPA(2)	202	197	-2.5	194	-4.0
TRANSPORT(1)	0.225	0.235	4.7	0.224	-0.4
TRANSPORT(2)	0.912	0.891	-2.3	0.916	0.4
ADF1(1)	1.000	0.997	-0.3	1.004	0.4
ADF1(2)	0.971	0.971	-0.1	0.968	-0.4
*Absorption cross sections are reduced due to neutron-producing non-fission reactions such as n2n and n3n					

Table B-44 Test Suite 11: Fission Product Yield and Kinetics Parameter Comparison for 17 × 17 WE Lattice

QOI	Serpent	Polaris	Diff (%)	NEWT	Diff (%)
Fission product yields					
¹³⁵ I	6.32E-02	6.05E-02	-4.3	6.29E-02	-0.5
¹³⁵ Xe	2.43E-03	4.96E-03	104.2	2.57E-03	5.7
¹⁴⁹ Pm	1.11E-02	9.00E-03	-19.3	6.81E-05	-99.4
Kinetics parameters					
INVVEL(1)	5.80E-08	5.77E-08	-0.6	5.89E-08	1.6
INVVEL(2)	2.44E-06	2.44E-06	0.2	2.45E-06	0.5
BETA(1)	1.75E-04	2.18E-04	25.0	2.09E-04	19.7
BETA(2)	9.67E-04	1.47E-03	51.5	1.41E-03	46.0
BETA(3)	9.50E-04	1.35E-03	42.2	1.30E-03	37.1
BETA(4)	2.80E-03	2.81E-03	0.5	2.70E-03	-3.4
BETA(5)	8.99E-04	9.47E-04	5.3	9.07E-04	0.9
BETA(6)	2.97E-04	3.19E-04	7.5	3.10E-04	4.5
BETA(Total)	6.09E-03	7.11E-03	16.9	6.84E-03	12.5
LAMBDA(1)	1.25E-02	1.25E-02	0.1	1.25E-02	0.0
LAMBDA(2)	3.17E-02	3.08E-02	-2.6	3.08E-02	-2.8
LAMBDA(3)	1.10E-01	1.15E-01	4.5	1.15E-01	4.3
LAMBDA(4)	3.21E-01	3.11E-01	-3.1	3.10E-01	-3.2
LAMBDA(5)	1.35E+00	1.24E+00	-7.8	1.23E+00	-8.4
LAMBDA(6)	8.89E+00	3.33E+00	-62.5	3.31E+00	-62.8
LAMBDA(Total)	9.73E-02	8.21E-02	-15.6	8.20E-02	-15.7

B.12 Test Suite 12 – PARCS Parameters for Fuel / Reflector Model

Purpose: The purpose of this test suite is to assess the accuracy of few-group homogenized cross section edits in NEWT and Polaris for reflector calculations compared with reference Serpent calculations. As mentioned in the description of Test Suite 11, Polaris uses a specialized treatment for the hydrogen transport cross section. For reflector cross section generation, this treatment leads to different homogenized transport cross sections and reflector ADFs. For this reason, ***Polaris transport cross sections and reflector ADFs are compared to Serpent without applied target or acceptance accuracy.***

Target Accuracy:

- 1.5% relative difference in absorption, downscatter, transport (NEWT only), and reflector ADF (NEWT only), and 5% relative difference in upscatter cross sections

Acceptance Accuracy:

- 3% relative difference in absorption, downscatter, transport (NEWT only), and reflector ADF (NEWT only), and 10% relative difference in upscatter cross sections

B.12.1 BWR

Description: BWR reflector cross sections are calculated by using the GE14 10 × 10 DOM lattice. The case matrix is shown in Table B-45. The BWR reflector geometries for bottom, top, and radial reflectors are shown in Figure B-68 through Figure B-70. Radial reflector model depicts reflector (dark brown) and baffle (beige) regions in Figure B-70.

Table B-45 Test Suite 12: BWR Case Matrix

Reflector location	TF (K)	TC (K)	Void fractions (%)
Top	950	560	0, 40, 70, 90
Bottom	950	560	0, 40, 70, 90
Radial	950	560	0, 40, 70, 90

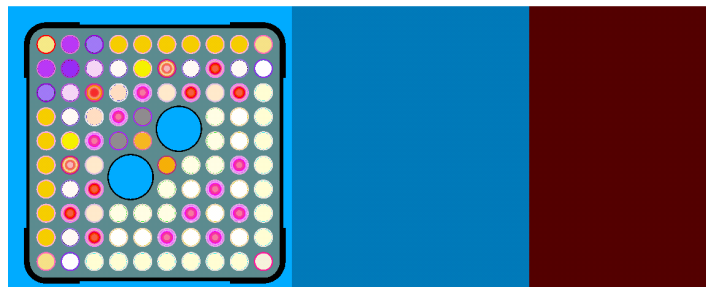


Figure B-68 Test Suite 12: BWR Bottom Reflector Geometry



Figure B-69 Test Suite 12: BWR Top Reflector Geometry



Figure B-70 Test Suite 12: BWR Radial Reflector Geometry

Results: For Polaris, 42 of 48 QOIs are within the target accuracy, and all 48 are within the acceptance accuracy. The QOIs outside of the target accuracy are the upscatter cross section for the radial reflector for all void fractions and the fast absorption cross section for the top reflector for the 70% and 90% void fraction.

For NEWT, 49 of 96 QOIs are within the target accuracy, and 74 of 96 are within the acceptance accuracy. The NEWT upscatter cross section requires further investigation: the QOI fails acceptance accuracy for the top and radial reflector for all void conditions, and it fails target accuracy for the bottom reflector for all void conditions. The NEWT thermal ADF value also requires further investigation: NEWT overestimates the Serpent value for the radial and bottom reflectors for all void conditions and the top reflector for 70% and 90% void fraction.

Table B-46 Test Suite 12: Reflector Cross Section Comparison for GE14 10 × 10 DOM Lattice at 0% Void Fraction

QOI	Serpent	Polaris	% relative difference	NEWT	% relative difference
Top reflector					
TRANSPORT(1)	1.81E-01	1.97E-01	8.5	1.80E-01	-0.8
TRANSPORT(2)	9.31E-01	9.17E-01	-1.5	9.29E-01	-0.2
ABS(1)*	9.28E-04	9.42E-04	1.5	9.59E-04	3.3
ABS(2)*	1.77E-02	1.75E-02	-1.0	1.75E-02	-0.8
SCAT(1,2)	2.90E-02	2.89E-02	-0.4	2.89E-02	-0.3
SCAT(2,1)	3.05E-04	3.13E-04	2.9	3.47E-04	13.9
ADF1(1)	1.069	1.006	-5.9	1.049	-1.9
ADF1(2)	0.896	0.877	-2.1	0.906	1.1
Radial reflector					
TRANSPORT(1)	1.82E-01	2.11E-01	16.0	1.81E-01	-0.6
TRANSPORT(2)	1.30E+00	1.28E+00	-1.6	1.29E+00	-0.6
ABS(1)*	5.49E-04	5.48E-04	-0.3	5.37E-04	-2.2
ABS(2)*	1.16E-02	1.17E-02	0.5	1.16E-02	0.3
SCAT(1,2)	4.27E-02	4.26E-02	-0.3	4.26E-02	-0.2
SCAT(2,1)	2.02E-04	2.16E-04	6.8	2.46E-04	21.7
ADF1(1)	1.101	1.000	-9.2	1.078	-2.1
ADF1(2)	1.070	1.029	-3.8	1.128	5.4
Bottom reflector					
TRANSPORT(1)	2.49E-01	2.64E-01	6.0	2.43E-01	-2.3
TRANSPORT(2)	1.21E+00	1.18E+00	-2.7	1.22E+00	0.9
ABS(1)*	1.26E-02	1.25E-02	-0.8	1.27E-02	0.8
ABS(2)*	3.56E-01	3.55E-01	-0.1	3.59E-01	1.0
SCAT(1,2)	2.23E-02	2.23E-02	-0.3	2.28E-02	2.3
SCAT(2,1)	4.38E-03	4.45E-03	1.5	4.72E-03	7.8
ADF1(1)	0.966	0.929	-3.9	0.965	-0.1
ADF1(2)	1.044	1.042	-0.1	1.002	-4.0
*Absorption cross sections are "reduced" due to neutron-producing non-fission reactions such as n2n and n3n					

Table B-47 Test Suite 12: Reflector Cross Section Comparison for GE14 10 × 10 DOM Lattice at 40% Void Fraction

QOI	Serpent	Polaris	% relative difference	NEWT	% relative difference
Top reflector					
TRANSPORT(1)	1.83E-01	1.98E-01	8.0	1.82E-01	-0.9
TRANSPORT(2)	9.30E-01	9.16E-01	-1.5	9.27E-01	-0.4
ABS(1)*	9.27E-04	9.41E-04	1.5	9.57E-04	3.3
ABS(2)*	1.77E-02	1.75E-02	-0.9	1.75E-02	-0.9
SCAT(1,2)	2.88E-02	2.87E-02	-0.4	2.87E-02	-0.3
SCAT(2,1)	3.13E-04	3.23E-04	3.1	3.59E-04	14.9
ADF1(1)	1.078	1.016	-5.8	1.057	-2.0
ADF1(2)	0.867	0.853	-1.6	0.887	2.4
Radial reflector					
TRANSPORT(1)	1.84E-01	2.12E-01	15.1	1.83E-01	-0.7
TRANSPORT(2)	1.30E+00	1.27E+00	-1.7	1.29E+00	-0.6
ABS(1)*	5.39E-04	5.39E-04	0.0	5.28E-04	-2.0
ABS(2)*	1.16E-02	1.17E-02	0.5	1.17E-02	0.4
SCAT(1,2)	4.26E-02	4.24E-02	-0.4	4.25E-02	-0.3
SCAT(2,1)	2.07E-04	2.22E-04	6.9	2.52E-04	21.8
ADF1(1)	1.111	1.011	-9.0	1.088	-2.1
ADF1(2)	1.053	1.023	-2.8	1.131	7.5
Bottom reflector					
TRANSPORT(1)	2.52E-01	2.66E-01	5.6	2.46E-01	-2.3
TRANSPORT(2)	1.20E+00	1.17E+00	-2.8	1.22E+00	0.9
ABS(1)*	1.27E-02	1.26E-02	-0.8	1.28E-02	0.7
ABS(2)*	3.52E-01	3.52E-01	-0.1	3.56E-01	1.0
SCAT(1,2)	2.23E-02	2.23E-02	-0.2	2.28E-02	2.2
SCAT(2,1)	4.52E-03	4.60E-03	1.6	4.89E-03	8.2
ADF1(1)	0.975	0.938	-3.8	0.972	-0.3
ADF1(2)	1.035	1.031	-0.4	0.996	-3.8
*Absorption cross sections are reduced due to neutron-producing non-fission reactions such as n2n and n3n					

Table B-48 Test Suite 12: Reflector Cross Section Comparison for GE14 10 × 10 DOM Lattice at 70% Void Fraction

QOI	Serpent	Polaris	% relative difference	NEWT	% relative difference
Top reflector					
TRANSPORT(1)	1.86E-01	2.00E-01	7.6	1.84E-01	-1.0
TRANSPORT(2)	9.30E-01	9.16E-01	-1.5	9.26E-01	-0.4
ABS(1)*	9.24E-04	9.38E-04	1.5	9.54E-04	3.2
ABS(2)*	1.77E-02	1.75E-02	-1.0	1.75E-02	-0.9
SCAT(1,2)	2.86E-02	2.85E-02	-0.4	2.85E-02	-0.5
SCAT(2,1)	3.19E-04	3.30E-04	3.4	3.67E-04	15.2
ADF1(1)	1.085	1.025	-5.5	1.063	-2.0
ADF1(2)	0.831	0.822	-1.1	0.858	3.2
Radial reflector					
TRANSPORT(1)	1.86E-01	2.11E-01	13.6	1.85E-01	-0.8
TRANSPORT(2)	1.29E+00	1.27E+00	-1.6	1.29E+00	-0.6
ABS(1)*	5.30E-04	5.32E-04	0.3	5.20E-04	-2.0
ABS(2)*	1.16E-02	1.17E-02	0.6	1.17E-02	0.4
SCAT(1,2)	4.23E-02	4.21E-02	-0.5	4.22E-02	-0.4
SCAT(2,1)	2.12E-04	2.26E-04	6.9	2.58E-04	21.7
ADF1(1)	1.119	1.021	-8.8	1.095	-2.1
ADF1(2)	1.026	1.011	-1.4	1.123	9.5
Bottom reflector					
TRANSPORT(1)	2.55E-01	2.68E-01	5.2	2.49E-01	-2.2
TRANSPORT(2)	1.20E+00	1.17E+00	-2.8	1.21E+00	0.9
ABS(1)*	1.26E-02	1.25E-02	-0.9	1.27E-02	0.6
ABS(2)*	3.50E-01	3.49E-01	-0.1	3.53E-01	1.0
SCAT(1,2)	2.22E-02	2.21E-02	-0.3	2.26E-02	1.9
SCAT(2,1)	4.67E-03	4.72E-03	1.2	5.03E-03	7.9
ADF1(1)	0.983	0.946	-3.7	0.979	-0.4
ADF1(2)	1.016	1.011	-0.5	0.981	-3.4
*Absorption cross sections are reduced due to neutron-producing non-fission reactions such as n2n and n3n					

Table B-49 Test Suite 12: Reflector Cross Section Comparison for GE14 10 × 10 DOM Lattice at 90% Void Fraction

QOI	Serpent	Polaris	% relative difference	NEWT	% relative difference
Top reflector					
TRANSPORT(1)	1.87E-01	2.01E-01	7.2	1.85E-01	-1.0
TRANSPORT(2)	9.29E-01	9.15E-01	-1.5	9.26E-01	-0.4
ABS(1)*	9.20E-04	9.34E-04	1.6	9.49E-04	3.2
ABS(2)*	1.77E-02	1.75E-02	-0.9	1.75E-02	-0.9
SCAT(1,2)	2.84E-02	2.83E-02	-0.3	2.82E-02	-0.5
SCAT(2,1)	3.24E-04	3.35E-04	3.2	3.73E-04	14.9
ADF1(1)	1.090	1.031	-5.4	1.068	-2.0
ADF1(2)	0.797	0.790	-0.8	0.827	3.8
Radial reflector					
TRANSPORT(1)	1.88E-01	2.12E-01	13.0	1.86E-01	-0.8
TRANSPORT(2)	1.29E+00	1.27E+00	-1.7	1.29E+00	-0.6
ABS(1)*	5.22E-04	5.24E-04	0.3	5.12E-04	-1.9
ABS(2)*	1.16E-02	1.17E-02	0.6	1.17E-02	0.5
SCAT(1,2)	4.21E-02	4.18E-02	-0.5	4.18E-02	-0.5
SCAT(2,1)	2.14E-04	2.30E-04	7.2	2.61E-04	21.9
ADF1(1)	1.124	1.028	-8.5	1.100	-2.1
ADF1(2)	0.995	0.992	-0.3	1.104	11.0
Bottom reflector					
TRANSPORT(1)	2.57E-01	2.69E-01	4.9	2.51E-01	-2.2
TRANSPORT(2)	1.19E+00	1.16E+00	-2.8	1.21E+00	0.9
ABS(1)*	1.26E-02	1.25E-02	-0.8	1.26E-02	0.6
ABS(2)*	3.48E-01	3.48E-01	-0.1	3.51E-01	1.0
SCAT(1,2)	2.20E-02	2.20E-02	-0.2	2.24E-02	1.7
SCAT(2,1)	4.74E-03	4.81E-03	1.3	5.13E-03	8.1
ADF1(1)	0.988	0.952	-3.7	0.983	-0.6
ADF1(2)	0.993	0.985	-0.8	0.961	-3.1
*Absorption cross sections are reduced due to neutron-producing non-fission reactions such as n2n and n3n					

B.12.2 PWR

Description: PWR reflector cross sections are calculated using the 17 × 17 WE lattice. The case matrix is shown in Table B-50.

Table B-50 Test Suite 12: PWR Case Matrix

Reflector location	TF (K)	TC (K)	PC (ppm)
Top	900	560	1,300
Bottom	900	560	1,300
Radial	900	560	1,300

Results: For Polaris, 7 of 12 QOIs are within the target accuracy, and 10 of 12 are within the acceptance accuracy. The QOIs outside of the target accuracy are the upscatter cross section for the radial reflector for all void fractions and the fast absorption cross section for the top reflector for the 70% and 90% void fraction.

For NEWT, 49 of 96 QOIs are within the target accuracy, and 74 of 96 are within the acceptance accuracy. The NEWT upscatter cross section requires further investigation: the QOI fails acceptance accuracy for the top and radial reflector for all void conditions and fails target accuracy for the bottom reflector for all void conditions. The NEWT thermal ADF value also requires further investigation: NEWT overestimates the Serpent value for the radial and bottom reflector for all void conditions and the top reflector for 70% and 90% void fraction.

Table B-51 Test Suite 12: Reflector Cross Section Comparison for 17 × 17 WE Lattice

QOI	Serpent	Polaris	% relative difference	NEWT	% relative difference
Top reflector					
TRANSPORT(1)	1.80E-01	1.96E-01	8.7	1.79E-01	-0.7
TRANSPORT(2)	9.30E-01	9.16E-01	-1.5	9.29E-01	-0.2
ABS(1)*	9.21E-04	9.40E-04	2.1	9.50E-04	3.2
ABS(2)*	1.77E-02	1.75E-02	-1.0	1.75E-02	-0.8
SCAT(1,2)	2.85E-02	2.84E-02	-0.3	2.84E-02	-0.2
SCAT(2,1)	3.19E-04	3.29E-04	3.2	3.63E-04	13.7
ADF1(1)	1.086	1.033	-4.9	1.081	-0.5
ADF1(2)	0.869	0.829	-4.5	0.869	0.1
Radial reflector					
TRANSPORT(1)	1.83E-01	2.05E-01	12.1	1.80E-01	-1.7
TRANSPORT(2)	1.30E+00	1.25E+00	-3.8	1.27E+00	-1.9
ABS(1)*	1.28E-03	1.24E-03	-3.1	1.26E-03	-1.2
ABS(2)*	3.67E-02	3.60E-02	-2.0	3.60E-02	-2.0
SCAT(1,2)	4.27E-02	4.10E-02	-3.8	4.18E-02	-2.0
SCAT(2,1)	5.24E-04	5.57E-04	6.3	5.99E-04	14.3
ADF1(1)	1.107	1.013	-8.5	1.100	-0.6
ADF1(2)	0.966	0.904	-6.4	0.973	0.7
Bottom reflector					
TRANSPORT(1)	2.48E-01	2.63E-01	6.1	2.42E-01	-2.2
TRANSPORT(2)	1.21E+00	1.17E+00	-2.7	1.22E+00	1.2
ABS(1)*	1.25E-02	1.24E-02	-0.8	1.26E-02	0.6
ABS(2)*	3.53E-01	3.52E-01	-0.1	3.56E-01	1.0
SCAT(1,2)	2.21E-02	2.20E-02	-0.2	2.26E-02	2.5
SCAT(2,1)	4.50E-03	4.56E-03	1.3	4.83E-03	7.4
ADF1(1)	0.973	0.940	-3.4	0.979	0.6
ADF1(2)	1.033	1.017	-1.6	0.992	-4.0
*Absorption cross sections are reduced due to neutron-producing non-fission reactions such as n2n and n3n					

B.13 Test Suite 13 – International Numerical Benchmarks

Purpose: The purpose of these international numerical benchmarks is for participants to propose and model benchmark cases that represent real world problems where there are no relevant benchmark experiments. Comparing results from a variety of modeling and simulation codes can provide a level of confidence in a particular code’s performance for a particular application. The following benchmarks have been chosen because of their relevance to LWR lattice physics. Accuracy and possible biases in k_{inf} and major actinides are compared to the reference solution in the benchmark or the average of the results published in the benchmark.

Target Accuracy:

- 200 pcm difference in k_{inf}
- 2% relative difference in isotope number densities for major actinides

Acceptance Accuracy:

- 400 pcm difference in k_{inf}
- 5% relative difference in isotope number densities for major actinides

B.13.1 BWR

Description: CE KENO, NEWT and Polaris models are created for the EGUNF Phase II BWR numerical benchmark specified in Table B-52. The benchmark is designed to assess the accuracy of calculations for gadolinium bearing fuel to support BWR burnup credit. The benchmark is based on Phase III-C benchmark [28] base geometry for an 8 × 8 ATRIUM design.

As part of the benchmark specifications, very small depletion steps (0.25 GWd/MTU) are used for depletion. Considering the large number of depletion steps, the benchmark assembly is depleted up to 15 GWd/MTU instead of 20 GWd/MTU as specified in the benchmark specifications.

Since EGUNF Phase II benchmark is not finalized for this test suite, CE KENO, NEWT and Polaris results for k_{inf} and isotopic concentrations of major actinides are compared to two MC depletion codes: Serpent 2.14 with ENDF/B-7.0 and SWAT4 with Japanese Evaluated Nuclear Data Library (JENDL)-4.

Table B-52 Test Suite 13: BWR Numerical Benchmark

Numerical benchmark	Assembly	Benchmarked neutronic parameters
EGUNF Phase II BWR Benchmark for Gadolinium Burnup	UOX 8 × 8 ATRIUM (large water box)	k_{inf} , isotopic distributions up to 15 GWd/MTU

Results:

Figure B-71 through Figure B-73 compare k_{inf} differences with respect to CE KENO results during depletion at 0, 40, and 70% void fractions. Similar trends with respect to CE KENO results are seen in Serpent, NEWT, and Polaris codes. SWAT4 and Serpent results show a difference as large as 800 pcm across all void fractions.

Relative differences of major actinide concentrations with respect to CE KENO results are compared at 8 GWd/MTU and 14 GWd/MTU burnups before and after gadolinium depletion peak. The results are presented in Table B-53 through Table B-55. All codes show good agreement in ^{235}U concentrations for all exposures and void fractions. The largest differences are observed in ^{238}Pu (14%) and ^{239}Pu (4%) concentrations.

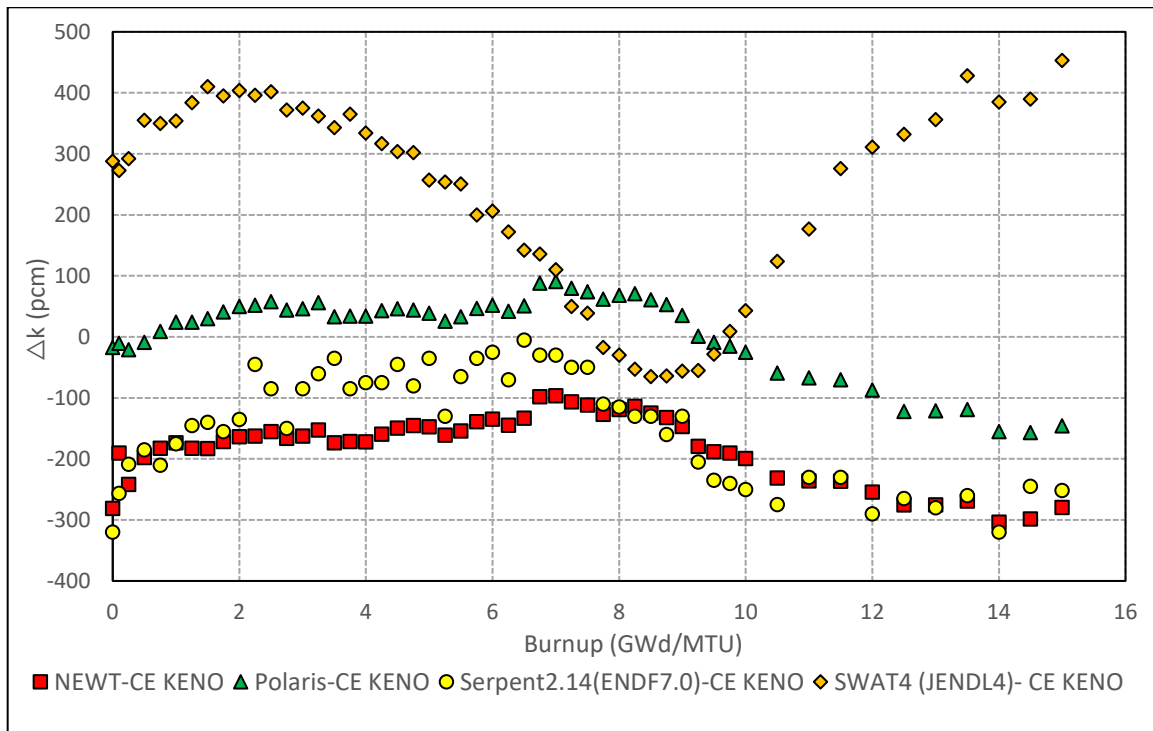


Figure B-71 Test Suite 13: BWR k_{inf} Differences with Depletion for 0% Void Fraction

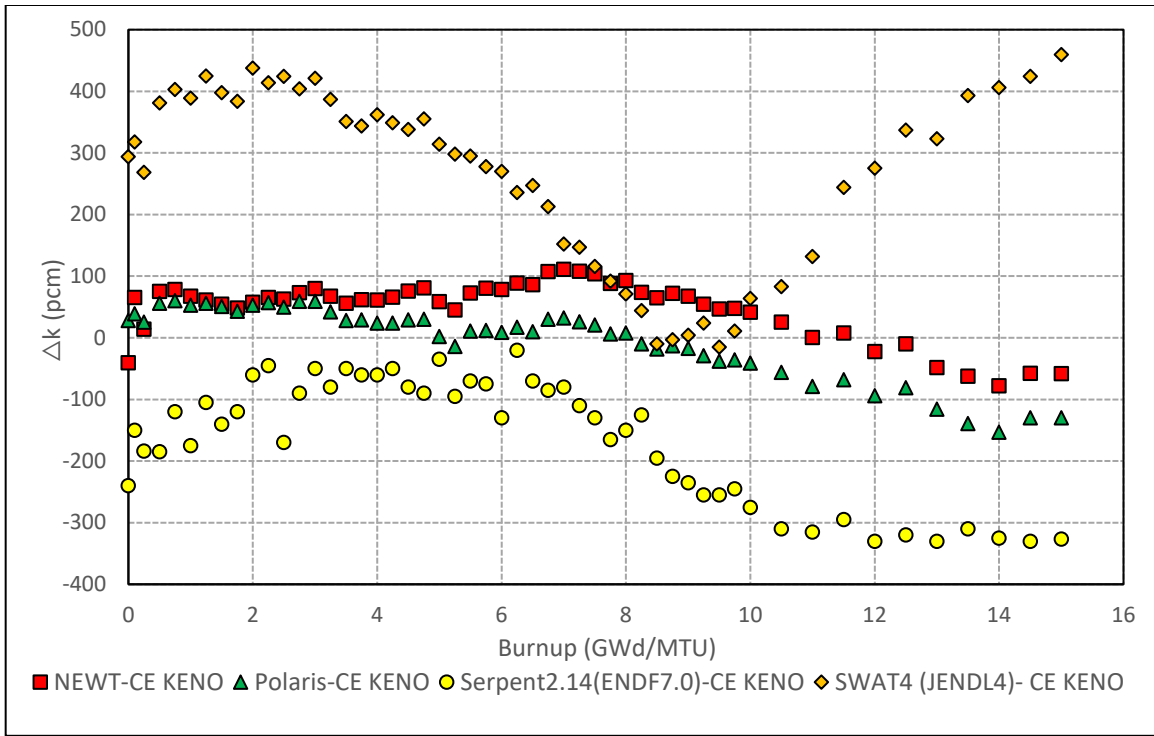


Figure B-72 Test Suite 13: BWR k_{inf} Differences with Depletion for 40% Void Fraction

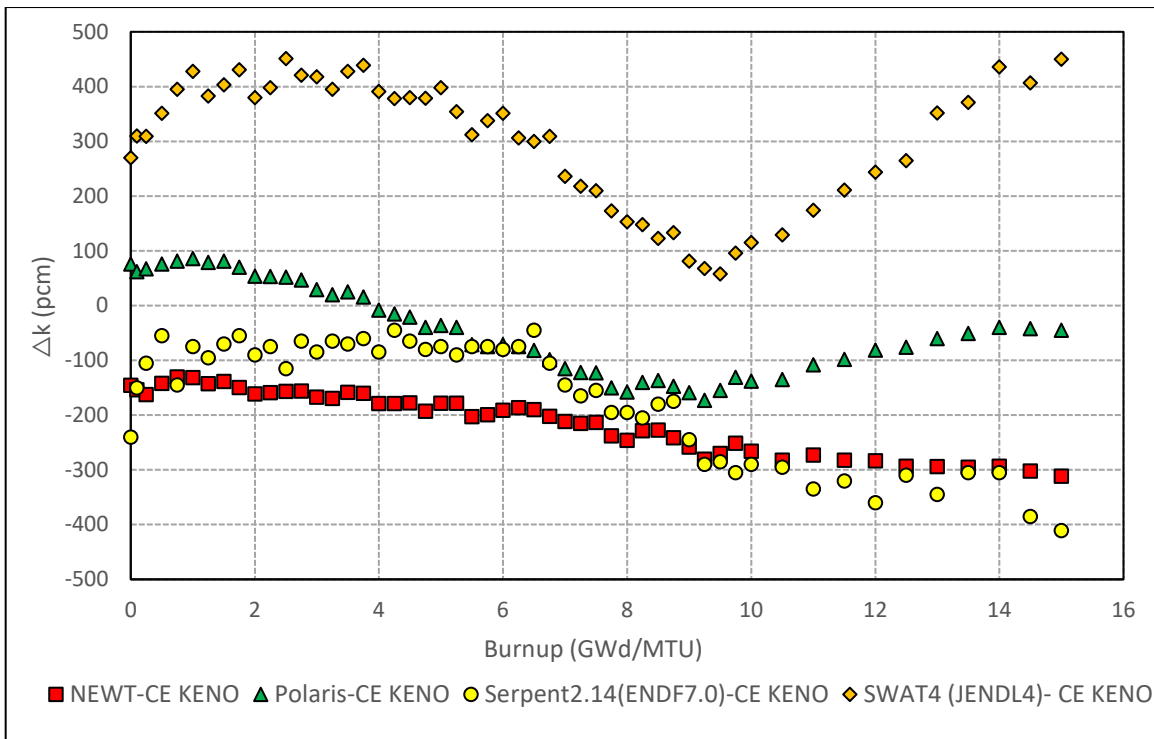


Figure B-73 Test Suite 13: BWR k_{inf} Differences with Depletion for 70% Void Fraction

Table B-53 Test Suite 13: Relative Differences in Isotopic Concentrations for 0% Void Fraction

Isotope	NEWT (%)	Polaris (%)	SWAT4 (%)	Serpent 2.14 (%)
8 GWd/MTU				
²³⁴ U	0.2	0.2	0.5	0.2
²³⁵ U	-0.1	-0.1	0.3	0.6
²³⁶ U	0.3	0.3	-1.0	-3.0
²³⁸ U	0.0	0.0	-0.2	-0.2
²³⁸ Pu	-1.7	-2.0	-2.6	-14.2
²³⁹ Pu	-1.2	-1.3	-4.4	-1.4
²⁴⁰ Pu	-1.0	-1.9	-0.3	0.4
²⁴¹ Pu	-0.7	-1.6	0.7	1.6
²⁴² Pu	-0.9	-2.0	2.8	-4.6
14 GWd/MTU				
²³⁴ U	0.1	0.4	0.1	0.2
²³⁵ U	-0.1	-0.2	1.4	0.5
²³⁶ U	0.3	0.3	-3.1	-0.5
²³⁸ U	0.0	0.0	0.1	0.0
²³⁸ Pu	-1.7	-1.9	-12.5	-6.7
²³⁹ Pu	-1.2	-1.3	-1.7	-4.3
²⁴⁰ Pu	-1.3	-1.8	-0.1	-0.3
²⁴¹ Pu	-0.8	-1.3	2.3	-0.8
²⁴² Pu	-0.5	-1.6	-4.0	-0.3

Table B-54 Test Suite 13: Relative Differences in Isotopic Concentrations for 40% Void Fraction

Isotope	NEWT (%)	Polaris (%)	SWAT4 (%)	Serpent 2.14 (%)
8 GWd/MTU				
²³⁴ U	0.1	0.3	0.1	0.1
²³⁵ U	-0.1	-0.1	0.6	0.2
²³⁶ U	0.2	0.3	-3.1	-0.5
²³⁸ U	0.0	0.0	-0.1	0.0
²³⁸ Pu	-1.8	-2.1	-14.3	-4.4
²³⁹ Pu	-1.8	-1.1	-1.2	-3.1
²⁴⁰ Pu	-1.5	-1.6	-0.3	0.0
²⁴¹ Pu	-0.9	-1.4	0.6	-0.5
²⁴² Pu	-0.6	-1.8	-6.0	-0.2
14 GWd/MTU				
²³⁴ U	0.1	0.5	0.1	0.2
²³⁵ U	-0.2	-0.1	1.4	0.5
²³⁶ U	0.3	0.3	-3.3	-0.5
²³⁸ U	0.0	0.0	-0.2	0.0
²³⁸ Pu	-2.0	-1.9	-11.9	-5.7
²³⁹ Pu	-1.9	-1.1	-1.3	-3.6
²⁴⁰ Pu	-1.6	-1.6	-0.8	-0.2
²⁴¹ Pu	-0.8	-1.0	1.5	-0.5
²⁴² Pu	-0.4	-1.4	-5.1	-0.3

Table B-55 Test Suite 13: Relative Differences in Isotopic Concentrations for 70% Void Fraction

Isotope	NEWT (%)	Polaris (%)	SWAT4 (%)	Serpent 2.14 (%)
8 GWd/MTU				
²³⁴ U	0.2	0.3	0.1	0.1
²³⁵ U	0.0	0.0	0.7	0.2
²³⁶ U	0.2	0.3	-3.2	-0.4
²³⁸ U	0.0	0.0	-0.1	0.0
²³⁸ Pu	-1.3	-2.1	-14.4	-3.6
²³⁹ Pu	0.9	-0.9	-1.2	-2.5
²⁴⁰ Pu	0.6	-1.5	-1.3	0.0
²⁴¹ Pu	0.8	-1.2	-0.4	-0.5
²⁴² Pu	0.4	-1.8	-7.4	-0.5
14 GWd/MTU				
²³⁴ U	0.3	0.6	0.0	0.2
²³⁵ U	0.0	-0.1	1.2	0.4
²³⁶ U	0.1	0.3	-3.5	-0.3
²³⁸ U	0.0	0.0	-0.1	0.0
²³⁸ Pu	-1.1	-2.0	-11.5	-4.8
²³⁹ Pu	1.1	-0.9	-1.3	-2.9
²⁴⁰ Pu	0.6	-1.5	-1.6	-0.1
²⁴¹ Pu	0.9	-0.8	0.8	-0.2
²⁴² Pu	0.4	-1.3	-6.3	-0.5

B.13.2 PWR

Description: TRITON/NEWT and Polaris models are created for the PWR numerical benchmarks specified in Table B-56. The evaluated EPRI depletion reactivity benchmark compares reactivity measurements of a 17 × 17 WE assembly with 104 IFBA pins at 10 GWd/MTU intervals. Measured depletion reactivity values are interpreted from 680 fission rate maps taken over 44 cycles from 4 different PWRs. The calculation approach used to infer the depletion reactivity from the measured plant data is described in detail in *Depletion Reactivity Benchmark for the International Handbook of Evaluated Reactor Physics Benchmark Experiments* [33].

Table B-56 Test Suite 13: PWR Numerical Benchmark

Numerical benchmark	Assembly	Benchmarked neutronic parameters
EPRI IFBA depletion reactivity [33]	UOX 17 × 17	k_{inf} , pin power distributions

Results: CE KENO, TRITON/NEWT, and Polaris results are shown in Table B-57 for the EPRI IFBA depletion reactivity benchmark. Good agreement is observed between the calculated and measured eigenvalues for all three codes. However, Polaris k_{inf} values show larger-than-expected biases after 40 GWd/MTU, which requires further investigation. The TRITON/NEWT results also require further investigation due to the large negative biases at BOL due to IFBA as shown in Test Suite 8 and 9.

Table B-57 EPRI IFBA Depletion Reactivity Benchmark Results

Burnup (GWd/MTU)	k(Burnup) – k(BOL)				Depletion reactivity bias C-E (pcm)		
	Experimental benchmark	CE KENO	TRITON/NEWT	Polaris	CE KENO	TRITON/NEWT	Polaris
10	0.0096	0.0090	0.0097	0.0095	-65	13	-6
20	-0.0421	-0.0428	-0.0418	-0.0420	-67	32	7
30	-0.1082	-0.1085	-0.1076	-0.1086	-25	64	-36
40	-0.1711	-0.1710	-0.1703	-0.1721	15	84	-95
50	-0.2265	-0.2266	-0.2257	-0.2284	-5	81	-191
60	-0.2729	-0.2733	-0.2724	-0.2759	-40	51	-295

B.14 Test Suite 14 – Variations in Vanished Zone Patterns

Purpose: Performance of the lattice physics calculations with respect to different vanished rod patterns in BWR lattices is tested.

Target Accuracy:

- 200 pcm difference in k_{inf}
- 1% RMS and 1.5% max difference in pin power distribution for BWR lattices
- 0.5% RMS and 1.5% max difference in pin power distribution for PWR lattices

Acceptance Accuracy:

- 400 pcm difference in k_{inf}
- 1.5% RMS and 2.5% max difference in pin power distribution for BWR and PWR lattices

B.14.1 BWR

Description: The vanished zone enrichment pattern from Test Suite 1 is adapted for three vanished zone patterns shown in Figure B-74. The case matrix for this test suite is listed in Table B-58.

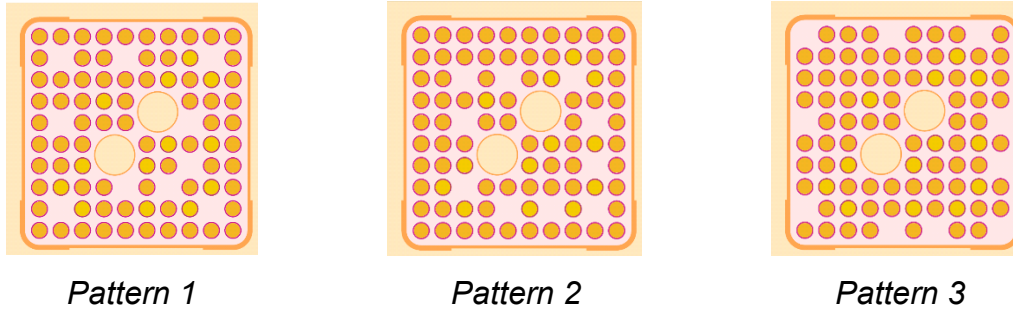


Figure B-74 Test Suite 14: Vanished Zone Patterns

Table B-58 Test Suite 14: BWR Case Matrix

Case number	TF (K)	TC (K)	Void fraction	PC (ppm)	Control rod poison (CR)	Pattern
1	950	560	0	0	0	1
2	950	560	40	0	0	1
3	950	560	70	0	0	1
4	950	560	90	0	0	1
5	950	560	0	0	0	2
6	950	560	40	0	0	2
7	950	560	70	0	0	2
8	950	560	90	0	0	2
9	950	560	0	0	0	3
10	950	560	40	0	0	3
11	950	560	70	0	0	3
12	950	560	90	0	0	3

Results: The k_{inf} differences for the case matrix are plotted in Figure B-75. No significant trend is observed with respect to vanished rod patterns.

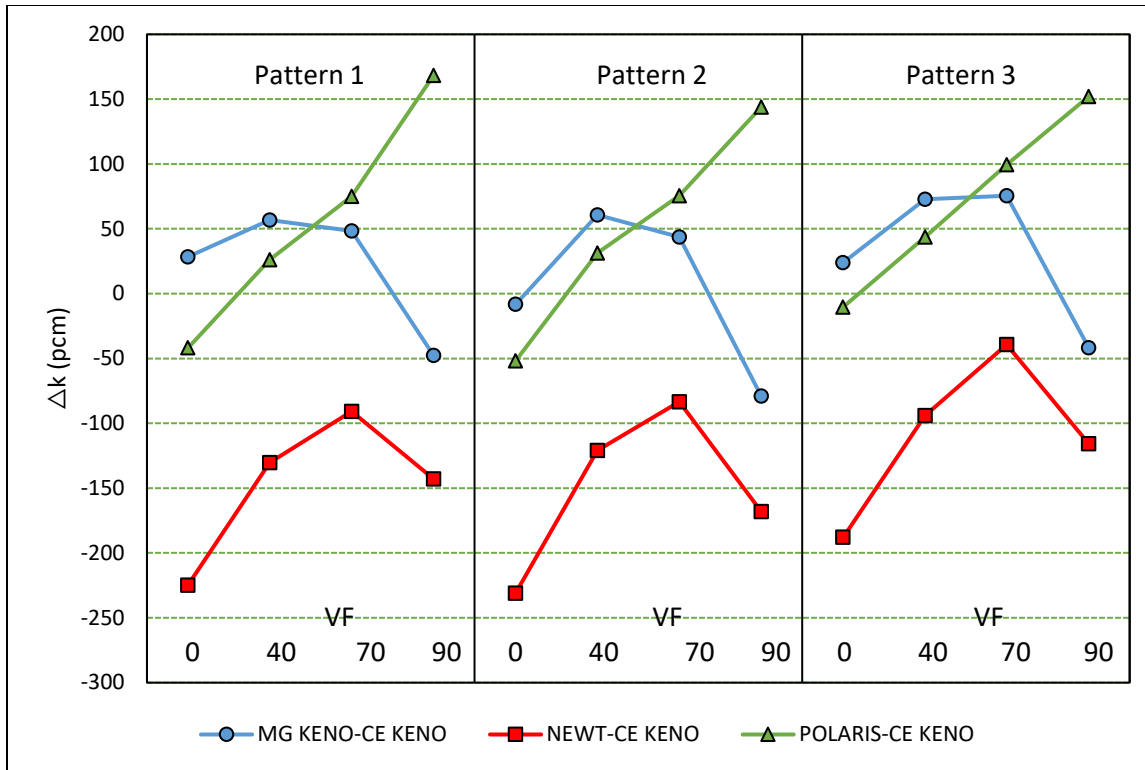


Figure B-75 Test Suite 14: k_{inf} Differences

APPENDIX C

RCA MEASUREMENTS FOR DEPLETION ASSESSMENT

Table C-1 shows the assembly design, enrichment, and burnup ranges covered by the selected RCA measurements for the UOX and MOX fuel samples. The RCA samples cover a burnup range from 36 to 52 GWd/MTU and provide data for early commercial assembly designs not covered in the 2D numerical benchmark validation suite. Previously validated representative samples [21,22,23] from each assembly design are used for depletion validation.

Table C-1 Selected RCA Samples

Reactor	Fuel	Assembly design	Enrichment ^{235}U wt %	Pu^{fiss} wt %	# of samples	Burnup (GWd/MTU)
Calvert Cliffs-1	PWR UOX	14 × 14	3.038	n/a	2	36.54, 46.5
Fukushima Daini-2	BWR UOX	8 × 8	3.41–3.91	n/a	2	43.99, 39.99
Gundremmingen	BWR MOX	9 × 9	0.253	1.15–5.53	1	51.7

RCA benchmark data are provided in previous reports [21,22,23].

The effect of isotope sets used in depletion calculations is shown in Figure C-1. For all isotopes, the effect of the *addnux* options 3 and 4 used in TRITON calculations is less than 1% in isotope concentrations. Although the isotopic concentrations do not change significantly, the difference in CPU time between the two isotope sets is more than fourfold for CE KENO depletion calculations. Therefore, *addnux*=3 option is employed in CE KENO depletion calculations in this test suite. The *addnux*=3 and *addnux*=4 differences for TRITON/NEWT depletion calculations will be used to evaluate the effect of *addnux*=3 in CE KENO depletion calculations.

Results of isotopic comparisons for the Calvert Cliffs-1 samples are shown in Figure C-2 and Figure C-3. NEWT results for Calvert Cliffs-1 samples show good agreement with the measured isotopic data. For both samples, relative differences in ^{235}U , ^{236}U , ^{238}U , ^{238}Pu , ^{240}Pu and ^{241}Pu are less than 3%. However, CE KENO results show larger relative differences for major actinides (~7%), which requires further investigation.

Results of isotopic comparisons for the Fukushima Daini-2 samples are shown in Figure C-4 and Figure C-5. CE KENO calculated isotope distributions show better agreement for the Fukushima Daini-2 samples compared to Calvert Cliffs-1 samples for ^{235}U .

Results of isotopic comparisons for the Gundremmingen samples are shown in Figure C-6. All three codes exhibit similar differences with measurements in general. CE KENO and NEWT relative differences for all major actinides are less than 5%. Relative difference for ^{239}Pu concentration is ~7% in Polaris calculations, while the difference stays below 2% for CE KENO and NEWT. Relatively large differences in ^{239}Pu concentrations between the three codes are also observable in Calvert Cliffs-1 samples and should be investigated in the future.

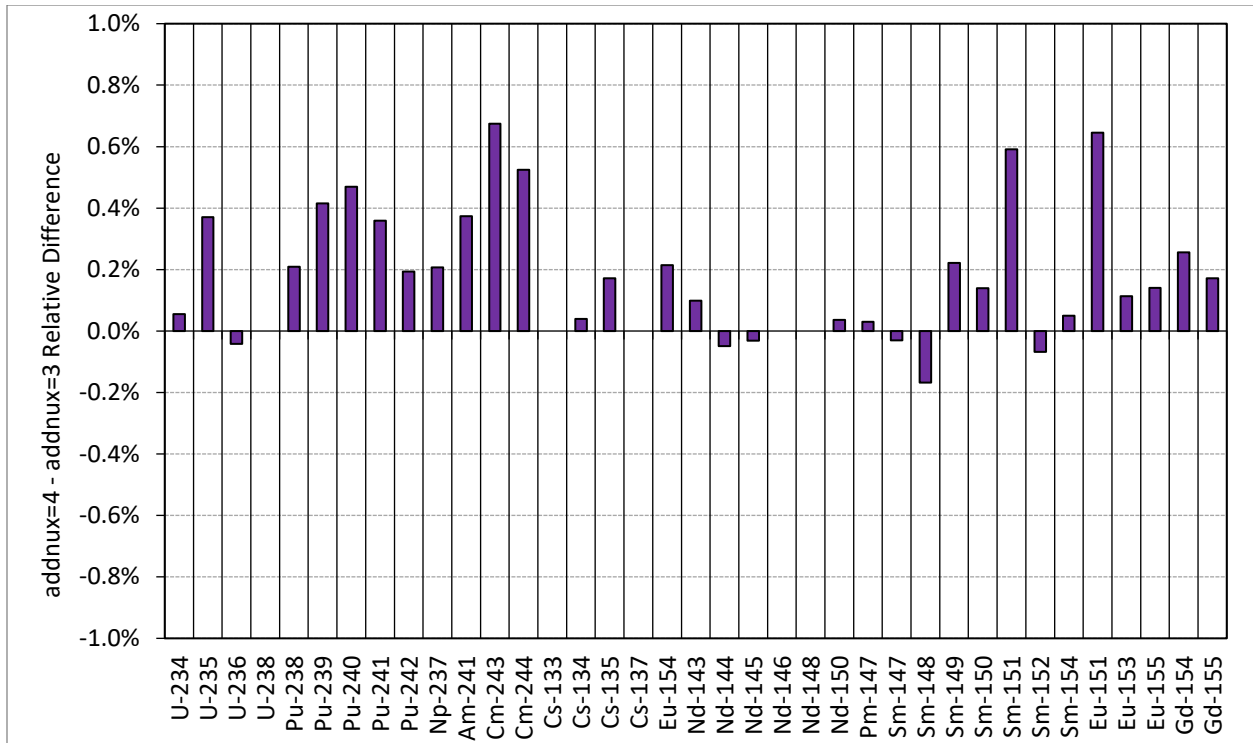


Figure C-1 Comparison of addnu=3 and addnu=4 Isotope Sets on Calvert Cliffs-1 MKP 109-3 Sample

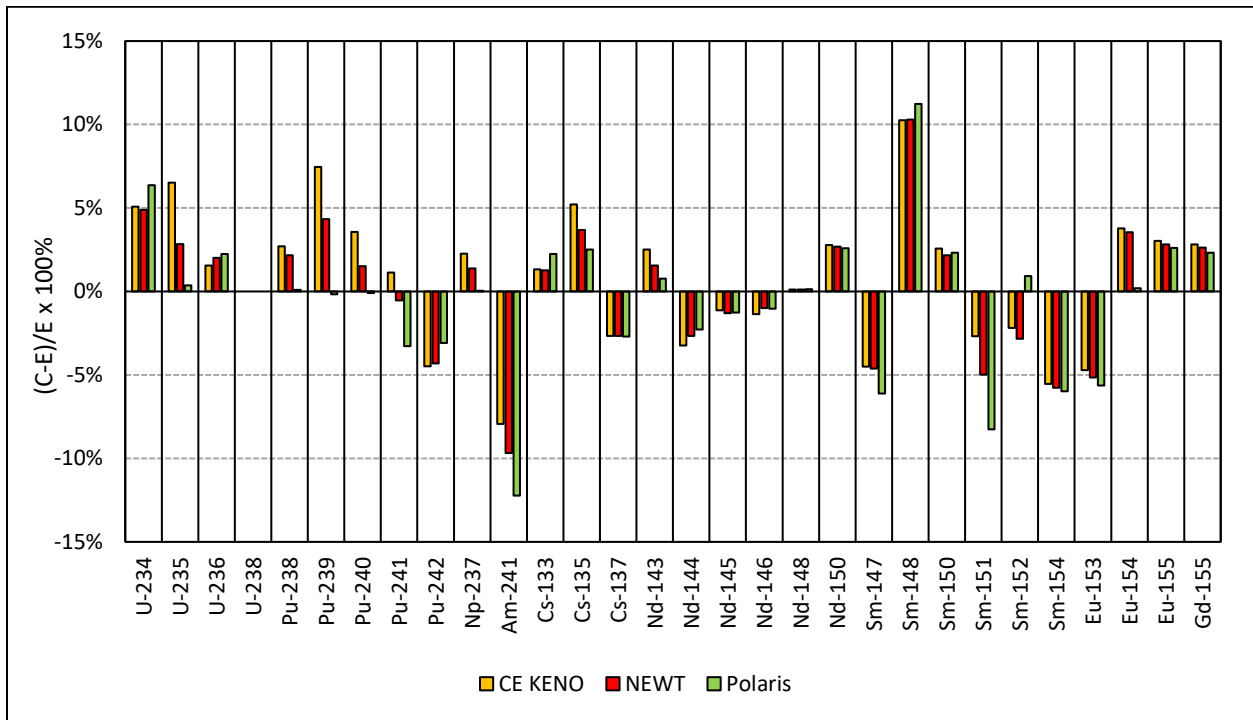


Figure C-2 Comparison of Isotopic Distributions for Calvert Cliffs-1 MKP 109-3 Sample

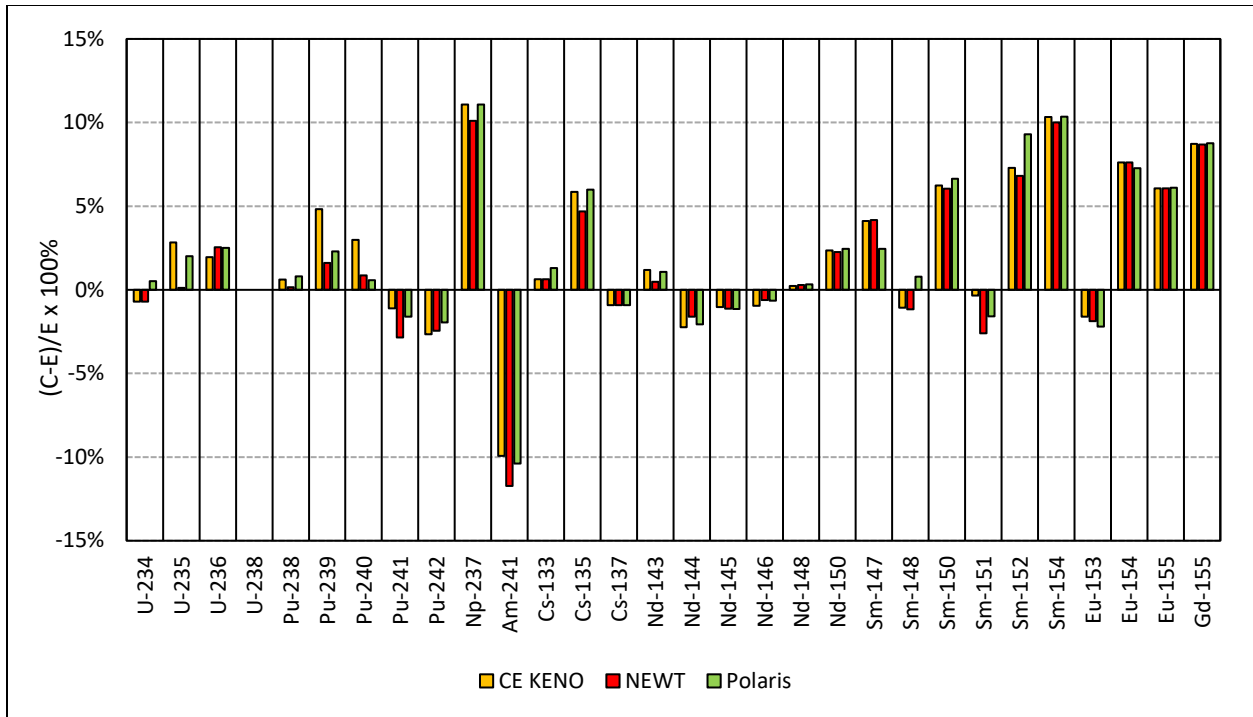


Figure C-3 Comparison of isotopic Distributions for Calvert Cliffs-1 MKP 109-2 Sample

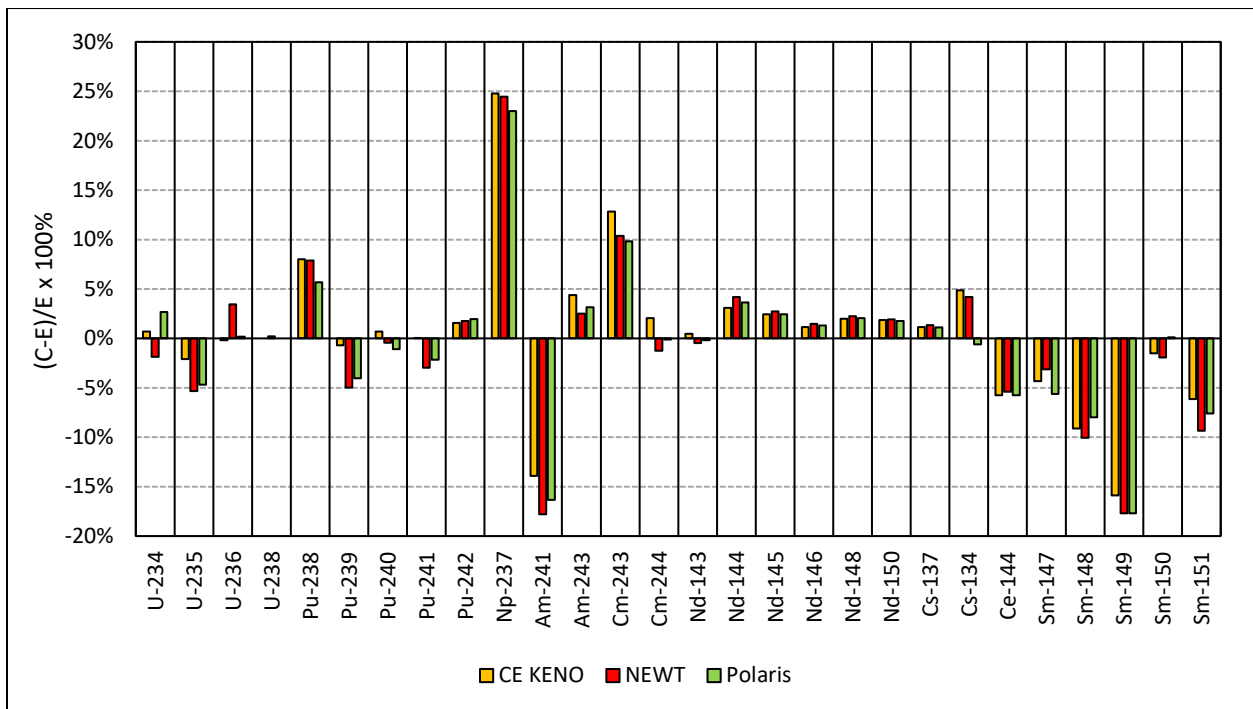


Figure C-4 Comparison of Isotopic Distributions for Fukushima SF98-5 Sample

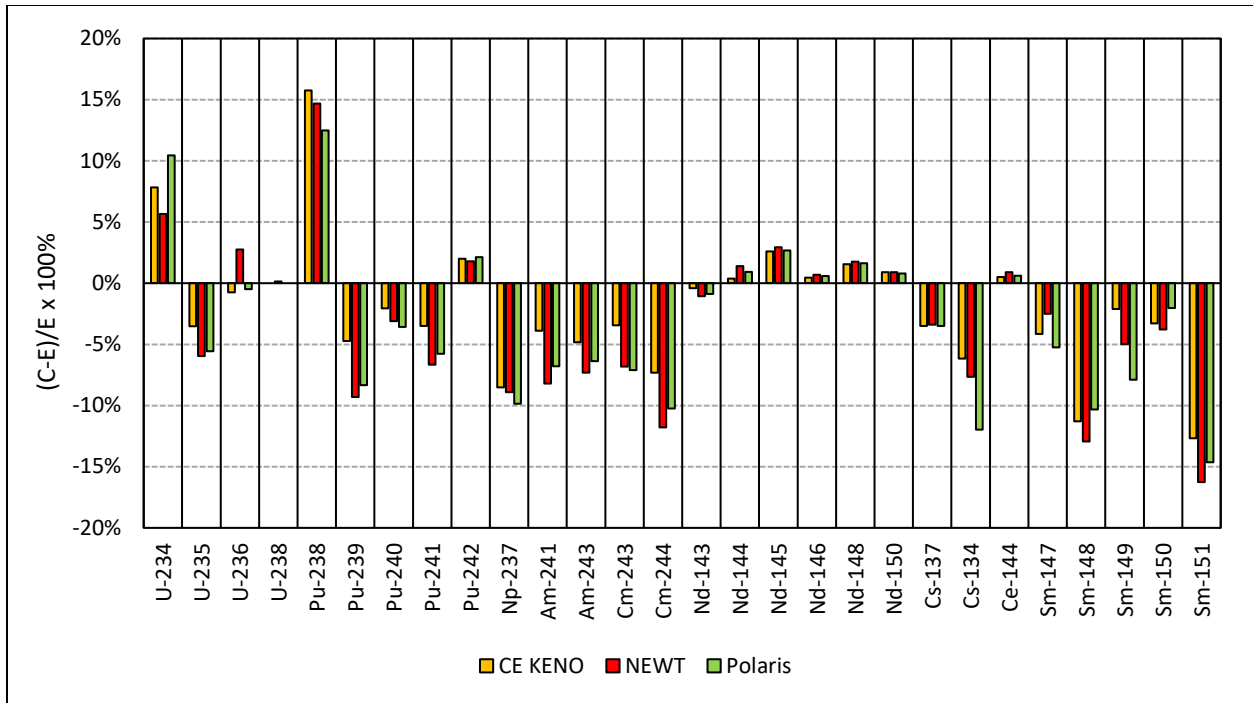


Figure C-5 Comparison of Isotopic Distributions for Fukushima SF98-6 Sample

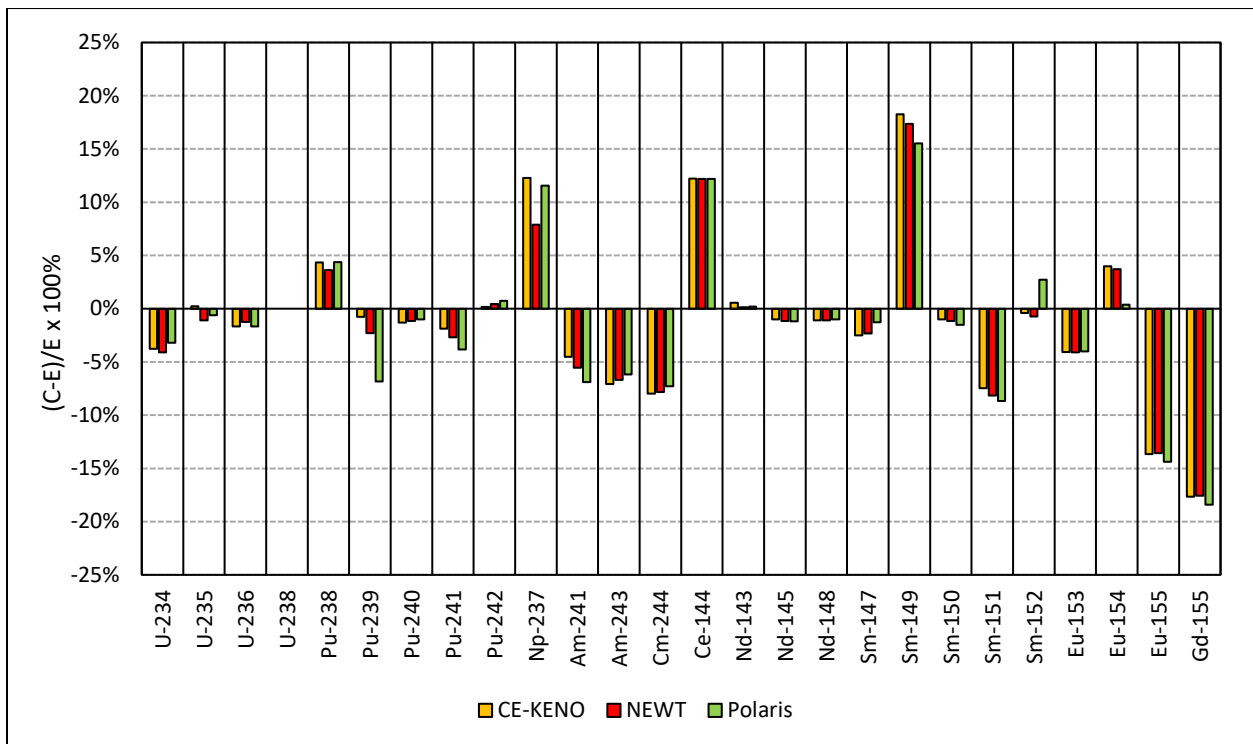


Figure C-6 Comparison of Isotopic Distributions for Gundremmingen GRM-1 Sample

APPENDIX D INPUT AND OUTPUT FILES

The non-proprietary models used in this report are described in this appendix and available as a separate archive of inputs and outputs. The test suites with proprietary design information are marked as “Proprietary” and stored separately as described in APPENDIX E.

Organization of the main directory structure of test suites are shown in Figure D-1. More detailed listings of each appendix directory and related subdirectories are provided in Figure D-2 through Figure D-7.

The input and output filenames for APPENDIX A and APPENDIX C tests are self-descriptive (e.g., “Fukushima_Daini-2-BWR-UOX/POL/sf98-5.inp” corresponds to Fukushima Daini-2 RCA model for sample SF98-5). The naming convention used for input files in APPENDIX B test suites follows the case matrices described in APPENDIX B. Each input file name is in the format of “Reactor-Lattice-State.Branch.Control.inp”. A detailed listing of each field used in the naming convention is provided in Table D-1. As an example, input name “P-W15-cz.tm293.2000ppm.inp” corresponds to PWR Westinghouse 15x15 lattice model at cold zero power state with moderator temperature set at 293K with 2000 ppm boron.

As samples, Polaris and TRITON/CE-KENO sequence input models for Fukushima Daini-2 SF98-5 RCA sample are also provided in Figure D-8 and Figure D-9, respectively.

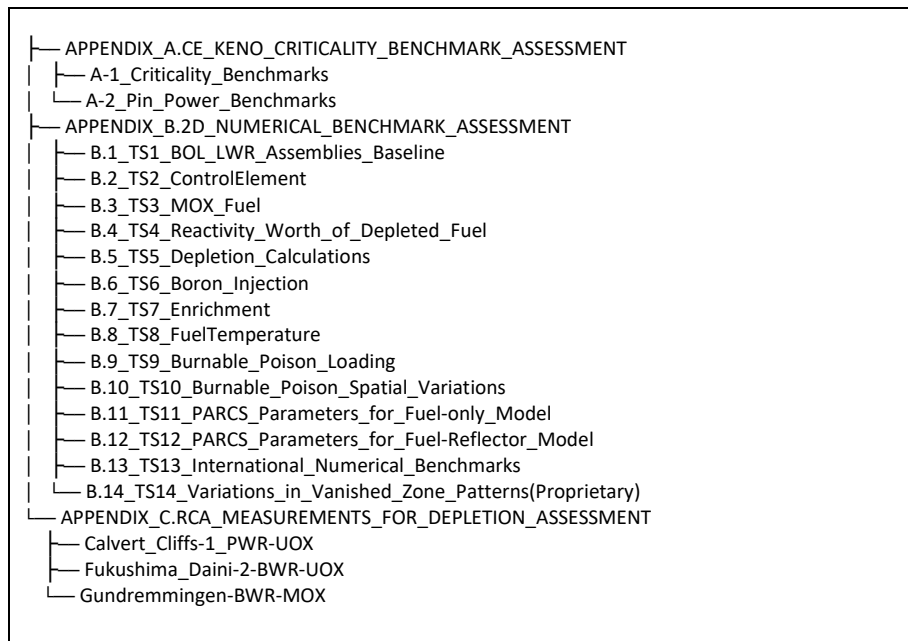


Figure D-1 Main Directory Structure of Input and Output Repository.

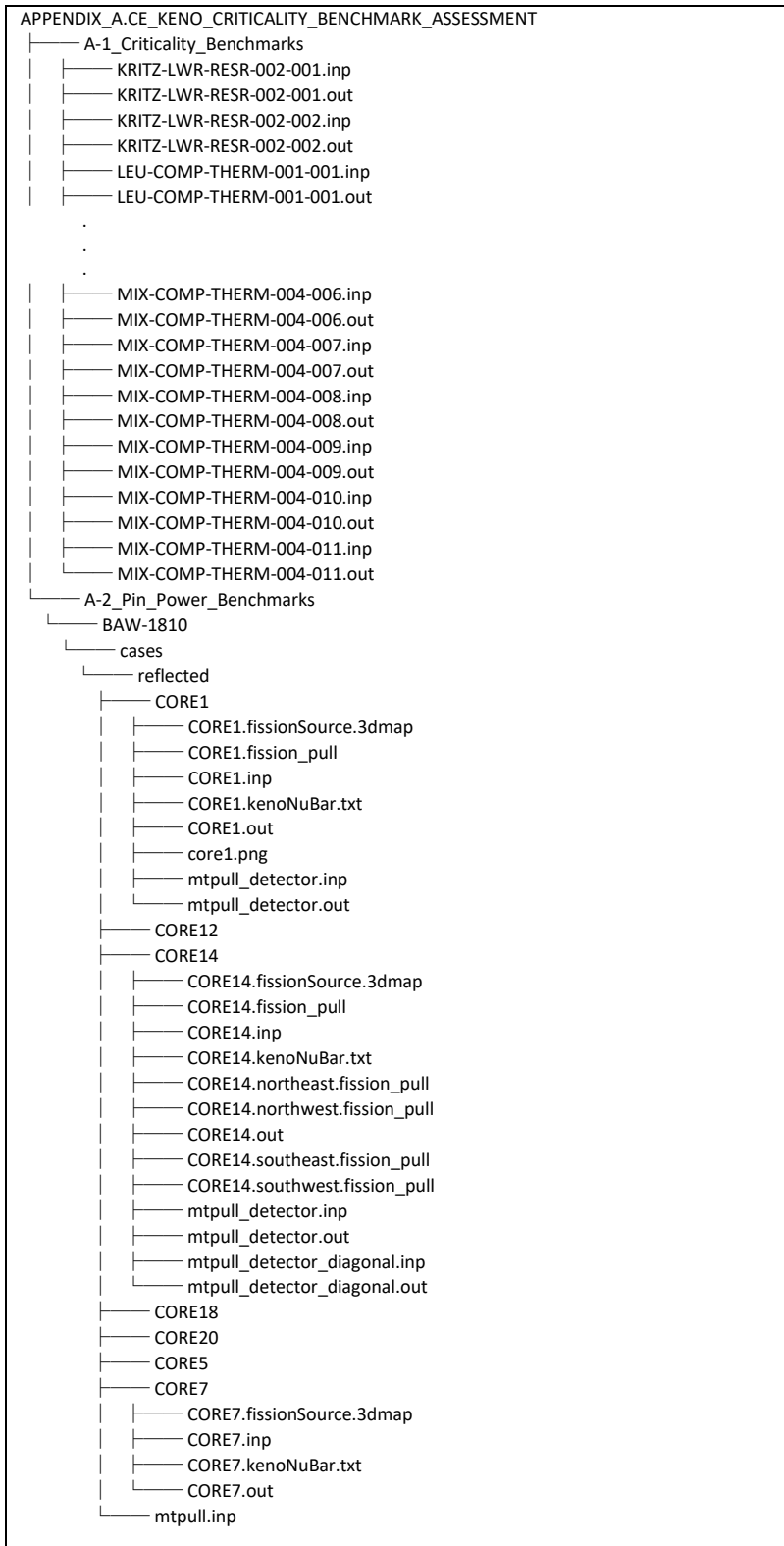


Figure D-2 Directory Structure (Partially Expanded) of APPENDIX A Inputs and Outputs

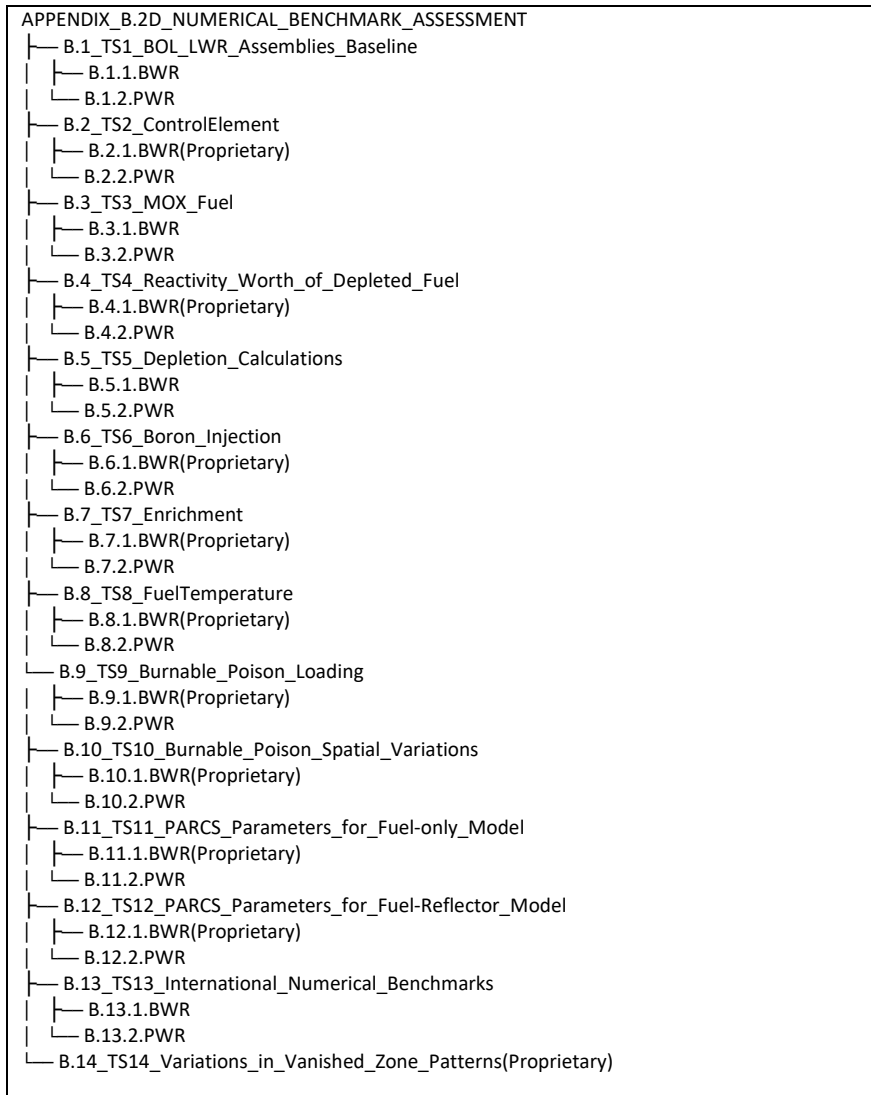


Figure D-3 Directory Structure of APPENDIX B Inputs and Outputs

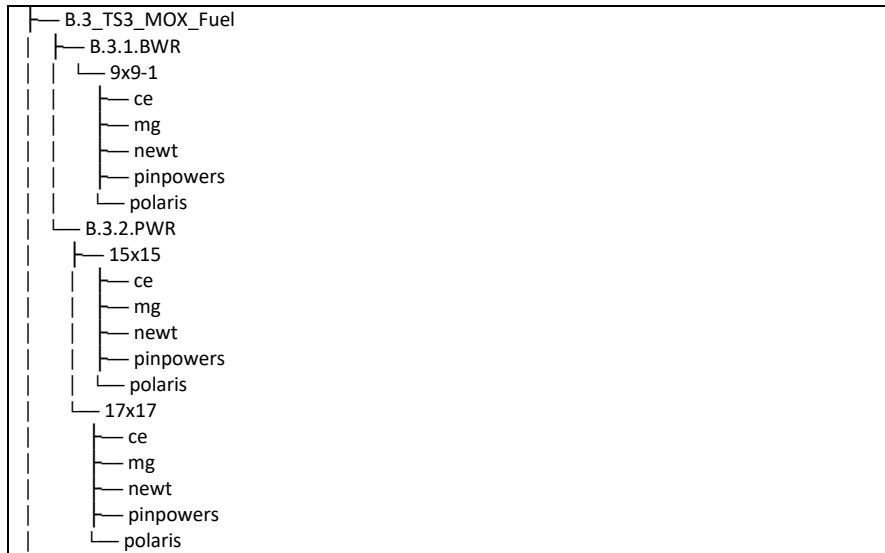


Figure D-4 Directory structure of APPENDIX A Test Suite 3 inputs and outputs

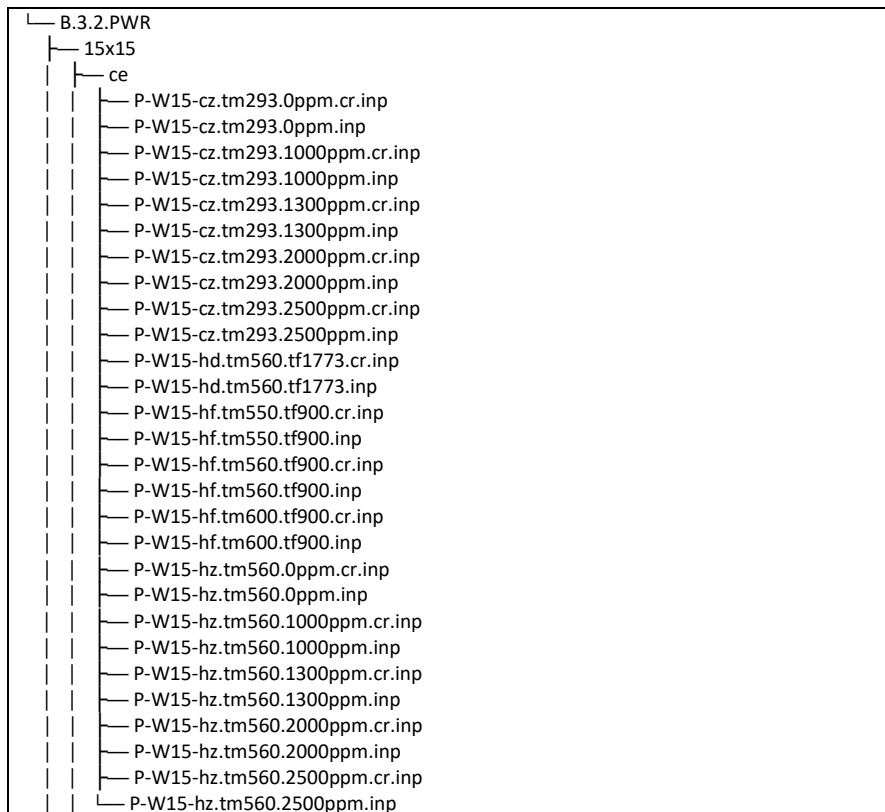


Figure D-5 Expanded Directory Structure of APPENDIX A Test Suite 3 PWR Inputs



Figure D-6 Expanded Directory Structure of APPENDIX A Test Suite 3 BWR Inputs

Table D-1 List of terms used in “Reactor-Lattice-State.Branch.Control.inp” Naming Convention for 2D Numerical Benchmark Assessment Test Suite Input Files

Field	Term	Explanation
Reactor	B	BWR
	P	PWR
Lattice*	W15	Westinghouse 15x15
	STEP3DOM	GNFJ STEP-3 9x9
	CE15	Combustion Engineering 15x15
	GE-14	General Electric 10x10
State	cz	cold zero power
	hf	hot full power
	hd	hot doppler
	hx	special hot zero power branch (BWR only)
	hz	hot zero power (PWR only)
Case	tmXXX	moderator/coolant temperature at XXX
	tfXXX	fuel temperature at XXX
	vXX	void fraction at XX
	bXXXX	boron concentration at XXXX ppm
	haf	Hafnium control element
	mar	Marathon control blades
	b4c	b4C control rods
	aic	AIC control rods
	inc	Inconel control rods
	b4cXX	b4c burnable absorber at XX locations or weight percent
	gdXX	gadolinia burnable absorber at XX locations (PWR only) or at XX weight percent
	ifbaXXX	ifba burnable absorber at XXX locations or at XXX weight percent
	pyXX	pyrex burnable absorber at XX locations
	waXX	waba burnable absorber at XX locations
	edge	gadolinia rod patterns at lattice edge
	int	gadolinia rod patterns at lattice interior
uXX	lattice average U ²³⁵ enrichment at XX	
Control	cr	rodded configuration

*only sample lattice names are listed

```

=polaris_6.3
title "8x8 Assembly model with large diagonal water rods"
lib "xn252v7.1"
sys BWR
geom FuelNode : ASSM 8 1.63
channel COOL
hgap 0.67 0.67 : MOD.1 MOD.1
box hspan=6.72 rad=0.9652 thick=0.23
opt KEFF UpscatterSuperGroup=1
deplete FUEL=yes GAD=yes
shield ALL=N FUEL=P GAD=R
basis ALL=no FUEL.100=yes
mat FUEL.100 : uo2_f100 temp=900 dens=9.943
  comp uvec100 : WT scale=PCT
    U234=0.036
    U235=3.910
    U238=96.054
  comp uo2_f100 : FORM uvec100=1 O=2
mat FUEL.101 : uo2_f100 temp=900 dens=9.943
mat FUEL.102 : uo2_f102 temp=900 dens=9.943
  comp uvec102 : WT scale=PCT
    U234=0.031
    U235=3.448
    U238=96.521
  comp uo2_f102 : FORM uvec102=1 O=2
mat FUEL.103 : uo2_f103 temp=900 dens=9.943
  comp uvec103 : WT scale=PCT
    U234=0.03
    U235=3.405
    U238=96.565
  comp uo2_f103 : FORM uvec103=1 O=2
mat FUEL.104 : uo2_f104 temp=900 dens=9.943
  comp uvec104 : WT scale=PCT
    U234=0.026
    U235=2.903
    U238=97.071
  comp uo2_f104 : FORM uvec104=1 O=2
mat FUEL.105 : uo2_f105 temp=900 dens=9.943
  comp uvec105 : WT scale=PCT
    U234=0.018
    U235=2.00
    U238=97.982
  comp uo2_f105 : FORM uvec105=1 O=2
mat GAD.50 : uo2gd_f50 temp=900 dens=9.943
  comp uox341 : UOX 3.41
  comp uo2gd_f50 : WT GD2O3=4.5 uox341=-100
mat GAD.60 : uo2gd_f50 temp=900 dens=9.943
mat COOL.1 : H2O temp=559 dens=0.5150
mat MOD.1 : H2O temp=559 dens=0.7401

pin 1 : 0.52700 0.61500 : FUEL.100 CLAD.1
pin 2 : 0.52700 0.61500 : FUEL.101 CLAD.1
pin 3 : 0.52700 0.61500 : FUEL.102 CLAD.1
pin 4 : 0.52700 0.61500 : FUEL.103 CLAD.1
pin 5 : 0.52700 0.61500 : FUEL.104 CLAD.1
pin 6 : 0.52700 0.61500 : FUEL.105 CLAD.1
pin 7 : 0.52700 0.61500 : GAD.50 CLAD.1
pin 8 : 0.52700 0.61500 : GAD.60 CLAD.1
pin W1 : 0.72364 0.81000 : MOD.1 CAN.1
pinmap 6

```

Figure D-8 Polaris Input File for Fukushima Daini SF98-5 Fuel Sample

```

5 1
4 8 3
4 3 5 4
4 3 5 W1 4
4 8 3 5 5 3
5 2 8 3 3 8 2
6 5 4 4 4 4 5 6

mesh COOL : nx=9 ny=9 ns=16 nr=2
mesh MOD : nf=4 nd=5 nx=10 ny=10 ns=16 nr=4
mesh FUEL : nr=3 ns=16
mesh GAD : nr=7 ns=16
mesh TUBE : ns=16
state
  ALL : temp=559
  FUEL : temp=900 dens=9.943
  MOD : dens=0.7401 temp=559
  COOL : dens=0.5150 temp=559

read history
power 13.45 33.95 41.84 41.84 0.0
dt 6 3 66 66 21
power 15.16 36.51 36.51 42.27 0.0
dt 5 122 122 8 117
power 15.16 36.51 36.51 0.0
dt 5 158.5 158.5 9
power 15.8 37.15 41.84 0.0
dt 4 72 10 81
power 17.29 38.64 38.64
dt 3 182.5 182.5
power 0
dt 2155
end history

end

```

Figure D-8 Polaris Input File for Fukushima Daini SF98-5 Fuel Sample (Continued)

```

=t6-depl parm={addnu=3)
BWR Validation sample5
ce_v7.1_endf
read comp
' 3.910 wt% U-235 tested
uo2 100 den=9.943 1 900 92234 0.036 92235 3.910 92238 96.054 end
'
' 3.910 wt% U-235 not tested
uo2 101 den=9.943 1 900 92234 0.036 92235 3.910 92238 96.054 end
'
' 3.448 wt% U-235 not tested
uo2 102 den=9.943 1 900 92234 0.031 92235 3.448 92238 96.521 end
'
' 3.405 wt% U-235 not tested
uo2 103 den=9.943 1 900 92234 0.03 92235 3.405 92238 96.565 end
'
' 2.903 wt% U-235 not tested
uo2 104 den=9.943 1 900 92234 0.026 92235 2.903 92238 97.071 end
'
' 2.000 wt% U-235 not tested
uo2 105 den=9.943 1 900 92234 0.018 92235 2.000 92238 97.982 end
'
' ba rod with 3.4 wt% U-235 /4.5 wt% Gd2O3 tested
uo2 50 den=9.943 0.955 900 92234 0.03 92235 3.410 92238 96.56 end
atom-gd2o3 50 9.943 2 64000 2 8016 3 0.045 900 end
uo2 51 den=9.943 0.955 900 92234 0.03 92235 3.410 92238 96.56 end
atom-gd2o3 51 9.943 2 64000 2 8016 3 0.045 900 end
uo2 52 den=9.943 0.955 900 92234 0.03 92235 3.410 92238 96.56 end
atom-gd2o3 52 9.943 2 64000 2 8016 3 0.045 900 end
uo2 53 den=9.943 0.955 900 92234 0.03 92235 3.410 92238 96.56 end
atom-gd2o3 53 9.943 2 64000 2 8016 3 0.045 900 end
uo2 54 den=9.943 0.955 900 92234 0.03 92235 3.410 92238 96.56 end
atom-gd2o3 54 9.943 2 64000 2 8016 3 0.045 900 end
uo2 55 den=9.943 0.955 900 92234 0.03 92235 3.410 92238 96.56 end
atom-gd2o3 55 9.943 2 64000 2 8016 3 0.045 900 end
uo2 56 den=9.943 0.955 900 92234 0.03 92235 3.410 92238 96.56 end
atom-gd2o3 56 9.943 2 64000 2 8016 3 0.045 900 end
'
' ba rod with 3.4 wt% U-235 /4.5 wt% Gd2O3 not tested
uo2 60 den=9.943 0.955 900 92234 0.03 92235 3.410 92238 96.56 end
atom-gd2o3 60 9.943 2 64000 2 8016 3 0.045 900 end
uo2 61 den=9.943 0.955 900 92234 0.03 92235 3.410 92238 96.56 end
atom-gd2o3 61 9.943 2 64000 2 8016 3 0.045 900 end
uo2 62 den=9.943 0.955 900 92234 0.03 92235 3.410 92238 96.56 end
atom-gd2o3 62 9.943 2 64000 2 8016 3 0.045 900 end
uo2 63 den=9.943 0.955 900 92234 0.03 92235 3.410 92238 96.56 end
atom-gd2o3 63 9.943 2 64000 2 8016 3 0.045 900 end
uo2 64 den=9.943 0.955 900 92234 0.03 92235 3.410 92238 96.56 end
atom-gd2o3 64 9.943 2 64000 2 8016 3 0.045 900 end
uo2 65 den=9.943 0.955 900 92234 0.03 92235 3.410 92238 96.56 end
atom-gd2o3 65 9.943 2 64000 2 8016 3 0.045 900 end
uo2 66 den=9.943 0.955 900 92234 0.03 92235 3.410 92238 96.56 end
atom-gd2o3 66 9.943 2 64000 2 8016 3 0.045 900 end
'' zirc2 clad
zirc2 300 1 559 end
zirc2 301 1 559 end
zirc2 302 1 559 end
zirc2 303 1 559 end
zirc2 304 1 559 end
zirc2 305 1 559 end
zirc2 306 1 559 end
zirc2 307 1 559 end
'
' h2o
h2o 400 den=0.5150 1 559 end
h2o 401 den=0.5150 1 559 end
h2o 402 den=0.5150 1 559 end
h2o 403 den=0.5150 1 559 end
h2o 404 den=0.5150 1 559 end
h2o 405 den=0.5150 1 559 end
h2o 406 den=0.5150 1 559 end
h2o 407 den=0.5150 1 559 end
h2o 408 den=0.7401 1 559 end
end comp
read burndata
power=13.45 burn=6 down=0 nlib=1 end
power=33.95 burn=3 down=0 nlib=1 end
power=41.84 burn=132 down=21 nlib=2 end

cylinder 2 0.281639896727 2.5 0.0
cylinder 3 0.344937019096 2.5 0.0
cylinder 4 0.398298961657 2.5 0.0
cylinder 5 0.445311776816 2.5 0.0
cylinder 6 0.48781461057 2.5 0.0
cylinder 7 0.527 2.5 0.0
cylinder 9 0.615 2.5 0.0
cuboid 10 0.815 -0.815 0.815 -0.815 2.5 0.0
media 50 1 1 vol=0.311481
media 51 1 -1 2 vol=0.311521
media 52 1 -2 3 vol=0.311475
media 53 1 -3 4 vol=0.311545
media 54 1 -4 5 vol=0.311446
media 55 1 -5 6 vol=0.311475
media 56 1 -6 7 vol=0.312363
media 300 1 -7 9 vol=0.789269
media 400 1 10 -9 vol=3.671006
boundary 10
unit 8
cylinder 1 0.199149480829 2.5 0.0
cylinder 2 0.281639896727 2.5 0.0
cylinder 3 0.344937019096 2.5 0.0
cylinder 4 0.398298961657 2.5 0.0
cylinder 5 0.445311776816 2.5 0.0
cylinder 6 0.48781461057 2.5 0.0

power=15.16 burn=5 down=0 nlib=1 end
power=36.51 burn=244 down=0 nlib=2 end
power=42.27 burn=8 down=117 nlib=1 end
power=15.16 burn=5 down=0 nlib=1 end
power=36.51 burn=317 down=9 nlib=2 end
power=15.80 burn=4 down=0 nlib=1 end
power=37.15 burn=72 down=0 nlib=1 end
power=41.84 burn=10 down=81 nlib=1 end
power=17.29 burn=3 down=0 nlib=1 end
power=38.64 burn=365 down=2155 nlib=2 end
end burndata
read depletion
-100 101 102 103 104 105 flux 50 51 52 53 54 55 56 60 61 62 63 64 65 66 end
end depletion
read keep_output
origen newt opus
end keep_output
read opus
units=grams
' nrank=37 sort=no
symnuc=u-234 u-235 u-236 u-238 np-237 pu-238 pu-239
pu-240 pu-241 pu-242 am-241 am-242m am-243 cm-242
cm-243 cm-244 cm-245 cm-246 nd-143 nd-144 nd-145
nd-146 nd-148 nd-150 cs-137 cs-134 eu-154 ce-144
ru-106 sm-147 sm-148 sm-149 sm-150 sm-151 sm-152
sm-154 o end
matl=100 end
end opus
read model
'BWR Fuel Bundle
read parameter
fdn=yes
flx=no
gen=1500
htm=no
ngp=100000
nsk=500
run=yes
tba=100
end parameter
read geom
unit 1
cylinder 1 0.527 2.5 0.0
cylinder 2 0.615 2.5 0.0
cuboid 3 0.815 -0.815 0.815 -0.815 2.5 0.0
media 100 1 1 vol=2.181172
media 300 1 2 -1 vol=0.789409
media 400 1 3 -2 vol=3.664793
boundary 3
unit 2
cylinder 1 0.527 2.5 0.0
cylinder 2 0.615 2.5 0.0
cuboid 3 0.815 -0.815 0.815 -0.815 2.5 0.0
media 101 1 1 vol=6.543515
media 300 1 2 -1 vol=2.368226
media 400 1 3 -2 vol=10.994378
boundary 3
unit 3
cylinder 1 0.527 2.5 0.0
cylinder 2 0.615 2.5 0.0
cuboid 3 0.815 -0.815 0.815 -0.815 2.5 0.0
media 102 1 1 vol=26.174944
media 300 1 2 -1 vol=9.472115
media 400 1 3 -2 vol=44.051927
boundary 3
unit 4
cylinder 1 0.527 2.5 0.0
cylinder 2 0.615 2.5 0.0
cuboid 3 0.815 -0.815 0.815 -0.815 2.5 0.0
media 103 1 1 vol=39.263925
media 300 1 2 -1 vol=14.205966
media 400 1 3 -2 vol=66.153108
boundary 3
unit 5
cylinder 1 0.527 2.5 0.0
cylinder 2 0.615 2.5 0.0
cuboid 3 0.815 -0.815 0.815 -0.815 2.5 0.0
media 104 1 1 vol=34.901489
media 300 1 2 -1 vol=12.627613
media 400 1 3 -2 vol=58.761033
boundary 3
unit 6
cylinder 1 0.527 2.5 0.0
cylinder 2 0.615 2.5 0.0
cuboid 3 0.815 -0.815 0.815 -0.815 2.5 0.0
media 105 1 1 vol=8.725337
media 300 1 2 -1 vol=3.156265
media 400 1 3 -2 vol=14.709571
boundary 3
unit 7
cylinder 1 0.199149480829 2.5 0.0

```

Figure D-9 TRITON/CE-KENO Input File for Fukushima Daini SF98-5 Fuel Sample

```

cylinder 7 0.527 2.5 0.0
cylinder 9 0.615 2.5 0.0
cuboid 10 0.815 -0.815 0.815 -0.815 2.5 0.0
media 60 1 1 vol=2.180365
media 61 1 -1 2 vol=2.180649
media 62 1 -2 3 vol=2.180324
media 63 1 -3 4 vol=2.180812
media 64 1 -4 5 vol=2.180121
media 65 1 -5 6 vol=2.180324
media 66 1 -6 7 vol=2.186543
media 300 1 -7 9 vol=5.524886
media 400 1 10 -9 vol=25.697039
boundary 10
unit 9
cylinder 1 0.527 2.5 0.0
cylinder 2 0.615 2.5 0.0
cuboid 3 0.815 -0.815 0.815 -0.815 2.5 0.0
media 408 1 1 vol=4.362529
media 300 1 2 -1 vol=1.578632
media 400 1 3 -2 vol=7.342005
boundary 3
global unit 10
cuboid 10 13.04 0.0 13.04 0.0 2.5 0.0
cuboid 11 13.24 -0.2 13.24 -0.2 2.5 0.0
cuboid 12 13.47 -0.43 13.47 -0.43 2.5 0.0
cuboid 13 14.14 -1.1 14.14 -1.1 2.5 0.0
array 1 10 place 1 1 1 0.815 0.815 0
media 400 1 11 -10 vol=26.433888
media 300 1 12 -11 vol=31.458595
media 408 1 13 -12 vol=97.590922
boundary 13
end geom
read array
ara=1 gbl=1 typ=cuboidal
nux=8 nuy=8 nuz=1
fill
6 5 4 4 4 5 6
5 2 8 3 3 8 2 5
4 8 3 5 5 3 8 4
4 3 5 9 4 5 3 4
4 3 5 4 9 5 3 4
4 8 3 5 5 3 8 4
5 1 7 3 3 8 2 5
6 5 4 4 4 4 5 6 end fill
end array
read bounds
all=mirror
end bounds
read grid
12
numxcells=16 numycells=16 numzcells=2
xmin=0.0 xmax=13.04
ymin=0.0 ymax=13.04
zmin=0.0 zmax=2.5
end grid
read plot
ttl='z=1.25 cm'
TYP=XY
XLR=14.14 YLR=-1.1 ZUL=1.25
XUL=-1.1 YUL=14.14 ZLR=1.25
NAX=2560 end
end plot
end data
end model
end

```

Figure D-9 TRITON/CE-KENO Input File for Fukushima Daini SF98-5 Fuel Sample (Continued)

APPENDIX E

PROPRIETARY INPUT AND OUTPUT FILES

GE-14 and SVEA-96 lattice designs used in this report contain proprietary design information and are described in this appendix and available as a separate archive of inputs and outputs. The list of the proprietary test suites is provided in Figure E-1.

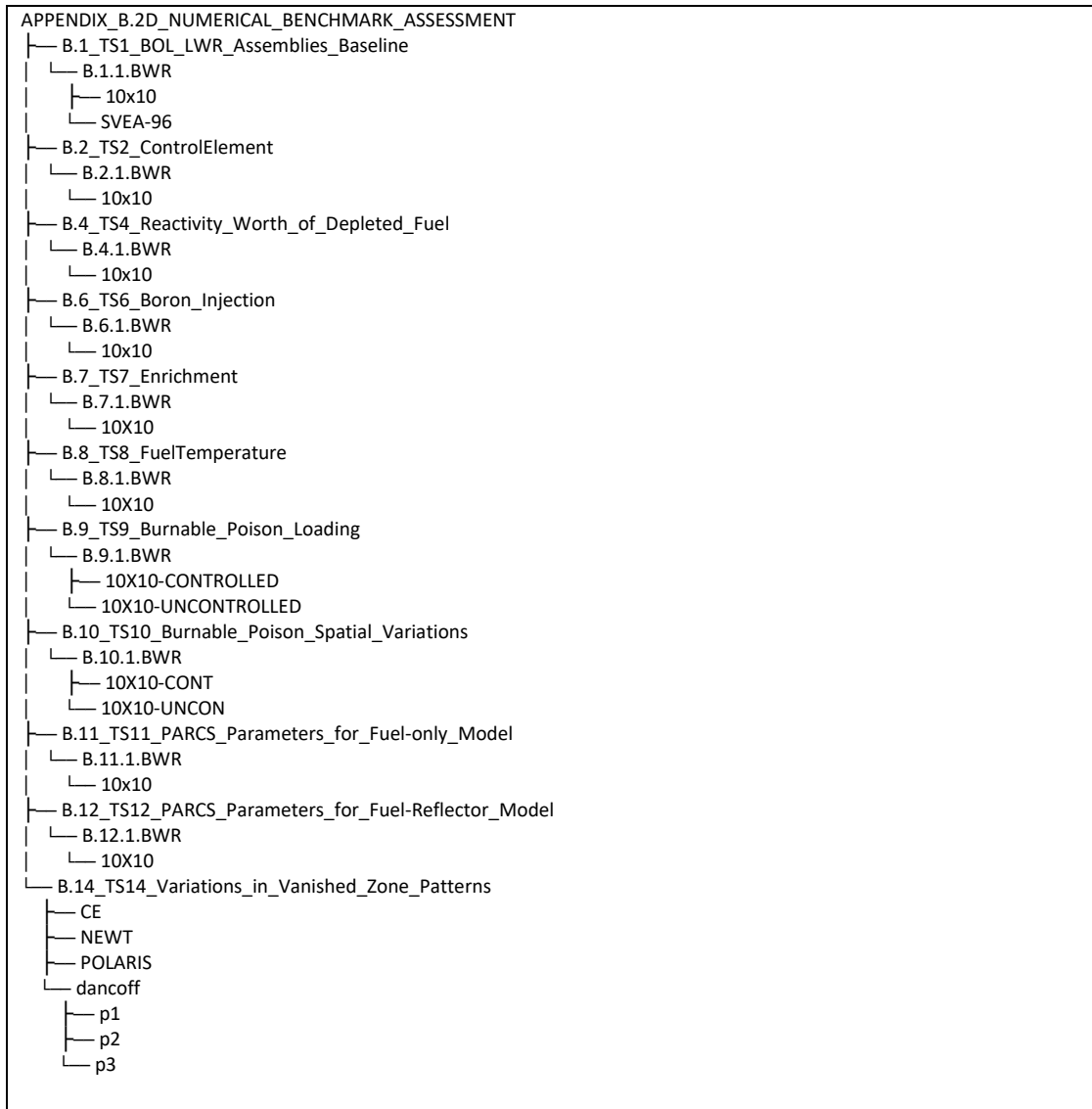


Figure E-1 Main Directory Structure of Proprietary Input Repository

APPENDIX F

SCALE 6.2.4 UPDATE

A new official version of SCALE 6.2, version 6.2.4, became available before the distribution of this report. Beside minor bug fixes and input/output format changes, changes to Polaris geometry engine were implemented in 6.2.4 compared to the SCALE 6.2 version used for calculations documented herein. In order to assure that any conclusion of this report has not changed especially regarding Polaris results, k_{inf} and pin power distributions for Test Suite 1 through Test Suite 14 were reevaluated using the latest SCALE 6.2.4 version.

Spot checks to CE KENO reference solutions were also performed to assure that similar differences with respect to the reference solution can be expected with the latest version as previously determined. The CE KENO reference solutions calculated with SCALE 6.2.4 for the BWR lattices exhibit on average a 20 pcm difference from previously calculated values. These changes in the results are attributed to several improvements in the Doppler broadening implementation. The maximum difference in CE KENO calculated k_{inf} is 52 pcm and corresponds to the 3000 K Doppler case at 90% void fraction in “Test Suite 8 - Fuel Temperature”.

All BWR Polaris results show consistent agreement between SCALE versions 6.2.2 and 6.2.4. The difference in k_{inf} values are less than 1 pcm and pin power differences are less than 0.01%.

SCALE 6.2.4 Polaris results for PWR lattices show differences for many cases compared to the SCALE 6.2 rev19189 Polaris results documented herein, if the same input files were used for the considered cases. These differences are mainly driven by changes to the Polaris geometry engine and changes in default coolant spatial mesh. To ensure a consistent comparison, the PWR lattice input files were slightly modified for the SCALE 6.2.4 runs to use two coolant regions for each unit cell as applied for the previous runs. Except for the IFBA lattice cases, the use of consistent meshing led to an average difference in k_{inf} of 20 pcm (with +/- 40 pcm maximum and minimum deviations) and to less than 0.04% difference in pin powers. The IFBA cases in “Test Suite 9 – Burnable Poison Loading” and “Test Suite 10 – Burnable Poison Spatial Variations” show differences up to 130 pcm (with average 20 pcm and rms 48 pcm) in k_{inf} values in SCALE 6.2.4 results compared to the previous results. The maximum difference in pin powers for these IFBA cases is below 0.06%.

Similar to BWR results, reference CE KENO results for PWR lattices show on average a 20 pcm difference in calculated k_{inf} values between 6.2.4 results and previous calculations, for consistent input files. The difference in k_{inf} is up to 47 pcm for the IFBA cases. Since both the reference solutions and the Polaris results change in the same direction, the differences between Polaris and CE KENO results for the PWR lattices still stay below the target criteria. Comparisons of the reported (SCALE 6.2 rev19189) and recent (SCALE 6.2.4) Polaris-CE KENO results are illustrated in Figure F-1 and Figure F-2 for Test Suite 9 and Test Suite 10.

Although changes to CE KENO and Polaris calculated k_{inf} and pin power distributions are observed, these changes are small and the difference in the results of the two codes stay below the acceptance criteria. Therefore, the use of the new SCALE 6.2.4 version for the reevaluated test suites did not lead to a significant change in the statistics shown in this report. The conclusions documented in this report are still valid.

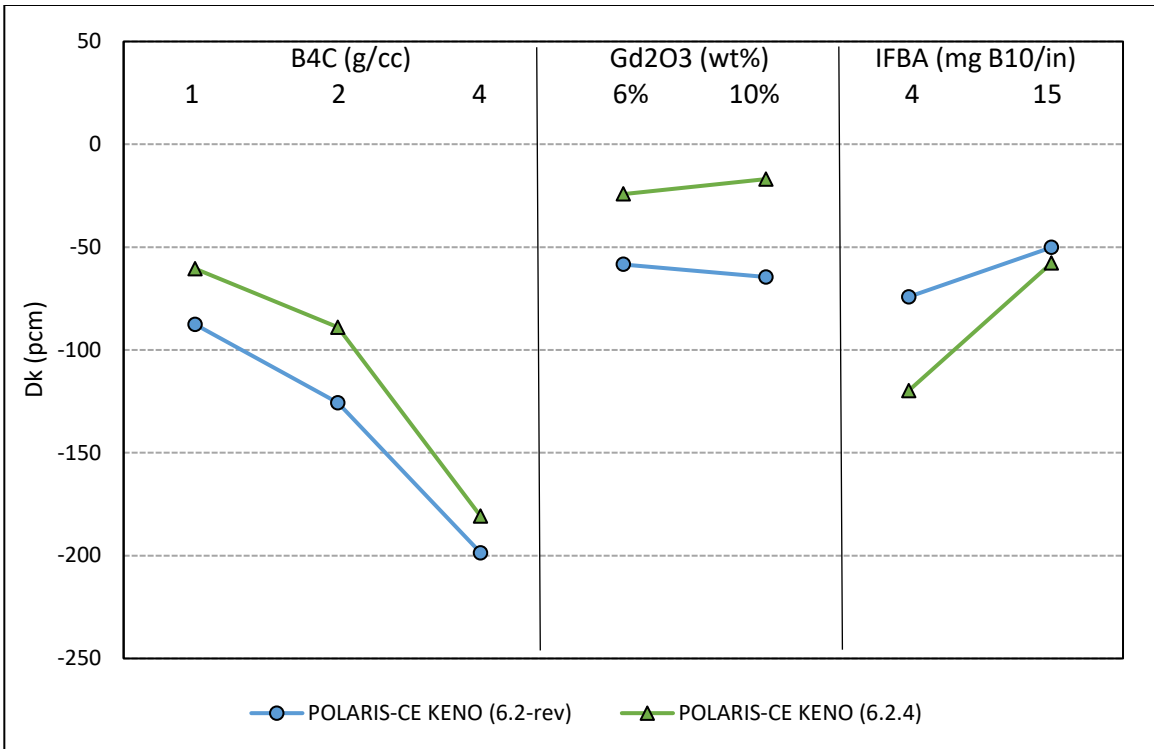


Figure F-1 Test Suite 9: Updated k_{inf} Differences for Uncontrolled PWR Cases

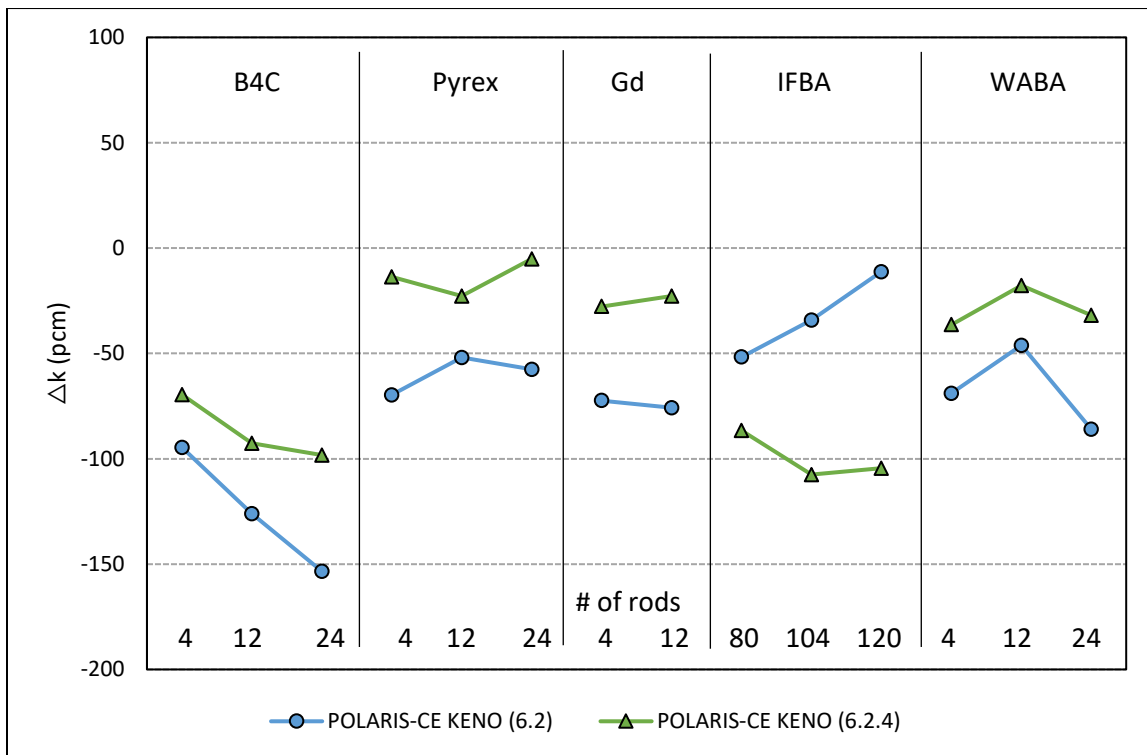


Figure F-2 Test Suite 10: Updated PWR k_{inf} Differences

BIBLIOGRAPHIC DATA SHEET

(See instructions on the reverse)

NUREG/CR-7284

2. TITLE AND SUBTITLE

SCALE 6.2 Lattice Physics Performance Assessment

3. DATE REPORT PUBLISHED

MONTH

YEAR

March

2023

4. FIN OR GRANT NUMBER

5. AUTHOR(S)

Ugur Mertuyrek, Matthew A. Jessee, Benjamin R. Betzler, and Stephen M. Bowman

6. TYPE OF REPORT

Technical

7. PERIOD COVERED (Inclusive Dates)

8. PERFORMING ORGANIZATION - NAME AND ADDRESS (If NRC, provide Division, Office or Region, U. S. Nuclear Regulatory Commission, and mailing address; if contractor, provide name and mailing address.)

Oak Ridge National Laboratory Managed
by UT-Battelle, LLC 1 Bethel Valley Road
Oak Ridge, TN 37831-6170

9. SPONSORING ORGANIZATION - NAME AND ADDRESS (If NRC, type "Same as above", if contractor, provide NRC Division, Office or Region, U. S. Nuclear Regulatory Commission, and mailing address.)

Division of Systems Analysis
Office of Nuclear Regulatory Research
U.S. Nuclear Regulatory Commission
Washington DC 20555-0001

10. SUPPLEMENTARY NOTES

L. Kyriazidis, NRC Project Manager

11. ABSTRACT (200 words or less)

The US Nuclear Regulatory Commission relies on the lattice physics analysis capabilities of the SCALE code system to perform confirmatory licensing analyses. Either SCALE lattice physics code—TRITON/NEWT or Polaris—can be used to calculate cross section data used by the PARCS nodal core simulator for full-core neutronics calculations. This report presents an assessment of the accuracy of SCALE lattice physics codes for preparation of PARCS cross section data to be used in light water reactor (LWR) analysis. Due to the nature of lattice physics calculations, critical reactor experiment benchmarks cannot be modeled in explicit detail in a lattice physics code. Therefore, either geometry approximations or axial buckling must be implemented to determine the critical water height. These modeling limitations have led to development of a three-phase assessment strategy. This report documents results for all test suites. Both TRITON/NEWT and Polaris exhibited acceptable accuracy for most test cases. For the few test cases in which acceptable accuracy criteria were not met, further code and data development are planned.

12. KEY WORDS/DESCRIPTORS (List words or phrases that will assist researchers in locating the report.)

lattice
physics LWR
Polaris
TRITON
PARCS

13. AVAILABILITY STATEMENT

unlimited

14. SECURITY CLASSIFICATION

(This Page)

unclassified

(This Report)

unclassified

15. NUMBER OF PAGES

16. PRICE



Federal Recycling Program



UNITED STATES
NUCLEAR REGULATORY COMMISSION
WASHINGTON, DC 20555-0001

OFFICIAL BUSINESS



@NRCgov



NUREG/CR-7284

SCALE 6.2 Lattice Physics Performance Assessment

March 2023